FAULT DIAGNOSIS IN NONLINEAR SYSTEMS USING LEARNING AND SLIDING MODE APPROACHES WITH APPLICATIONS FOR SATELLITE CONTROL SYSTEMS

by

Qing Wu

B.A.Sc., Huazhong University of Science and Technology, 1999

M.A.Sc., Huazhong University of Science and Technology, 2002

A THESIS SUBMITTED IN PARTIAL FULFILLMENT
OF THE REQUIREMENTS FOR THE DEGREE OF
DOCTOR OF PHILOSOPHY
in the School
of
Engineering Science

SIMON FRASER UNIVERSITY
Spring 2008

APPROVAL

Name: Qing Wu

Degree: Doctor of Philosophy

Title of thesis: Fault Diagnosis in Nonlinear Systems Using Learning and Sliding Mode Approaches with Applications for Satellite Control Systems

Examining Committee: Dr. Daniel Lee
Chair

Dr. Mehrdad Saif, Senior Supervisor

Dr. Farid Golnaraghi, Supervisor

Dr. John D. Jones, Supervisor

Dr. Ahmad Rad, Internal Examiner

Dr. Kash Khorasani, External Examiner,
Professor of Electrical & Computer Engineering,
Concordia University

Date Approved: April 3, 2008

Declaration of Partial Copyright Licence

Abstract

In this thesis, model based fault detection, isolation, and estimation problem in several classes of nonlinear systems is studied using sliding mode and learning approaches.

First, a fault diagnosis scheme using a bank of repetitive learning observers is presented. The diagnostic observers are established in a generalized observer scheme, and the observer inputs are repetitively updated using the output estimation error in a proportional-integral structure.

Next, a framework for robust fault diagnosis using sliding mode and learning approaches is proposed to deal with various types of faults in a class of nonlinear systems with triangular input form. In the designed diagnostic observers, first order and second order sliding modes are used respectively, to achieve robust state estimation in the presence of uncertainties, and additional online estimators are established to characterize the faults. In order to guarantee that the sliding mode is able to distinguish the system uncertainties from the faults, two iterative adaptive laws are used to update the sliding mode switching gains. Moreover, different online fault estimators are developed using neural state space models, iterative learning algorithms, and wavelet networks.

Another class of nonlinear systems where an unmeasurable part of state can be described as a nonlinear function of the output and its derivatives is considered next. Accordingly, a class of fault diagnosis schemes using high order sliding mode differentiators (HOSMDs) and online estimators are proposed, where neural adaptive estimators and iterative neuron PID estimators are designed. Additionally, a fault diagnosis scheme using HOSMDs and neural networks based uncertainty observers is designed in order to achieve a better performance in robust fault detection. If the

uncertainties can be accurately estimated, the generated diagnostic residual is more sensitive to the onset of faults.

Finally, a fault diagnosis scheme using Takagi-Sugeno (TS) fuzzy models, neural networks, and sliding mode is developed. The availability of TS fuzzy models makes this fault diagnosis scheme applicable to a wider class of nonlinear systems. The proposed fault diagnosis schemes are applied to several types of satellite control systems, and the simulation results demonstrate their performance.

Keywords: Fault Diagnosis; Observer; Sliding Mode; Learning; Fuzzy Model; Neural Networks; Satellite Control Systems

Dedication

To my father, Zhengqi Wu, and my mother, Yueling Sun.

Acknowledgments

My great gratitude goes primarily to my Senior Supervisor Dr. Mehrdad Saif for his support, patience, guidance, and enthusiastic assistant to my research. I appreciate his time, effort, suggestions, and comments during this thesis and related research.

I would like to give my special thanks to Dr. Farid Golnaraghi and Dr. John D. Jones for serving as my supervisory committee members, to Dr. Ahmad Rad for willing to be Internal Examiner, to Dr. Kamal K. Gupta for chairing my Examining Committee, to Dr. Kash Khorasani for being the External Examiner. I am very grateful to them for taking their precious time to review my thesis.

I wish to express my gratitude to all my past and current colleagues, particularly the members of the Diagnostic and Control Laboratory: Dr. Weitian Chen, Dr. Wen Chen, Mr. Guangqing Jia, Mrs. Esther Liu, Mrs. Jinyun Ren, Mr. Yifeng Huang, Mr. Qingguo Li, Mr. Jimmy Tsai, Mr. Esmaeil Tafazzoli, etc.

Many thanks are given to my friends in SFU: Dr. Wei Luo, Mrs. Huanhuan Wu, Mrs. Vicky Hu, Mr. Jianyuan Liu, Mrs. Lan Jiang, Mr. Guangxing Zuo, Mrs. Cindy Feng, etc.

Furthermore, I am particularly indebted to my father Zhengqi Wu and my mother Yueling Sun for their encouragement, support, and love.

The financial support from the Natural Science and Engineering Research Council (NSERC) of Canada, the Canadian Space Agency (CSA), the School of Engineering Science, and Simon Fraser University is gratefully acknowledged.

Contents

List of Tables

List of Figures

Table of Acronyms

BP:	Back-Propagation
EKF:	Extended Kalman Filter
FD:	Fault Diagnosis
FNO:	Fuzzy-Neural Observer
FNSMO:	Fuzzy-Neural Sliding Mode Observer
HOSMD:	High Order Sliding Mode Observer
IFAC:	International Federation of Automatic Control
ILO:	Iterative Learning Observer
INPID:	Iterative Neuron PID
LMI:	Linear Matrix Inequality
MIMO:	Multiple Input Multiple Output
MSFF:	Multiple Satellite Formation Flying
NSS:	Neural State Space
NAE:	Neural Adaptive Observer
PCA:	Principal Component Analysis
PI:	Proportional-Integral
PID:	Proportional-Integral-Derivative
PLS:	Partial Least Square
PSD:	Proportional-Summation-Derivative
RBF:	Radial Basis Function
RGDA:	Robust Gradient Descent Algorithm

RILA:	Robust Iterative Learning Algorithm
RLO:	Repetitive Learning Observer
SMO:	Sliding Mode Observer
TS:	Takagi-Sugeno

Nomenclatures

A	system state matrix
B	system input matrix
b_i	radius of ball
C	system output matrix
C	damping coefficient in flexible satellite
c_{ij}	translation in wavelet network
$d_{i,j}$	mapping from output to state
E	modulus of elasticity of the appendage
e_y	system output error
F_d	constant disturbance force
f	nonlinear function
f_a	additive fault
G	switching gain matrix of sliding mode
G^*	optimal switching gain of sliding mode
g_i	switching gain vector of sliding mode
h	nonlinear function
$h^\dagger$	nonlinear function
I	sectional area moment of inertia
J	moment of inertia of central hub
J_1	moment of inertia of each appendage
J_M	symmetric momentum of inertia
K	gain of PID-type estimator

$K_{j,i}$	Kalman gain
k	index of iterative or repetitive learning domain
k_ξ	Lipschitz constant
L	Length of appendage
L_i	gain for local linear observer
l	distance from a point to the center of the hub
M	Earth's mass
$\hat{M}$	fault estimator
m	mass of satellite
m_l	mass of leader satellite
m_f	mass of follower satellite
P	symmetric positive definite matrix
p_i	generalized coordinate
$P_{j,i}$	covariance matrix of state estimation error
Q	symmetric positive definite matrix
q_d	relative trajectory
$q_{i,j}$	coefficient vector
$\mathbf{q}$	first three quaternion
q_4	the fourth quaternion
$R_{j,i}$	estimated covariance of measurement noise
r	distance in polar coordinate or radius of the hub
r_i	diagnostic residual
S	equivalent state estimation error vector
$\bar{S}$	equivalent state estimation error matrix
s_i	equivalent state estimation error
T_f	beginning time of fault
T_m	beginning time of estimator
T_d	disturbance torque
t	index of continuous time or discrete time
u	input vector

u^*	control signal for healthy system
u_f	control force of follower satellite
u_i	the ith element of input vector
u_t	control torque
$\hat{V}$	parameter of fault estimator
$\tilde{V}$	parameter estimation error
V^*	optimal parameter
V_M	bound of parameter
V_l	Lyapunov function
V_s	Lyapunov function
$\hat{W}$	parameter of fault estimator
$\tilde{W}$	parameter estimation error
W^*	optimal parameter
W_M	bound of parameter
x	state vector
$\hat{x}$	state vector of observer
$\tilde{x}$	state estimation error
y	system output vector
$\hat{y}$	output vector of observer
$\tilde{y}$	output estimation error
$\dot{y}_D$	derivative of y using HOSMDs
$z_{i,j}^{(k)}$	external input of PID-type estimator
$\mathcal{B}_{i,j}^{(k)}$	coefficient matrix
α	positive constant
β_i	positive constant
Γ_1	symmetric positive definite matrix
Γ_2	symmetric positive definite matrix
Γ_3	symmetric positive definite matrix
γ_i	learning rate
δ_f	fault estimation error

Chapter 1

Introduction

1.1 System Monitoring and Fault Diagnosis

Modern control engineering systems are becoming increasingly complex resulting in more sophisticated control laws. Hence, all the control performance specifications, the reliability, and the operating safety become critical requirements. Traditionally, the system monitoring and timely fault diagnosis capabilities have been of utmost importance in safety-critical systems, such as civil and military aircraft, nuclear power reactors, etc. However, with the development of modern technologies, other factors have been playing a major role in identifying the need for these capabilities in other technical systems. Many contributing factors have caused automatic fault detection, isolation, estimation, and accommodation problem to become an active area in a large variety of industries and systems.

Due to the wide applications of electronics and computer technologies, the sophistication level of many industrial control systems has largely increased. A good example is manufacturing modern automobiles. Many functions, such as anti-lock brakes and combustion control, are now electronically executed and are used on many vehicles. Productivity and economics are basic driving forces for fault diagnosis requirements. A trivial fault may gradually evolve to a complete failure that can result in plant shutdown and, therefore, loss of revenue.

Environmental considerations become an important reason for developing fault

diagnosis strategies. Without any prevention and protection, the consequences caused by faults can be extremely serious to the environment. For instance, nuclear material leaking from a nuclear reactor may lead to unrecoverable pollution to the neighboring earth, air, and water. For the sake of human security, fault diagnosis is essential to provide valuable information for preventing catastrophe.

In summary, fault diagnosis is extremely important, considering the production and economic loss, environmental impact, and safety of humans. Therefore, online system monitoring and fault diagnosis have become an attractive subject in the area of control systems.

1.2 Literature Review for Fault Diagnosis

1.2.1 Basic Concept of Fault Diagnosis

In order to address the contributions of fault diagnosis (FD) in a unified framework, the Technical Committee SAFEPROCESS of the International Federation of Automatic Control (IFAC) defined common terminology in the field of fault diagnosis. In their terminology list, a *fault* is referred to as "*an unpermitted deviation of at least one characteristic property or variable of the system from acceptable/usual/standard behavior.*" This definition specifies a fault as a process abnormality or symptom. Different from a *failure*, which is defined as a "*permanent interruption of a system's ability to perform a required function under specified operating conditions*", the term *fault* is mainly used to indicate a malfunction that can be tolerable at its present stage.

Faults can be classified according to a variety of criteria. Based on their locations, faults can be classified into *actuator faults*, *component faults*, *sensor faults*, and so on. For example, for a mechatronic system, damage in the bearings, deficiencies in force or momentum, or defects in the gears are typical actuator faults. Cracks, ruptures, fracture, leaks, and any loose component of the system are considered component faults. Furthermore, scaling errors, drift, and dead zones in sensors contribute to sensor faults. In some literature, *state faults* and *output faults* have been used to

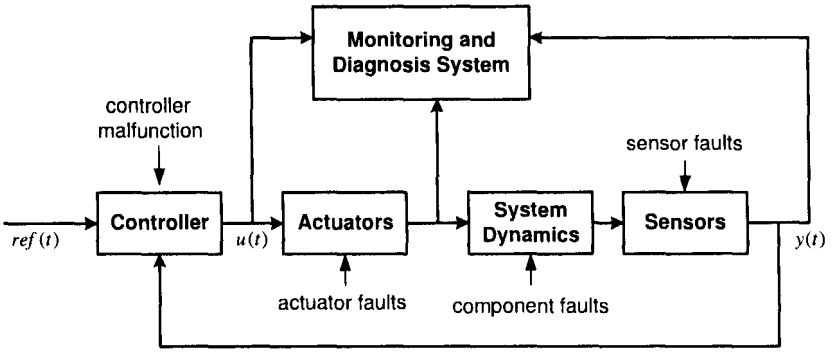

Figure 1.1: Diagram of a closed-loop control system with diagnosis system

mathematically describe the locations of the faults. According to their time-behavior, faults can be divided into *abrupt faults* and *incipient faults*, where the abrupt faults represent sudden changes in system dynamics, and the incipient faults depict small and slowly developing deviations from normal status. According to their relations to other parts of the system, faults can be categorized into *additive faults* and *multiplicative faults*, where the additive faults are described as additional functions which are added in the system's dynamical equations, while the multiplicative faults are represented by the product of a variable with the faults.

To prevent any undesirable consequences, a monitoring system is necessary to detect and isolate faults as quickly as possible. A diagram of fault diagnosis for control systems is shown in Figure 1.1. A fault diagnosis procedure is typically comprised of three tasks: 1) *fault detection* makes a binary-decision whether and when any abnormal event in the monitored system happens, or if everything works well. Fault detection can be achieved from either the direct observation of system inputs and outputs, or the use of certain types of redundant relations. 2) *fault isolation* determines the locations and/or types of the faults. 3) *fault identification* or *fault estimation* specifies the magnitude of the fault. Fault detection, isolation, and estimation are usually referred to as fault diagnosis. After a fault has been diagnosed, in some applications, the systems are required to be fault-tolerant, which is usually achieved via passive or active controller reconfigurations. This procedure is usually referred to as *fault accommodation.*

1.2.2 Fault Diagnosis Methodologies

Manual diagnosis of control systems has been conducted for a very long time. However, automatic diagnosis first appeared after computers became available. In the 1970's, the first research report on fault diagnosis based on analytical redundancy approaches was published at MIT. Since then, the research on fault diagnosis has been intensified in the last three decades, and it gradually became a multidisciplinary subject which integrates control theory, information theory, principles of reliability, statistics, artificial intelligence, etc. Today, the unsolved problems in fault diagnosis attract the attention of more and more researchers and practitioners. Contributions in this area have been summarized in many books [1], [2], [3], [4], [5], [6].

Traditionally, limit checking is a straightforward and easy way for diagnosing faults. For example, when a sensor signal is out of its normal range, an alarm is generated to indicate an abnormal event. Thresholds are usually used to predefine the normal range. When the thresholds are functions of some variables or parameters, the limit checking method can be considered as a model-based diagnosis method.

Another class of traditional fault diagnosis methods is based on *hardware redundancy*, where duplicated sensors, actuators, and components are equipped to measure and/or control a particular variable. In this mechanism, outputs from identical components are compared for consistency. The major problems encountered with hardware redundancy are the cost of the additional equipment and extra space required to accommodate the equipment. Moreover, extra equipment increases the system complexity, which may bring additional diagnostic requirements. Therefore, in the last three decades, fault diagnosis using *analytical redundancy* techniques has received considerable interest from industrial practitioners as well as academic researchers [7].

In spite of the overlap between different diagnostic approaches, one systematic way to classify the analytical redundancy based fault diagnosis methodologies was proposed in [8], [9], and [10], where fault diagnosis schemes are categorized into *quantitative model-based* methods, *qualitative model-based* methods, and *process history-based* methods.

Fault diagnostic strategies are usually functions of knowledge representation schemes,

which, in turn, are largely influenced by the kind of prior knowledge available. The model-based prior knowledge can be generally classified as quantitative and qualitative. In quantitative models, prior knowledge is expressed in terms of mathematical functional relationships between the inputs and outputs of the system. In this thesis, we mainly focus on quantitative model-based fault diagnosis methods. Thus, the characteristics of quantitative model-based fault diagnosis schemes will be summarized in Section 1.2.3.

In contrast to quantitative models, the relationships in qualitative model equations are described in terms of qualitative functions centered around different units in a process. The qualitative models can be established using qualitative causal models or abstraction hierarchies. In the qualitative causal models, digraphs, fault trees, and qualitative physics are the typical qualitative knowledge forms. With respect to abstraction hierarchy, abstraction at different levels is possible along two dimensions: structural and functional. Moreover, the two fundamental search strategies are topographic and symptomatic, where topographic searches conduct malfunction analysis using a template of normal operation, and symptomatic searches look for symptoms to lead the search to the fault location.

In comparison to assuming prior knowledge about the model is available, process history based methods only assume a large amount of historical process data can be obtained. Data can be transformed and expressed as a priori knowledge to the diagnostic system using different feature extraction methods. The feature extraction process can be either quantitative or qualitative. Methods that extract quantitative information can be widely classified into non-statistical or statistical methods. One class of typical and important non-statistical methods is based on neural networks. Principal component analysis (PCA)/partial least square (PLS), and statistical pattern classifiers constitute a primary component of statistical feature extraction methods. In addition, expert systems and trend modeling methods are the two major methods that extract qualitative history information.

A thorough review regarding these three classes of fault diagnosis schemes is found in [8], [9], [10].

1.2.3 Quantitative Model-based Fault Diagnosis Methods

In the last thirty years, quantitative model-based fault diagnosis schemes have been significantly investigated, and many contributions have been summarized in the books [2], [3], [4], [5], [6]. From this literature, *residual generation* and *parameter estimation* are two main systematic methods used in the quantitative model-based fault diagnosis schemes.

In the residual generation based fault diagnosis schemes, a mathematical model of the dynamic system being considered is first constructed; then the residual signals produced from the consistency checking of different variables are evaluated to diagnose faults. Normally, the consistency checking in analytical redundancy compares the available system measurements with their estimation/observation. For different purposes, the generated residual can be quite different. For example, a signal that is zero, or small, in the fault free case, and nonzero when a fault occurs is enough for fault detection. But for fault isolation and estimation, more sophisticated residuals that contain the information of faults have to be developed. The most frequently used residual generation fault diagnosis schemes are observer-based approaches and parity space approaches.

The second class of quantitative model-based fault diagnosis schemes treats faults as deviations in system parameters. Considering a system with a nominal model $\mathcal{M}(\theta_0)$, we use parameter estimation methods to obtain an estimation $\hat{\theta}$ of θ_0. If the deviation of $\hat{\theta}$ from θ_0 is above a threshold, then we can conclude that a fault has occurred. Through comparing $\hat{\theta}$ with θ_0, we can achieve fault diagnosis. However, this method is limited by the following two aspects: 1) the assumption that a fault can be modeled as a deviation of system parameters is so restricted that it is probably unrealistic for many practical faults; 2) as the number of faults increases, the dimension of the parameter θ may become so large that computing the estimation of θ is cumbersome. Therefore, compared with parameter estimation methods, residual generation methods have received more investigation.

For control systems, the quantitative model-based fault diagnosis schemes have

the following advantages: 1) No additional hardware components are needed to implement fault diagnosis algorithms. A model-based fault diagnosis algorithm can be implemented in software on process control and monitoring computers. Moreover, in many situations, the available measurements for controller design are sufficient for developing fault diagnosis algorithms, therefore no extra sensors are required. Under these circumstances, only powerful computers with more storage capacity and computing ability are needed to implement fault diagnosis schemes. 2) The fault diagnosis results using quantitative models can help establish a fault accommodation algorithm using controller reconfiguration approaches. In many applications, the fault diagnosis algorithms are designed based on the same linear or nonlinear models as those for the controllers design. The location and magnitude of the faults can be directly or indirectly used to design fault-tolerant controllers. Therefore, quantitative model-based fault diagnosis algorithms and fault accommodation algorithms can be designed and implemented in a unified framework. 3) Quantitative model-based fault diagnosis schemes can be implemented online, providing real-time monitoring and diagnosis.

In spite of these advantages, some challenging issues in the quantitative model-based fault diagnosis schemes are still under further investigation, in order to solve the following problems: 1) Robust fault diagnosis for nonlinear uncertain systems is needed. Due to the universal existence of nonlinearities and uncertainties in practical situations, an effective model-based fault diagnosis scheme should be robust, i.e., it should be insensitive or even invariant to modeling uncertainties, without losing sensitivity to faults. 2) Accurate fault estimation in the presence of uncertainties is needed. The accuracy of fault estimation should be guaranteed even when the system has suffered from modeling uncertainties and disturbances. 3) Online implementation of fault diagnosis algorithms is needed. Now most fault diagnosis schemes are required to detect, isolate, and estimate various faults in a real-time environment, so that the engineers have more time to react before faults turn into failures. Therefore, fault diagnosis algorithms should not be too complicated to be realized. 4) The consistency between theoretical properties and practical applications is needed. Analytical properties such as robustness, sensitivity, and stability should be guaranteed

rigorously in theory as well as in practice. In conclusion, many issues of the quantitative model-based fault diagnosis schemes in nonlinear uncertain systems need further investigation.

1.3 Thesis Motivation

With the development of space technologies, a variety of space vehicles, such as launchers, satellites, and space shuttles, have been constructed and utilized in various space missions, such as global positioning, Earth observation, atmosphere data collection, space science, and communication. The dynamics of this class of systems have the following characteristics: 1) The safety and reliability of the space vehicles are so crucial that fault diagnosis schemes are indispensable. 2) Various linear and nonlinear mathematical models of the space vehicles are already available for the design of controllers and/or state observers. The attitude dynamics of the space vehicles can be represented by linear systems when small attitude is deviated from local vertical local horizontal orientation. However, the attitude dynamics of the space vehicles are inherently nonlinear, especially when the space vehicles make a large angle maneuver or have flexible appendages; therefore, different nonlinear models must be used to describe their dynamics. Moreover, one key space technology is to distribute functionality of a large space vehicle to a group of smaller, low-cost, cooperative space vehicles. Flying two or more satellites in a specific formation is usually referred to as a multiple satellite formation flying (MSFF) system. The relative distances and orientations between the satellites are controlled for formation reconfiguration and collision avoidance [11], [12]. The dynamics of the MSFF systems can also be described by nonlinear mathematical equations. 3) The vehicles in space are subject to internal modeling uncertainties and external disturbances and noises. For example, gravity-gradient torque, aerodynamics torque, and Earth magnetic torque constitute the primary environmental disturbances for space vehicles in low Earth orbit (LEO), within 1000km. 4) In order to guarantee the normal operation of space vehicles, online fault diagnosis is essential to provide real-time information for the space vehicles to accommodate the faults as soon as possible. Therefore, fault diagnosis for satellite

control systems have attracted significant attentions, and quite a few research results have been published, e.g., [13], [14], [15], [16], [17], [18], [19], [20], [21].

Several classes of satellite control systems investigated in this thesis are summarized in Figure 1.2. These systems not only include the typical satellite attitude and orbital control systems, but they also have the dynamical systems of flexible satellites, and multiple satellites. In order to realize health monitoring for these various satellite control systems, the designed fault diagnosis schemes need to at least satisfy the following requirements:

- both linear and nonlinear models of different satellite control systems should be able to be used in the design of fault diagnosis schemes;
- the fault diagnosis schemes should be able to deal with nonlinear systems where not all states are measurable;
- the fault diagnosis schemes should be effective in the presence of uncertainties;
- the fault diagnosis schemes should be implementable in real-time environment; and
- the fault diagnosis schemes should be able to theoretically and practically guarantee the robustness, sensitivity, and stability.

Due to the dual relationship between the state feedback control and the full order observer design, the main design procedure in model-based fault diagnosis becomes an equivalent state feedback control problem. Hence, in recent years, robust fault diagnosis schemes for nonlinear systems using adaptive techniques, artificial intelligence methodologies, and sliding mode approaches have been considerably developed.

The fault diagnosis schemes using a variety of adaptive approaches have been studied by a number of researchers in the last ten years, e.g., [22], [23], [24], [25], [26]. In this class of fault diagnosis schemes, the parameters of the proposed observer are adaptively updated using the output estimation error. After the estimation error dynamics are stabilized, the estimators that contain these parameters are used to characterize the faults. Wang and Daley only considered linear systems without uncertainties and

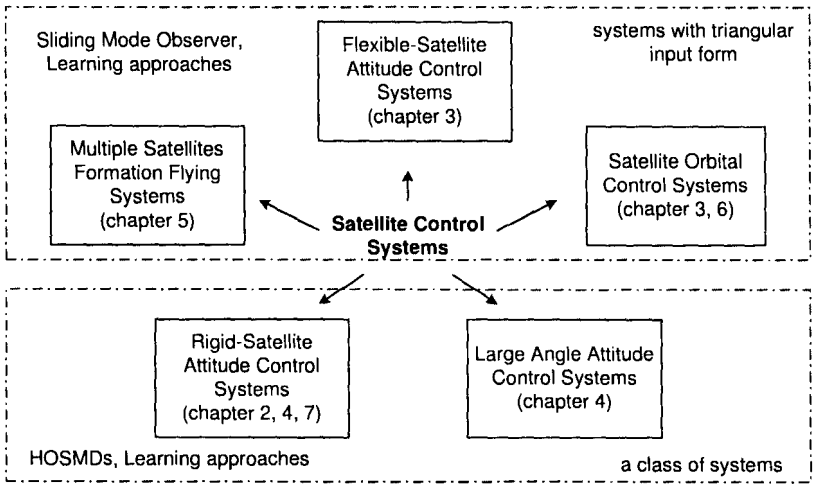

Figure 1.2: Summary of several classes of satellite control systems in this thesis

disturbances [22], [23]. Jiang et al. and Xu and Zhang used robust adaptive techniques to estimate not only constant faults, but also time-varying faults in the presence of uncertainties [24], [25]. Since 1994, Polycarpou et al. have explored the robust fault diagnosis schemes in a class of nonlinear systems using learning methodologies, such as neural networks, [27], [28], [29], [30], [31], [32], and [33]. Due to the powerful abilities of neural networks in function approximation and pattern recognition, neural networks-based fault diagnosis schemes have been extensively studied, where neural networks are usually developed as predictors of the nonlinear models and/or a fault classifier; e.g., [34], [35], [36]. However, the mathematical models that can fully or partially characterize the system dynamics are not explicitly utilized.

As a result, neural networks based observers have been designed and used for fault diagnosis in nonlinear systems; e.g., [37], [38], [39], [40], [41], [42], [43], [44], [45], [46], [47], [48]. In their work, neural networks are integrated with the observer design methods, where the neural networks are only employed to approximate the possible faults. In [31], robustness is achieved by using a dead-zone operator, where the parameter update algorithm is insensitive to the estimation error less than a threshold, which is deemed to be caused by modeling uncertainties. Moreover, a bank of neural networks

based online approximators are adopted to estimate the magnitude of the faults. Although this is a unified framework of the robust fault diagnosis schemes using learning methodologies, the selection of a proper approximator is still based on trial-and-error methods. For a specific problem with specific requirement, an *ad hoc* online estimator will works better than a general one. For example, the transient process and steady-state error of fault estimation are expected to be reduced and even eliminated. Moreover, projection operators are used in the parameter update algorithms in order to avoid parameter drift caused by modeling uncertainties, approximation errors, or noise. However, the procedure of designing this projection operator is not straightforward. Additionally, the use of a dead-zone operator, which achieves a robust fault detection, however, reduces the accuracy of the fault estimation.

In recent years, another family of learning approaches, named *iterative learning observers* (ILO), have been proposed and used in the fault diagnosis for some kinds of systems [49], [50], [51], [52], [53]. The ILO was inspired by iterative learning control algorithms [54], [55], where the observer input is always updated by previous information. The advantage of iterative learning observers is they can be easily implemented, because the structure of an ILO is simple. Additionally, the stability of the ILO-based fault diagnosis schemes can be guaranteed by selecting suitable coefficients that satisfy Lyapunov functions. For an arbitrary time-varying fault, iterative learning algorithms achieve better approximation performance than adaptive algorithms which perform well only for constant or periodic fault signals [49], [51], [52], [53]. However, so far, Proportional-type iterative learning observers are mainly used, where only the output estimation error at the current iteration is iteratively updated in the form of a linear discrete-time filter. Due to the availability of various iterative learning control strategies, other types of iterative learning observers can be developed to reduce the required iteration number and to avoid unnecessary overshoot and transient process in the fault estimation.

Furthermore, due to the inherent robustness of sliding mode to modeling uncertainties, the fault diagnosis schemes using sliding mode observers have been investigated by many researchers for several years; for example, [56], [57], [58], [59], [60], [61], [62], [63], [64], [65], [66], [67], [68], [69], [70], [71], [72]. sliding mode observers can be applied

to the robust fault diagnosis schemes in at least two ways: 1) The fault is treated in the same way as other unknown inputs such as system uncertainties, and both the fault and the system uncertainties are counteracted by the sliding mode. Consequently, the sliding motion is still maintained even after a fault occurs. Through a series of matrix transformations, a fault estimation or reconstruction signal can be explicitly established using an equivalent output estimation error injection method. 2) In the second class of robust FD schemes using sliding mode observers, the fault is treated in a different way from the system uncertainties. Prior to the occurrence of any fault, the sliding mode works only to eliminate the effect of the system uncertainties. After a fault occurs, the sliding motion is supposed to be destroyed, and other learning or adaptive techniques are adopted to estimate the fault. So far, the second method has not been explicitly developed, and the key point is properly selecting an appropriate switching gain of the sliding mode in order to successfully distinguish the modeling uncertainties from the faults. If the gain is too large, observer will exhibit excessive chattering before reaching sliding mode, and even the faults may be counteracted by the sliding mode. If the gain is too small, the observer may never be able to reach a sliding mode and converge to a real state value.

In recent years, various high order sliding mode observers and/or differentiators have been designed for state observation [73], [74], [75], [76], [77], [78], [79], [80], [81], [82], and fault diagnosis in nonlinear systems; for example, super-twisting algorithms [83], [50], [84], [85], [86], [87]. Compared with first order (classic) sliding mode observers, high order sliding mode observers not only hold their robustness to system uncertainties, but they also reduce or remove chattering effects and can provide a smooth or at least piece-wise smooth observation within a finite time. Moreover, a high order sliding mode demonstrates its unique strength in state observation of a class of nonlinear systems with a relative degree of more than one. However, high order sliding mode observers/differentiators based fault diagnosis schemes have just attracted many researchers' attentions in the last few years.

Moreover, wavelet networks, at least, have the same *universal approximation* property as neural networks [88], [89]. This property can theoretically guarantee the fault estimation accuracy if the wavelet network is chosen as an alternative of the neural

networks based fault estimator. Moreover, the wavelet networks coefficients have an explicit link with some appropriate transform. This link will help provide good initial values for some learning algorithms. Additionally, a reduced-size wavelet network achieves the same approximation quality as neural networks. This feature simplifies the structure of the fault estimators, making the fault diagnosis schemes easier to implement.

Fuzzy logic, in the last several years, has been extensively used in system modeling, control, and pattern recognition [90], [91], [92], [93], [94], [95], [96], [97], [98]. The most significant applications of fuzzy models to fault diagnosis are using their classification and reasoning abilities [99], [100]. Correspondingly, the designed fuzzy model based fault diagnosis schemes are mainly qualitative model based or process history based. Moreover, research has shown that fuzzy models have the same approximation ability as neural networks under certain conditions. Therefore, fuzzy models can replace the neural networks in the fault diagnosis schemes using learning approaches. In addition, at least two approaches are used to construct fuzzy models: 1) identification using input-output data; and 2) derivation from given mathematical equations for nonlinear systems. Consequently, linear model based fault diagnosis schemes can be extended to more general nonlinear systems through fuzzy models. In fact, fuzzy-model-based fault diagnosis schemes have only been partly developed [101], [102], [103], and [104].

In summary, according to the above analysis, the existing fault diagnosis schemes for nonlinear systems can still be improved. Hence, in this thesis, our research focuses on the design and analysis of fault detection, isolation, and estimation strategies using learning and sliding mode methodologies, as well as their applications to a variety of satellite control systems. A diagram illustrating the hierarchy of analytical redundancy based fault diagnosis schemes is shown in Figure 1.3.

Through my research, the following objectives were achieved:

- extend several existing fault diagnosis methods to more general nonlinear dynamic systems;
- develop a framework of robust fault diagnosis schemes using sliding mode and learning approaches;

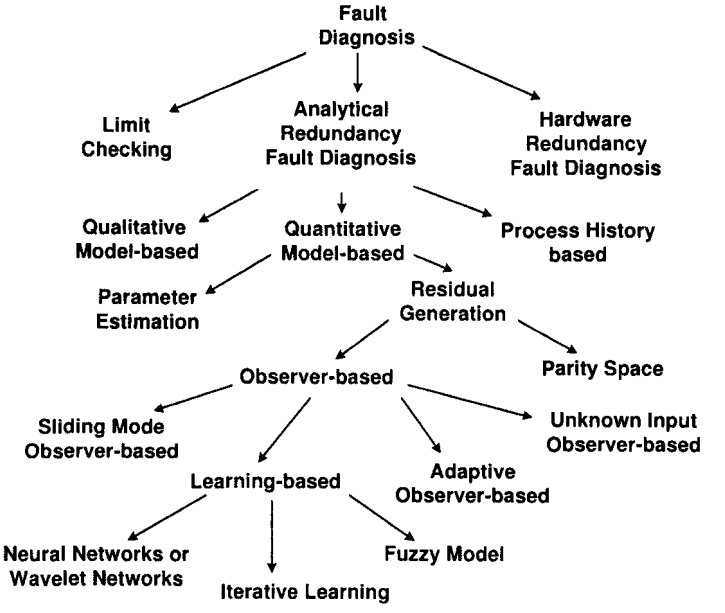

Figure 1.3: Hierarchical structure of the fault diagnosis schemes in this thesis

- establish more learning strategies for robust fault isolation and estimation;
- relax some restrictive assumptions on the fault diagnosis schemes based on learning approaches; and
- apply the proposed fault diagnosis schemes to a variety of satellite control systems.

1.4 Thesis Contributions and Outline

The contributions of this thesis are summarized as follows.

- **Actuator fault detection, isolation, and estimation using a bank of repetitive learning observers**

  In Chapter 2, inspired by previous proportional-type ILO, a novel fault diagnosis scheme using Proportional-Integral (PI) type repetitive learning observer (RLO) is developed for a class of discrete-time nonlinear systems based on a generalized

observer structure. In this fault diagnosis scheme, in order to isolate one fault among N possible faults, N observers are designed to generate N residuals, and the ith residual is sensitive to all faults except the ith one. Consequently, fault detection and isolation become straightforward by observing and comparing the residuals generated by each observer. After detecting and locating the fault, the parameter of the corresponding PI type repetitive learning observer is updated to estimate the magnitude of the fault. In order to demonstrate its performance, this fault detection, isolation, and estimation scheme will be applied to the nonlinear dynamics of a satellite attitude control system.

- **Robust fault detection, isolation, and estimation using sliding mode and learning strategies**

  Chapter 3 explores a novel framework for fault diagnosis schemes using sliding mode and learning approaches. The proposed fault diagnosis schemes are particularly designed for a class of nonlinear systems with a triangular input form. The designed fault diagnostic observer has three features: 1) The variable switching gain is updated by using an iterative learning algorithm and an iterative fuzzy model, respectively, which guarantees the sliding motion as well as reducing the gain value. With a time-varying switch gain, the sliding mode is only expected to eliminate the effect of the modeling uncertainties on system dynamics. 2) After any fault occurs, the sliding motion is destroyed due to the variable sliding mode gain. Correspondingly, a bank of online learning estimators are activated to isolate and estimate the fault. 3) This fault diagnostic observer is suitable for cases of a single fault as well as for cases of multiple faults.

  After setting up the architecture of the robust fault diagnostic observer, we focus on the development of the online fault estimators in this class of fault diagnosis schemes. First, a neural state space (NSS) model based fault estimator is built, which has a nonlinear state space structure. Then, an iterative learning based fault estimator is designed. These two kinds of fault estimators are designed and analyzed in Chapter 3 in detail, but here is a brief introduction:

- *Neural state space model-based estimator*

  A neural state space model is a special type of recurrent neural network [105], [106], [107], [108]. When NSS models are used as a fault estimator, it demonstrates the following features: 1) The NSS models have the same approximation ability as neural networks. Hence, under some assumptions, the characteristics of faults can be accurately specified. 2) The NSS models have a similar structure as linear state space models, consequently, the theoretical properties of the fault diagnosis schemes using NSS models can be rigorously analyzed by extending some properties of linear state space systems. In Chapter 3, a fault diagnosis scheme using an estimator based on sliding modes and NSS models is applied to a satellite orbital control system.

- *PID-type iterative learning estimator*

  Although neural networks based estimators can approximate the fault with satisfactory accuracy under certain conditions, inevitably, overshoot and transient process in the fault estimation occur because the estimators need time to update their parameters to approximate the abrupt changes caused by faults. Accordingly, we build an iterative learning estimator, which has the following characteristics: 1) The tracking trajectory becomes time-varying, but iteration-invariant. 2) The architecture of the iterative learning estimator is simple and deterministic, and only the proportional, integral, and derivative information of the output estimation error is used. 3) The parameters of the estimator are updated in the iteration domain rather than in the time domain. This strategy not only guarantees the convergence of the update process when the tracking trajectory is time-varying and iteration-invariant, but it also reduces or even eliminates the transient process and overshoot in the fault estimation. This fault diagnosis scheme using sliding mode and PID-type iterative learning estimator is applied to a flexible satellite control system.

- **Robust fault detection, isolation, and estimation using high order**

sliding mode differentiators and learning approaches

In Chapter 4, the fault diagnosis problem in a class of nonlinear systems are studied, where the unmeasurable state is a nonlinear function of the system output and its derivatives. For this class of particular nonlinear systems, high order sliding mode differentiators (HOSMDs) are first used to obtain the derivatives of the system output. Then the unmeasurable system state is estimated according to the system dynamics and the system output and its derivatives which have been obtained via HOSMDs. Thereafter, a fault diagnostic observer is constructed, where the online estimators are again used to isolate and estimate possible faults. Two types of fault estimators are discussed in detail in Chapter 4, and here are some characteristics of these two fault estimators.

– *Neural adaptive estimator*

The neural adaptive estimator (NAE) is inspired by discrete-time proportional type iterative learning observers and artificial neural networks. The neural adaptive estimator has the following advantages: 1) Its structure is simpler than general feed-forward or recurrent multiple-layer neural networks, and only the numbers of previous estimator inputs and outputs need to be determined. As a result, if appropriate parameter update laws are chosen, the algorithm is more easily implemented and can satisfy more strict real-time computational requirements. 2) Theoretical properties of the NAE-based fault diagnosis scheme are more easily analyzed than general neural networks-based fault diagnosis schemes. The fault diagnosis scheme using HOSMDs and neural adaptive estimator is applied to a typical satellite attitude control system.

– *Iterative neuron PID estimator*

The PID-type iterative learning estimator mentioned in Chapter 3 is actually a linear combination of previous information of the state estimation error and its differences. In order to accelerate the convergence rate, the hyperbolic tangent activation function is used to formulate an iterative

neuron PID estimator. Still, only the proportional, integral, and derivative information of the state estimation error are used to build the fault estimator. Not only does the deterministic observer structure simplify the procedure of selecting a suitable architecture of the fault estimator, but the nonlinear relationship between the input and output of the estimator also speeds the approximation process. Moreover, in order to increase the fault estimation accuracy, four robust adaptive algorithms are adopted to iteratively update the parameters of this fault estimator. This strategy can also reduce the transient time and overshoot in the fault estimation because the parameters are updated in the iteration domain rather than in the time domain. To illustrate the performance of this fault diagnosis scheme, it is applied to a satellite attitude control system with large angle maneuver.

- **Robust fault detection, isolation, and estimation using a second-order sliding mode and wavelet networks**

  In Chapter 5, we apply a second order sliding mode and wavelet networks to the fault diagnostic observer design for the class of systems which is discussed in Chapter 3. The second order sliding mode is only used to estimate the system state in the presence of modeling uncertainties. The sliding motion is destroyed by the onset of faults, and then a bank of wavelet networks are activated to specify the faults. Although the basic idea of the fault diagnosis scheme in this chapter is the same as that in Chapter 3, the distinguished features of the second order sliding mode and wavelet networks provide flexibility in the design of fault diagnosis schemes. The proposed fault diagnosis scheme is applied to a multiple satellites formation flying system.

- **Fault detection, isolation, and estimation using fuzzy models, neural networks, and sliding modes**

  In Chapter 6, the fault detection, isolation, and estimation schemes using sliding modes and learning approaches is extended to a class of nonlinear systems,

which can be represented by Takagi-Sugeno (TS) fuzzy models. A TS fuzzy observer is first developed to estimate the system state, and then neural networks are integrated to form a fuzzy-neural observer, where the neural networks are supposed to estimate the faults. A modified back-propagation algorithm is used to update the parameters of the neural networks, where only the output information is used. In order to increase the robustness of this fault diagnosis scheme and to reduce the approximation error caused by the system uncertainties and estimator itself, sliding modes are utilized to construct a fuzzy-neural sliding mode diagnostic observer. The neural networks is still used to isolate and estimate possible faults. Finally, the proposed fault diagnosis scheme is applied to a reduced-order satellite orbital control system.

- **Fault diagnosis using high order sliding mode differentiators and uncertainty observers**

  Chapter 7 proposes a novel robust fault diagnosis scheme for the class of nonlinear systems discussed in Chapter 4, This fault diagnosis scheme is different from previous ones. The system modeling uncertainty is estimated by using learning approaches, rather than passively being counteracted by a sliding mode. As a result, the residual is designed in such a way that it only has relationships with the uncertainty estimation error and faults. If an accurate estimation of the uncertainty is realized, the fault signature on the residual becomes more evident, and fault detection and isolation is achieved more easily. In the design of the uncertainty observers, we still need to use the information of the unmeasurable state, which, again, is estimated via the high order sliding mode differentiators. This proposed robust fault diagnosis scheme is applied to a typical satellite attitude control system.

To summarize the approaches used in this thesis, a diagram showing the relationship between the different approaches in this thesis is described by Figure 1.4. The bi-directional arrows in this diagram indicate the two approaches at the end of each side are used together in this thesis.

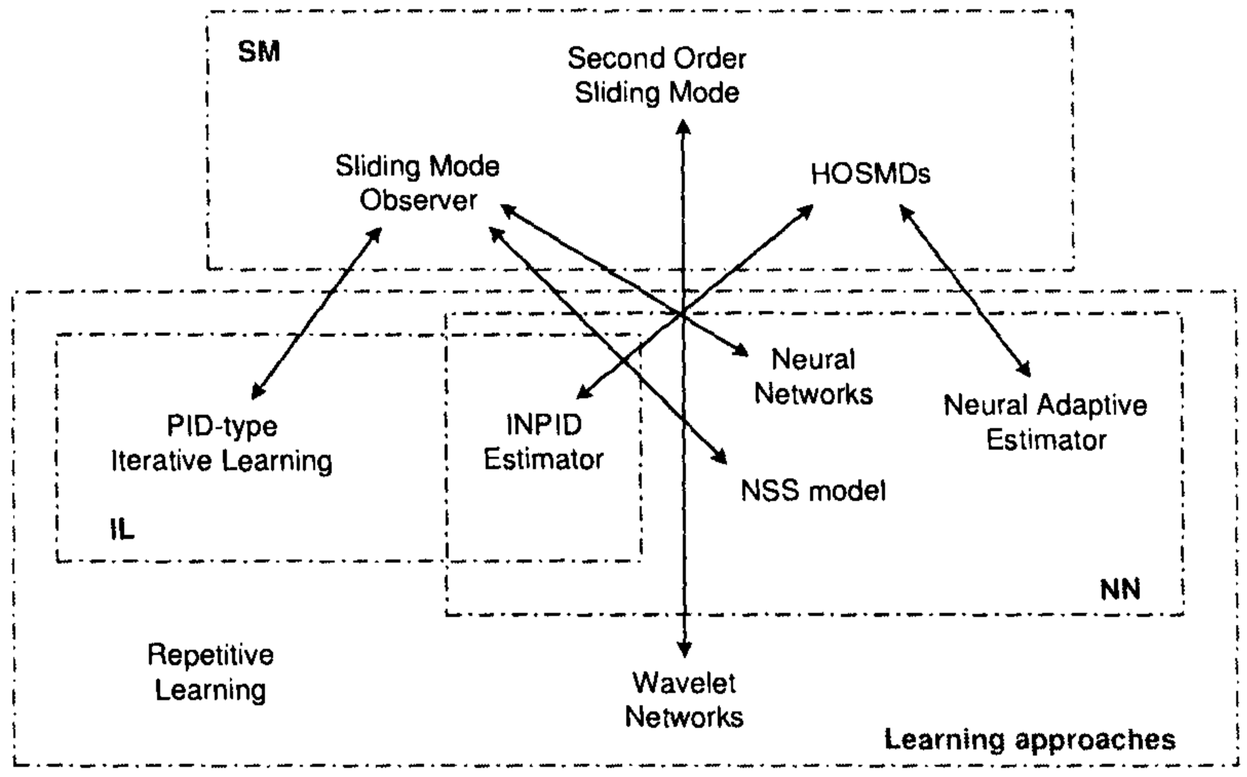

Figure 1.4: Relationship between the approaches in this thesis

Chapter 2

Actuator Fault Diagnosis in Nonlinear Systems Using Repetitive Learning Observers (RLOs)

In this chapter, the fault diagnosis problem for a class of discrete-time nonlinear systems are investigated using a bank of Proportional-Integral (PI) type repetitive learning observers (RLOs). The proposed fault diagnosis scheme is applied to a satellite attitude control system.

2.1 Introduction

Due to the universal existence of nonlinearities in practical systems, fault detection, isolation, and estimation in nonlinear systems has received considerable attention in the last few years. On one hand, many researchers considered extending fault diagnosis approaches for linear systems to the cases of nonlinear systems. On the other hand, various nonlinear system modeling and control strategies are used to design fault diagnosis schemes.

In the nonlinear fault diagnosis schemes, an important class of approaches was originally proposed in [27] and further developed in [28], [29], [30], [31], [32], and [33]. The characteristics of this class of FD schemes are to approximate the nonlinear fault functions by using online learning estimators. So far, the online fault estimators include adaptive observers [22], [23] [25], neural networks [34], [35], [36], and neural networks based observers [46], [47], [48]. One common feature of these online approximators is their parameters are updated in the time domain.

In recent years, another class of online estimators, named iterative learning observers (ILOs), was proposed and applied to the nonlinear fault diagnosis problems; e.g., [49], [50], [51], [52], [53]. This class of iterative learning observers, in fact, inherits the idea of iterative learning control ([54], [55]), but it is different in the design and implementation. The iterative learning control methods require the system to execute the whole process multiple times, whereas the ILOs update the parameters to approximate unknown input functions recursively. In the ILOs-based fault diagnosis schemes, the time-varying tracking trajectory becomes constant at each measurable time, which increases the estimation accuracy if the iteration number is sufficiently large. Moreover, the ILOs are easily implemented because only one or two coefficients need to be designed and the updating process is repeatable in the iteration domain. However, in those previous work on ILOs, only the observer input is iteratively updated in a proportional way for continuous time systems.

In addition, two observer design schemes have been used to design fault diagnosis strategies. The first scheme is called *dedicated observer scheme* [1]. In this scheme, to isolate one fault among N possible faults, N observers are designed to generate N residuals, and the ith residual is expected to be only sensitive to the ith fault, but insensitive to others. The other scheme is called *generalized observer scheme* [7], where N observers are also designed to produce N residuals. However, the difference is that the ith residual is sensitive to all possible faults, except the ith one. For these two schemes, once the residuals are generated, the decision making for fault isolation becomes straightforward. In this chapter, we adopt the second observer scheme to design a fault diagnosis approach because, when using the generalized observer scheme, we only need to consider how to make the ith residual insensitive

to the ith fault, and other residuals are naturally sensitive to the faults due to the nonlinearity and coupling of the dynamic systems.

Satellites play an ever increasing important role in various space missions, such as global positioning, Earth observation, space science, and communication. In order to achieve high-accuracy performance on pointing requirements, three-axis attitude control systems are usually installed on the satellites. As a result, a variety of controller design methods have been developed for the multi-input-multi-output (MIMO) attitude control systems by many researchers and engineers. Nevertheless, the research regarding fault diagnosis for those kinds of systems is not thorough as for controller design. This fact motivates us to develop more model-based fault diagnosis schemes and apply them to the satellite attitude control systems.

This chapter is arranged as follows. In Section 2.2, the system of interest is first described and some necessary assumptions are introduced. Then, in Section 2.3, Section 2.4, and Section 2.5, a bank of PI-type repetitive learning diagnostic observers are designed, and their corresponding fault detection, isolation, and estimation strategies are proposed and analyzed theoretically. Section 2.6 provides a simulation example where the proposed fault diagnosis scheme is applied to a satellite control system. Finally, Section 2.7 gives conclusions.

2.2 Problem Formulation

The class of discrete-time nonlinear dynamic systems in this chapter is described by the following difference equation:

$$\begin{aligned} x(t+1) &= f(x(t),t) + Bu(t) \\ y(t) &= Cx(t) \end{aligned} \tag{2.1}$$

where $x = [x_1, \cdots, x_n]^\top \in \Re^n$ is the state vector, $u = [u_1, \cdots, u_m]^\top \in \Re^m$ is the control input vector, and $y = [y_1, \cdots, y_p]^\top \in \Re^p$ is the output vector of the system, respectively. The term $B = [b_1, \cdots, b_m]$ is called the actuator distribution matrix, where b_i is the ith column vector. The symbol t denotes the index of discrete time domain in this chapter, but it represents continuous time in the later chapters.

When an actuator fault occurs, the corresponding system can be described by a faulty model of (2.1). Since the system has a total of m actuators, m possible faulty models are available. For example, if the lth actuator is faulty, the corresponding faulty model is presented by

$$\begin{aligned} x(t+1) &= f(x(t),t) + \sum_{j=1}^{m} b_j u_j(t) + b_l u_l^f(t) \\ y(t) &= Cx(t) \end{aligned} \tag{2.2}$$

where $u_l^f(t)$ is an additive faulty signal in the lth actuator.

Throughout this chapter, the following assumptions are introduced in the design and analysis of the RLOs-based fault detection, isolation, and estimation scheme.

Assumption 2.1 Only a finite constant actuator fault is supposed to occur at one time; that is, $u_j^f(t) \equiv \theta_j$ for $t \geq t_f$ and $\lim_{t\to\infty} |u_j(t) - \theta_j| \neq 0$, $j \in 1, 2, \cdots, m$, where θ_j is a finite constant, t_f is the time when the fault becomes constant, $u_j(t)$ is the healthy actuator output, and u_j^f is the finite constant fault signal in the jth actuator. Constant bias or offset in an actuator can be described by this kind of fault.

Assumption 2.2 The nonlinear system function $f(x,t)$ is Lipschitz at output y with a positive constant k_f; i.e.,

$$\|f(y, x_2, t) - f(\hat{y}, \hat{x}_2, t)\| \leq k_f \|y - \hat{y}\| \tag{2.3}$$

where x can be divided into two components, $x_1 = y$ and x_2.

Assumption 2.3 The nonlinear function $f(x,t)$ can be decomposed into a linear matrix component and a nonlinear function part; i.e.,

$$f(x,t) = Ax + \xi(x,t), \tag{2.4}$$

and the nonlinear function part is Lipschitz with another constant k_ξ; i.e.,

$$\|\xi(x,t) - \xi(\hat{x},t)\| < k_\xi \|x - \hat{x}\|. \tag{2.5}$$

Assumption 2.4 A symmetric positive definite matrix P exists which satisfies the following Lyapunov function:

$$A^{\top}PA - P = -Q \tag{2.6}$$

where Q is also a symmetric positive definite matrix.

Remark 2.1 *In this chapter, we study a class of discrete-time nonlinear systems that is of the form (2.1), or a class of continuous-time nonlinear systems that can be discretized into (2.1). The studied systems satisfy Assumption 2.1, 2.2, 2.3, and 2.4. These assumptions are used in the design and analysis of the proposed RLOs-based actuator fault detection, isolation, and estimation scheme.*

2.3 Design of Repetitive Learning Observers

Based on the faulty model (2.2) and Assumption 2.1, a specific faulty model of system (2.1) becomes

$$\begin{aligned} x(t+1) &= f(x(t),t) + \sum_{j=1}^{m} b_j u_j(t) + b_l\theta_l \\ y(t) &= Cx(t). \end{aligned} \tag{2.7}$$

Based on (2.7), we design m repetitive learning observers for all m faulty models as

$$\begin{aligned} \hat{x}_i(t,k+1) &= f(\hat{x}_i(t,k)) + \sum_{j=1}^{m} b_j u_j(t) + b_i\hat{\theta}_i(t,k) \\ \hat{y}_i(t,k) &= C\hat{x}_i(t,k), \qquad\qquad i = 1,\cdots,m \\ \hat{\theta}_i(t,k) &= \hat{\theta}_i(t,k-1) + q_{i,1}d_{i,1}\tilde{y}_i(t,k) + q_{i,2}d_{i,2}(\delta\tilde{y}_i(t,k)) \end{aligned} \tag{2.8}$$

where $\tilde{y}_i(t,k) = y(t+1) - \hat{y}_i(t,k) = C(x(t+1) - \hat{x}_i(t,k))$ is the ith output estimation error at sampling time t and at the kth repetition, $\delta\tilde{y}_i(t,k) = \tilde{y}_i(t,k) - \tilde{y}_i(t,k-1)$, k is the index of the repetitive learning domain, $d_{i,j} \in \Re^{n\times p}(j = 1,2)$ is a mapping from the output to the state, and $q_{i,j} \in \Re^{1\times n}(j = 1,2)$ is the coefficient vector, which determines the convergence rate of the repetitive learning algorithm.

The repetitive learning algorithm is implemented in the following way. At each sampling time t, $\hat{y}_i(t,0)$ is set to be $y(t+1)$; i.e., $\tilde{y}_i(t,0) = 0$ at the initialization phase. Then, all the m observers repetitively update their parameters $\hat{\theta}_i(t,k)$ using a PI-type algorithm in the repetitive learning domain. When k reaches the maximum repetition number k_m, or $\|\tilde{y}_i(t,k)\|$ is less than a tolerance error $\epsilon_{\tilde{y}}$, the repetitive learning process at time t ceases.

The initial value of $\hat{x}_i(t,0)$ is obtained by using the mapping operator $d_{i,j}$ from $\hat{y}_i(t,0)$ to $\hat{x}_i(t,0)$. Since not all state variables are available, $\hat{x}_i(t,0)$ is not always equal to $x(t+1)$; that is, $\tilde{x}_i(t,0)$ is not always zero. However, $\tilde{x}_i(t,0)$ becomes small if $\hat{x}(t,0)$ is well obtained by using the mapping operator. Moreover, this initialization is implemented at each sampling time t. Therefore, the estimation error will not accumulate as the discrete time t increases.

In order to investigate the properties of the proposed RLOs, we obtain the dynamics of the estimation error in the repetitive learning domain by subtracting (2.8) from (2.7); i.e.,

$$\begin{aligned} \tilde{x}_i(t,k+1) &= f(x(t)) - f(\hat{x}_i(t,k)) + b_l\theta_l - b_i\hat{\theta}_i(t,k) \\ \tilde{y}_i(t,k) &= C\tilde{x}_i(t,k) \end{aligned} \tag{2.9}$$

where $\tilde{x}_i(t,k)$ is the ith state estimation error at the kth repetition and at time t.

2.4 RLOs-based Actuator Fault Detection and Isolation

Fault detection is the primary task in a fault diagnosis scheme. In order to detect and locate an actuator fault, we design a bank of residuals $r_i(t) = \|\tilde{y}_i(t,k)\|, i = 1,\ldots,m$. If only one residual approaches zero while the others are nonzero (e.g., $r_l(t) \to 0$, and $r_i(t) \neq 0, (i \neq l)$), then the lth actuator is considered to be faulty. Regarding this fault detection and isolation scheme for (2.7), we have the following theorem.

Theorem 2.1 *When the lth actuator is faulty, the lth observer output $\hat{y}_l(t,k)$ converges to the system output $y(t+1)$ as the repetition number k approaches infinity;*

that is,

$$\|\tilde{y}_l(t,k)\| \to 0 \quad as \quad k \to \infty \tag{2.10}$$

provided the following inequality is satisfied,

$$\left\| \begin{bmatrix} \hat{e}_1 & \hat{e}_2 \\ \hat{e}_1 & \rho_1 \end{bmatrix} \right\|_{\inf} < 1 \tag{2.11}$$

where $\|\cdot\|_{\inf}$ *is the infinity norm of a matrix. The variables* $\hat{e}_1$, $\hat{e}_2$, *and* ρ_1 *are defined in the following proof.*

Proof: The lth pair of estimation error dynamics in the repetitive learning domain is described as

$$\begin{aligned} \tilde{x}_l(t,k+1) &= f(x(t)) - f(\hat{x}_l(t,k)) + b_l(\theta_l - \hat{\theta}_l(t,k)) \\ \tilde{y}_l(t,k) &= C\tilde{x}_l(t,k). \end{aligned} \tag{2.12}$$

From (2.8) and (2.12), we can obtain that

$$\begin{aligned} \tilde{y}_l(t,k+1) - \tilde{y}_l(t,k) &= -C(f(\hat{x}_l(t,k)) - f(\hat{x}_l(t,k-1))) \\ &\quad -Cb_l(\hat{\theta}_l(t,k) - \hat{\theta}_l(t,k-1)) \\ &= -C(f(\hat{x}_l(t,k)) - f(\hat{x}_l(t,k-1))) \\ &\quad -Cb_l(q_{l,1}d_{l,1}\tilde{y}_l(t,k) + q_{l,2}d_{l,2}\delta\tilde{y}_l(t,k)). \end{aligned} \tag{2.13}$$

Thus, we have

$$\begin{aligned} \|\delta\tilde{y}_l(t,k+1)\| &\leq \|C\|(k_f + \|b_l q_{l,2} d_{l,2}\|)\|\delta\tilde{y}_l(t,k)\| \\ &\quad + \|Cb_l q_{l,1} d_{l,1}\|\|\tilde{y}_i(t,k)\|. \end{aligned} \tag{2.14}$$

Based on (2.13), we have

$$\begin{aligned} \tilde{y}_l(t,k+1) &= (I - Cb_l q_{l,1} d_{l,1})\tilde{y}_l(t,k) \\ &\quad -C(f(\hat{x}_l(t,k)) - f(\hat{x}_l(t,k-1))) \\ &\quad -Cb_l q_{l,2} d_{l,2}\delta\tilde{y}_l(t,k), \end{aligned} \tag{2.15}$$

and

$$\begin{aligned}\|\tilde{y}_l(t,k+1)\| &\leq \|I - Cb_lq_{l,1}d_{l,1}\|\|\tilde{y}_l(t,k)\| \\ &\quad +\|C\|(k_f + \|b_lq_{l,2}d_{l,2}\|)\|\delta\tilde{y}_l(t,k)\|. \end{aligned} \tag{2.16}$$

Considering (2.14) and (2.16), we obtain

$$\begin{bmatrix} \|\delta\tilde{y}_l(t,k+1)\| \\ \|\tilde{y}_l(t,k+1)\| \end{bmatrix} \leq \begin{bmatrix} \hat{e}_1 & \hat{e}_2 \\ \hat{e}_1 & \rho_1 \end{bmatrix} \begin{bmatrix} \|\delta\tilde{y}_l(t,k)\| \\ \|\tilde{y}_l(t,k)\| \end{bmatrix} \tag{2.17}$$

where the symbol "$\leq$" applies to each element of the vector, $\hat{e}_1 = \|C\|(k_f+\|b_lq_{l,2}d_{l,2}\|)$, $\hat{e}_2 = \|Cb_lq_{l,1}d_{l,1}\|$, and $\rho_1 = \|I - Cb_lq_{l,1}d_{l,1}\|$.

Taking the inf-norm on both sides of (2.17), and according to the basic property of the vector norm, we can derive that if

$$\left\| \begin{bmatrix} \hat{e}_1 & \hat{e}_2 \\ \hat{e}_1 & \rho_1 \end{bmatrix} \right\|_{\inf} < 1, \tag{2.18}$$

and $\|\tilde{y}_l(t,0)\|$ and $\|\delta\tilde{y}_l(t,0)\|$ are both finite numbers, then both $\|\tilde{y}_l(t,k)\|$ and $\|\delta\tilde{y}_l(t,k)\|$ converge to zero as k approaches infinity. ∎

Remark 2.2 *The inequality (2.18) is only a sufficient condition to guarantee the convergence of the lth observer output estimation error.*

In order to isolate the fault, we want to show that the output estimation errors of all RLOs except the lth one do not approach zero. If so, the fault isolation becomes straightforward.

Theorem 2.2 *If matrix CB is of full column rank, then the residual $r_i(t) \neq 0, (i \neq l)$, and the fault isolation problem can be effectively solved by evaluating the residuals.*

Proof: For $i \neq l$, we have the estimation error dynamics as follows,

$$\begin{aligned}\tilde{x}_i(t,k+1) &= f(x(t)) - f(\hat{x}_i(t,k)) + b_l\theta_l - b_i\hat{\theta}_i(t,k) \\ \tilde{y}_i(t,k) &= C\tilde{x}_i(t,k). \end{aligned} \tag{2.19}$$

If matrix CB has full column rank, Cb_l and Cb_i are independent. Additionally, $\hat{\theta}_i(t,k)$ is updated using $\tilde{y}_i(t,k)$, and, in general, $\hat{\theta}_i(t,k) \neq \theta_l$ for $i \neq l$. Therefore, generally, $\tilde{y}_i(t,k)$ for $i \neq l$ will not approach zero. ∎

Summarizing Theorem 2.1 and 2.2, if the lth actuator is faulty, then only the lth residual $r_l(t)$ is zero and others are nonzero. Therefore, the proposed PI-type RLOs are effective for fault detection and isolation.

2.5 RLOs-based Actuator Fault Estimation

In the event of a fault, the location as well as the size of the fault must be determined. In this section, we estimate the fault by updating the parameter $\hat{\theta}_l(t,k)$ in the repetitive learning domain. Regarding the fault estimation using RLOs, we have the following theorem.

Theorem 2.3 *When the lth actuator is faulty, if the sufficient condition (2.18) in Theorem 2.1 and the following inequality are both satisfied,*

$$\rho_2 = \|I - (q_{l,1}d_{l,1} + q_{l,2}d_{l,2})Cb_l\| < 1, \tag{2.20}$$

then

$$\lim_{k\to\infty} \|\theta_l - \hat{\theta}_l(t,k)\| = 0. \tag{2.21}$$

Proof: Subtracting both sides of $\hat{\theta}_l(t,k+1)$ from θ_l in (2.8), we have

$$\begin{aligned}
\tilde{\theta}_l(t,k+1) &= \tilde{\theta}_l(t,k) - q_{l,1}d_{l,1}\tilde{y}_l(t,k+1) - q_{l,2}d_{l,2}\delta\tilde{y}_l(t,k+1) \\
&= \tilde{\theta}_l(t,k) - (q_{l,1}d_{l,1} + q_{l,2}d_{l,2})\tilde{y}_l(t,k+1) + q_{l,2}d_{l,2}\tilde{y}_l(t,k) \\
&= \tilde{\theta}_l(t,k) - (q_{l,1}d_{l,1} + q_{l,2}d_{l,2})C(f(x(t)) - f(\hat{x}_l(t,k))) \\
&\quad -(q_{l,1}d_{l,1} + q_{l,2}d_{l,2})Cb_l\tilde{\theta}_l(t,k) + q_{l,2}d_{l,2}\tilde{y}_l(t,k).
\end{aligned} \tag{2.22}$$

Taking the norm on both sides of (2.22), and according to Assumption 2.2, we obtain

$$\|\tilde{\theta}_l(t,k+1)\| \leq \rho_2\|\tilde{\theta}_l(t,k)\| + \hat{e}_3\|\tilde{y}_l(t,k)\| \tag{2.23}$$

where

$$\rho_2 = \|I - (q_{l,1}d_{l,1} + q_{l,2}d_{l,2})Cb_l\|$$

and

$$\hat{e}_3 = \|(q_{l,1}d_{l,1} + q_{l,2}d_{l,2})Ck_f\| + \|q_{l,2}d_{l,2}\|.$$

Therefore, if the sufficient condition in Theorem 2.1 is satisfied to guarantee $\|\tilde{y}_l(t,k)\| \to 0$, and the parameters of the observers are carefully chosen to guarantee $0 < \rho_2 < 1$, then $\lim_{k\to\infty} \|\tilde{\theta}_l(t,k)\| = 0$. ∎

Remark 2.3 *So far, we do not have a systematic way to choose the learning coefficients $q_{i,1}$ and $q_{i,2}$, and we still have to use a trial-and-error method. In order to guarantee (2.11) and (2.20), not only do the system dynamics need to satisfy certain assumptions, but also the learning coefficients need to be set to small values in numerical computation.*

In addition to fault detection, isolation, and estimation, the PI-type repetitive learning observers can be used to estimate the system state. This property is guaranteed by the following theorem.

Theorem 2.4 *For $i = l$, if the conditions in Theorem 2.1 and 2.3 are all guaranteed, and the following inequality is also satisfied,*

$$\lambda_{min}(Q) > k_\xi\|P\| + 2k_\xi\|P\|\|A\| \tag{2.24}$$

where P and Q are both defined in Assumption 2.4, and $\lambda_{min}(Q)$ is the minimum eigenvalue of Q, then the system state estimation error obtained by the lth observer ultimately approaches zero.

Proof: Based on Assumption 2.3, the dynamics of the state estimation error are

$$\begin{aligned}\tilde{x}_l(t,k+1) &= f(x(t)) - f(\hat{x}_l(t,k)) + b_l(\theta_l - \hat{\theta}_l(t,k)) \\ &= A\tilde{x}_l(t,k) + (\xi(x(t)) - \xi(\hat{x}_l(t,k))) + b_l\tilde{\theta}_l(t,k).\end{aligned} \tag{2.25}$$

We design a Lyapunov function as

$$V_l(k) = \tilde{x}_l(t,k)^\top P \tilde{x}_l(t,k). \tag{2.26}$$

Based on the results derived from Theorem 2.3 and Assumption 2.4, we compute the difference of $V_l(k)$ to be

$$\begin{aligned}
&V_l(k+1) - V_l(k) \\
&= \tilde{x}_l(t,k+1)^\top P \tilde{x}_l(t,k+1) - \tilde{x}_l(t,k)^\top P \tilde{x}_l(t,k) \\
&= \tilde{x}_l(t,k)^\top (A^\top P A - P)\tilde{x}_l(t,k) \\
&\quad +2\tilde{x}_l(t,k)^\top A^\top P(\xi(x(t)) - \xi(\hat{x}(t,k))) \\
&\quad +(\xi(x(t)) - \xi(\hat{x}_l(t,k)))^\top P(\xi(x(t)) - \xi(\hat{x}_l(t,k))) \\
&\quad +\tilde{\theta}_l(t,k)^\top b_l^\top P b_l \tilde{\theta}_l(t,k) + 2\tilde{x}_l(t,k)^\top A^\top b_l \tilde{\theta}_l(t,k) \\
&\quad +2\tilde{\theta}_l(t,k)^\top b_l^\top (\xi(x(t)) - \xi(\hat{x}_l(t,k))) \\
&\leq -\tilde{x}_l(t,k)^\top Q \tilde{x}_l(t,k) + k_\xi \|P\| \|\tilde{x}_l(t,k)\|^2 \\
&\quad +2k_\xi \|P\| \|A\| \|\tilde{x}_l(t,k)\|^2 + \|P\| \|b_l\| \|\tilde{\theta}_l(t,k)\|^2 \\
&\quad +2(\|A\| + k_\xi)\|b_l\| \|\tilde{\theta}_l(t,k)\| \|\tilde{x}_l(t,k)\| \\
&\leq -\beta_1 \|\tilde{x}_l(t,k)\|^2 + 2\beta_2 \|\tilde{x}_l(t,k)\| \|\tilde{\theta}_l(t,k)\| + \beta_3 \|\tilde{\theta}_l(t,k)\|^2 \\
&= -\beta_1 \Big(\|\tilde{x}_l(t,k)\| - \frac{\beta_2}{\beta_1} \|\tilde{\theta}_l(t,k)\| \Big)^2 + \Big(\frac{\beta_2^2}{\beta_1} + \beta_3 \Big) \|\tilde{\theta}_l(t,k)\|^2
\end{aligned} \tag{2.27}$$

where

$$\beta_1 = \lambda_{\min}(Q) - k_\xi \|P\| - 2k_\xi \|P\| \|A\| \tag{2.28}$$

$$\beta_2 = \|A\| \|b_l\| + \|b_l\| k_\xi \tag{2.29}$$

$$\beta_3 = \|P\| \|b_l\|^2. \tag{2.30}$$

If

$$\lambda_{min}(Q) > k_\xi \|P\| + 2k_\xi \|P\| \|A\| \tag{2.31}$$

$$\|\tilde{x}_l(t,k)\| > \frac{\beta_2 + \sqrt{\beta_2^2 + \beta_1 \beta_3}}{\beta_1} \|\tilde{\theta}_l(t,k)\| \tag{2.32}$$

we obtain $\Delta V_l(k) < 0$, which implies $\hat{x}_l(t,k)$ is ultimately bounded, since β_2 and β_3 are finite positive numbers. This bound depends on the fault estimation error. Based on the results in Theorem 2.3, $\|\tilde{x}_l(t,k)\|$ approaches zero as $k \to 0$.

For $(i \neq l)$, we can prove that $\tilde{x}_i(t,k) \neq 0$ in a similar way as that in Theorem 2.2. Therefore, the lth observer alone can be used to estimate the system state. ∎

The propose fault diagnosis scheme in this chapter is implemented using the following algorithm:

- Step 1: Determine mapping operators $d_{i,j}$, and coefficient $q_{i,j}$ based on system dynamics and using a trial-and-error method.
- Step 2: Set maximum repetition number k_m and tolerance error $\epsilon_{\tilde{y}}$.
- Step 3: Obtain system output $y(t+1)$ from (2.1).
- Step 4: Construct m RLOs for m possible faulty models, and obtain $\tilde{y}_i(t,k)$ and $\delta\tilde{y}_i(t,k)$ at the kth repetition.
- Step 5: Update $\hat{\theta}_i(t,k)$ of RLOs in repetition domain.
- Step 6: If $k = k_m$ or $\|\tilde{y}_i(t,k)\| < \epsilon_{\tilde{y}}$, then compute residual $r_i(t) = \|\tilde{y}_i(t,k)\|$, and record $\hat{\theta}_i(t,k)$ and $\hat{x}_i(t,k)$. Otherwise, $k := k+1$, and goes to Step 4.
- Step 7: Use $r_i(t)$ to detect fault based on Theorem 2.1.
- Step 8: Use $r_i(t)$ to isolate fault based on Theorem 2.2.
- Step 9: Use $\hat{\theta}_l(t,k)$ to estimate fault based on Theorem 2.3.
- Step 10: Estimate system state using $\hat{x}_l(t,k)$.

2.6 Application to a Satellite Attitude Control System

In this section, we apply the proposed RLOs-based fault diagnosis scheme to a dynamic satellite attitude control system. This satellite works in a circular orbit in an

inverse square gravitational field. The attitude of the satellite is assumed to have no effect on the orbit. We define I_1, I_2, I_3 as the principal axis moments of inertia of the satellite, $\omega = [\omega_1, \omega_2, \omega_3]^\top$ as the angular velocity of the satellite, and $\theta = [\theta_1, \theta_2, \theta_3]^\top$ as the pitch, yaw, and roll angles of the satellite, respectively.

The angular velocity has the following nonlinear relationship with the three attitude angles:

$$\begin{aligned} \omega &= \begin{bmatrix} \omega_1 \\ \omega_2 \\ \omega_3 \end{bmatrix} = \begin{bmatrix} (\omega_0 + \dot{\theta}_1)\sin\theta_2 + \dot{\theta}_3 \\ (\omega_0 + \dot{\theta}_1)\cos\theta_2\cos\theta_3 + \dot{\theta}_2\sin\theta_3 \\ -(\omega_0 + \dot{\theta}_1)\cos\theta_2\sin\theta_3 + \dot{\theta}_2\cos\theta_3 \end{bmatrix} \\ &= R(\theta)\dot{\theta} + \omega_c(\theta) = T(\theta, \dot{\theta}) \end{aligned} \tag{2.33}$$

where

$$R(\theta) = \begin{bmatrix} \sin\theta_2 & 0 & 1 \\ \cos\theta_2\cos\theta_3 & \sin\theta_3 & 0 \\ -\cos\theta_2\sin\theta_3 & \cos\theta_3 & 0 \end{bmatrix}, \quad \omega_c(\theta) = \begin{bmatrix} \omega_0\sin\theta_2 \\ \omega_0\cos\theta_2\cos\theta_3 \\ -\omega_0\cos\theta_2\sin\theta_3 \end{bmatrix}. \tag{2.34}$$

The motion equation about the mass center of the satellite is provided in [109] as,

$$I\dot{\omega} + \tilde{\omega}I\omega = 3\omega_0^2\tilde{\xi}_c I\xi_c + u + T_d \tag{2.35}$$

where $I = diag\{I_1, I_2, I_3\}$, $u = [u_1, u_2, u_3]^\top$ is the control torque vector, and $T_d = [T_{d1}, T_{d2}, T_{d3}]^\top$ is the disturbance torque vector. The vector ξ_c is written as

$$\xi_c = \begin{bmatrix} -\sin\theta_1\cos\theta_2 \\ \cos\theta_1\sin\theta_3 + \sin\theta_1\sin\theta_2\cos\theta_3 \\ \cos\theta_1\cos\theta_3 - \sin\theta_1\sin\theta_2\sin\theta_3 \end{bmatrix}, \tag{2.36}$$

and $\tilde{\omega}$ is the skew symmetric matrix of the vector ω, which is defined as,

$$\tilde{\omega} = \begin{bmatrix} 0 & -\omega_3 & \omega_2 \\ \omega_3 & 0 & -\omega_1 \\ -\omega_2 & \omega_1 & 0 \end{bmatrix}. \tag{2.37}$$

Defining the state vector to be $x = [\theta^\top, \omega^\top]^\top$, we obtain the dynamics of the satellite motion in a nonlinear state space form as

$$\begin{aligned} \dot{x} &= \begin{bmatrix} R^{-1}(\theta)(\omega - \omega_c(\theta)) \\ I^{-1}(-\tilde{\omega} I\omega + 3\omega_0^2 \tilde{\xi}_c I \xi_c) \end{bmatrix} + \begin{bmatrix} 0 \\ I^{-1} \end{bmatrix} u + \begin{bmatrix} 0 \\ I^{-1} \end{bmatrix} T_d \\ y &= [\theta_1, \theta_2, \theta_3]^\top. \end{aligned} \tag{2.38}$$

In the simulation, the parameter values of the satellite dynamics are listed in Table 2.1. The system dynamics is discretized using Euler's method with a sampling rate equal to 1000Hz. This sampling rate is determined using a trial-and-error method. If the sampling rate is too large, the discrete-time system can not represent the original continuous-time system. However, a too small sampling rate causes the repetitive learning algorithm hard to be implemented in real-time.

A sliding mode controller was designed in [110] to control the satellite output to track the designated reference, which is,

$$\theta_r = (1 - \mathrm{e}^{-at}(\sin at + \cos at))\theta^* \tag{2.39}$$

where $a = 0.353$ and $\theta^* = [180, 45, 75]^\top$ (deg). The control torque is disturbed by $\varsigma_u = 1\% * rand$; i.e., $T_d = \varsigma_u u$, while the Euler angles have measurement noise with $\varsigma_y = 0.01\% * rand$; i.e., $\theta_{measure} = (1 + \varsigma_y)\theta$, where $rand$ is a Gaussian white noise.

In the design of the repetitive learning observers, the parameters to be determined are $d_{i,j}$ and $q_{i,j}$. Based on the analysis in Section 2.3, $d_{i,j} \in \Re^{n \times p}$ is the operator that inversely maps the output to the state, and $q_{i,j} \in \Re^{1 \times n}$ is the vector that balances the

Table 2.1: Parameters of a satellite attitude control system

Parameters	Values (unit)
Principal moment of inertia I_1	874.6 (kg m^2)
Principal moment of inertia I_2	888.2 (kg m^2)
Principal moment of inertia I_3	97.6 (kg m^2)
Orbital rate ω_0	7.29 $\times 10^{-5}$ (rad/s)

convergence rate of the state and parameter estimation. In this simulation, we choose

$$d_{i,j} = \begin{bmatrix} 1 & 0 & 0 \\ 0 & 1 & 0 \\ 0 & 0 & 1 \\ 0.7071\Delta & 0 & \Delta \\ 0.183\Delta & 0.9659\Delta & 0 \\ 0.683\Delta & 0.2588\Delta & 0 \end{bmatrix} \tag{2.40}$$

where Δ is the difference operator. The matrix $d_{i,j}$ is chosen based on (2.33) and measured angles. In numerical computation, $d_{i,j}$ can be treated as a time-varying left-multiply matrix on $\tilde{y}_i(t,k)$ and $\delta\tilde{y}_i(t,k-1)$ at each sampling time. Moreover, the coefficient vector, $q_{i,j}$, is defined to be a vector such that only the $(n-m+i)$th element, $q_{i,j}^{(n-m+i)}$, which corresponds to the ith actuator is nonzero; that is,

$$\begin{aligned} q_{1,1} &= \begin{bmatrix} 0 & 0 & 0 & 10^{-6} & 0 & 0 \end{bmatrix} \\ q_{1,2} &= \begin{bmatrix} 0 & 0 & 0 & 10^{-7} & 0 & 0 \end{bmatrix} \\ q_{2,1} &= \begin{bmatrix} 0 & 0 & 0 & 0 & 10^{-6} & 0 \end{bmatrix} \\ q_{2,2} &= \begin{bmatrix} 0 & 0 & 0 & 0 & 10^{-7} & 0 \end{bmatrix} \\ q_{3,1} &= \begin{bmatrix} 0 & 0 & 0 & 0 & 0 & 10^{-6} \end{bmatrix} \\ q_{3,2} &= \begin{bmatrix} 0 & 0 & 0 & 0 & 0 & 10^{-7} \end{bmatrix}. \end{aligned}$$

Note that the coefficient vector may affect the precision of fault estimation.

The simulation results are shown from Figure 2.1 to 2.8, where Figure 2.1 illustrates the time-behavior of the system output when no fault occurs. The sliding mode control algorithm offers a satisfactory control performance in the presence of disturbances. Figure 2.2 to Figure 2.5 portray the simulation results of case 1, where a fault occurs in the second actuator beginning from $t = 20sec$. Figure 2.6 and Figure 2.8 demonstrate the results of case 2, where another fault occurs in the third actuator since $t = 22sec$. Clearly, when the ith actuator is faulty, only the residual produced by the ith observer approaches zero, while the other residuals approach nonzero values.

The corresponding parameter $\hat{\theta}_i$ is able to specify the fault in a short time. Moreover, in both these two cases, after the fault has been characterized, the ith observer provides an estimation of the system state. The chattering in the simulation results are due to the existence of system uncertainties and measurement noises, which directly affect the output estimation error. However, the time-varying uncertainty and noise become constant values in the repetitive learning domain at each discrete time. Hence, the performance of fault estimation is not influenced too much as long as the output estimation error approaches zero in time. Since there is no explicit robust strategies in the proposed fault diagnosis scheme, the proposed FD scheme can only be tolerant to small magnitude of disturbances and noises. In summary, these two simulation cases demonstrate that the proposed repetitive learning observers are effective in diagnosing finite constant faults in actuators for a class of nonlinear systems.

2.7 Conclusions

In this chapter, inspired by ILOs, a bank of m nonlinear repetitive learning observers was designed for the detection, isolation, and estimation of m possible constant actuator faults in a class of discrete time nonlinear systems. The RLOs preserve the simplicity in structure of ILOs, and use a PI-type algorithm to update their parameters. The system dynamics work in a discrete time domain and the observer parameters are updated in a repetitive learning domain, where the discrete time domain and the repetitive learning domain form a 2-dimensional structure. Based on RLOs, m residuals were generated to detect and locate a fault, where only the ith residual that is associated with the ith faulty actuator is insensitive to the fault. This strategy results in straightforward fault detection and isolation. Moreover, the observer parameter that isolates the fault was used to estimate the constant fault function. Sufficient conditions for effective fault isolation and estimation were derived analytically. The theoretical analysis is exemplified by an application of the proposed fault diagnosis scheme to the dynamics of a satellite attitude control system. The simulation results verify the accuracy of the fault diagnosis scheme.

Although the proposed RLOs-based fault diagnosis scheme has the advantages

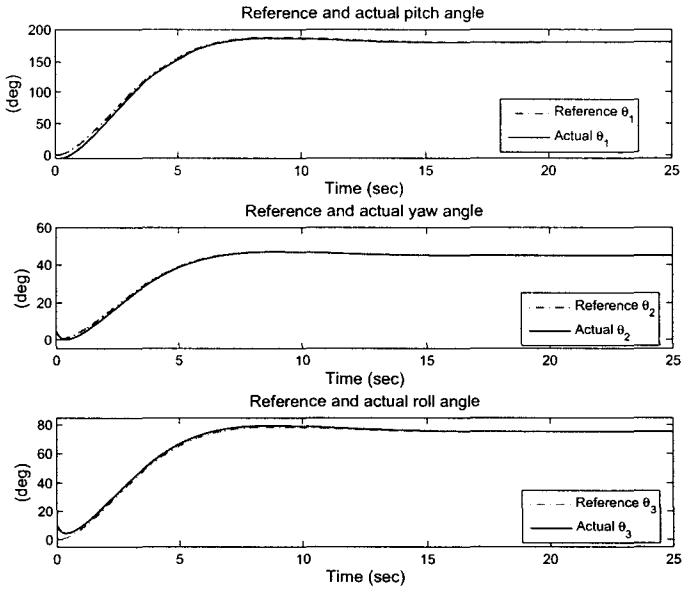

Figure 2.1: System output in the fault-free case

that the structure of RLOs is simple and only two coefficients of each observer need to be selected beforehand, the types of faults investigated in this chapter are confined to finite constant faults. The applicability of the proposed fault diagnosis scheme to a time-varying single fault and even multiple faults need further study. In addition, from simulation results, the system uncertainty and noise have to be very small in order to guarantee a successful fault diagnosis because no robust strategy is utilized in this fault diagnosis scheme. Therefore, robust fault diagnosis in the presence of system uncertainties is still a challenging issue for theoretical research as well as real applications.

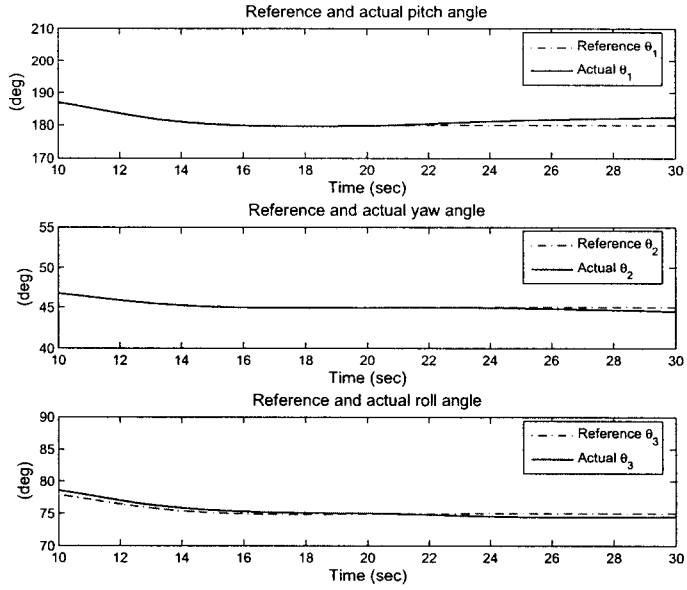

Figure 2.2: System output when a fault occurs at the second actuator

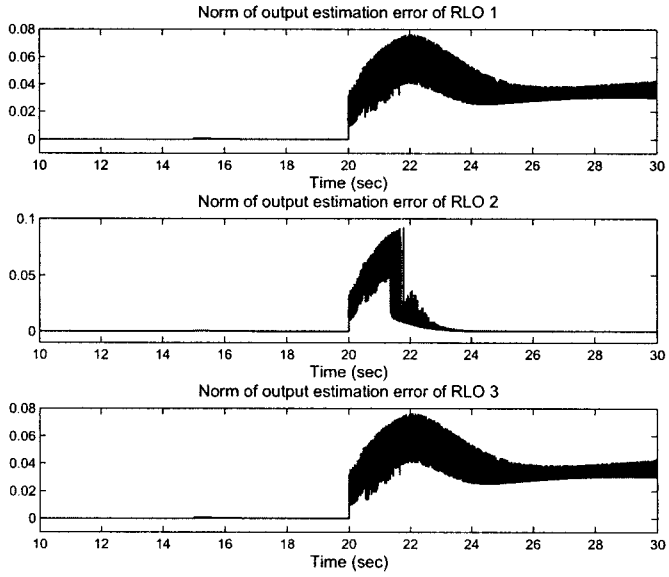

Figure 2.3: Fault detection and isolation results when a fault occurs at the second actuator

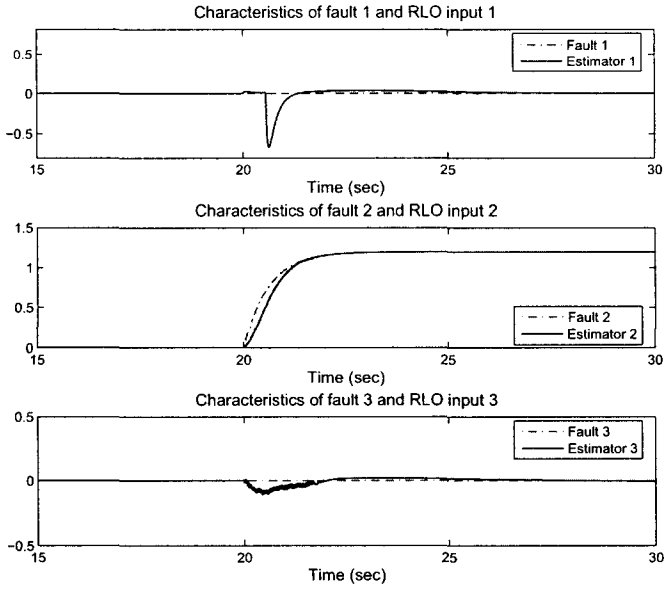

Figure 2.4: Fault estimation result when a fault occurs at the second actuator

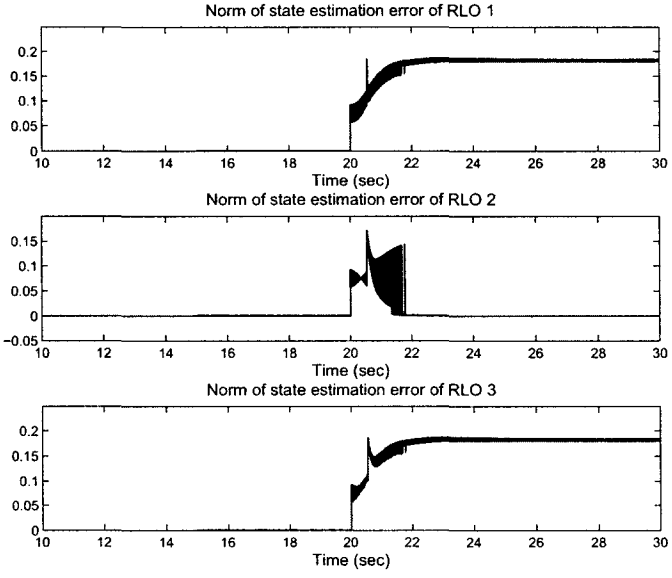

Figure 2.5: Norm of state estimation error of the three observers when a fault occurs at the second actuator

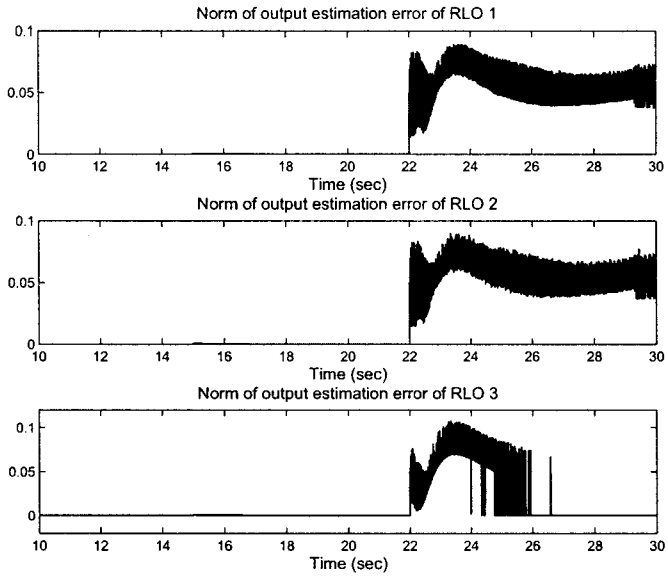

Figure 2.6: Fault detection and isolation results when a fault occurs at the third actuator

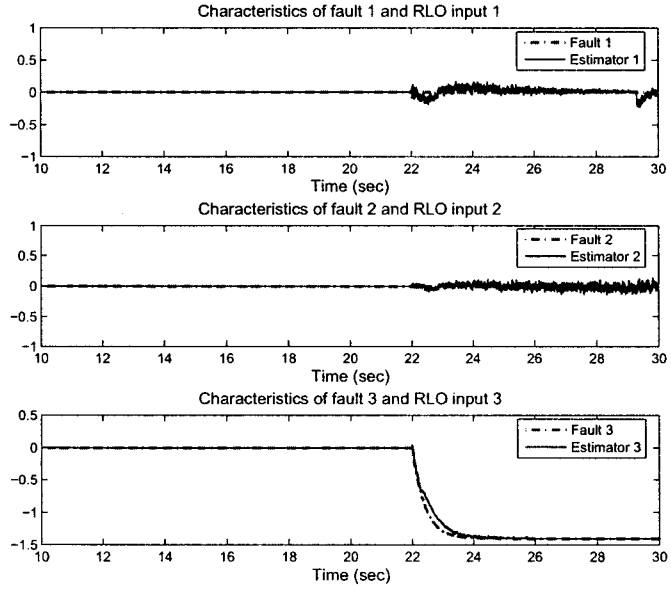

Figure 2.7: Fault estimation result when a fault occurs at the third actuator

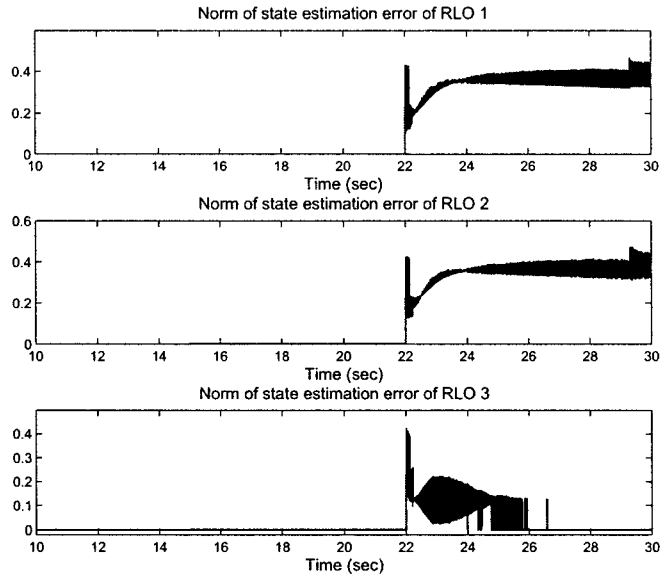

Figure 2.8: Norm of state estimation errors of the three observers when a fault occurs at the third actuator

Chapter 3

Fault Diagnosis Using Sliding Mode and Learning Approaches

In this chapter, a unified framework of a fault diagnosis scheme using sliding mode and learning approaches in a class of nonlinear systems is established.

3.1 Introduction

In general, a model-based fault diagnosis scheme generates a residual via comparing the measurable output of a system with the output generated through the system's mathematical model. Then, fault diagnostic decisions are made based on this residual. Early fault diagnosis approaches were based on the assumption that the system under consideration was linear and sufficiently accurate mathematical model was available. Although model-based fault diagnosis schemes are attractive due to their powerful information processing capabilities, efficient diagnosis relies on the robustness of the residual with respect to the system uncertainties. This issue is referred to as *robust fault diagnosis.*

For linear systems, robust fault diagnosis can be achieved via unknown input observers and eigenstructure assignment methods, both of which decouple the effect of uncertainties from the residual. These two approaches do not make assumptions on the size and the time functions, or on the frequency characteristics of the faults or

of the unknown inputs. For nonlinear systems, robust fault diagnosis schemes using learning approaches have been significantly investigated. For example, fault diagnosis schemes using feedforward neural networks, iterative learning observers, adaptive observers, and other methods have received a great deal of attention. To realize robust fault diagnosis, dead-zone operators are usually adopted in the learning algorithms to ensure that the fault estimators are insensitive to the error signal under a certain threshold which is deemed to be caused by system uncertainties, thereby preventing false alarms [27], [28], [29], [30], [31], [32], and [33]. However, several issues still need further study in this class of fault diagnosis methodologies. One issue is that, in all likelihood, the dead-zone operators reduce the accuracy of the fault approximation. Another issue concerns the projection operators which can confine the parameter estimation vectors to a predefined compact and convex region in the presence of system uncertainties and approximation errors. A third issue is that the online fault estimators should be easily implementable to satisfy the requirement of real-time computation. In addition, an accurate fault estimation is helpful for controller reconfiguration to achieve fault tolerance. Hence, an estimation of a fault with a fast transient process and less overshoot is preferred. This expectation motivates us to develop more learning approaches to diagnose faults for different specific situations.

Due to the inherent robustness property of a sliding mode to system uncertainties, sliding mode techniques have been studied for system observation by many researchers [111], [112], [113], [114], [115], [116], [117], [66], [48], [118], [119], [120], and [121]. In summary, the existing sliding mode observer design methods can be classified into two categories: 1) SMO designs based on equivalent control methods, and 2) SMO designs based on the Lyapunov method.

In addition to the applications of a sliding mode to linear systems, in recent years, sliding mode techniques have been extended to design fault diagnosis schemes for nonlinear dynamic systems. One approach to using a sliding mode observer in fault diagnosis is that the observer maintains a sliding motion even in the presence of faults, and the fault signals are reconstructed by manipulating the equivalent output injection signals. In order to guarantee the stability of the fault diagnosis scheme, the bound of the system uncertainties is usually estimated and involved in the design

of the discontinuous term. The practical importance of this class of sliding mode observer-based fault diagnosis approaches is that it allows small faults to be detected, even if large modeling errors occur. However, a large amount of chattering occurs when this method is implemented by digital computers at a given sampling frequency. Some researchers have proposed a variety of approaches to reduce the unnecessary chattering. One method is to use a continuous saturation function to replace the discontinuous *sign* function. Other methods involve adaptively estimating the bound of the system uncertainties [122], [123] or constructing an adaptive switching gain [124], [125], [126]. However, these methods have not been widely used in sliding mode observer based fault diagnosis.

In this chapter, a class of nonlinear diagnostic observers is established and applied to the fault diagnosis of a class of nonlinear systems. The diagnostic observer integrates an adaptive sliding mode and a bank of online estimators. The sliding mode in this class of observers is used only to eliminate the effect of system uncertainties, and the observer is designed such that the sliding motion is destroyed when any fault occurs. In order to estimate the state as soon as possible and to prevent the sliding mode eliminating the deviation caused by faults, the switching gain of the sliding mode is updated by an iterative learning algorithm and an iterative fuzzy model, respectively. After the occurrence of faults, a bank of online estimators is activated to isolate and identify the incipient and/or abrupt faults. Neural networks based models and online estimators based on iterative learning algorithms are established to characterize the faults. The advantage of this class of robust fault diagnosis schemes is that it is able to not only detect various faults in the presence of system uncertainties, but also isolate and estimate the faults with satisfactory accuracy. Theoretical results are verified by applying the proposed fault diagnosis schemes to a fourth-order satellite orbital control system and a flexible satellite control system, both of which belong to the class of nonlinear systems with triangular input form.

The organization of this chapter is as follows. In Section 3.2, the investigated problem and some preliminaries are stated. The diagnostic observer using sliding modes and learning approaches is proposed in Section 3.3, where two update laws for the sliding mode switching gain are established, respectively. In Section 3.4, the

analytical properties of the proposed fault diagnosis scheme are rigorously analyzed. After this analysis, two kinds of online fault estimators are developed to characterize the fault functions. These two estimator based fault diagnosis schemes are applied to a satellite orbital control system and a flexible control system in Section 3.5 and Section 3.6, respectively. Finally, conclusions are given in Section 3.7.

3.2 Problem Formulation

In this chapter, a class of nonlinear input-output dynamic systems subject to system uncertainties and additive state faults is described by the following differential equations:

$$\begin{aligned} \dot{x}_1(t) &= x_2(t) \\ \dot{x}_2(t) &= A_{21}x_1 + A_{22}x_2 + \xi(x,u,t) + \eta(x,u,t) + \beta(t-T_f)f_a(x,u,t) \\ y(t) &= x_1(t) \end{aligned} \tag{3.1}$$

where $x_1(t) = [x_{1,1}, \cdots, x_{1,p}]^\top \in \Re^p, (p = n/2)$, and $x_2(t) = [x_{2,1}, \cdots, x_{2,p}]^\top \in \Re^p$ are two components of the state vector $x = [x_1^\top, x_2^\top]^\top$, $y(t) \in \Re^p$ is the output vector, and $u(t) \in \Re^m$ is the control vector of the system. The terms $\xi : \Re^n \times \Re^m \times \Re^+ \to \Re^p$, $\eta : \Re^n \times \Re^m \times \Re^+ \to \Re^p$, and $f_a : \Re^n \times \Re^m \times \Re^+ \to \Re^p$ are all smooth vector fields. The matrices $A_{21} \in \Re^{p\times p}$ and $A_{22} \in \Re^{p\times p}$ describe the linear characteristics of the system, while $\xi(x,u,t)$ denotes the nonlinear dynamics. The nonlinear function vector $\eta = [\eta_1, \cdots, \eta_p]^\top$ represents the modeling uncertainties and disturbances in the system dynamics. The nonlinear function vector $f_a(x,u,t) = [f_a^{(1)}(x,u,t), \cdots, f_a^{(p)}(x,u,t)]^\top$ denotes any change in the system dynamics due to additive state faults, which probably occur in the actuators and/or in the system components. The term $\beta(t-T_f) = diag\{\beta_1(t-T_f), \cdots, \beta_p(t-T_f)\}$ is a diagonal time profile function matrix which satisfies

$$\beta_i(t-T_f) = \begin{cases} 0 & t < T_f \\ 1 & t \geq T_f \end{cases} \qquad i = 1, \cdots, p \tag{3.2}$$

where T_f denotes the beginning time of a fault.

We can write the system dynamics (3.1) into a new form as

$$\begin{aligned} \dot{x}(t) &= Ax(t) + D\xi(x,u,t) + D\eta(x,u,t) + D\beta(t-T_f)f_a(x,u,t) \\ y(t) &= Cx(t) \end{aligned} \tag{3.3}$$

where matrix A is defined to be

$$A = \begin{bmatrix} 0_p & I_p \\ A_{21} & A_{22} \end{bmatrix},$$

and $C = [I_p \quad 0_p]$, $D = [0_p \quad I_p]^\top$, 0_p is a $p \times p$ zero matrix, and I_p is a $p \times p$ identity matrix.

For the sake of designing and analyzing the proposed fault diagnosis scheme conveniently, the following assumptions are introduced.

Assumption 3.1 The system uncertainties $\eta(x,u,t)$ is possibly an unstructured nonlinear function of x, u, and t, but bounded; i.e., a known constant η_0 exists such that $\|\eta(x,u,t)\| \leq \eta_0$.

For many dynamic systems, considerable system modeling and identification methods result in relatively small $\eta(t)$. The upper bound of the state modeling uncertainties is used in the design of the proposed diagnostic sliding mode observer and in the robustness analysis of the proposed fault diagnosis scheme. Throughout this thesis, $\|\cdot\|$ represents the Euclidean vector norm or induced matrix 2-norm.

Assumption 3.2 The nonlinear dynamic component $\xi(x,u,t)$ of system (3.1) is Lipschitz at the state x with three known constants k, k_1, and k_2; that is,

$$\|\xi(x,u,t) - \xi(\hat{x},u,t)\| \leq k\|x-\hat{x}\| \leq k_1\|x_1-\hat{x}_1\| + k_2\|x_2-\hat{x}_2\|. \tag{3.4}$$

Assumption 3.3 The magnitude of the state fault is bounded by a finite constant; i.e., $\|f_a(t)\| \leq f_m$, and the system state variables would deviate from their normal values but they will remain finite after the state fault occurs. Moreover, the fault is assumed to occur after all the state variables have been observed in the original regulation phase by using the sliding mode.

The finiteness of the fault and the system state are not only required for state observation, but also guarantee the feasibility of characterizing the fault using on-line approximators. The assumption on the onset of the fault helps to individually investigate the state observation and fault diagnosis.

Assumption 3.4 Matrix A is stable, which implies that A_{22} is also stable; i.e., a symmetric positive definite matrix Γ_2 exists that satisfies the following Lyapunov function:

$$A_{22}^{\top}\Gamma_2 + \Gamma_2 A_{22} = -Q \tag{3.5}$$

where Q is also a positive definite matrix.

Even if matrix A is unstable, the linear part of the system (3.1) is stabilized by designing a Luenberger gain.

Remark 3.1 *The dynamic system (3.1) can represent a family of systems which have triangular input form. Many mechanical or equivalent systems can be classified into (3.1) because usually only displacements or angles are measurable. For such class of systems, it is possible to design an observer which does not use the input derivative. In real applications such as satellite jet control or AC motor with PWM control, the exact information of the input derivative is hard to obtained [115], [127].*

Remark 3.2 *Sliding mode observers for the class of systems with triangular input form have been studied in [115], [66]. In these methods, the states are stabilized recursively, one by one in finite time, and the switching gain of the sliding mode observer is held constant. The constant switching gain is acceptable when the objective is only to observe the states. However, when the effect of system uncertainties needs to be eliminated, and for the sliding motion to be destroyed when a fault occurs, a time-varying switching gain is preferable.*

3.3 Fault Diagnosis Using Sliding Modes and Learning Approaches

3.3.1 Design of a Fault Diagnostic Observer

Based on system (3.1), a nonlinear diagnostic observer is proposed as follows:

$$\begin{aligned}\dot{\hat{x}}_1(t) &= \hat{x}_2(t) + g_1(t)\text{sign}(\Gamma_1 s_1(t)) + \beta(t - T_m)\hat{M}_1(t) \\ \dot{\hat{x}}_2(t) &= A_{21}\hat{x}_1 + A_{22}\hat{x}_2 + \xi(\hat{x}, u, t) + g_2(t)\text{sign}(\Gamma_2 s_2(t)) + \beta(t - T_m)\hat{M}_2(t) \\ \hat{y}(t) &= \hat{x}_1(t) \end{aligned} \tag{3.6}$$

where $\hat{x}_1 \in \Re^p$ and $\hat{x}_2 \in \Re^p$ are the estimated state vectors, and $\hat{y} \in \Re^p$ is the output vector of the observer. The term *sign* is a signum function, and $\hat{M}_1(t) = [\hat{M}_{1,1}, \cdots, \hat{M}_{1,p}]^\top$, $\hat{M}_2(t) = [\hat{M}_{2,1}, \cdots, \hat{M}_{2,p}]^\top$ are online fault estimator vectors, which are explicitly discussed in later sections.

In order to separate the roles of the sliding mode from the online fault estimators, in the beginning, we disable the fault estimators $\hat{M}_1(t)$ and $\hat{M}_2(t)$ before all the state estimation errors reach the sliding manifold. Moreover, the fault is assumed to occur after the activation of the fault estimators; i.e., $T_m < T_f$.

The terms $\Gamma_1 \in \Re^{p\times p}$ and $\Gamma_2 \in \Re^{p\times p}$ are both symmetric positive definite matrices, and Γ_2 satisfies Assumption 3.4. The terms $s_1(t) = [s_{1,1}, \cdots, s_{1,p}]^\top \in \Re^p$, and $s_2(t) = [s_{2,1}, \cdots, s_{2,p}]^\top \in \Re^p$ are named equivalent state estimation errors, which are calculated according to the anti-peaking structure [115] as follows:

$$\begin{cases} s_1(t) = x_1(t) - \hat{x}_1(t) & \\ s_2(t) = (g_1(t)\text{sign}(\Gamma_1 s_1(t)))_{eq}, & \text{if } \tilde{x}_1(t) = 0 \text{ and } \dot{\tilde{x}}_1(t) = 0 \\ \quad\ = 0, & \text{otherwise} \end{cases} \tag{3.7}$$

where $(g_1(t)\text{sign}(\Gamma_1 s_1(t)))_{eq}$, named equivalent output injection, is the average value of the discontinuous term in the sliding mode, which itself is enough to keep $\tilde{x}_1$ on the sliding manifold; i.e., $\dot{\tilde{x}}_1(t) = \tilde{x}_2(t) - (g_1(t)\text{sign}(\Gamma_1 s_1(t)))_{eq}$, when $\dot{\tilde{x}}_1(t) = 0$ and $\tilde{x}_1(t) = 0$, where $\tilde{x}_1(t) = x_1 - \hat{x}_1$ and $\tilde{x}_2 = x_2 - \hat{x}_2$ are defined as the state estimation

errors. The switching gain $g_1(t) = diag\{g_{1,1}, \cdots, g_{1,p}\}$ and $g_2(t) = diag\{g_{2,1}, \cdots, g_{2,p}\}$ are two diagonal matrices.

The principle of the anti-peaking structure is that the output estimation error is not used to construct the state estimation error before reaching the sliding manifold. Hence, the output estimation error $\tilde{x}_1$ reaches the sliding manifold prior to $\tilde{x}_2$. From (3.7), the state estimation error $\tilde{x}_2$ is constructed by using the equivalent output injection as

$$\tilde{x}_2(t) = (g_1(t)\text{sign}(\Gamma_1\tilde{x}_1(t)))_{eq} \tag{3.8}$$

after $\tilde{x}_1(t)$ reaches the sliding manifold.

Several methods have been proposed to compute the equivalent output injection. For example, Utkin *et al.* used a low pass filter to eliminate high frequency chattering [112], and others computed the equivalent output injection by adding a small positive number, δ, in the denominator of the discontinuous term [56]. In this chapter, we use the second method to obtain the equivalent output injection.

The dynamics of the observer can be written in a new vector form as

$$\begin{aligned} \dot{\hat{x}}(t) &= A\hat{x} + D\xi(\hat{x}, u, t) + G(t)\text{sign}(\Gamma S(t)) + \beta(t - T_m)\hat{M}(t) \\ \hat{y}(t) &= C\hat{x} \end{aligned} \tag{3.9}$$

where $G(t) = diag\{g_{1,1}(t), \cdots, g_{1,p}(t), g_{2,1}(t) \cdots, g_{2,p}(t)\}$ is the diagonal switching gain matrix. The equivalent state estimation errors are constructed into a new vector $S(t) = [s_1^\top(t),\ s_2^\top(t)]^\top$. The new matrix $\Gamma = diag\{\Gamma_1, \Gamma_2\}$ is still a positive definite matrix.

Defining $\tilde{y}(t) = y(t) - \hat{y}(t)$ as the output estimation error, we can derive the dynamics of the estimation error by subtracting (3.9) from (3.3) as follows:

$$\begin{aligned} \dot{\tilde{x}}(t) &= A\tilde{x}(t) + D(\xi(x, u, t) - \xi(\hat{x}, u, t)) + D\eta(x, u, t) - G(t)\text{sign}(\Gamma S) + \tilde{M}(t) \\ \tilde{y}(t) &= C\tilde{x}(t) \end{aligned} \tag{3.10}$$

where $\tilde{M}(t) = D\beta(t - T_f)f_a(t) - \beta(t - T_m)\hat{M}(t)$ is defined as the fault estimation error.

The estimation error dynamics (3.10) will be used in the property analysis of the proposed fault diagnosis scheme.

3.3.2 Fault Diagnosis Strategy Using a Diagnostic Observer

In model-based fault diagnosis methods, a residual is usually generated to diagnose faults. Due to the universal existence of system uncertainties and noise, robust fault diagnosis strategies are necessary to avoid a false alarm. One robust fault diagnosis approach uses a dead-zone operator in the learning algorithm, which leads the online estimators to specify only the signal with magnitude above a certain threshold [31]. However, this method reduces the accuracy of fault estimation. Another way to ensure robust fault diagnosis is to set a nonzero threshold for the residual when making diagnostic decisions. Adaptive or optimal threshold for timely fault diagnosis have been investigated [128], [129], [130], [131], [132], [133]. In previous work, designing an effective time-varying diagnostic threshold significantly depends on extensive prior knowledge of the system and faults. In practice, an *ad hoc* threshold is required for a specific problem.

In this chapter, the measurable output estimation error is used as the residual signal, and a constant threshold is set for robust fault diagnosis. After the sliding mode forces all the state estimation errors to reach the sliding manifold,

$$\begin{cases} \text{No fault has occured, and } \hat{M}_1(t), \hat{M}_2(t) \text{ are set to zero} & \text{if } \|\tilde{y}(t)\|_\lambda < \epsilon_\lambda \\ \text{A fault has occured, } \hat{M}_1(t), \hat{M}_2(t) \text{ are activated} & \text{if } \|\tilde{y}(t)\|_\lambda \geq \epsilon_\lambda \end{cases} \tag{3.11}$$

where $\|\tilde{y}(t)\|_\lambda$ is the λ-norm of $\tilde{y}(t)$, which is defined as $\|\tilde{y}(t)\|_\lambda = \sup_{t\in[T_0,t']} \mathrm{e}^{-\lambda t}\|\tilde{y}(t)\|$, where $\lambda > 0$, T_0 is defined in Section 3.4, and t' is the time when the proposed observer terminates. The term ϵ_λ is the threshold for robust fault detection. Since $\|\tilde{y}(t)\|_\lambda \leq \sup_{t\in[T_0,t']} \|\tilde{y}(t)\|$, a bound of $\|\tilde{y}(t)\|$ can be selected as the threshold.

In order to make the sliding mode term eliminate only the deviation in the system dynamics caused by uncertainties, the switching gain $G(t)$ is set to be upper bounded by G_0, i.e., $\|G(t)\| < G_0$. This issue will be discussed in more detail in the robustness analysis of this FD scheme, Section 3.4.1. The setting of the upper bound distinguishes the effect of faults from that of the system uncertainties. Moreover, the output of the online estimator $\hat{M}(t)$ is used to determine the location, and to estimate the magnitude of the faults.

In addition to the upper bound, the switching gain is supposed to have a lower

bound, which is the minimum gain to guarantee the sliding motion prior to the occurrence of any fault. The lower bound of the switching gain is discussed in the stability analysis of this fault diagnosis scheme, Section 3.5.2. Based on the above analysis, under the guarantee of sliding motion, the switching gain needs to be reduced as much as possible in order to increase the sensitivity to a fault. In numerical computation, the switching gain is set as the lower bound when the state estimation errors reach zero by using a sliding mode in the original regulation phase.

3.3.3 Sliding Mode Gain Design Using an Iterative Learning Algorithm

For sliding mode observers, a larger switching gain can enable the state estimation errors to approach the sliding manifold more quickly, but it may also cause unnecessary high-frequency chattering. Furthermore, since the sliding mode term in the diagnostic observer is used only to eliminate the effect of system uncertainties, the switching gain can not be too large because, in that case, the effect of faults will also be destroyed by the sliding mode. On the contrary, when a fault occurs, the sliding motion should be destroyed immediately, and then the online fault estimator should specify the fault as soon as possible. Therefore, a time-varying switching gain is more desirable for the purpose of our study.

Adaptation laws for the switching gain of sliding mode controllers were investigated in [124], [126]. In this section, two iterative methods are designed to update the switching gain of the proposed sliding mode observer.

A Proportional-type (*P-type*) iterative learning update law is first proposed to update the switching gain as follows:

$$G_{k+1}(t) = G_k(t) + \Phi(t)|\bar{S}_k(t)|\text{sign}(\bar{S}_k(t)\bar{S}_{k-1}(t)) \tag{3.12}$$

where the diagonal matrix $\bar{S} = diag\{s_{1,1}, \cdots, s_{1,p}, s_{2,1}, \cdots, s_{2,p}\}$ is defined for the updating of the switching gain, and k indicates the kth iteration at time t. $\Phi(t) \in \Re^{n\times n}$ is a positive definite iterative learning coefficient matrix which determines the rate of adaptation. The operator $|\cdot|$ takes the absolute value of each element of a

vector or a matrix.

From the adaptation law (3.12), we see that if the state estimation error has not reached the sliding manifold (the switching gain should be larger), the element of $\text{sign}(\bar{S}_k(t)\bar{S}_{k-1}(t))$ is +1, and the switching gain will increase correspondingly. If the state estimation error crosses the sliding manifold (the switching gain should be reduced), the element of $\text{sign}(\bar{S}_k(t)\bar{S}_{k-1}(t))$ is -1, and the gain will decrease correspondingly.

The purpose of the iterative learning update law (3.12) is to search for an optimal switching gain $G^*(t)$ at each time t which can sufficiently minimize the state estimation error. The convergence property of this iterative learning update law (3.12) is analyzed in the following theorem.

Theorem 3.1 *If the inequality (3.17) holds, the update law (3.12) for the sliding mode switching gain is convergent.*

Proof: Subtracting G^* from both sides of (3.12) yields

$$\Delta G_{k+1} = \Delta G_k - \Phi|\bar{S}_k|\text{sign}(\bar{S}_k\bar{S}_{k-1}) \tag{3.13}$$

where G^* is the optimal gain which makes the state estimation error exactly reach the sliding manifold. We define $\Delta G_k = G^* - G_k$. Taking the inner product on both sides of (3.13) with themselves via Φ^{-1}, we obtain

$$\begin{aligned} \Delta G_{k+1}^\top \Phi^{-1} \Delta G_{k+1} &= \Delta G_k^\top \Phi^{-1} \Delta G_k + |\bar{S}_k|^\top \Phi |\bar{S}_k| \\ &\quad -2\Delta G_k^\top |\bar{S}_k| \text{sign}(\bar{S}_k\bar{S}_{k-1}). \end{aligned} \tag{3.14}$$

Integrating both sides of (3.14) over the time interval [0, t] results in

$$\begin{aligned} \|\Delta G_{k+1}\|^2_{\Phi^{-1}} &= \|\Delta G_k\|^2_{\Phi^{-1}} + \|\bar{S}_k\|^2_\Phi \\ &\quad -2\int_0^t \Delta G_k^\top(\tau)|\bar{S}_k(\tau)|\text{sign}(\bar{S}_k(\tau)\bar{S}_{k-1}(\tau))d\tau \\ &= \|\Delta G_k\|^2_{\Phi^{-1}} + \|\bar{S}_k\|^2_\Phi - 2\int_0^t |\Delta G_k^\top(\tau)||\bar{S}_k(\tau)|d\tau \end{aligned} \tag{3.15}$$

where $\|\cdot\|_{\Phi^{-1}}$ is defined as

$$\|\Delta G_k\|_{\Phi^{-1}} = \left\{ \int_0^t \Delta G_k^\top(\tau)\Phi^{-1}\Delta G_k(\tau)d\tau \right\}^{1/2}. \tag{3.16}$$

If the estimation error dynamics satisfies dissipativity; i.e., a positive constant α exists such that

$$\begin{aligned} \int_0^t |\Delta G_k^\top(\tau)||\bar{S}_k(\tau)|d\tau &\geq \int_0^t \Delta G_k^\top(\tau)\bar{S}_k(\tau)d\tau \\ &\geq \frac{1+\alpha}{2}\int_0^t \bar{S}_k(\tau)^\top\Phi\bar{S}_k(\tau)d\tau \\ &= \frac{1+\alpha}{2}\|\bar{S}_k\|_\Phi^2, \end{aligned} \tag{3.17}$$

then, from (3.15), we have

$$\|\Delta G_{k+1}\|_{\Phi^{-1}}^2 \leq \|\Delta G_k\|_{\Phi^{-1}}^2 - \alpha\|\bar{S}_k\|_\Phi^2. \tag{3.18}$$

This inequality implies that the sequence $\{\|\Delta G_k\|_{\Phi^{-1}}\}$ will monotonously decrease with increasing k as long as $\|\bar{S}_k\|_\Phi$ is nonzero. Because $\{\|\Delta G_k\|_{\Phi^{-1}}\}$ is bounded from below, the monotonous decrease of $\{\|\Delta G_k\|_{\Phi^{-1}}\}$ means $\|\bar{S}_k\|_\Phi \to 0$ as $k \to \infty$. Thus, $G_k(t) \to G^*(t)$ as $k \to \infty$, that is, the iterative learning update law is convergent. ∎

The inequality (3.17) is generated by choosing a suitable iterative learning coefficient matrix $\Phi(t)$. Normally, a small $\Phi(t)$ results in a steadily but slowly converging process. A large $\Phi(t)$ leads to a fast convergence, while the iterative learning process may be unstable. In practice, $\Phi(t)$, for increasing the switching gain, can be set to a different value than $\Phi(t)$ for decreasing the switching gain.

In the ideal case, the optimal switching gain at each time t is obtained through iteratively updating the switching gain to drive $\bar{S}_k(t)$ to the sliding manifold. In practical computation, a maximum iteration number is set to prevent overtime updating. The maximum iteration number is usually set to a large value in order to guarantee the convergence of the switching gain to its optimal value.

3.3.4 Sliding Mode Gain Design Using an Iterative Fuzzy Model

In the above *P-type* iterative learning update algorithm, because the coefficient matrix $\Phi(t)$ is held constant during the increasing or decreasing updating of the switching gain, reaching the optimal value of the gain may take more iterations. In order to obtain better performance, we consider using an iterative fuzzy model to update the coefficient matrix $\Phi(t)$ via the following update law:

$$G_{i,i}(k+1) = G_{i,i}(k) + \Phi_{i,i}(k)|\bar{S}_{i,i}(k)| \tag{3.19}$$

where k still denotes iteration number, and the subscript (i,i) represents the ith diagonal element of a matrix.

According to the analysis in Section 3.3.3, when tuning the switching gain, we need to consider the magnitude of the estimation error, as well as its position relative to the sliding manifold. Therefore, according to the principle of the iterative learning algorithm (3.12), we determine $\Phi_{i,i}(k)$ based on the values of $\bar{S}_{i,i}(k-1)$ and $\bar{S}_{i,i}(k)$.

We first define the inputs of the fuzzy model as $inp_1 = \bar{S}_{i,i}(k-1)$ and $inp_2 = \bar{S}_{i,i}(k)$. Then, in fuzzification of these two inputs, we map the crisp values of $\bar{S}_{i,i}(k-1)$ and $\bar{S}_{i,i}(k)$ into several fuzzy sets: NL, NB, NM, NS, PS, PM, PB, and PL, where N stands for negative, P positive, L large, B big, M medium, and S small. The membership functions for these fuzzy sets are shown in Figure 3.1.

In Figure 3.1, the triangular membership functions are used to separately map the $\bar{S}_{i,i} > 0$ and $\bar{S}_{i,i} < 0$ into two groups of fuzzy sets, because $\Delta G_{i,i}$ should be different when $\text{sign}(\bar{S}_{i,i}(k-1))\text{sign}(\bar{S}_{i,i}(k)) < 0$ and $\text{sign}(\bar{S}_{i,i}(k-1))\text{sign}(\bar{S}_{i,i}(k)) > 0$.

A fuzzy linguistic model (Mamdani model), shown in Table 3.1, is designed, where rule n is denoted as

$$R_n: \quad \textbf{If } inp_1 \text{ is } A_{1,n} \textbf{ and } inp_2 \text{ is } A_{2,n}, \textbf{ then } \Phi_{i,i}(k) \text{ is } \bar{\Phi}^n_{i,i} \tag{3.20}$$

where R_n denotes the nth rule, $n = 1, \cdots, N_r$, and N_r is the number of rules. $A_{m,n}$ and $\bar{\Phi}^n_{i,i}$ are fuzzy sets described by membership functions $\mu_{A_{m,n}}(inp_m) :\rightarrow [0,\ 1]$ and $\mu_{\bar{\Phi}_m} :\rightarrow [0,\ 1]$.

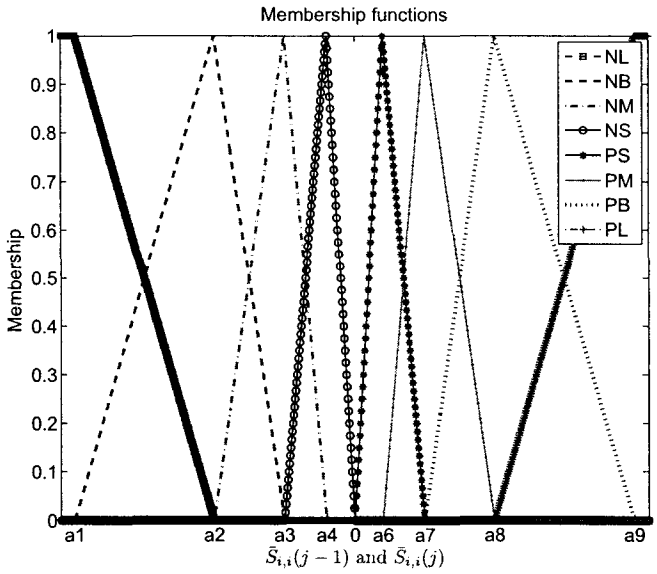

Figure 3.1: Membership functions for fuzzification of $\bar{S}_{i,i}(k-1)$ and $\bar{S}_{i,i}(k)$

Table 3.1: Fuzzy rule base for the coefficient gain $\bar{\Phi}^n_{i,i}$

$\bar{S}_{i,i}(k-1) \setminus \bar{S}_{i,i}(k)$	NL	NB	NM	NS	PS	PM	PB	PL
NL	Φ_{PL}	Φ_{PB}	Φ_{PM}	Φ_{PS}	Φ_{NS}	Φ_{NM}	Φ_{NB}	Φ_{NL}
NB	Φ_{PL}	Φ_{PB}	Φ_{PM}	Φ_{PS}	Φ_{NS}	Φ_{NM}	Φ_{NB}	Φ_{NL}
NM	Φ_{PL}	Φ_{PB}	Φ_{PM}	Φ_{PS}	Φ_{NS}	Φ_{NM}	Φ_{NB}	Φ_{NL}
NS	Φ_{NL}	Φ_{NB}	Φ_{NM}	Φ_{NS}	Φ_{NS}	Φ_{NM}	Φ_{NB}	Φ_{NL}
PS	Φ_{NL}	Φ_{NB}	Φ_{NM}	Φ_{NS}	Φ_{NS}	Φ_{NM}	Φ_{NB}	Φ_{NL}
PM	Φ_{NL}	Φ_{NB}	Φ_{NM}	Φ_{NS}	Φ_{PS}	Φ_{PM}	Φ_{PB}	Φ_{PL}
PB	Φ_{NL}	Φ_{NB}	Φ_{NM}	Φ_{NS}	Φ_{PS}	Φ_{PM}	Φ_{PB}	Φ_{PL}
PL	Φ_{NL}	Φ_{NB}	Φ_{NM}	Φ_{NS}	Φ_{PS}	Φ_{PM}	Φ_{PB}	Φ_{PL}

Then, an inference mechanism is used to calculate the degree to which each rule fires for a given fuzzified input pattern (inp_1, inp_2) by considering the label sets and rule. A rule is considered to fire when the conditions upon which it depends occur. Since these conditions are defined by fuzzy sets which have degrees of membership, a rule will have a degree of firing, called *firing strength*, ω_n. In this work, the firing strength is calculated by the product of the degrees of membership; that is,

$$\omega_n = \prod_{m=1}^{2} \mu_{A_{m,n}}(inp_m). \tag{3.21}$$

Finally, a defuzzifier converts the resulting fuzzy sets defined by the inference mechanism to the output of the model to a standard crisp signal. Here, we use the center-of-gravity, or *centroid*, method to calculate $\Phi_{i,i}(k)$ as follows:

$$\Phi_{i,i}(k) = \frac{\sum_{n=1}^{N_r} \omega_n \bar{\Phi}_{i,i}^n}{\sum_{n=1}^{N_r} \omega_n}. \tag{3.22}$$

Actually, the centroid method of defuzzification takes a weighted sum of the designated consequences of the rules based on the firing strengths of the rules.

Remark 3.3 *Comparing the iterative learning algorithm (3.12) and (3.19), clearly (3.12) is equivalent to a Proportional-type controller with a constant coefficient, whereas (3.19) is equivalent to a coefficient-varying Proportional-type controller. Therefore, based on the performance of different Proportional-type controllers, if the coefficient matrix is carefully updated, the switching gain will take less time to reach an optimal value when it is updated by the iterative fuzzy model.*

3.4 Properties of the Fault Diagnosis Scheme

The purpose of this section is to obtain some theoretical guarantees with respect to the robustness and sensitivity of the proposed observer-based fault diagnosis scheme.

3.4.1 Robustness Analysis

Robustness of a fault diagnosis scheme refers to its ability to prevent a false alarm in the presence of system uncertainties. As for the robust FD scheme described above, its robustness is achieved by setting a threshold on the generated residual.

Based on Assumption 3.3, we consider the time interval between the first-time observation of states by using a sliding mode and the occurrence of any fault; i.e., $t \in [T_0, T_x)$, where T_0 denotes the time that all states have been estimated via the sliding mode in the initial regulation phase, and T_x refers to the onset time of an additive state fault. The finite-time convergence of the state estimation errors to zero via the sliding mode will be given in Section 3.4.2. Regarding the robustness of this fault diagnosis scheme, we have the following theorem.

Theorem 3.2 *The proposed robust fault diagnosis scheme guarantees that* $\|\tilde{y}(t)\|_\lambda < \epsilon_\lambda$, *when* $T_0 < t < T_x$.

Proof: Using a contradiction method [31], we suppose that a time t_e exists (where $T_0 < t_e < T_x$) such that $\|\tilde{y}(t)\|_\lambda < \epsilon_\lambda$ for $T_0 < t < t_e$ and

$$\|\tilde{y}(t_e)\|_\lambda = \epsilon_\lambda. \tag{3.23}$$

After the occurrence of a sliding motion in the initial regulation phase and prior to any fault, the dynamics of the estimation error are

$$\begin{aligned} \dot{\tilde{x}}(t) &= A\tilde{x}(t) + D(\xi(x,u,t) - \xi(\hat{x},u,t)) + D\eta(t) - G(t)\text{sign}(\Gamma S) \\ \tilde{y}(t) &= C\tilde{x}(t), \qquad\qquad \tilde{x}(T_0) = 0. \end{aligned} \tag{3.24}$$

By solving the differential equation (3.24), we obtain

$$\begin{aligned} \tilde{x}(t_e) &= \mathrm{e}^{A(t_e-T_0)}\tilde{x}(T_0) + \int_{T_0}^{t_e} \mathrm{e}^{A(t_e-\tau)}\Big(D(\xi(x,\tau) - \xi(\hat{x},\tau)) \\ &\quad + D\eta(\tau) - G(\tau)\text{sign}(\Gamma S(\tau))\Big)d\tau \\ &= \int_{T_0}^{t_e} \mathrm{e}^{A(t_e-\tau)}\Big(D(\xi(x,\tau) - \xi(\hat{x},\tau)) + D\eta(\tau) \\ &\quad - G(\tau)\text{sign}(\Gamma S(\tau))\Big)d\tau, \end{aligned} \tag{3.25}$$

and

$$\begin{aligned}\|\tilde{x}(t_e)\| &\leq \int_{T_0}^{t_e} \|\mathrm{e}^{A(t_e-\tau)}\| \Big(\|D\| \|\xi(x) - \xi(\hat{x})\| + (\|D\|\eta_0 + \|G\|) \Big) d\tau \\ &< \int_{T_0}^{t_e} k_3 \|\tilde{x}(\tau)\| d\tau + l \end{aligned} \tag{3.26}$$

where $k_3 = k\|D\| \sup_{\tau\in[0,t'-T_0]} \|\mathrm{e}^{A\tau}\|$, and

$$l = (\|D\|\eta_0 + \|G\|) \int_0^{\infty} \|\mathrm{e}^{At}\| dt. \tag{3.27}$$

The terms k_3 and l are both finite numbers because matrix A is stable, and $\|D\|$ and $\|G\|$ are finite values.

Using the Gronwall Lemma, we have

$$\|\tilde{x}(t_e)\| < l\, \mathrm{e}^{k_3(t_e-T_0)}. \tag{3.28}$$

Multiplying $\mathrm{e}^{-\lambda t}$ on both sides of (3.28), and taking $\lambda > (t_e/T_0 - 1)k_3$, we obtain

$$\mathrm{e}^{-\lambda t}\|\tilde{x}(t_e)\| < l\, \mathrm{e}^{-\lambda t + k_3 t_e - k_3 T_0}. \tag{3.29}$$

Taking the supremum on both sides of the above inequality, we obtain

$$\|\tilde{x}(t_e)\|_\lambda \;<\; l. \tag{3.30}$$

Therefore, the output estimation error is

$$\|\tilde{y}(t_e)\|_\lambda < \|C\|_\lambda l = \epsilon_\lambda, \tag{3.31}$$

which contradicts (3.23). Thus, we concluded that for all $T_0 < t < T_x$, the output estimation error $\tilde{y}(t)$ remains within the bound ϵ_λ, and, consequently, the outputs of the fault estimators remain zero. ∎

Moreover, in order to keep $\|\tilde{y}(t)\|_\lambda < \epsilon_\lambda$ during the period before any fault, the upper bound of the switching gain $G(t)$ is set to

$$G_0 = \frac{\epsilon_\lambda}{\|C\|_\lambda \int_0^{\infty} \|\mathrm{e}^{At}\| dt} - \|D\|\eta_0. \tag{3.32}$$

Using the proposed diagnostic observer, the threshold is chosen only according to the characteristics of the system, and it is not affected by the initial estimation error. Moreover, using sliding mode, the threshold for fault diagnosis can be chosen smaller than a system that does not use sliding mode.

3.4.2 Sensitivity Analysis

Not only does the fault diagnosis system need to be robust against the system uncertainties, but it should also be sensitive to any fault. However, an inherent tradeoff exists between the robustness and sensitivity of the fault diagnosis scheme because high sensitivity to faults may reduce the robustness to system uncertainties. The sensitivity property in this thesis specifies the set of faults that can be reliably detected, and it focuses on the characteristics of the fault diagnosis scheme in the time interval between the occurrence of a fault and the time of its detection.

Theorem 3.3 *Consider the fault diagnosis scheme presented by (3.6). If a time interval $t_x > 0$ exists such that the state fault $f_a(t)$ satisfies*

$$\left\| \int_{T_x}^{T_x+t_x} e^{A(T_x+t_x-\tau)} D f_a(\tau) d\tau \right\| \geq 2l, \tag{3.33}$$

then the fault estimator $\hat{M}(t)$ will be activated to approximate the fault, that is, $\|\tilde{y}(T_x + t_x)\| \geq \epsilon_\lambda$.

Proof: In the time interval between the occurrence of a state fault and the adaptation of the fault estimator $\hat{M}(t)$, the dynamics of the estimation error satisfy

$$\begin{aligned} \dot{\tilde{x}}(t) &= A\tilde{x}(t) + D(\xi(x,u,t) - \xi(\hat{x},u,t)) + D\eta(t) - G(t)\text{sign}(\Gamma S) + Df_a(t) \\ \tilde{y}(t) &= C\tilde{x}(t). \end{aligned} \tag{3.34}$$

Solving (3.34) for any $t_x > 0$ gives

$$\begin{aligned} \tilde{x}(T_x + t_x) &= \int_{T_0}^{T_x+t_x} \mathrm{e}^{A(T_x+t_x-\tau)} \Big[D(\xi(x) - \xi(\hat{x})) + D\eta(\tau) - G(\tau)\text{sign}(\Gamma S(\tau)) \Big] d\tau \\ &\quad + \int_{T_x}^{T_x+t_x} \mathrm{e}^{A(T_x+t_x-\tau)} D f_a(\tau) d\tau. \end{aligned} \tag{3.35}$$

Then using the triangle inequality on (3.35), we obtain

$$\begin{aligned}\|\tilde{x}(T_x+t_x)\| &\leq \int_{T_0}^{T_x+t_x} \left\|e^{A(T_x+t_x-\tau)}\right\| \|D\| \|\xi(x)-\xi(\hat{x})\| d\tau \\ &\quad + \int_{T_0}^{T_x+t_x} \left\|e^{A(T_x+t_x-\tau)}\right\| (\|G\|+\|D\|\eta_0) d\tau \\ &\quad + \left\| \int_{T_x}^{T_x+t_x} e^{A(T_x+t_x-\tau)} D f_a(\tau) d\tau \right\| \\ &\leq \int_{T_0}^{T_x+t_x} k_3 \|\tilde{x}(\tau)\| d\tau + l + \left\| \int_{T_x}^{T_x+t_x} e^{A(T_x+t_x-\tau)} D f_a(\tau) d\tau \right\| \quad (3.36)\end{aligned}$$

Using the Gronwall inequality again, we obtain

$$\|\tilde{x}(T_x+t_x)\| \leq \left(l + \left\| \int_{T_x}^{T_x+t_x} e^{A(T_x+t_x-\tau)} D f_a(\tau) d\tau \right\| \right) e^{k_3(T_x+t_x-T_0)}. \quad (3.37)$$

Computing λ-norm on both sides of (3.37), when $\lambda > k_3$, we have

$$\|\tilde{x}(T_x+t_x)\|_\lambda \leq \left\| \int_{T_x}^{T_x+t_x} e^{A(T_x+t_x-\tau)} D f_a(\tau) d\tau \right\| + l. \quad (3.38)$$

According to the basic property of matrix norm, we have

$$\begin{aligned}\|\tilde{y}(T_x+t_x)\|_\lambda &\leq \|C\|_\lambda \|\tilde{x}(T_x+t_x)\|_\lambda \\ &\leq \|C\|_\lambda \left\| \int_{T_x}^{T_x+t_x} e^{A(T_x+t_x-\tau)} D f_a(\tau) d\tau \right\| + \epsilon_\lambda. \quad (3.39)\end{aligned}$$

We use the triangle inequality again, and obtain

$$\|\tilde{y}(T_x+t_x)\|_\lambda \geq \|C\|_\lambda \left\| \int_{T_x}^{T_x+t_x} e^{A(T_x+t_x-\tau)} D f_a(\tau) d\tau \right\| - \epsilon_\lambda. \quad (3.40)$$

Therefore, if the nonlinear fault function satisfies (3.33), then $\|\tilde{y}(T_x+t_x)\|_\lambda \geq \epsilon_\lambda$, which implies the online fault estimators will be activated, and the state faults are detected correspondingly. ∎

3.5 Fault Isolation and Estimation Using Neural State Space Models

3.5.1 Fault Estimator Design Using Neural State Space Models

Neural state space (NSS) models have been investigated for system modeling and control in [105], [106], [107], and [108]. Inherently, being recurrent neural networks, the NSS models not only have similar nonlinear approximation abilities as feed-forward neural networks, but they also have state-space-like structures, which may bring convenience to the theoretical analysis.

Based on NSS models, the fault estimators are designed as

$$\begin{aligned}\dot{\hat{M}}_{1,i}(t) &= \hat{W}_{1,i}^{(1)}\hat{M}_{1,i}(t) + \hat{W}_{1,i}^{(2)}(t)\sigma\big(\hat{W}_{1,i}^{(3)}(t)\hat{M}_{1,i}(t) + \hat{W}_{1,i}^{(4)}(t)\tilde{x}_{1,i}(t)\big)\\ \dot{\hat{M}}_{2,i}(t) &= \hat{W}_{2,i}^{(1)}\hat{M}_{2,i}(t) + \hat{W}_{2,i}^{(2)}(t)\sigma\big(\hat{W}_{2,i}^{(3)}(t)\hat{M}_{2,i}(t) + \hat{W}_{2,i}^{(4)}(t)s_{2,i}(t)\big)\end{aligned} \tag{3.41}$$

where $i = 1, \cdots, p$, and $\hat{W}_{i,j}^{(l)}$, $(i = 1, 2; j = 1, \cdots, p; l = 1, \cdots, 4)$ are the parameters of the ith NSS models. The activation function is set to be a tangent hyperbolic function, i.e.,

$$\sigma(z) = \frac{1 - e^{-z}}{1 + e^{-z}}. \tag{3.42}$$

The parameters of a NSS model can be updated by many optimization algorithms that are usually used for neural networks. Here, an extended Kalman filter (EKF)-like algorithm is used to update the parameters in $\hat{M}_1(t)$ and $\hat{M}_2(t)$, respectively.

$$K_{1,i}(t) = P_{1,i}(t)H_{1,i}(t)\left[H_{1,i}(t)^{\top}P_{1,i}(t)H_{1,i}(t) + R_{1,i}(t)\right]^{-1} \tag{3.43}$$

$$\dot{P}_{1,i}(t) = -\mathcal{B}_{1,i}^{(1)}K_{1,i}(t)H_{1,i}^{\top}(t)P_{1,i}(t) \tag{3.44}$$

$$\dot{\hat{W}}_{1,i}(t) = \mathcal{B}_{1,i}^{(2)}K_{1,i}(t)\tilde{x}_{1,i}(t) \tag{3.45}$$

and

$$K_{2,i}(t) = P_{2,i}(t)H_{2,i}(t)\left[H_{2,i}(t)^{\top}P_{2,i}(t)H_{2,i}(t) + R_{2,i}(t)\right]^{-1} \tag{3.46}$$

$$\dot{P}_{2,i}(t) = -\mathcal{B}_{2,i}^{(1)}K_{2,i}(t)H_{2,i}^{\top}(t)P_{2,i}(t) \tag{3.47}$$

$$\dot{\hat{W}}_{2,i}(t) = \mathcal{B}_{2,i}^{(2)}K_{2,i}(t)s_{2,i}(t) \tag{3.48}$$

where $K_{1,i}, K_{2,i} \in \Re^p$ are the Kalman gain matrices, $P_{1,i}, P_{2,i} \in \Re^{p\times p}$ are the covariance matrix of the state estimation error, and $H_{1,i}, H_{2,i} \in \Re^p$ are defined as

$$H_{1,i}(t) = \frac{\partial \hat{x}_{1,i}(t)}{\partial \hat{W}_{1,i}}, \tag{3.49}$$

$$H_{2,i}(t) = \frac{\partial \hat{x}_{2,i}(t)}{\partial \hat{W}_{2,i}}. \tag{3.50}$$

The terms $\mathcal{B}_{1,i}^{(1)}$, $\mathcal{B}_{1,i}^{(2)}$, $\mathcal{B}_{2,i}^{(1)}$, and $\mathcal{B}_{2,i}^{(2)}$ are four $p \times p$ diagonal coefficient matrices whose elements are positive update rates. The scalar $R_{1,i}$ and $R_{2,i}$ are the estimated covariance of measurement noise. For single-input and single-output systems, $R_{1,i}$ and $R_{2,i}$ can be estimated in a similar way to that in [134], i.e.,

$$\dot{R}_{1,i} = \frac{e_{1,i}^2(t) - R_{1,i}(t)}{t} \tag{3.51}$$

$$\dot{R}_{2,i} = \frac{e_{2,i}^2(t) - R_{2,i}(t)}{t} \tag{3.52}$$

where $e_{1,i}(t) = \tilde{x}_{1,i}(t) - \hat{M}_{1,i}(t)$, and $e_{2,i}(t) = s_{2,i}(t) - \hat{M}_{2,i}(t)$.

The convergence of this EKF-like algorithm is analyzed in the following theorem.

Theorem 3.4 *The parameter update algorithm (3.43) - (3.45) is convergent, provided that $P_{1,i}$ is a positive definite matrix.*

Proof: If $P_{1,i}(t)$ holds positive definite, the following inequality can be guaranteed,

$$H_{1,i}(t)^\top P_{1,i}(t) H_{1,i}(t) > 0. \tag{3.53}$$

Since, for SISO systems, $R_{1,i}(t)$ is the estimated variance of noise, it is nonnegative for all time. Hence, with (3.53) we have

$$0 < H_{1,i}(t)^\top P_{1,i}(t) H_{1,i}(t) < H_{1,i}(t)^\top P_{1,i}(t) H_{1,i}(t) + R_{1,i}(t). \tag{3.54}$$

Consider a positive Lyapunov function candidate:

$$V(t) = \frac{1}{2}\tilde{x}_{1,i}^2(t). \tag{3.55}$$

The derivative of (3.55) with respect to time t is

$$\begin{aligned}\dot{V}(t) &= \dot{\tilde{x}}_{1,i}\tilde{x}_{1,i} \\ &= \left(\frac{\partial \tilde{x}_{1,i}}{\partial \hat{W}_{1,i}}\right)^{\top}\frac{\partial \hat{W}_{1,i}}{\partial t}\tilde{x}_{1,i} \\ &= -H_{1,i}^{\top}\mathcal{B}_{1,i}^{(2)}K_{1,i}\tilde{x}_{1,i}^{2} \\ &= -H_{1,i}^{\top}\mathcal{B}_{1,i}^{(2)}P_{1,i}H_{1,i}\left[H_{1,i}^{\top}P_{1,i}H_{1,i}+R_{1,i}\right]^{-1}\tilde{x}_{1,i}^{2}. \end{aligned} \tag{3.56}$$

Therefore, if $P_{1,i}(t)$ remains positive definite for all time, then $\dot{V}(t) < 0$, which implies the state estimation error $\tilde{x}_{1,i}$ will converge to zero. ∎

In numerical computation, the guarantee of (3.53) for all time is not an easy task. Usually, $P_{1,i}$ and $P_{2,i}$ are set to large diagonal matrices, and $R_{1,i}$ and $R_{2,i}$ are set to small numbers in order to hold $R_{1,i} > 0$ and $R_{2,i} > 0$, and to prevent the denominators in (3.43) and (3.46) from being zero. Moreover, pre-training of the NSS models is necessary in order to achieve satisfactory estimation accuracy.

3.5.2 Stability Analysis

In this section, we explore the stability of the proposed fault diagnosis scheme. Prior to any fault, only the sliding mode observer works to estimate the state of the system. Therefore, the dynamics of the state estimation error before the occurrence of any fault are given by

$$\dot{\tilde{x}}_1 = \tilde{x}_2 - g_1(t)\text{sign}(\Gamma_1\tilde{x}_1) \tag{3.57}$$

$$\dot{\tilde{x}}_2 = A_{21}\tilde{x}_1 + A_{22}\tilde{x}_2 + \xi(x_1,x_2) - \xi(\hat{x}_1,\hat{x}_2) + \eta(t) - g_2(t)\text{sign}(\Gamma_2 s_2). \tag{3.58}$$

Regarding the stability of (3.57) and (3.58), we have the following theorem.

Theorem 3.5 *If the system (3.1) satisfies Assumptions 3.1-3.4, and the following inequalities are guaranteed*

$$\lambda_{\min}(Q) > 2k_2\|\Gamma_2\| \tag{3.59}$$

$$\lambda_{\min}(g_1(t)) > \|\tilde{x}_2\| \tag{3.60}$$

$$\lambda_{\min}(g_2(t)) > \eta_0 \tag{3.61}$$

where Q is defined in Assumption 3.4, then the proposed observer can estimate the states of the system in finite time, i.e., the state estimation error $\tilde{x}(t)$ asymptotically approach zero.

Proof: We first consider the dynamics of the output estimation error $\tilde{x}_1$, and design a Lyapunov function as

$$V_1 = \tilde{x}_1^\top \Gamma_1 \tilde{x}_1 \tag{3.62}$$

where Γ_1 was defined in Chapter 3.3.1.

Based on (3.57), computing the time derivative of V_1 with respect to time t gives

$$\begin{aligned} \dot{V}_1 &= \dot{\tilde{x}}_1^\top \Gamma_1 \tilde{x}_1 + \tilde{x}_1^\top \Gamma_1 \dot{\tilde{x}}_1 \\ &= (\tilde{x}_2 - g_1 \text{sign}(\Gamma_1 \tilde{x}_1))^\top \Gamma_1 \tilde{x}_1 + \tilde{x}_1^\top \Gamma_1 (\tilde{x}_2 - g_1 \text{sign}(\Gamma_1 \tilde{x}_1)) \\ &= 2(\Gamma_1 \tilde{x}_1)^\top \tilde{x}_2 - 2(\Gamma_1 \tilde{x}_1)^\top g_1 \text{sign}(\Gamma_1 \tilde{x}_1). \end{aligned} \tag{3.63}$$

By properly choosing $g_1(t)$ to satisfy $\lambda_{\min}(g_1(t)) > \|\tilde{x}_2\|$, we have $\dot{V}_1 < 0$, which means $\tilde{x}_1$ reaches the sliding manifold in a finite time t_1. Moreover, after t_1, we have

$$s_2 = (g_1 \text{sign}(\Gamma_1 s_1))_{eq} = \tilde{x}_2$$

and the dynamics of the state estimation error $\tilde{x}_2$ becomes

$$\dot{\tilde{x}}_2 = A_{22}\tilde{x}_2 + \xi(x_1, x_2) - \xi(\hat{x}_1, \hat{x}_2) + \eta(t) - g_2(t)\text{sign}(\Gamma_2 \tilde{x}_2). \tag{3.64}$$

Let us consider another Lyapunov function candidate:

$$V_2 = \tilde{x}_2^\top \Gamma_2 \tilde{x}_2 \tag{3.65}$$

where Γ_2 is defined in Assumption 3.4.

The time derivative of V_2 with respect to t is

$$\begin{aligned}
\dot{V}_2 &= \dot{\tilde{x}}_2^\top \Gamma_2 \tilde{x}_2 + \tilde{x}_2^\top \Gamma_2 \dot{\tilde{x}}_2 \\
&= \tilde{x}_2^\top A_{22}^\top \Gamma_2 \tilde{x}_2 + \tilde{x}_2^\top \Gamma_2 A_{22} \tilde{x}_2 \\
&\quad +2\tilde{x}_2^\top \Gamma_2 (\xi(x_1, x_2) - \xi(\hat{x}_1, \hat{x}_2)) + 2\tilde{x}_2^\top \Gamma_2 (\eta(t) - g_2 \text{sign}(\Gamma_2 \tilde{x}_2)) \\
&\leq \tilde{x}_2^\top (A_{22}^\top \Gamma_2 + \Gamma_2 A_{22}) \tilde{x}_2 + 2\|\tilde{x}_2^\top\| \|\Gamma_2\| (k_1 \|\tilde{x}_1\| + k_2 \|\tilde{x}_2\|) \\
&\quad +2\tilde{x}_2^\top \Gamma_2 (\eta(t) - g_2 \text{sign}(\Gamma_2 \tilde{x}_2)) \\
&= -\tilde{x}_2^\top Q \tilde{x}_2 + 2k_2 \|\Gamma_2\| \|\tilde{x}_2\|^2 + 2\tilde{x}_2^\top \Gamma_2 (\eta(t) - g_2 \text{sign}(\Gamma_2 \tilde{x}_2)) \\
&< -\rho \|\tilde{x}_2\|^2 + 2\tilde{x}_2^\top \Gamma_2 (\eta(t) - g_2 \text{sign}(\Gamma_2 \tilde{x}_2)) \qquad (3.66)
\end{aligned}$$

where $A_{22}^\top \Gamma_2 + \Gamma_2 A_{22} = -Q$ is the Lyapunov function defined in Assumption 3.4, and $\rho = \lambda_{\min}(Q) - 2k_2\|\Gamma_2\|$. Therefore, when the inequalities $\rho = \lambda_{\min}(Q) - 2k_2\|\Gamma_2\| > 0$ and $\lambda_{\min}(g_2) > \eta_0$ are satisfied, then $\tilde{x}_2$ goes to zero after finite time $t_2 > t_1$. ∎

From the above proof, it is concluded that for a class of systems, if the switching gains are properly chosen to guarantee (3.59) and (3.60), the proposed observer can estimate their states in finite time. This result implies that both the state estimation error and the output estimation error are zero or close to zero prior to the occurrence of any fault, which means the threshold for fault detection can be very small.

After a state fault occurs, the estimation error would first deviate from zero because the fault works as a new unknown input to the system. However, due to the compensation of the NSS models $\hat{M}_1(t)$ and $\hat{M}_2(t)$, theoretically, the state estimation error should return zero, if the NSS models can exactly specify the fault. In practice, due to the existence of fault estimation error, the state estimation error will not exactly be zero, but it will remain within a small bound.

After the occurrence of a state fault, the dynamics of the estimation error become

$$\dot{\tilde{x}}_1 = \tilde{x}_2 - g_1(t)\text{sign}(\Gamma_1 s_1) - \hat{M}_1(\hat{W}_1, \tilde{x}_1, t) \qquad (3.67)$$

$$\begin{aligned}
\dot{\tilde{x}}_2 &= A_{21}\tilde{x}_1 + A_{22}\tilde{x}_2 + \xi(x_1, x_2) - \xi(\hat{x}_1, \hat{x}_2) + \eta(t) - g_2(t)\text{sign}(\Gamma_2 s_2) \\
&\quad + f_a(t) - \hat{M}_2(\hat{W}_2, \tilde{x}_2, t). \qquad (3.68)
\end{aligned}$$

The stability of (3.67) and (3.68) is provided in the following theorem.

Theorem 3.6 *If system (3.1) satisfies Assumptions 3.1-3.4, the inequalities (3.59)-(3.61) are all satisfied, and the following conditions (3.69) and (3.70) are both guaranteed*

$$\lambda_{\min}(g_1(t)) > \|\tilde{x}_2\| + \delta_{M_1} \tag{3.69}$$

$$\Gamma_2 Z^\top = K_2^\top \mathcal{B}_2^{(2)} \Gamma_3 \tag{3.70}$$

then the state estimation error $\tilde{x}_2$ is uniformly bounded, where δ_{M_1}, Z, K_2, $\mathcal{B}_2^{(2)}$, and Γ_3 are defined in the following proof.

Proof: We first consider the convergence of $\tilde{x}_1$. From the above analysis, when $\hat{M}_1(t)$ is activated, $\tilde{x}_1$ is already zero by using the sliding mode. Moreover, $\hat{M}_1(t)$ is initialized to be zero. Therefore, $\hat{M}_1(t)$ can be assumed not to go to infinity in a finite time. In another words, $\hat{M}_1(t)$ is bounded by a finite number δ_{M_1}; i.e., $\|\hat{M}_1(t)\| < \delta_{M_1}$, within a finite time.

By still choosing the first Lyapunov function as $V_1 = \tilde{x}_1^\top \Gamma_1 \tilde{x}_1$, and computing its time derivative with respect to time t, we obtain

$$\begin{aligned}
\dot{V}_1(t) &= \dot{\tilde{x}}_1^\top \Gamma_1 \tilde{x}_1 + \tilde{x}_1^\top \Gamma_1 \dot{\tilde{x}}_1 \\
&= (\tilde{x}_2 - g_1(t)\text{sign}(\Gamma_1 s_1) - \hat{M}_1(t))^\top \Gamma_1 \tilde{x}_1 \\
&\quad + \tilde{x}_1^\top \Gamma_1 (\tilde{x}_2 - g_1(t)\text{sign}(\Gamma_1 s_1) - \hat{M}_1(t)) \\
&= 2(\Gamma_1 \tilde{x}_1)^\top (\tilde{x}_1 - \hat{M}_1) - 2(\Gamma_1 \tilde{x}_1)^\top g_1(t)\text{sign}(\Gamma_1 \tilde{x}_1).
\end{aligned} \tag{3.71}$$

When we choose $\lambda_{\min}(g_1) > \|\tilde{x}_2\| + \delta_{M_1}$, then $\dot{V}_1(t) < 0$, which implies $\tilde{x}_1$ converges to the sliding manifold in a finite time.

Based on the universal nonlinear approximation ability of NSS models, (3.68) can be rewritten as

$$\begin{aligned}
\dot{\tilde{x}}_2 &= A_{21}\tilde{x}_1 + A_{22}\tilde{x}_2 + \xi(x_1, x_2) - \xi(\hat{x}_1, \hat{x}_2) + \eta(t) - g_2(t)\text{sign}(\Gamma_2 s_2) \\
&\quad + \hat{M}_2(W_2^*, \tilde{x}_2, t) - \hat{M}_2(\hat{W}_2, \tilde{x}_2, t) + \upsilon_x(t)
\end{aligned} \tag{3.72}$$

where $\upsilon_x(t)$ denotes a network approximation error defined as

$$\upsilon_x(t) = f_a(t) - \hat{M}_2(W_2^*, \tilde{x}_2, t). \tag{3.73}$$

The *optimal* parameter W_2^* is selected such that the L_2-norm distance between $f_a(t)$ and $\hat{M}_2(W_2^*, \tilde{x}_2, t)$ is minimized. Note that the artificial parameter W_2^* is only used for the analysis and is not for the parameter design of the fault diagnosis scheme.

Assuming $\hat{M}_{2,i}(t)$ is a smooth function, we can formulate the ith NSS model as

$$\begin{aligned}\hat{M}_{2,i}(\hat{W}_{2,i}, \tilde{x}_{2,i}, t) &= \hat{M}_{2,i}(W_{2,i}^*, \tilde{x}_{2,i}, t) + \left(\frac{\partial \hat{M}_{2,i}}{\partial \hat{W}_{2,i}}\right)^\top (\hat{W}_{2,i} - W_{2,i}^*) + \hat{M}_{2,i}^0(\hat{W}_{2,i}, \tilde{x}_{2,i}, t) \\ &= \hat{M}_{2,i}(W_{2,i}^*, \tilde{x}_{2,i}, t) - Z_i^\top \tilde{W}_{2,i} + \hat{M}_{2,i}^0(\hat{W}_{2,i}, W_{2,i}^*, \tilde{x}_{2,i}, t) \qquad (3.74)\end{aligned}$$

where $\tilde{W}_{2,i} = W_{2,i}^* - \hat{W}_{2,i}$ is the parameter estimation error vector, $\hat{M}_{2,i}^0(\hat{W}_{2,i}, \tilde{x}_{2,i}, t)$ represents the higher order term of the Taylor series expansion of $\hat{M}_{2,i}(\hat{W}_{2,i}, \tilde{x}_{2,i}, t)$ with respect to $W_{2,i}^*$, and $Z_i \in \Re^p$ is the derivative of the ith NSS model output $\hat{M}_{2,i}$ with respect to its parameter vector $\hat{W}_{2,i}$; i.e., $Z_i = \frac{\partial \hat{M}_{2,i}}{\partial \hat{W}_{2,i}}$.

Based on (3.74), we have

$$\hat{M}_2(W_2^*, \tilde{x}_2, t) = \hat{M}_2(\hat{W}_2, \tilde{x}_2, t) + Z^\top \tilde{W}_2 - \hat{M}_2^0(\hat{W}_2, W_2^*, \tilde{x}_2, t) \qquad (3.75)$$

where $\hat{M}_{2,i}(W_{2,i}^*, \tilde{x}_{2,i}, t)$, $\hat{M}_{2,i}(\hat{W}_{2,i}, \tilde{x}_{2,i}, t)$, and $\hat{M}_{2,i}^0(\hat{W}_{2,i}, W_{2,i}^*, \tilde{x}_{2,i}, t)$ are the ith element of the vectors $\hat{M}_2(W_2^*, \tilde{x}_2, t)$, $\hat{M}_2(\hat{W}_2, \tilde{x}_2, t)$ and $\hat{M}_2^0(W_2^*, \hat{W}_2, \tilde{x}_2, t)$, respectively. The matrix $Z = diag\{Z_1, \cdots, Z_p\} \in \Re^{p^2 \times p}$, and $\tilde{W}_2 = [\tilde{W}_{2,1}^\top, \cdots, \tilde{W}_{2,p}^\top]^\top \in \Re^{p^2}$.

By substituting (3.75) into (3.72), we obtain

$$\begin{aligned}\dot{\tilde{x}}_2 &= A_{21}\tilde{x}_1 + A_{22}\tilde{x}_2 + \xi(x_1, x_2) - \xi(\hat{x}_1, \hat{x}_2) + \eta(t) - g_2(t)\text{sign}(\Gamma_2 s_2) \\ &\quad + Z^\top \tilde{W}_2 + \bar{v}_x(t) \qquad (3.76)\end{aligned}$$

where $\bar{v}_x(t) = v_x(t) - \hat{M}_2^0$ is comprised of a network approximation error and a higher order term. Based on the properties of NSS models, $\bar{v}_x(t)$ is bounded by a finite number.

Based on (3.48), we can obtain

$$\dot{\tilde{W}}_2 = -\dot{\hat{W}}_2 = -\mathcal{B}_2^{(2)} K_2 \tilde{x}_2 \qquad (3.77)$$

where $\mathcal{B}_2^{(2)} = diag\{\mathcal{B}_{2,1}^{(2)}, \cdots, \mathcal{B}_{2,p}^{(2)}\} \in \Re^{p^2 \times p^2}$, and $K_2 = diag\{K_{2,1}, \cdots, K_{2,p}\} \in \Re^{p^2 \times p}$.

The second Lyapunov function is defined as

$$V_2 = \tilde{x}_2^\top \Gamma_2 \tilde{x}_2 + \tilde{W}_2^\top \Gamma_3 \tilde{W}_2 \qquad (3.78)$$

where $\Gamma_3 \in \Re^{p^2 \times p^2}$ is also a symmetric positive definite matrix to be determined.

Based on (3.70), (3.76), and (3.77), the derivative of V_2 with respect to t is

$$\begin{aligned}
\dot{V}_2 &= \tilde{x}_2^\top (A_{22}^\top \Gamma_2 + \Gamma_2 A_{22})\tilde{x}_2 + 2\tilde{x}_2^\top \Gamma_2 (\xi(x_1, x_2) - \xi(\hat{x}_1, \hat{x}_2)) \\
&\quad + 2\tilde{x}_2^\top \Gamma_2 (\eta(t) + \bar{v}_x(t) - g_2(t)\text{sign}(\Gamma_2 \tilde{x}_2)) + 2\tilde{x}_2^\top \Gamma_2 Z^\top \tilde{W}_2 \\
&\quad - 2\tilde{x}_2^\top K_2^\top \mathcal{B}_2^{(2)} \Gamma_3 \tilde{W}_2 \\
&< -\rho \|\tilde{x}_2\|^2 + 2\tilde{x}_2^\top \Gamma_2 (\eta(t) - g_2(t)\text{sign}(\Gamma_2 \tilde{x}_2)) + 2\|\tilde{x}_2\| \|\Gamma_2\| \|\bar{v}_x\| \\
&< -\rho \|\tilde{x}_2\|^2 - 2g_3 \|\tilde{x}_2\| \|\Gamma_2\| + 2\|\bar{v}_x\| \|\tilde{x}_2\| \|\Gamma_2\| \qquad (3.79)
\end{aligned}$$

where $g_3 > 0$ is guaranteed by choosing $\lambda_{\min}(g_2(t)) > \eta_0$. If $g_3 > \|\bar{v}_x\|$, then $\dot{V}_2 < 0$, which means the approximation error is also eliminated by the sliding mode term, and $\tilde{x}_2$ can reach the sliding manifold in a finite time. If $0 < g_3 < \|\bar{v}_x\|$, (3.79) is continuously written as

$$\begin{aligned}
\dot{V}_2 &< -\rho \|\tilde{x}_2\|^2 + 2(\|\bar{v}_x\| - g_3)\|\Gamma_2\| \|\tilde{x}_2\| \\
&= -\rho \Big(\|\tilde{x}_2\| - \frac{\|\bar{v}_x\| - g_3}{\rho} \|\Gamma_2\| \Big)^2 + \frac{(\|\bar{v}_x\| - g_3)^2 \|\Gamma_2\|^2}{\rho} \qquad (3.80)
\end{aligned}$$

Therefore, when

$$\|\tilde{x}_2\| \geq \frac{2(\|\bar{v}_x\| - g_3)\|\Gamma_2\|}{\rho}, \qquad (3.81)$$

$\dot{V}_2 < 0$, which means $\tilde{x}_2$ is uniformly bounded. ∎

Remark 3.4 *The conditions (3.69) and (3.70) are sufficient conditions to guarantee the boundedness of $\tilde{x}_2$ theoretically. It is not easy to test (3.69) and (3.70). In practice, simulation results demonstrate that the fault diagnosis algorithm works well even without checking these two conditions.*

Remark 3.5 *The above analysis guarantees uniform boundedness of the state estimation error. If the NSS model $\hat{M}_2(t)$ can estimate the fault with certain accuracy, and g_2 is chosen large enough, then the estimation error asymptotically converges to zero. Moreover, the performance of this fault diagnosis scheme can be improved by reducing the system uncertainties, properly increasing the switching gain g_2, and carefully selecting the online approximator $\hat{M}_2(t)$.*

The proposed fault diagnosis scheme in Section 3.3.1 can be implemented using the following algorithm:

- Step 1: Initialize the diagnostic observer (3.6).
- Step 2: Update sliding mode switching gain based on iterative learning algorithm (3.12) or iterative fuzzy model (3.19).
- Step 3: Start NSS model-based fault estimators $\hat{M}(t)$ at $t = T_m$.
- Step 4: Obtain $\tilde{x}_1(t)$ and $s_2(t)$ based on system dynamics (3.1) and the observer (3.6).
- Step 5: Compare $\|\tilde{y}(t)\|$ with a threshold ϵ_λ.
- Step 6: If $\|\tilde{y}(t)\| \geq \epsilon_\lambda$, then fault occurs, and the parameters of the fault estimator (3.41) are updated using EKF-like algorithms. Otherwise, no fault occurs.
- Step 7: Use $\hat{M}(t)$ to isolate and estimate the fault.

3.5.3 Application to a Satellite Orbital System

In this section, the proposed robust fault diagnosis scheme is applied to a fourth-order dynamic satellite system which has been described in [31]. The nominal model of the system is

$$\begin{aligned} \dot{r} &= v & r(0) &= r_0 \\ \dot{v} &= r\omega^2 - \frac{k}{mr^2} + \frac{u_1}{m} & v(0) &= 0 \\ \dot{\phi} &= \omega & \phi(0) &= 0 \\ \dot{\omega} &= -\frac{2v\omega}{r} + \frac{u_2}{mr} & \omega(0) &= \omega_0 \end{aligned} \tag{3.82}$$

where $m = 200$kg is the mass of the satellite, (r, ϕ) are the polar coordinates of the satellite, v is the radial speed, and ω is the angular velocity. Control inputs u_1 and u_2 are the radial and tangential thrust forces, respectively. The parameter $k = K_E m$, where $K_E = 3.986 \times 10^5 \text{km}^3/\text{s}^2$ is derived from a parameter of the Earth

($M_E = 5.974 \times 10^{24}$kg). The satellite is first observed in perigee, 375 km above the surface of the Earth, resulting in $r_0 = R_E + 375$km ($R_E = 6.378 \times 10^3$km). The initial angular speed, ω_0, is computed using the orbital mechanics $\omega_0 = \sqrt{(e_{orbit}+1)K_E/r_0^3}$, where $e_{orbit} = 0.162$ is the eccentricity. The Cartesian coordinates of the satellite are the measured variables; i.e., $y_1 = r\sin(\phi)$, $y_2 = r\cos(\phi)$. In order to compare the results with those in [31], we use a similar local diffeomorphism in [135]; i.e.,

$$\begin{aligned} z_1 &= r\sin(\phi) \\ z_2 &= r\cos(\phi) \\ z_3 &= v\sin(\phi) + r\omega\cos(\phi) \\ z_4 &= v\cos(\phi) - r\omega\sin(\phi) \end{aligned}$$

the system (3.82) is transformed into the form represented by

$$\begin{aligned} \dot{z}_1 &= z_3 \\ \dot{z}_2 &= z_4 \\ \dot{z}_3 &= \frac{-z_1}{(z_1^2+z_2^2)^{3/2}}\frac{k}{m} + \frac{u_1 z_1 + u_2 z_2}{(z_1^2+z_2^2)^{1/2}}\frac{1}{m} \\ \dot{z}_4 &= \frac{-z_2}{(z_1^2+z_2^2)^{3/2}}\frac{k}{m} + \frac{u_1 z_2 - u_2 z_1}{(z_1^2+z_2^2)^{1/2}}\frac{1}{m} \\ y_1 &= z_1 \\ y_2 &= z_2 \end{aligned} \tag{3.83}$$

where $z_1(0) = 0$, $z_2(0) = r_0$, $z_3(0) = r_0\omega_0$, and $z_4(0) = 0$.

In the simulation, the mass of the satellite is assumed to be underestimated by $\varsigma_z = 3\%$ ($m^* = m(1-\varsigma_z), k^* = k(1-\varsigma_z)$). The system (3.83) can be converted into a state space model where (A, C) are given by

$$A = \begin{bmatrix} 0 & 0 & 1 & 0 \\ 0 & 0 & 0 & 1 \\ 0 & 0 & 0 & 0 \\ 0 & 0 & 0 & 0 \end{bmatrix}, \quad C = \begin{bmatrix} 1 & 0 & 0 & 0 \\ 0 & 1 & 0 & 0 \end{bmatrix}.$$

The nonlinear term $\xi(z,u)$ is expressed as

$$\xi(z,u) = \begin{bmatrix} 0 \\ 0 \\ -\dfrac{z_1}{(z_1^2+z_2^2)^{3/2}}\dfrac{k^*}{m^*} + \dfrac{u_1 z_1 + u_2 z_2}{(z_1^2+z_2^2)^{1/2}}\dfrac{1}{m^*} \\ -\dfrac{z_2}{(z_1^2+z_2^2)^{3/2}}\dfrac{k^*}{m^*} + \dfrac{u_1 z_2 - u_2 z_1}{(z_1^2+z_2^2)^{1/2}}\dfrac{1}{m^*} \end{bmatrix}$$

and the state uncertainty is represented by

$$\eta(z,u,t) = \begin{bmatrix} 0 \\ 0 \\ -\dfrac{\varsigma_\eta(2+\varsigma_\eta)}{(1+\varsigma_\eta)^2}\dfrac{z_1}{(z_1^2+z_2^2)^{3/2}}\dfrac{k^*}{m^*} - \dfrac{\varsigma_z}{m^*}\dfrac{u_1 z_1 + u_2 z_2}{(z_1^2+z_2^2)^{1/2}} \\ -\dfrac{\varsigma_\eta(2+\varsigma_\eta)}{(1+\varsigma_\eta)^2}\dfrac{z_2}{(z_1^2+z_2^2)^{3/2}}\dfrac{k^*}{m^*} - \dfrac{\varsigma_z}{m^*}\dfrac{u_1 z_2 - u_2 z_1}{(z_1^2+z_2^2)^{1/2}} \end{bmatrix}$$

where $\varsigma_\eta = 2\%$ is a coefficient of the uncertainty. Thus, the dynamics of the state and sensor uncertainties can be expressed as

$$\eta_z = \left[0, \quad -\varsigma\frac{u_1}{m^*}, \quad 0, \quad -\varsigma\frac{u_2}{m^* r}\right]^\top \tag{3.84}$$

$$\eta_y = \left[\varsigma_y r\sin(\varphi), \quad \varsigma_y r\sin(\varphi)\right]^\top \tag{3.85}$$

If we define $x_1 = [z_1 \ z_2]^\top$ and $x_2 = [z_3 \ z_4]^\top$, (3.83) can be represented in a triangular input form as (3.1). Therefore, the proposed robust fault diagnosis scheme can be applied to this dynamic system.

Based on (3.83), we design a diagnostic observer as follows,

$$\begin{aligned}
\dot{\hat{z}}_1 &= \hat{z}_3 + g_1(t)\text{sign}(y_1 - \hat{y}_1) + \hat{M}_1(t) \\
\dot{\hat{z}}_2 &= \hat{z}_4 + g_2(t)\text{sign}(y_2 - \hat{y}_2) + \hat{M}_2(t) \\
\dot{\hat{z}}_3 &= \frac{-\hat{z}_1}{(\hat{z}_1^2+\hat{z}_2^2)^{3/2}}\frac{k}{m} + \frac{u_1\hat{z}_1 + u_2\hat{z}_2}{(\hat{z}_1^2+\hat{z}_2^2)^{1/2}}\frac{1}{m} + g_3(t)\text{sign}(s_3(t)) + \hat{M}_3(t) \\
\dot{\hat{z}}_4 &= \frac{-\hat{z}_2}{(\hat{z}_1^2+\hat{z}_2^2)^{3/2}}\frac{k}{m} + \frac{u_1\hat{z}_2 - u_2\hat{z}_1}{(\hat{z}_1^2+\hat{z}_2^2)^{1/2}}\frac{1}{m} + g_4(t)\text{sign}(s_4(t)) + \hat{M}_4(t) \\
\hat{y}_1 &= \hat{z}_1 \\
\hat{y}_2 &= \hat{z}_2
\end{aligned} \tag{3.86}$$

where $\hat{z}_1(0) = -0.1$, $\hat{z}_2(0) = r_0 - 0.5$, $\hat{z}_3(0) = r_0\omega_0 + 0.25$, and $\hat{z}_4(0) = 0.01$. The equivalent estimation error $s_3(t)$, $s_4(t)$ are computed according to the anti-peaking structure (3.7), and $\hat{M}_1(t) \sim \hat{M}_4(t)$ are four neural state space models. In order to demonstrate the performance of this robust fault diagnosis scheme, a single incipient fault, a single abrupt fault, and multiple faults are tested. The possible faults could be system component faults, actuator faults or a combination of them. Here, in fault detection and isolation, we indicate the occurrence of faults and determine which state channel is faulty. Locating the faulty variable or actuator needs further work.

Example 1-Single incipient fault: Consider an incipient state fault $f_a^{(3)}(t)$ which occurs in the third state

$$f_a^{(3)}(t) = \beta(t-2)\Big(-1.1\sin(\frac{\pi t}{2})\Big)$$

where $\beta(t - T_x)$ is the time profile function defined in Chapter 3.3.1.

In this example, the switching gain of the sliding mode term is updated using an iterative learning algorithm and an iterative fuzzy model.

Case 1-Adaptive switching gain using an iterative learning algorithm: The initial switching gains of the four sliding mode terms are $g_1(0) = 5$, $g_2(0) = 5$, $g_3(0) = 60$, and $g_4(0) = 60$. The learning coefficient matrix $\Phi = diag\{10^{-3}, 10^{-6}, 10^{-3}, 5\times 10^{-3}\}$ when the gains increase, and $\Phi = diag\{10^{-2}, 85, 7 \times 10^{-5}, 0.14\}$ when the gains decrease. Figure 3.2 compares the outputs of the nominal system with those of the faulty system. Under system uncertainties and state faults, the practical system output deviate from the output of the nominal system.

Figure 3.3 shows the dynamics of the system states and observer states, (The variables x_3 and x_4 are shown for the sake of illustration and discussion. They may not be available for measurement in practical situations). Clearly under the performance of a sliding mode, the system states can be observed in a small period of time. Moreover, after $\tilde{x}_1$ reaches the sliding manifold, the second observer state, $\hat{x}_2$, begins to approach the actual state x_2.

Figure 3.4 portrays the evolution of the adaptive switching gains. The gains are kept steady after the state estimation errors reach the sliding manifold because we desire to keep the switching gain under control and not allow it to become large. A

over-large gain could counteract the effect of the fault.

Figure 3.5 depicts the norm of the output estimation error, which can be used to detect the occurrence of faults. From the figure, as a fault appears, the norm of the output estimation error immediately exceeds a threshold, which successfully indicates the onset of the fault. However, selection of the diagnostic threshold depends on the magnitude of the fault; that is, larger faults result in bigger differences between the output and its estimation. Hence, (3.11) may fail to work in real applications due to the presence of uncertainty.

Figure 3.6 illustrates the characteristics of the fault function and output of the neural state space models. When an incipient fault occurs, both of the two NSS models in the state dynamics generate nonzero signals, which, with a proper threshold, can be used to indicate the occurrence of the fault. However, only the NSS model that corresponds to the faulty state specifies the dynamics of the fault, and the output of the NSS models associated with other healthy states returns back to zero or close to zero. Therefore, this robust fault diagnosis scheme is useful for fault isolation and estimation of single incipient fault.

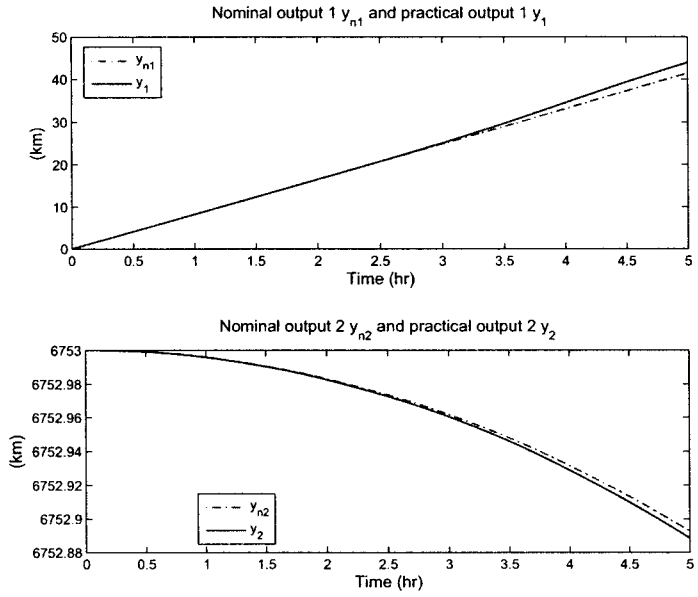

Figure 3.2: Nominal system output and faulty system output for case 1 of Example 1

Table 3.2: Values of switching gain $\bar{\Phi}^n_{i,i}$

$g_i \setminus \bar{\Phi}^n_{i,i}$	Φ_{NL}	Φ_{NB}	Φ_{NM}	Φ_{NS}	Φ_{PS}	Φ_{PM}	Φ_{PB}	Φ_{PL}
g_1	-1.6	-1.4	-1.1	-0.7	10^{-8}	3×10^{-8}	6×10^{-8}	10^{-7}
g_2	-10	-7	-2.5	-1.3	10^{-9}	5×10^{-9}	7×10^{-9}	10^{-8}
g_3	-14.1	-13	-12	-10	5×10^{-12}	10^{-11}	5×10^{-11}	10^{-10}
g_4	-0.7	-0.5	-0.3	-0.1	7×10^{-5}	10^{-4}	3×10^{-4}	10^{-3}

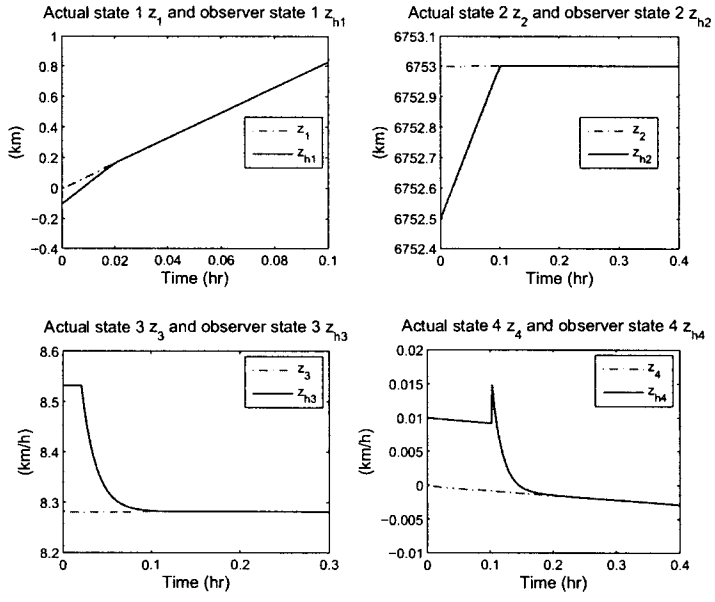

Figure 3.3: System states and observer states for case 1 of Example 1

Case 2-Adaptive switching gain using an iterative fuzzy model: The characteristics of the system and the fault is set to be the same as those in case 1. The only difference is that the switching gain is updated using the iterative fuzzy model which was introduced in Section 3.3.4. The initial gain matrix is still set to $diag\{5, 5, 60, 60\}$. We use the functions in Figure 3.1 as the fuzzification membership functions, where the coordinates on the x-axis are set to [-0.1, -0.05, -0.01, -0.002, 0, 0.002, 0.01, 0.05, 0.1]. The crisp rule consequent of $\bar{\Phi}^n_{i,i}$ in the fuzzy rule base is set in Table 3.2.

Figure 3.7 shows the time-behavior of the switching gains in the four sliding mode terms. Clearly, the sliding mode using an iterative fuzzy model to update the switching

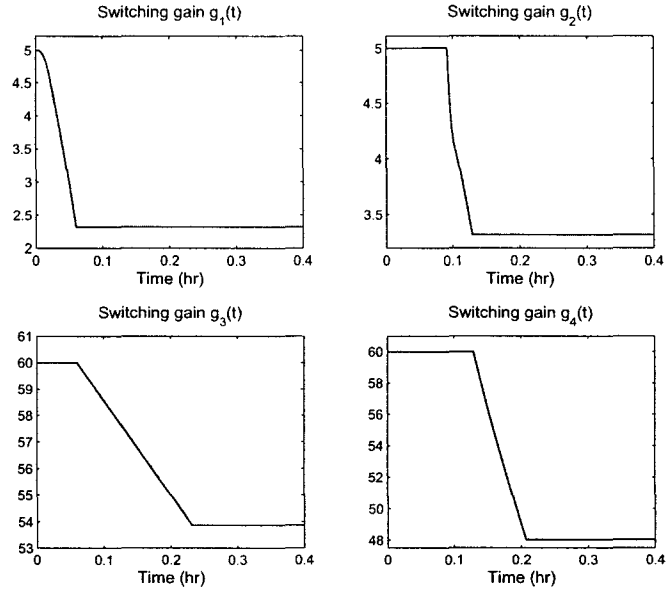

Figure 3.4: Four sliding mode switching gains updated using the iterative learning algorithm for case 1 of Example 1

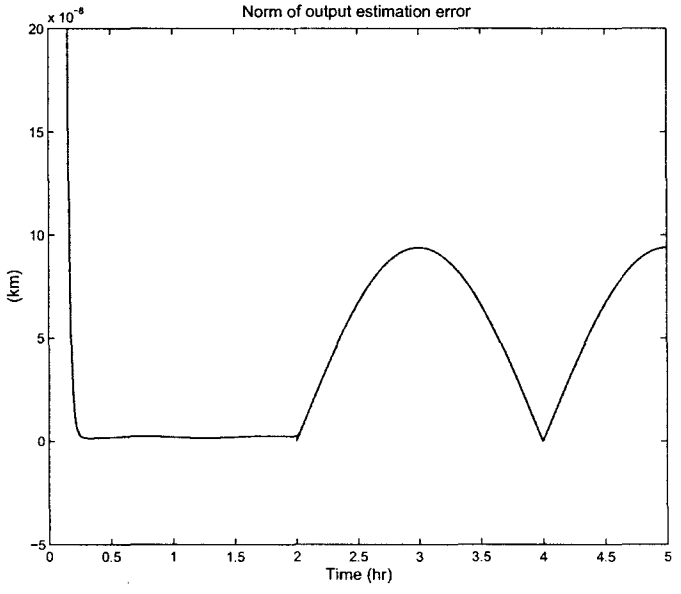

Figure 3.5: Norm of output estimation error for case 1 of Example 1

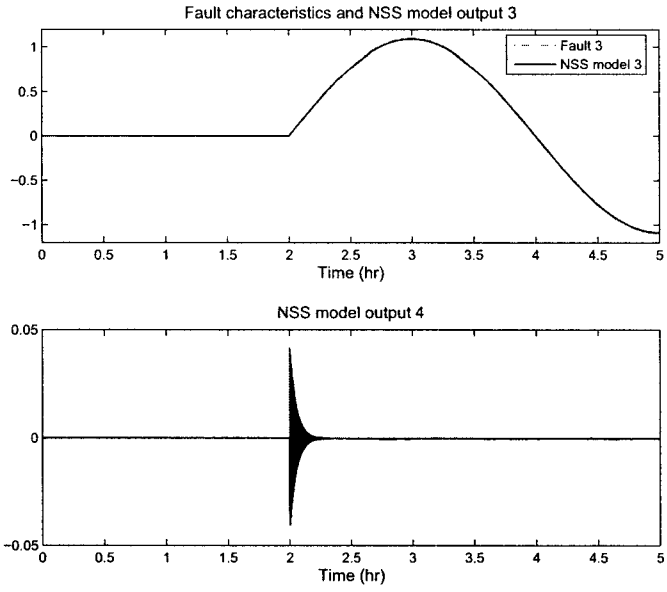

Figure 3.6: Incipient state fault 3 and the NSS model output 3 and 4 for case 1 of Example 1

gains takes less time to reach the sliding manifold than the sliding mode using the iterative learning method. This feature is expected because the update law using a fuzzy model is equivalent to a varying-coefficient proportional-type controller, while the update law using the learning algorithm is equivalent to a traditional constant-coefficient proportional-type controller.

In Figure 3.8, the NSS models also indicate the occurrence of the fault, and the NSS model corresponding to the faulty state estimates the fault successfully.

Example 2-Single abrupt fault: Unlike incipient faults, an abrupt fault may cause great change in the structure and/or parameters of the system in a very short time. Here, we consider the case of an abrupt fault $f_a^{(4)}(t) = -1 \times \beta(t - 2.5)$, which is assumed to occur in the fourth state at $t = 2.5$ hour. The initial estimation errors and uncertainties are set to be the same as those in Example 1; therefore, the sliding mode term is the same. The switching gain is updated using the iterative fuzzy model. Figure 3.9 shows the characteristics of the fault and the outputs of two NSS models. From this figure, when an abrupt fault occurs, both of the two NSS models

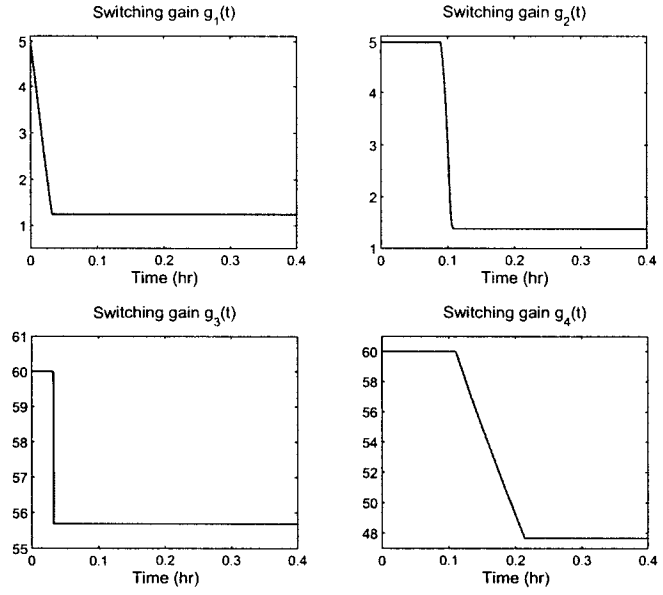

Figure 3.7: Four adaptive switching gains updated using the iterative fuzzy model for case 2 of Example 1

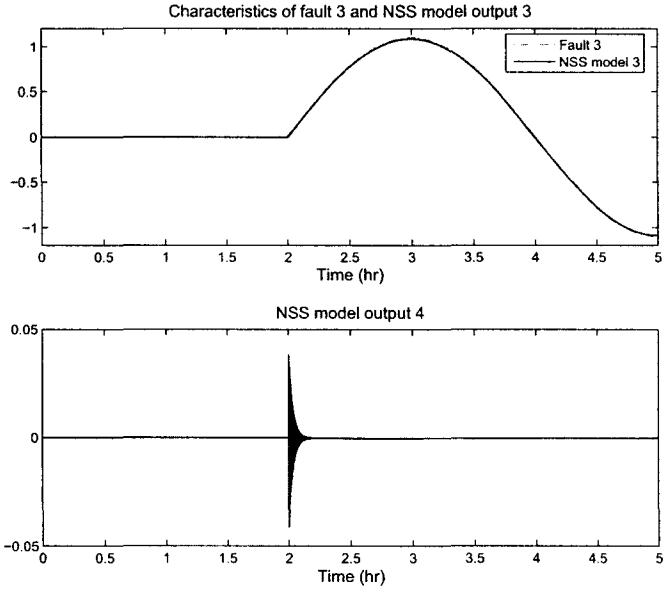

Figure 3.8: Fault 3 and the NSS model output 3 and 4 for case 2 of Example 1

generate a large amount of chattering. Then, only the NSS model associated with the faulty state specifies the fault, while the outputs of the NSS models associated with the healthy states return zero or stay close to zero. When the fault changes so abruptly that the NSS models can not update their parameters in a timely manner to approximate the fault, and signum functions are used, the transient process with chattering in the fault estimation signal occurs.

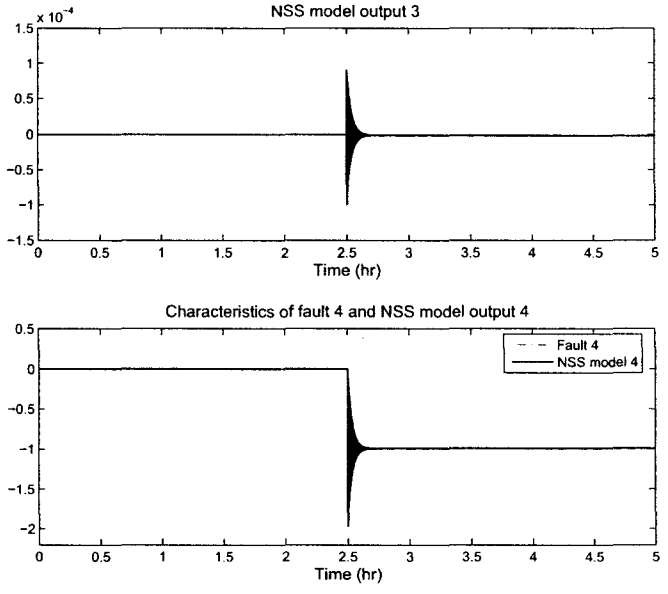

Figure 3.9: Abrupt fault 4 and the corresponding NSS model output 3 and 4 in Example 2

Example 3-Multiple faults: We now consider the effectiveness of this FD scheme for multiple faults. An incipient fault $f_a^{(3)}(t) = -1 \times \beta(t-2)$ and an abrupt fault

$$f_a^{(4)}(t) = \beta(t-2) \times \left(0.9\sin(2\pi t)\cos(2\pi t) + 0.8\sin(\frac{\pi t}{2})\cos(\frac{\pi t}{2}) + 0.7\sin(\frac{\pi t}{4})\cos(\frac{\pi t}{4})\right)$$

occur simultaneously in the third and fourth states, respectively. The diagnostic results are shown in Figure 3.10, where the NSS models in the third and fourth state demonstrate the characteristics of the two faults, respectively. Although some chattering occurs in the early phase of fault approximation, the NSS models successfully

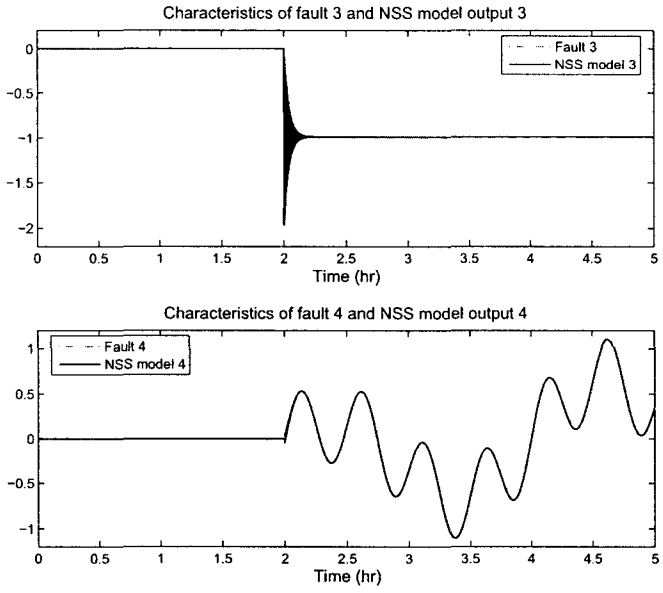

Figure 3.10: Abrupt fault 3, incipient fault 4 and the corresponding NSS model output 3 and 4 in Example 3

estimate the faults shortly after. Therefore, the proposed fault diagnosis scheme is also effective for multiple faults.

3.6 Fault Isolation and Estimation Using Iterative Learning Estimators

3.6.1 Design of PID-type Iterative Learning Fault Estimators

In this section, a bank of PID-type iterative learning estimators is proposed to diagnose faults. The advantage of this kind of estimator is its parameters are updated in the iteration domain such that the overshoot and transient process of fault estimation can be reduced or even eliminated. Here, $\hat{M}_1(t) = [\hat{M}_{1,1}(t), \cdots, \hat{M}_{1,p}(t)]^\top \in \Re^p$ represents a bank of PID-type iterative learning estimators associated with $\hat{x}_1$, and $\hat{M}_2(t) = [\hat{M}_{2,1}(t), \cdots, \hat{M}_{2,p}(t)]^\top \in \Re^p$ denotes another bank of PID-type iterative learning estimators associated with $\hat{x}_2$. At each time t, the estimators $\hat{M}_{i,j}$, $(i = 1, 2; j = 1, \ldots, p)$

are iteratively updated according to the following rule [136]:

$$\hat{M}_{i,j}(t) = \frac{K \cdot \sum_{l=1}^{3} \omega_{i,j}^{(l)}(t) z_{i,j}^{(l)}(t-\tau)}{\sum_{l=1}^{3} \omega_{i,j}^{(l)}(t)} \tag{3.87}$$

where K is the gain, $\omega_{i,j}^{(l)}(t), (l = 1, \cdots, 3)$ are the three parameters of the (i,j)th observer input, and τ is the sampling time interval in the iteration domain. Three external inputs of $\hat{M}_{i,j}(t)$ are chosen as

$$\begin{cases} z_{i,j}^{(1)}(t) = s_{i,j}(t) \\ z_{i,j}^{(2)}(t) = z_{i,j}^{(1)}(t) - \hat{M}_{i,j}(t) \\ z_{i,j}^{(3)}(t) = \Delta z_{i,j}^{(2)}(t) = z_{i,j}^{(2)}(t) - z_{i,j}^{(2)}(t-\tau) \end{cases} \tag{3.88}$$

If we define

$$W_{i,j}(t) = \left[\frac{K\omega_{i,j}^{(1)}(t)}{\sum_{l=1}^{3} \omega_{i,j}^{(l)}(t)} \quad \frac{K\omega_{i,j}^{(2)}(t)}{\sum_{l=1}^{3} \omega_{i,j}^{(l)}(t)} \quad \frac{K\omega_{i,j}^{(3)}(t)}{\sum_{l=1}^{3} \omega_{i,j}^{(l)}(t)} \right]^{\top}$$

and

$$z_{i,j}(t) = [z_{i,j}^{(1)}(t) \quad z_{i,j}^{(2)}(t) \quad z_{i,j}^{(3)}(t)]^{\top},$$

then $\hat{M}_{i,j}(t) = W_{i,j}^{\top}(t) z_{i,j}(t-\tau)$.

The following adaptive law is used to update the parameters of (3.87):

$$\begin{aligned} \Delta W_{i,j}(t) &= W_{i,j}(t) - W_{i,j}(t-\tau) \\ &= \frac{\alpha_1 \tilde{x}_{i,j}(t) z_{i,j}(t-\tau)}{\alpha_2 + z_{i,j}^{\top}(t-\tau) z_{i,j}(t-\tau)} \end{aligned} \tag{3.89}$$

where α_1 is the learning rate and α_2 is a small positive number used to prevent the denominator becoming zero.

The proposed fault diagnosis scheme in Section 3.6.1 can be implemented using the following algorithm:

- Step 1: Initialize the diagnostic observer (3.6).
- Step 2: Update sliding mode switching gain based on an iterative learning algorithm (3.12) or an iterative fuzzy model (3.19).

- Step 3: Start PID-type iterative learning fault estimators $\hat{M}_{i,j}(t)$ at $t = T_m$.
- Step 4: Obtain $\tilde{x}_1(t)$ and $s_2(t)$ based on system dynamics (3.1) and the observer (3.6).
- Step 5: Compare $\|\tilde{y}(t)\|$ with a threshold ϵ_λ.
- Step 6: If $\|\tilde{y}(t)\| \geq \epsilon_\lambda$, then fault occurs, and the parameters of the fault estimators (3.87) are updated using PID-type iterative learning algorithms. Otherwise, no fault occurs.
- Step 7: Use $\hat{M}_{i,j}(t)$ to isolate and estimate the fault.

3.6.2 Stability Analysis

In this section, stability of the proposed fault diagnosis scheme using PID-type iterative learning estimators is explored. Prior to any fault, the stability of the estimation error dynamics can be investigated in the same way as that in Section 3.5.2.

Firstly, after the occurrence of a state fault, the estimation error deviates from zero firstly, because the fault works as a new unknown input to the system. However, due to the compensation of the observer input $\hat{M}(t)$, theoretically, the state estimation error should return to zero if $\hat{M}(t)$ exactly specifies the fault. In practice, due to the existence of fault estimation error, the state estimation error remains within a small bound. This property is shown in the following theorem.

Theorem 3.7 *If conditions (3.59)-(3.61) and the following equality and inequality are both satisfied,*

$$\lambda_{\min}(g_1) > \|\tilde{x}_2\| + \delta_{M_1} \tag{3.90}$$

$$\Gamma_2 Z_2^\top(t-\tau) = \bar{Z}_2(t-\tau)\Gamma_3 \tag{3.91}$$

where Z_2 and $\bar{Z}_2$ are defined later, then the state estimation error $\tilde{x}_2$ is uniformly bounded.

Proof: The boundedness of $\tilde{x}_1$ is proved using the same method in Theorem 3.6. Then, we consider the stability of $\tilde{x}_2$.

The structure of the PID-type iterative learning estimator is similar to that of the radial basis function (RBF) networks. Although only three inputs exist, and the output of the estimator is a linear combination of the inputs, the PID-type iterative learning estimator only needs to approximate a constant value in the iteration domain at each sampling time. Therefore, due to the approximation ability of RBF networks, it is reasonable to assume that the fault function $f_a(t)$ can be approximated by the PID-type iterative learning estimator as

$$f_a(t) = \hat{M}_2(W_2^*, t) + \upsilon_x \tag{3.92}$$

where υ_x denotes the network approximation error. The optimal parameter W_2^* is selected such that the L_2 norm distance between $f_a(t)$ and $\hat{M}_2(W_2^*, t)$ is minimized. Note that the artificial parameter W_2^* is only used for theoretical analysis and is not for the estimator design.

Based on (3.89), we have

$$\hat{M}_2(W_2^*, t) = \hat{M}_2(W_2, t) + Z_2^\top(t-\tau)\tilde{W}_2 \tag{3.93}$$

where $Z_2 = diag\{z_{2,1}(t-\tau), \cdots, z_{2,p}(t-\tau)\} \in \Re^{3p\times p}$, $\tilde{W}_2 = [\tilde{W}_{2,1}^\top, \cdots, \tilde{W}_{2,p}^\top]^\top \in \Re^{3p}$, and $\tilde{W}_2 = W_2^* - W_2$.

Substituting (3.92) and (3.93) into (3.68), we obtain

$$\begin{aligned}\dot{\tilde{x}}_2 &= A_{21}\tilde{x}_1 + A_{22}\tilde{x}_2 + \xi(x_1, x_2) - \xi(\hat{x}_1, \hat{x}_2) + \eta(t) - g_2(t)\text{sign}(\Gamma_2 s_2) \\ &\quad + Z_2^\top(t-\tau)\tilde{W}_2 + \upsilon_x.\end{aligned} \tag{3.94}$$

Based on (3.89), we have

$$\begin{aligned}\dot{W}_{i,j} &\approx \frac{\Delta W_{i,j}}{\Delta t} \\ &= \frac{\alpha_1 \tilde{x}_{i,j}(t) z_{i,j}(t-\tau)}{\tau(\alpha_2 + z_{i,j}^\top(t-\tau) z_{i,j}(t-\tau))}.\end{aligned} \tag{3.95}$$

Hence,

$$\begin{aligned}\dot{\tilde{W}}_2 &= -\dot{W} \\ &= -\bar{Z}_2(t-\tau)\tilde{x}_2\end{aligned} \tag{3.96}$$

where

$$\bar{Z}_2 = \begin{bmatrix} \frac{\alpha_1 z_{2,1}(t-\tau)}{\tau(\alpha_2 + z_{2,1}^\top(t-\tau)z_{2,1}(t-\tau))} & & \\ & \ddots & \\ & & \frac{\alpha_1 z_{2,p}(t-\tau)}{\tau(\alpha_2 + z_{2,p}^\top(t-\tau)z_{2,p}(t-\tau))} \end{bmatrix}$$

The second Lyapunov function is still defined as

$$V_2 = \tilde{x}_2^\top \Gamma_2 \tilde{x}_2 + \tilde{W}_2^\top \Gamma_3 \tilde{W}_2 \tag{3.97}$$

where $\Gamma_3 \in \Re^{p^2 \times p^2}$ is also a symmetric positive definite matrix to be determined.

Based on (3.91), (3.94) and (3.96), the derivative of V_2 with respect to t is

$$\begin{aligned} \dot{V}_2 &= \tilde{x}_2^\top (A_{22}^\top \Gamma_2 + \Gamma_2 A_{22})\tilde{x}_2 + 2\tilde{x}_2^\top \Gamma_2 (\xi(x_1, x_2) - \xi(\hat{x}_1, \hat{x}_2)) \\ &\quad + 2\tilde{x}_2^\top \Gamma_2 (\eta(t) + \upsilon_x(t) - g_2(t)\text{sign}(\Gamma_2 \tilde{x}_2)) \\ &\quad + 2\tilde{x}_2^\top \Gamma_2 Z_2^\top (t-\tau)\tilde{W}_2 - 2\tilde{x}_2^\top \bar{Z}_2^\top (t-\tau)\Gamma_3 \tilde{W}_2 \\ &< -\rho\|\tilde{x}_2\|^2 + 2\tilde{x}_2^\top \Gamma_2 (\eta(t) - g_2(t)\text{sign}(\Gamma_2 \tilde{x}_2)) + 2\|\tilde{x}_2\|\|\Gamma_2\|\|\upsilon_x\| \\ &< -\rho\|\tilde{x}_2\|^2 - 2g_3\|\tilde{x}_2\|\|\Gamma_2\| + 2\|\upsilon_x\|\|\tilde{x}_2\|\|\Gamma_2\| \end{aligned} \tag{3.98}$$

where $g_3 > 0$ is guaranteed by choosing $\lambda_{\min}(g_2(t)) > \eta_0$. If $g_3 > \|\upsilon_x\|$, then $\dot{V}_2 < 0$, which means the approximation error is also eliminated by the sliding mode, and $\tilde{x}_2$ can reach the sliding manifold in a finite time. If $0 < g_3 < \|\upsilon_x\|$, (3.98) is continuously written as

$$\begin{aligned} \dot{V}_2 &< -\rho\|\tilde{x}_2\|^2 + 2(\|\upsilon_x\| - g_3)\|\Gamma_2\|\|\tilde{x}_2\| \\ &= -\rho\Big(\|\tilde{x}_2\| - \frac{\|\upsilon_x\| - g_3}{\rho}\|\Gamma_2\|\Big)^2 + \frac{(\|\upsilon_x\| - g_3)^2\|\Gamma_2\|^2}{\rho} \end{aligned} \tag{3.99}$$

Therefore, when

$$\|\tilde{x}_2\| \geq \frac{2(\|\upsilon_x\| - g_3)\|\Gamma_2\|}{\rho}, \tag{3.100}$$

then $\dot{V}_2 < 0$, which means $\tilde{x}_2$ is uniformly bounded. ∎

Remark 3.6 *Theorem 3.7 guarantees the uniform boundedness of the state estimation error. If (3.90) and (3.91) are satisfied, and $g_1(t)$ and $g_2(t)$ are properly updated, then the estimation error converges to zero in a finite time. Moreover, the performance of this fault diagnosis scheme can be improved by properly choosing the switching gains, and carefully designing the online estimators.*

3.6.3 Application for a Flexible Satellite Control System

In this section, the dynamics of a satellite with flexible appendages is first presented. Then, the proposed fault diagnosis scheme is tested on this flexible satellite.

The model of a flexible satellite is composed of a rigid central hub, which represents the satellite body, and two flexible appendages, which are usually solar arrays, antennas, or any other flexible structures. The satellite is assumed to maneuver in a circular orbit. A series of axes has been defined in [137] when deriving the motion equation of this satellite:

X_c, Y_c, Z_c – Axes of right-handed coordinate frame,
X_0, Y_0, Z_0 – Axes of an inertial frame,
X_s, Y_s, Z_s – Axes of an orbital frame.

When the satellite is slewed around the axis Z_s, which is normal to the orbital plane, the flexible appendages are deformed. We assume that the appendages suffer elastic transverse bending only in the orbital plane $X_s - Y_s$. In [137], considering the configuration of the satellite, assuming that the pitch maneuver excites the two flexible appendages anti-symmetrically is reasonable.

The governing equations of the satellite motion were developed via the Lagrangian procedure. The spatial discretization method was used to derive a group of ordinary differential equations to describe the motion of the satellite, although the vibration of the appendages can be described by partial differential equations. As a result, the appendage deflections, which are strictly confined in the orbital plane, are expressed in terms of a set of admissible or shape functions as

$$\delta(l,t) = \sum_{i=1}^{N} \Psi_i(l-r)p_i(t) \tag{3.101}$$

where $p_i(t)$ are the generalized coordinates associated with these functions, l is the distance from a point on the appendage to the center of the hub, and r is the radius of the hub. Here, we assume that N modes are sufficient for the computation of elastic deformation. Ψ_i are the shape functions that satisfy the geometric and physical boundary conditions. The shape functions are given in [137] as

$$\Psi_i(l-r) = 1 - \cos\left(\frac{i\pi(l-r)}{L}\right) + \frac{1}{2}(-1)^{i+1}\left(\frac{i\pi(l-r)}{L}\right)^2 \tag{3.102}$$

where L is the length of the appendage.

The formulation of the governing equations of this kind of spacecraft is discussed in [138] and is expressed as

$$\begin{aligned}
&[J + 2J_1 + \mathbf{p}^\top \mathbf{M_{pp}} \mathbf{p}]\ddot{\psi} + \mathbf{m}_{\psi\mathbf{p}}^\top \dot{\mathbf{p}} + 2(\dot{\psi} + \omega_0)\dot{\mathbf{p}}^\top \mathbf{M_{pp}} \mathbf{p} \\
&\quad + 3\omega_0^2 \sin(2\psi)[J_1 - \frac{1}{2}\mathbf{p}^\top \mathbf{M_{pp}} \mathbf{p}] + 3\omega_0^2 \cos(2\psi)\mathbf{m}_{\psi\mathbf{p}}^\top \mathbf{p} = u_t \\
&\mathbf{M_{pp}}\ddot{\mathbf{p}}^\top + \mathbf{m}_{\psi\mathbf{p}}\ddot{\psi} + \frac{3}{2}\omega_0^2 \sin(2\psi)\mathbf{m}_{\psi\mathbf{p}} + \mathbf{C_{pp}}\dot{\mathbf{p}} \\
&\quad + [\mathbf{K_{pp}} - (\dot{\psi}^2 + 2\dot{\psi}\omega_0 + 3\omega_0^2 \sin^2\psi)\mathbf{M_{pp}}]\mathbf{p} = 0
\end{aligned} \tag{3.103}$$

where ψ is the pitch angle, $\mathbf{p} = [p_1, \cdots, p_N]^\top$ is the vector of the generalized coordinates of the appendage flexibility , ω_0 is the orbital rate, J and J_1 are the mass moments of inertia of the central hub and each appendage, respectively, u_t is the control torque, and $\mathbf{M_{pp}}$, $\mathbf{m}_{\psi\mathbf{p}}$, $\mathbf{C_{pp}}$ and $\mathbf{K_{pp}}$ are the following modal integrals:

$$\begin{aligned}
[\mathbf{M_{pp}}]_{i,j} &= 2\int_r^{r+L} \Psi_i(l-r)\Psi_j(l-r)dl \\
[\mathbf{m}_{\psi\mathbf{p}}]_{i,j} &= 2r\int_r^{r+L} l\Psi_i(l-r)dl \\
[\mathbf{C_{pp}}]_{i,j} &= 2\int_r^{r+L} CI\Psi_i''(l-r)\Psi_j''(l-r)dl \\
[\mathbf{K_{pp}}]_{i,j} &= 2\int_r^{r+L} EI\Psi_i''(l-r)\Psi_j''(l-r)dl
\end{aligned} \tag{3.104}$$

where $\Psi_i'' = (\partial^2\Psi_i/\partial l^2)$, C and E are the damping coefficient and modulus of elasticity of the appendages, and I is the sectional area moment of inertia with respect to the appendage bending axis.

When satellite maneuvers are relatively fast, the nonlinear terms associated with the pitch angle ψ will dominate over the terms associated with the flexibility generalized coordinates, $\mathbf{p}$. Hence, the quadratic terms, $\mathbf{p}^\top \mathbf{M_{pp}} \mathbf{p}$ and $\dot{\mathbf{p}}^\top \mathbf{M_{pp}} \mathbf{p}$ can be neglected and resulting in simplified motion equations,

$$\begin{pmatrix} J_t & \mathbf{m}_{\psi\mathbf{p}}^\top \\ \mathbf{m}_{\psi\mathbf{p}} & \mathbf{M_{pp}} \end{pmatrix} \begin{pmatrix} \ddot{\psi} \\ \ddot{\mathbf{p}} \end{pmatrix} + \begin{pmatrix} 0 & 0 \\ 0 & \mathbf{C_{pp}} \end{pmatrix} \begin{pmatrix} \dot{\psi} \\ \dot{\mathbf{p}} \end{pmatrix} + \begin{pmatrix} 0 & 0 \\ 0 & \mathbf{K_{pp}} \end{pmatrix} \begin{pmatrix} \psi \\ \mathbf{p} \end{pmatrix} = \begin{pmatrix} u_t \\ 0 \end{pmatrix} + \begin{pmatrix} h_1 \\ \mathbf{h_2} \end{pmatrix} \tag{3.105}$$

where

$$\begin{aligned} J_t &= J + 2J_1 \\ h_1 &= -3\omega_0^2 J_1 \sin(2\psi) - 3\omega_0^2 \cos(2\psi) \mathbf{m}_{\psi\mathbf{p}}^\top \mathbf{p} \\ \mathbf{h_2} &= (\dot{\psi}^2 + 2\dot{\psi}\omega_0 + 3\omega_0^2 \sin^2\psi)\mathbf{M_{pp}}\mathbf{p} - \frac{3}{2}\omega_0^2 \sin 2\psi \mathbf{m}_{\psi\mathbf{p}}. \end{aligned}$$

When we choose the state vector to be $x = [\psi,\ \mathbf{p},\ \dot{\psi},\ \dot{\mathbf{p}}]^\top$ and the output vector to be $y = [\psi,\ \mathbf{p}]^\top$, the above equations can be written into a form similar to (3.1). So, the proposed fault diagnosis scheme in this section can be applied to the satellite with flexible appendages.

The simulation for the fault diagnosis in system (3.105) is presented here. The satellite is assumed to maneuver in a circular orbit at an altitude of 400 km. The nominal parameters of this satellite are listed in Table 3.3. In the simulation, because the system has only one control torque, u_t, we consider the case when a single actuator fault occurs at the 8th *second*. An incipient fault and an abrupt fault are tested. The fault functions are described as

$$f_a^{(3)}(t) = \beta(t-8)\big(0.4\sin(2\pi t/2) + 0.5\sin(2\pi t/4) + 0.6\sin(2\pi t/8)\big) \tag{3.106}$$

and

$$f_a^{(3)}(t) = -\beta(t-8) \tag{3.107}$$

The system dynamics are assumed to be subject to disturbances and measurement noises. In simulation, the disturbance in the control torque is set to be a random

Table 3.3: Nominal parameters of the satellite with flexible appendages

Parameters	Values (unit)
Moment of inertia of central hub J	3972 (kg m^2)
Moment of inertia of appendage J_1	500 (kg m^2)
Appendage structural damping CI	545 (kg m^3/s)
Appendage stiffness EI	1500 (kg m^3/s)
Appendage length L	30 (m)
Appendage radius r	1 (m)
Orbital rate ω_0	0.0047 (rad/s)
Number of coordinates N	5

signal with a maximum magnitude 0.05, and the measurement noises are set to be random signals with maximum magnitude 0.5%.

Moreover, this FD scheme can be easily extended to the case of multiple state faults. The state is divided into four parts: $x = [x_1, x_{2,1}, \cdots, x_{2,N}, x_3, x_{4,1}, \cdots, x_{4,N}]^\top$, and only x_1 and $x_{2,1}, \ldots, x_{2,N}$ are measurable. Correspondingly, a group of observer inputs are constructed as $\hat{M} = [\hat{M}_1, \hat{M}_{2,1}, \cdots, \hat{M}_{2,N}, \hat{M}_3, \hat{M}_{4,1}, \cdots, \hat{M}_{4,N}]^\top$.

In the simulation design, the gain of the PID-type iterative learning estimator is set to $K = 1$. The initial values of the external inputs are all set to 0.5. Simulation results are shown from Figure 3.11 to Figure 3.14. Several conclusions can be derived from these figures. Firstly, system performance deteriorates when an actuator fault occurs. Secondly, prior to the onset of any fault, the sliding mode works to reduce the estimation error close to zero, which illustrates that the proposed fault diagnosis scheme is robust to system uncertainties with certain magnitudes. Thirdly, whether an incipient fault or an abrupt fault occurs in a state channel, the corresponding observer input can characterize the fault with satisfactory accuracy in the presence of uncertainties and measurement noises. Other fault estimators still remain zero or close to zero, which implies this FD scheme is able to locate and estimate the actuator fault effectively. However, large magnitude of measurement noises impact the fault estimation performance and probably fail the fault diagnosis scheme. Therefore, the parameters of the sliding mode and fault estimators need to be adjusted carefully, and filters are necessary in some cases.

3.7 Conclusions

In this chapter, a unified framework of robust fault diagnosis schemes using sliding mode and learning approaches was proposed for a class of nonlinear systems, which has, or can be transformed into, a triangular input form. In this class of FD schemes, the purpose of the sliding mode is only to deal with the effect of system uncertainties, where the sliding mode with an adaptive switching gain helps to distinguish the fault from other unknown inputs. The adaptive switching gain is updated using an iterative learning algorithm followed by an iterative fuzzy model. The robustness with respect to uncertainties and the sensitivity to faults were rigorously analyzed thereafter. After the state estimation errors are stabilized by the sliding mode, two kinds of online fault estimators were respectively designed to specify the faults. One fault estimator is based on neural state space models, and the other uses an iterative learning algorithm. The stability of these two observer-based fault diagnosis schemes were investigated. To exemplify the theoretical results, the proposed robust fault diagnosis schemes using sliding mode and learning approaches were applied to a satellite orbital control system and a flexible satellite control system. The simulation results illustrate that the proposed fault diagnosis schemes can successfully detect, isolate, and estimate a single abrupt/incipient fault as well as multiple faults.

Although the studied robust fault diagnosis schemes are feasible for a class of nonlinear systems with triangular input form, some typical satellite control systems can not be classified into this family; e.g., the satellite attitude control systems in Chapter 2. Therefore, other types of fault diagnosis schemes should be designed based on the different dynamics of the satellite control systems.

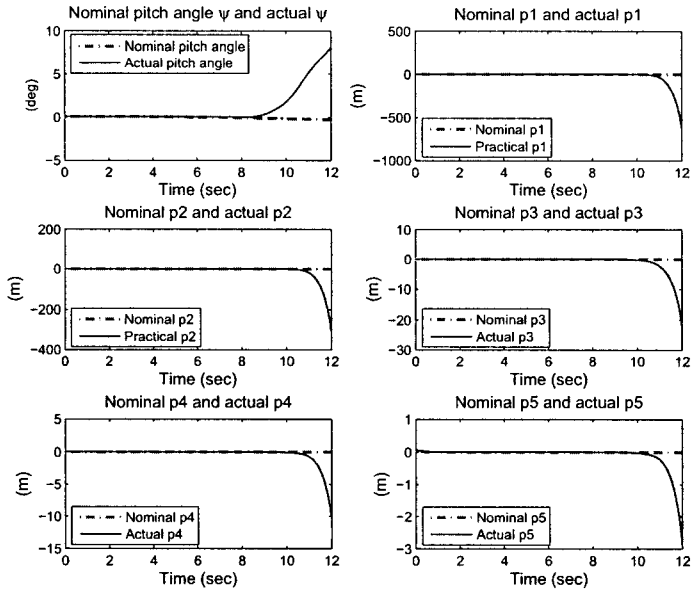

Figure 3.11: Nominal system output, actual system output and observer output when an incipient state fault occurs at the 8th second

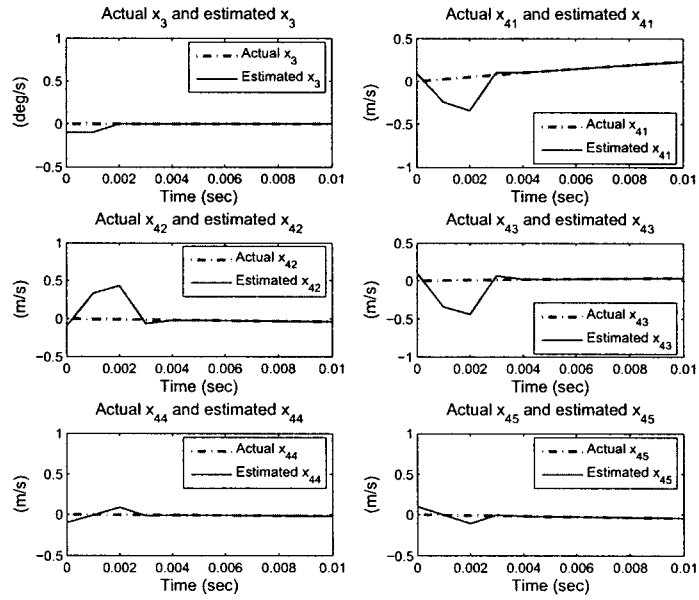

Figure 3.12: Actual states and estimated states using the proposed diagnostic observer

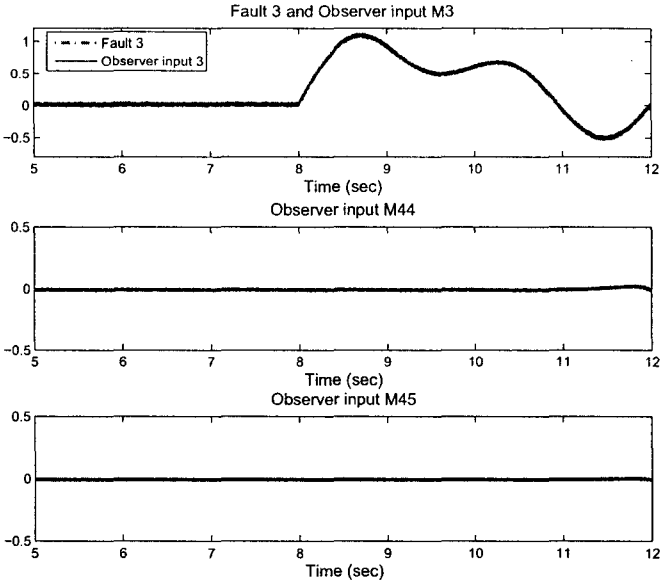

Figure 3.13: Incipient state fault $f_a^{(3)}(t)$, fault estimator $\hat{M}_3(t)$, and the observer inputs $\hat{M}_{4,4}(t)$ and $\hat{M}_{4,5}(t)$

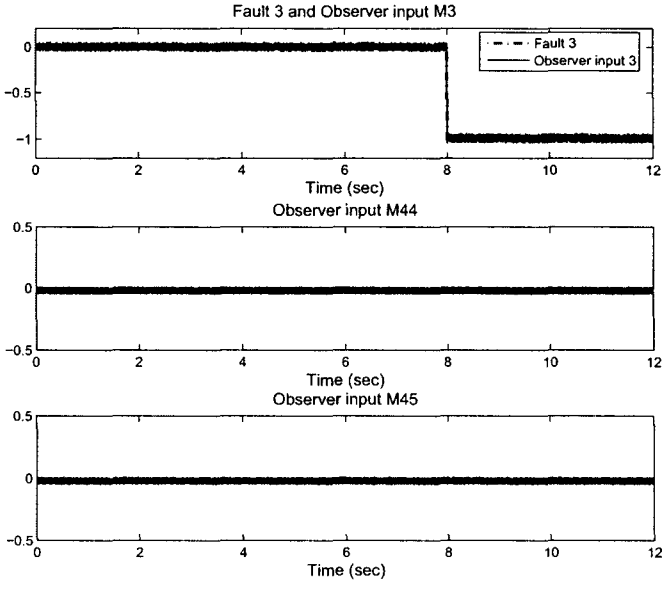

Figure 3.14: Abrupt state fault $f_a^{(3)}(t)$, fault estimator $\hat{M}_3(t)$, and the observer inputs $\hat{M}_{4,4}(t)$ and $\hat{M}_{4,5}(t)$

Chapter 4

Fault Diagnosis Using High Order Sliding Mode Differentiators and Learning Approaches

In this chapter, a class of nonlinear systems is studied where the unmeasurable system state can be described as a nonlinear function of the system output and its derivatives. Correspondingly, fault diagnosis schemes using high order sliding mode differentiators (HOSMDs) and two learning approaches are proposed for this class of nonlinear systems.

4.1 Introduction

In Chapter 3, a unified framework of fault detection, isolation, and estimation schemes using sliding mode and learning approaches was proposed for a class of nonlinear systems which have, or can be transformed into, a triangular input form. The proposed fault diagnosis strategies have been successfully applied to some satellite control systems, such as satellite orbital control systems and flexible satellite control systems. Unfortunately, some typical satellite attitude control systems cannot be formulated in this way.

Through studying the dynamics of a typical satellite attitude control system, we

can easily see that the three unmeasurable angular velocities can be represented by nonlinear functions of Euler angles and their derivatives with respect to time. This feature implies that if we can obtain the exact derivatives of the measurable Euler angles, the angular velocities can be precisely estimated. Additionally, according to previous research [139], the accurate information of all the state variables of the system being studied is helpful for designing algorithms to diagnose faults in system components and/or actuators. Therefore, the method for obtaining the exact derivatives of the system output becomes a primary task.

Exact differentiators have been studied for several years. For a dynamic system with a finite relative degree more than one, the system is invertible if the exact derivatives of the state and output are available. The invertibility of a control system makes the controller design easier. As a result, various exact differentiators were designed by many researchers; e.g., algebraic differentiators [140], high order sliding mode differentiators [83], [84], [85]. These differentiators have been used in the design of fault diagnosis schemes [87], [141]. Among these exact differentiators, HOSMDs are distinguished from others since it can ensure the best-possible error asymptotic order when the input noise is a measurable (Lebesgue) bounded function of time.

Moreover, although neural networks have powerful nonlinear approximation abilities, for a specific problem, *ad hoc* neural networks models should be designed. For example, a variety of neural networks based models with different adaptive laws were proposed to design state observers for different kinds of systems; e.g., [37], [38], [39], [40], [41], [42], [43]. Moreover, the last chapter shows that recurrent neural networks and iterative learning estimators are both successful for fault isolation and estimation. If these two techniques can be combined, the performance of the designed fault diagnosis scheme is expected to be better. Actually, similar strategies have been used in controller designs, such as single neuron PSD control [136], [142], and neural network direct control [143].

In this chapter, the advantages of high order sliding mode differentiators, neural networks, and iterative learning algorithms are integrated. The purpose of the HOSMDs is to obtain an exact derivative of the system output, which will be used to

estimate the unmeasurable state of the system. Then, diagnostic observers using neural adaptive estimators and iterative neuron PID estimators are proposed respectively. After that, for the purpose of demonstrating their performance, these two kinds of diagnostic observers are applied to a satellite attitude control system and a satellite system with large angle maneuver, respectively.

The remaining parts of this chapter are organized as follows. In Section 4.2, the system under study is described mathematically, and some necessary assumptions are given. In Section 4.3, the high order sliding mode differentiators are introduced and their properties that were provided in [84] are briefly reviewed. In Section 4.4, the fault diagnosis scheme using HOSMDs and neural adaptive estimators is proposed and applied to the satellite attitude control system studied in Chapter 2. Then, in Section 4.5, the fault diagnosis scheme using HOSMDs and the iterative neuron PID estimators is discussed and applied to a large angle satellite attitude control system. Finally, conclusions are presented.

4.2 Problem Formulation

The class of nonlinear dynamic systems with modeling uncertainties and additive state faults is presented as

$$\dot{x}_1 = h(x_1, x_2) \tag{4.1}$$

$$\dot{x}_2 = f(x_1, x_2) + Bu(t) + \eta(t) + \beta(t - T_f) f_a(t) \tag{4.2}$$

$$x_2 = h^{\dagger}(x_1, \dot{x}_1) \tag{4.3}$$

$$y = x_1 \tag{4.4}$$

where $x_1 \in \Re^n$, $x = [x_1^\top, x_2^\top]^\top$ is the vector of the system state, $u(t) = [u_1, \cdots, u_m]^\top$ and $y(t)$ are the system input and output vectors. Function vectors $f(x_1, x_2) = [f_1(x_1, x_2), \cdots, f_n(x_1, x_2)]^\top$ and $h(x_1, x_2) = [h_1(x_1, x_2), \cdots, h_n(x_1, x_2)]^\top$ describe the system state and output dynamics, respectively, $\eta(t) = [\eta_1(t), \cdots, \eta_n(t)]^\top$ denotes the uncertainty vector, and $f_a(t) = [f_a^{(1)}(t), \cdots, f_a^{(n)}(t)]^\top$ is the fault function vector. Moreover, $B \in \Re^{n \times m}$ is the control matrix, and, in (4.3), $h^{\dagger}$ is a pseudo-inverse

function of (4.1), which implies the state x_2 can be described as a nonlinear function of the system output and its derivative. The time profile function $\beta(t)$ is the same as that in Chapter 3.

For the sake of designing and analyzing the actuator fault diagnosis scheme conveniently, the following assumptions are introduced.

Assumption 4.1 All the functions in $f(x_1, x_2)$ and $h(x_1, x_2)$ are known.

Assumption 4.2 The state function $f(x(t))$ is differentiable at $\hat{x}_2$, which is

$$A(t) = \left.\frac{\partial f}{\partial x}\right|_{x=\hat{x}_2}$$

where $A(t)$ is an $n \times n$ matrix. So, the following equation is derived through a series expansion of $f(x)$ at $\hat{x}_2$.

$$f(x_1, x_2) - f(x_1, \hat{x}_2) = A(t)\tilde{x}_2(t) + \xi(x_1, x_2, \hat{x}_2) \tag{4.5}$$

where $\xi(x_1, x_2, \hat{x}_2) = o(\|\tilde{x}_2(t)\|)$, which contains the nonlinear high-order term of the state estimation error $\tilde{x}_2(t) = x_2(t) - \hat{x}_2(t)$.

Assumption 4.3 The nonlinear component $\xi(x_1, x_2)$ is Lipschitz at $\tilde{x}_2$ with a known constant k_ξ; that is

$$\|\xi(y, x_2) - \xi(y, \hat{x}_2)\| < k_\xi \|x_2 - \hat{x}_2\|. \tag{4.6}$$

Assumption 4.4 Matrix A is stable, which implies a symmetric positive definite matrix Γ_1 exists such that

$$A^\top \Gamma_1 + \Gamma_1 A = -Q \tag{4.7}$$

where Q is also a positive definite matrix. Even if the matrix A is unstable, we can stabilize the linear part of the system by using a Luenberger gain.

Assumption 4.5 The minimum and maximum eigenvalues of the symmetric positive definite matrix Γ_1 in Assumption 4.4 are ζ_1 and ζ_2, which satisfy

$$0 < \zeta_1 \leq \|\Gamma_1\| \leq \zeta_2. \tag{4.8}$$

The purpose of this study is to design an actuator fault detection, isolation, and estimation scheme for system (4.1)-(4.4) under Assumption 4.1-4.5.

4.3 High Order Sliding Mode Differentiators

From system (4.1)-(4.4), the relative degree from the input, u, to the output, y, is more than one. When $f(x_1, x_2)$ and $h(x_1, x_2)$ are general nonlinear functions, the observer design for (4.1) and (4.2) becomes a challenging task if high order sliding mode techniques are not used.

Equations (4.3) and (4.4) indicate that the unmeasurable state x_2 can be represented as a nonlinear function of the system output and its derivative. Therefore, if we can obtain the derivatives of y, the state x_2 can be estimated using (4.3) and (4.4).

In this chapter, second order or third order sliding mode differentiators [83] are used to obtain the first and second order derivatives of y, which are formulated as follows:

1. Second Order Sliding Mode Differentiator

$$\begin{aligned} \dot{z}_0 &= v_0 \\ v_0 &= -\lambda_0 |z_0 - y|^{2/3} sign(z_0 - y) + z_1 \\ \dot{z}_1 &= v_1 \\ v_1 &= -\lambda_1 |z_1 - v_0|^{1/2} sign(z_1 - v_0) + z_2 \\ \dot{z}_2 &= -\lambda_2 sign(z_2 - v_1). \end{aligned} \tag{4.9}$$

2. Third Order Sliding Mode Differentiator

$$\begin{aligned} \dot{z}_0 &= v_0 \\ v_0 &= -\lambda_0 |z_0 - y|^{3/4} sign(z_0 - y) + z_1 \\ \dot{z}_1 &= v_1 \\ v_1 &= -\lambda_1 |z_1 - v_0|^{2/3} sign(z_1 - v_0) + z_2 \\ \dot{z}_2 &= v_2 \\ v_2 &= -\lambda_2 |z_2 - v_1|^{1/2} sign(z_2 - v_1) + z_3 \\ \dot{z}_3 &= -\lambda_3 sign(z_3 - v_2) \end{aligned} \tag{4.10}$$

where λ_0, λ_1, λ_2, and λ_3 are diagonal positive coefficient matrices, and for a vector $x = [x_1, \cdots, x_n]^\top$, $|x|^{q_1/q_2} sign(x)$ is defined as $\left[|x_1|^{q_1/q_2} sign(x_1), \cdots, |x_n|^{q_1/q_2} sign(x_n)\right]^\top$.

The parameters of the differentiator can be easily adjusted because the estimation accuracy is not very sensitive to their values. However, a tradeoff exists: the larger the parameters, the faster the convergence and the higher sensitivity to input noises and the sampling interval.

It has been proved that if no measurement noise exists and all the coefficients are chosen properly, then, within a finite time, both the 2nd-order and 3rd-order sliding mode differentiators can guarantee

$$z_0 = y; \; z_1 = \dot{y}; \; z_2 = \ddot{y}. \tag{4.11}$$

If measurement noise exists with a magnitude less than ϵ, and all the coefficients are chosen properly, the high order sliding mode differentiators can ensure

$$\begin{aligned} |z_i - y^{(i)}| &\leq \mu_i \epsilon^{(n-i+1)/(n+1)}, \quad i = 0, 1, \cdots, n \\ |v_i - y^{(i+1)}| &\leq \nu_i \epsilon^{(n-i)/(n+1)}, \quad i = 0, 1, \cdots, n-1 \end{aligned} \tag{4.12}$$

where μ_i and ν_i are positive constants which are only dependent on the parameters of the differentiators [85].

4.4 Fault Diagnosis Using HOSMDs and Neural Adaptive Estimators

4.4.1 Diagnostic Neural Adaptive Observer Design

A neural adaptive observer which is used to diagnose faults is designed as follows,

$$\begin{aligned} \dot{\hat{x}}_2 &= f(y, \hat{x}_2) + Bu + \beta(t - T_m)\hat{M}_2(t), \quad \hat{x}_2(0) = x_{2D}(0) \\ x_{2D} &= h^\dagger(y, \dot{y}_D) \end{aligned} \tag{4.13}$$

where $\hat{x}_2 \in \Re^n$ is the estimated state, $\dot{y}_D$ is the first-order derivative of y computed via the high order sliding mode differentiators, and x_{2D} is the calculated state using

y and $\dot{y}_D$. If the high order sliding mode differentiators can exactly compute the derivative of y, then x_{2D} is completely equal to x_2. Moreover, we assume that the neural adaptive estimator $\hat{M}_2(t)$ is activated after all the states are estimated via HOSMDs, but before the occurrence of any fault. This assumption guarantees the performance of the neural adaptive estimators.

In addition, $\hat{M}_2(t)$, the diagnostic observer input, is described as

$$\hat{M}_{2,j}(t) = W_j(t)\sigma(V_j(t)I_j(t)) \tag{4.14}$$

where $\hat{M}_{2,j}$ is the jth element of $\hat{M}_2$, W_j and $V_j = [V_{j,1}, \cdots, V_{j,p+q}]$ are the parameters of $\hat{M}_{2,j}$, and τ denotes the time delay. The activation function is still a tangent hyperbolic function. The external input $I_j(t)$ is defined as

$$I_j(t) = [\hat{M}_{2,j}(t-\tau), \cdots, \hat{M}_{2,j}(t-p\tau), \tilde{x}_{2D,j}(t-\tau), \cdots, \tilde{x}_{2D,j}(t-q\tau)]^\top \tag{4.15}$$

where $\tilde{x}_{2D,j}$ is the jth element of $\tilde{x}_{2D}$, which is defined as $\tilde{x}_{2D} = x_{2D} - \hat{x}_2$. Suitable p and q are selected based on the time delay of practical systems and real time requirement. Large values of p and q may take more computational time and cause unnecessary delay.

Similar to neural state space models, the parameters of the neural adaptive estimators can be updated using a variety of optimization algorithms. Here, in order to achieve a fast convergence rate, the EKF-like algorithm is used as follows:

$$K_j(t) = P_j(t)H_j(t)[H_j^\top P_j H_j + R_j]^{-1} \tag{4.16}$$

$$\dot{P}_j(t) = -\mathcal{B}_{1,j}K_j(t)H_j^\top(t)P_j(t) \tag{4.17}$$

$$\dot{\hat{\theta}}_j(t) = \mathcal{B}_{2,j}K_j(t)\Xi[\tilde{x}_{2D,j}(t)] \tag{4.18}$$

where the parameter vector is defined as

$$\hat{\theta}_j(t) = [W_j(t), V_{j,1}, \cdots, V_{j,p+q}]^\top, \tag{4.19}$$

and the dead-zone operator $\Xi[\cdot]$ is defined to be

$$\Xi[\tilde{x}_{2D,j}(t)] = \begin{cases} \tilde{x}_{2D,j}(t) & \text{if } |\tilde{x}_{2D,j}(t)| \geq \epsilon_i \\ 0 & \text{if } |\tilde{x}_{2D,j}(t)| < \epsilon_i \end{cases} \tag{4.20}$$

where ϵ_i is a threshold for robust fault diagnosis.

The dead-zone operator assures that the parameter adaptation is insensitive to fault estimation errors under a certain magnitude, allowing the fault diagnosis scheme to be robust with respect to system uncertainties.

When the exact derivative of y is available using the high order sliding mode differentiators, the dynamics of the unmeasurable state estimation error is obtained by subtracting (4.13) from (4.1), resulting in

$$\begin{aligned} \dot{\tilde{x}}_2 &= \dot{\tilde{x}}_{2D} \\ &= f(y, x_{2D}) - f(y, \hat{x}_2) + \eta(t) + \beta(t - T_f) f_a(t) - \beta(t - T_m)\hat{M}_2(t). \end{aligned} \quad (4.21)$$

The proposed fault diagnosis scheme using HOSMDs and neural adaptive estimators is implemented using the following algorithm:

- Step 1: Based on (4.1) - (4.4), obtain the first order derivative of system output y using HOSMDs (4.9) or (4.10).
- Step 2: Design a neural adaptive observer based on (4.13) and (4.14).
- Step 3: If all states are estimated by HOSMDs, then activate the neural adaptive estimator (4.14) at $t = T_m$. Otherwise, $\hat{M}_{2,j}(t) = 0$ and goes to Step 1.
- Step 4: Update the parameters of the neural adaptive estimator using an EKF-like algorithm.
- Step 5: Compare $\hat{M}_{2,j}(t)$ with a predetermined threshold to detect fault.
- Step 6: Use $\hat{M}_{2,j}(t)$ to isolate and estimate fault.

4.4.2 Property Analysis

In this section, the convergence property of the observer input $\hat{M}_2(t)$ is first investigated. Then, the stability of the proposed fault diagnosis scheme is analyzed.

Based on (4.14), the jth neural adaptive estimator $\hat{M}_{2,j}$ can be rewritten as

$$\hat{M}_{2,j}(t) = W_j(t)\sigma\left(\sum_{i=1}^{p} V_{j,i}\hat{M}_{2,j}(t-i\tau) + \sum_{i=1}^{q} V_{j,p+i}\tilde{x}_{2D,j}(t-i\tau)\right). \tag{4.22}$$

If the time t is denoted as $t = k\tau$, and we set the time delay as one, then (4.22) is expressed as

$$\hat{M}_{2,j}(k+1) = W_j\sigma\left(\sum_{i=1}^{p} V_{j,i}\hat{M}_{2,j}(k-i+1) + B_j(k)\right) \tag{4.23}$$

where $B_j(k) = \sum_{i=1}^{q} V_{j,p+i}\tilde{x}_{2D,j}(k-i+1)$ is the bias.

We define a vector $z = [z_1(k), \cdots, z_p(k)]^\top$, where $z_i(k) = \hat{M}_{2,j}(k-i+1)$, for $i = 1, \cdots, p$ as a new state vector of the observer input. Hence, (4.23) can be written as

$$z_1(k+1) = W_j\sigma\left(\sum_{i=1}^{p} V_{j,i}z_i(k) + B_j(k)\right). \tag{4.24}$$

Let $z^* = [z_1^*, \cdots, z_p^*]$ be the equilibrium point of (4.24), which is well known to satisfy $z(k+1) = z(k) = z^*$, $k = 0, 1, 2, \cdots$. Due to the recursive property of the state z, clearly the equilibrium equation can be represented by

$$z_1^* = W_j\sigma\left(\sum_{i=1}^{p} V_{j,i}z_i^* + B_j\right) \tag{4.25}$$

and $z_1^* = z_2^* =, \cdots, = z_p^*$.

Lemma 1 The system $x(k+1) = \Phi x(k)$ is asymptotically stable if and only if all the eigenvalues of Φ are located within the unit circle of the complex plane [144].

A theorem regarding the stability of the equilibrium point of (4.24) is presented as follows.

Theorem 4.1 *The equilibrium point z^* of (4.24) is asymptotically stable if the absolute value of $W_j \cdot \Delta \cdot \sum_{i=1}^{p} V_{j,i}$ is less than one, where Δ is of the following form:*

$$\Delta = \frac{1}{2}\left[1 - \sigma^2\left(\sum_{i=1}^{p} V_{j,i}z_1^* + B_j\right)\right]. \tag{4.26}$$

Proof: Taking an approximation of $z_1(k+1)$ around the equilibrium point z_1^* by means of Taylor series, we have

$$\begin{aligned} z_1(k+1) &= W_j\sigma\left(\sum_{i=1}^{p} V_{j,i}z_i(k) + B_j\right) \\ &\simeq W_j\sigma\left(\sum_{i=1}^{p} V_{j,i}z_i^* + B_j\right) + W_j\cdot\Delta\cdot\sum_{i=1}^{p} V_{j,i}(z_1 - z_1^*). \end{aligned} \tag{4.27}$$

The first order derivative of $z_1(k+1)$ evaluated at the equilibrium point z_1^* is $W_j\cdot\Delta\cdot\sum_{i=1}^{p} V_{j,i}$. The value of Δ is within the interval (0, 1/2). Therefore, the equilibrium point z^* is asymptotically stable if the absolute value of $W_j\cdot\Delta\cdot\sum_{i=1}^{p} V_{j,i}$ is less than one. ∎

Remark 4.1 *For a healthy system with an ideal observer, $\tilde{x}_2$ is supposed to approach zero. As a result, $\hat{M}_2(t)$ becomes an autonomous system, and $\hat{M}_2(t)$ is asymptotically stable to the equilibrium point zero. When a fault occurs, B_j in (4.24), which contains $\tilde{x}_2$, is not longer zero. The value of $W_j\cdot\Delta\cdot\sum_{i=1}^{p} V_{j,i}$ is modified to satisfy the Theorem 4.1. The observer input $\hat{M}_2$ will be asymptotically stable to the nonzero fault function.*

After investigating the properties of the neural adaptive estimators, we study the stability of the neural adaptive observer based fault diagnosis scheme using a Lyapunov approach.

Based on the fundamental approximation theory, the fault function can be approximated by (4.22) in a compact set, provided $f_a(t)$ is a smooth function of the system states. Therefore, if the structure and parameters of the neural adaptive estimators are carefully adjusted, a bank of neural adaptive estimators exists that is able to approximate the fault function with sufficient accuracy; i.e.,

$$\max\|f_a(x_2,t) - \hat{M}_2(t)\| \le \delta_f. \tag{4.28}$$

Regarding the boundedness of $\tilde{x}_2$, we have the following theorem.

Theorem 4.2 *Consider the nonlinear dynamics (4.1)-(4.4) under Assumptions 4.1-4.5, and the proposed neural adaptive observer (4.13), when the high order sliding*

mode differentiators work well, and the neural adaptive estimators are carefully tuned, then the state estimation error $\tilde{x}_2$ is bounded by a ball with radius b, i.e.,

$$\|\tilde{x}_2\| \leq \frac{2\gamma}{\rho_1} = b. \tag{4.29}$$

Proof: Consider a Lyapunov function candidate

$$V(t) = \tilde{x}_2^\top(t)\Gamma_1\tilde{x}_2(t) \tag{4.30}$$

where Γ_1 is defined in Assumption 4.4.

Based on Assumption 4.1-4.5, and the estimation error dynamics (4.21) after the occurrence of any fault, the derivative of $V(t)$ with respect to time t is

$$\begin{aligned}
\dot{V}(t) &= \dot{\tilde{x}}_2^\top\Gamma_1\tilde{x}_2 + \tilde{x}_2^\top\Gamma_1\dot{\tilde{x}}_2 \\
&= \tilde{x}_2^\top(A^\top\Gamma_1 + \Gamma_1 A)\tilde{x}_2 + 2\tilde{x}_2^\top\Gamma_1(\xi(y,x_2) - \xi(y,\hat{x}_2)) \\
&\quad +2\tilde{x}_2^\top\Gamma_1\eta(t) + 2\tilde{x}_2^\top\Gamma_1(f_a(t) - \hat{M}_2(t)) \\
&< -\lambda_{\min}(Q)\|\tilde{x}_2\|^2 + 2k_\xi\|\tilde{x}_2\|\|\Gamma_1\| + 2\eta_0\|\tilde{x}_2\|\|\Gamma_1\| + 2\delta_f\|\tilde{x}_2\|\|\Gamma_1\| \\
&= -\rho_1\|\tilde{x}_2\|^2 + 2\gamma\|\tilde{x}\| \\
&= -\rho_1\Big(\|\tilde{x}_2\| - \frac{\gamma}{\rho_1}\Big)^2 + \frac{\gamma^2}{\rho_1}
\end{aligned} \tag{4.31}$$

where $\rho_1 = \lambda_{\min}(Q)$, and $\gamma = \|\Gamma_1\|(k_\xi + \eta_0 + \delta_f)$.

The inequality (4.31) implies that if $\|\tilde{x}_2\| \geq \frac{2\gamma}{\rho_1}$ then $\dot{V}$ is negative and $\tilde{x}_2$ is uniformly bounded. ∎

4.4.3 Application to a Satellite Attitude Control System

In this section, the proposed fault diagnosis scheme using high order sliding mode differentiators and neural adaptive estimators is applied to the satellite attitude control system, which has been studied in Section 2.6.

The dynamics of the satellite attitude control system is given in Section 2.6. A third order sliding mode differentiator is used to obtain the derivatives of the three angles. In order to guarantee the performance of the HOSMD, the sampling time

interval is set to 5×10^{-4}. The coefficients in the HOSMD are set to $\lambda_0 = \lambda_1 = \lambda_2 = \lambda_3 = 40$.

The jth neural adaptive estimator is selected to be

$$\hat{M}_{2,j}(t) = W_j(t)\sigma\left(\sum_{i=1}^{3} V_{j,i}\hat{M}_{2,j}(t - i\tau) + V_{j,4}\tilde{x}_{2D,j}(t - \tau)\right) \tag{4.32}$$

where the delays $p = 3$ and $q = 1$ are chosen based on a trial-and-error method. The initial values of the parameters in the EKF algorithm are set to $P_j(0) = 100I_5$, and $R_j(0) = 2 \times 10^{-5}$. The neural adaptive estimators are pre-trained before being used for fault isolation and estimation. In the simulation, $\hat{M}_2(t)$ is not activated until $t = 7.5sec$, and we assume a fault exists in the third actuator; i.e.,

$$f_a^{(3)}(t) = -3.2\beta(t - 10)\sin((t - 10)/0.35) \tag{4.33}$$

The control torque is assumed to be subject to disturbance by $\varsigma_u = 1\% * rand$; i.e., $T_d = \varsigma_u u$, while the Euler angles have measurement noise with $\varsigma_y = 0.5\% * rand$; i.e., $\theta_{measure} = (1 + \varsigma_y)\theta$, where $rand$ is still a Gaussian white noise.

The simulation results are shown in Figure 4.1 to 4.3. Figure 4.1 and Figure 4.2 demonstrate the system states can be accurately estimated by using third order sliding mode differentiators, no matter if the system is healthy or faulty. Figure 4.3 illustrates that if the threshold for fault diagnosis is set to ± 0.5, only the output of the third estimator is out of the threshold after the $10th$ second and the others are not. The activation of the fault estimator causes a large magnitude of chattering. That is due to the transient learning process of neural adaptive estimators. The appearance of peaks in the fault estimation is because corrupting measurement noise is introduced into the HOSMDs, and the system itself is sensitive to modeling uncertainties. Detailed discussion and methods attenuating the coupling peaks can be found in [87]. This result implies the observer inputs can effectively detect and isolate the fault if a proper threshold is chosen. Moreover, only the estimator $\hat{M}_{2,3}(t)$ can characterize the fault with a satisfactory performance.

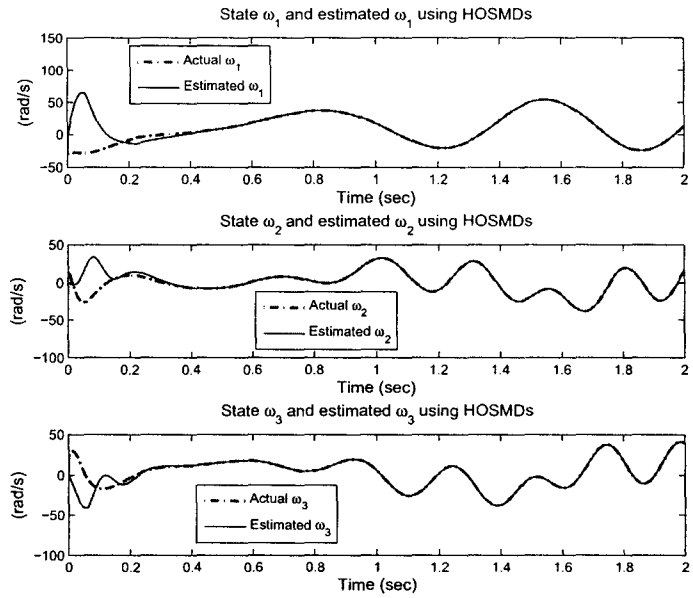

Figure 4.1: Actual states and estimated states using third order sliding mode differentiators

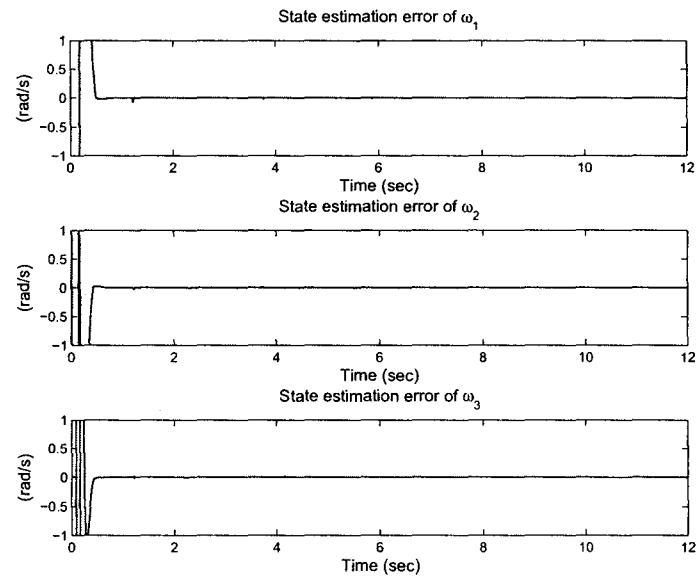

Figure 4.2: Time-behavior of state estimation error

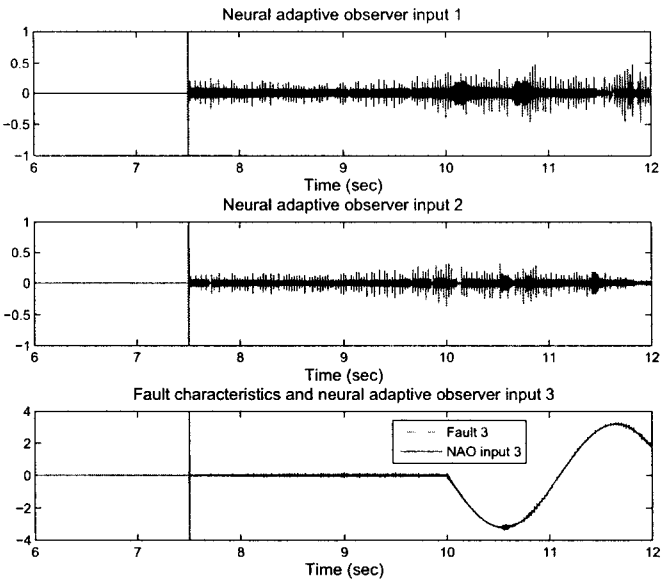

Figure 4.3: Characteristics of the fault $f_a^{(3)}(t)$ and neural adaptive estimators

4.5 Fault Diagnosis Using HOSMDs and Iterative Neuron PID Estimators

In previous chapters, fault estimators based on neural networks and iterative learning algorithm were designed. Although the PID-type iterative learning fault estimator is able to reduce the overshoot and eliminate the transient-time process in fault estimation, it may take too much time in the iterative learning process because the PID-type iterative learning fault estimator is a linear combination of three inputs. Moreover, the nonlinear activation functions in neural networks allow the neural networks to approximate nonlinear functions. Therefore, inspired by this principle, an iterative neuron PID fault estimator is proposed in this section.

4.5.1 Iterative Neuron PID Fault Observer Design

The structure of the fault diagnostic observer is the same as (4.13), and the only difference is the observer input $\hat{M}_2(t)$, which is defined as the fault estimator. We

assume the fault diagnosis algorithm is implemented using computers. Hence, at each sampling time of t, $\hat{M}_2(t)$ is iteratively updated in an iteration domain; i.e.,

$$\begin{aligned}\hat{M}_{2,i}(k+1) &= \hat{M}_{2,i}(k) + W_i(k)\sigma\Big(V_{i,1}(k)z_{i,1}(k) \\ &\quad + V_{i,2}(k)z_{i,2}(k) + V_{i,3}(k)z_{i,3}(k)\Big)\end{aligned} \tag{4.34}$$

where k is the index of the iterative learning domain, W_i, $V_{i,j}$, for $i = 1, \cdots, n$, and $j = 1, \cdots, 3$ are the parameters of the estimator, and $\sigma(\cdot)$ is still the tangent hyperbolic function. Defining $e_i(k) = \tilde{x}_{2D,i} - \hat{M}_{2,i}(k)$, we design the external inputs of $\hat{M}_{2,i}(k+1)$ to be

$$\begin{cases} z_{i,1}(k) &= e_i(k) \\ z_{i,2}(k) &= \Delta e_i(k) = e_i(k) - e_i(k-1) \\ z_{i,3}(k) &= \Delta^2 e_i(k) = e_i(k) - 2e_i(k-1) + e_i(k-2) \end{cases} \tag{4.35}$$

The parameters to be updated are formulated in a vector form as

$$\theta_i(k) = [W_i(k),\ V_{i,1}(k),\ V_{i,2}(k),\ V_{i,3}(k)]^{\mathsf{T}}. \tag{4.36}$$

To update the parameters of this fault estimator, four update laws are designed and analyzed, respectively.

Algorithm 1: Robust gradient descent algorithm (RGDA)–The robust gradient descent algorithm is designed as

$$\theta_i(k+1) = \theta_i(k) + \gamma_i H_i(k)\Xi[e_i(k)] \tag{4.37}$$

where $H_i(k)$ is the derivative of $\hat{M}_{2,i}(k)$ with respect to $\theta_i(k)$. The positive scalar γ_i is the learning rate, which balances the convergence speed. The dead-zone operator $\Xi[\cdot]$ is defined as

$$\Xi[e_i(k)] = \begin{cases} e_i(k) & \text{if } |e_i(k)| \geq \epsilon_i \\ 0 & \text{if } |e_i(k)| < \epsilon_i \end{cases} \tag{4.38}$$

where ϵ_i is a threshold for robust fault diagnosis. The dead-zone operator guarantees that the parameter updating is insensitive to estimation error under a certain magnitude, which realizes robustness with respect to system uncertainties.

The convergence of the proposed robust gradient descent algorithm is analyzed by considering a cost function as

$$J(\theta_i(k)) = \frac{1}{2}e_i^2(k). \tag{4.39}$$

The purpose of the parameter updating law is to decrease the cost function $J(\theta_i(k))$, that is,

$$\Delta J(\theta_i(k)) = J(\theta_i(k+1)) - J(\theta_i(k)) < 0. \tag{4.40}$$

Based on the first-order Taylor series expansion of $J(\theta_i(k+1))$ around $\theta_i(k)$ and using (4.37), we have

$$\begin{aligned} J(\theta_i(k+1)) &= J(\theta_i(k) + \Delta\theta_i(k)) \\ &\approx J(\theta_i(k)) + \nabla J(\theta_i)^\top \Delta\theta_i(k) \\ &= J(\theta_i(k)) - H_i(k)^\top e_i(k)\Delta\theta_i(k) \\ &= J(\theta_i(k)) - \gamma_i \|H_i(k)\|^2 e_i(k)\Xi[e_i(k)] \end{aligned} \tag{4.41}$$

where $\nabla J(\theta_i)$ is the gradient of $J(\theta_i)$ at $\theta_i(k)$. When $|e_i(k)| \geq \epsilon_i$, $J(\theta_i(k+1)) < J(\theta_i(k))$, which implies the parameter updating process is convergent. When $|e_i(k)| < \epsilon_i$, $\Delta J(\theta_i(k)) = 0$, and the parameters stop updating, which shows the robustness of the algorithm.

The convergence rate of the gradient descent algorithm is inherently slow, especially when the fixed learning rate is not properly chosen. Therefore, an adaptive law with a time-varying learning rate is used.

Algorithm 2: Robust extended Kalman filter algorithm–The robust EKF algorithm is formulated in a discrete-time form as

$$\begin{aligned} K_i(k) &= P_i(k)H_i(k)[H_i(k)^\top P_i(k)H_i(k) + R_i(k)]^{-1} \\ P_i(k+1) &= P_i(k) - K_i(k)H_i(k)^\top P_i(k) \\ \theta_i(k+1) &= \theta_i(k) + K_i(k)\Xi[e_i(k)] \end{aligned} \tag{4.42}$$

where $K_i(k)$ is the Kalman gain, $P_i(k)$ is the covariance matrix of the state estimation error, $H_i(k)$ is still the derivative of $\hat{M}_{2,i}(k)$ with respect to $\theta_i(k)$, and $R_i(k)$ is the

noise covariance matrix. $\Xi[\cdot]$ is the robust operator described in (4.37). According to [134], $R_i(k)$ is recursively computed via

$$R_i(k) = R_i(k-1) + [e_i(k)^2 - R_i(k-1)]/k \tag{4.43}$$

Convergence of the EKF algorithm is investigated in previous section.

Remark 4.2 *Both the robust gradient descent algorithm and the robust EKF algorithm belong to optimization algorithms, and their convergence properties can be analyzed using the same cost function. In these two algorithms, $\Delta\theta_i(k)$ are both proportional to the fault estimation error $e_i(k)$. However, the learning rate of the gradient descent algorithm is a pre-determined number, γ_i, while the learning rate of the EKF algorithm is an iteration-varying term, $P_i(k)[H_i(k)^\top P_i(k)H_i(k)+R_i(k)]^{-1}$, which leads to a faster convergence process. The local convergence of RGDA can be guaranteed rigorously, while the convergence of EKF algorithm is harder to analyze. Chapter (3.5.1) provides a method to investigate the convergence of EKF algorithm.*

Algorithm 3: Robust iterative learning algorithm (RILA) 1–A robust iterative learning algorithm is proposed to update each parameter respectively; that is

$$\begin{cases} W_i(k+1) &= W_i(k) + d_0\Xi[e_i(k)] \\ V_{i,1}(k+1) &= V_{i,1}(k) + d_1\Xi[z_{i,1}(k)] \\ V_{i,2}(k+1) &= V_{i,2}(k) + d_2\Xi[z_{i,2}(k)] \\ V_{i,3}(k+1) &= V_{i,3}(k) + d_3\Xi[z_{i,3}(k)] \end{cases} \tag{4.44}$$

where $d_0 \sim d_3$ are the iterative learning rates.

Algorithm 4: Robust iterative learning algorithm (RILA) 2–Another robust iterative learning algorithm is proposed by considering the directions of the parameters variation; that is

$$\begin{cases} W_i(k+1) &= W_i(k) + d_0|\Xi[e_i(k)]|sign(e_i(k))sign(e_i(k-1)) \\ V_{i,1}(k+1) &= V_{i,1}(k) + d_1|\Xi[z_{i,1}(k)]|sign(z_{i,1}(k))sign(z_{i,1}(k-1)) \\ V_{i,2}(k+1) &= V_{i,2}(k) + d_2|\Xi[z_{i,2}(k)]|sign(z_{i,2}(k))sign(z_{i,2}(k-1)) \\ V_{i,3}(k+1) &= V_{i,3}(k) + d_3|\Xi[z_{i,3}(k)]|sign(z_{i,3}(k))sign(z_{i,3}(k-1)) \end{cases} \tag{4.45}$$

Defining a vector $S_i(k) = [e_i(k),\ z_{i,1}(k),\ z_{i,2}(k),\ z_{i,3}(k)]^\top$ and the coefficient matrix $D = diag\{d_0, d_1, d_2, d_3\}$, (4.45) can be formulated into a vector form as

$$\theta_{i,k+1} = \theta_{i,k} + D|\Xi[S_{i,k}]| \cdot sign(S_{i,k}) \cdot sign(S_{i,k-1}) \tag{4.46}$$

where the dot multiplication operator "$\cdot$" represents the product of the corresponding element in two vectors. The *sign* function and dead-zone operator, $\Xi[\cdot]$, operate on each element of a vector. For simplicity of expression, the iteration index k is written as a subscript.

The convergence of RILA 2 is investigated in the following theorem, and the convergence of RILA 1 can be similarly derived.

Theorem 4.3 *The robust iterative learning algorithm (4.45) is convergent, if the inequality (4.51) is satisfied.*

Proof: When the parameters are updated, we assume an optimal parameter θ_i^* exists which enables the observer input to precisely characterize the fault. Subtracting both sides of (4.46) from θ_i^* yields

$$\Delta\theta_{i,k+1} = \Delta\theta_{i,k} - D|S_{i,k}| \cdot sign(S_{i,k}) \cdot sign(S_{i,k-1}) \tag{4.47}$$

where $\Delta\theta_{i,k} = \theta_i^* - \theta_{i,k}$. Doing inner product of both sides of (4.47) with themselves via D^{-1}, we have

$$\begin{aligned} \Delta\theta_{i,k+1}^\top D^{-1}\Delta\theta_{i,k+1} &= \theta_{i,k}^\top D^{-1}\theta_{i,k} + |S_{i,k}^\top|D|S_{i,k}| \\ &\quad -2\Delta\theta_{i,k}^\top|S_{i,k}| \cdot sign(S_{i,k}) \cdot sign(S_{i,k-1}). \end{aligned} \tag{4.48}$$

Integrating (4.48) over the time interval $[0,\ t]$ results in

$$\begin{aligned} \|\Delta\theta_{i,k+1}\|_{D^{-1}}^2 &= \|\Delta\theta_{i,k}\|_{D^{-1}}^2 + \|S_{i,k}\|_D^2 \\ &\quad -2\int_0^t \Delta\theta_{i,k}^\top(\tau)|S_{i,k}(\tau)| \cdot sign(S_{i,k}) \cdot sign(S_{i,k-1})d\tau \\ &= \|\Delta\theta_{i,k}\|_{D^{-1}}^2 + \|S_{i,k}\|_D^2 - 2\int_0^t |\Delta\theta_{i,k}^\top(\tau)||S_{i,k}(\tau)|d\tau \end{aligned} \tag{4.49}$$

where $\|\cdot\|_{D^{-1}}$ is a functional norm defined as

$$\|\Delta\theta_{i,k}\|^2_{D^{-1}} = \int_0^t \Delta\theta_{i,k}^\top(\tau)D^{-1}\Delta\theta_{i,k}(\tau)d\tau. \tag{4.50}$$

If a positive constant α exists such that

$$\begin{aligned}\int_0^t \Delta\theta_{i,k}^\top(\tau)S_{i,k}(\tau)d\tau &\geq \frac{1+\alpha}{2}\int_0^t S_{i,k}^\top(\tau)DS_{i,k}(\tau)d\tau \\ &= \frac{1+\alpha}{2}\|S_{i,k}\|^2_D,\end{aligned} \tag{4.51}$$

then,

$$\begin{aligned}\|\Delta\theta_{i,k+1}\|^2_{D^{-1}} &\leq \|\Delta\theta_{i,k}\|^2_{D^{-1}} + \|S_{i,k}\|^2_D - (1+\alpha)\|S_{i,k}\|^2_D \\ &= \|\Delta\theta_{i,k}\|^2_{D^{-1}} - \alpha\|S_{i,k}\|^2_D.\end{aligned} \tag{4.52}$$

Inequality (4.52) shows that the sequence $\{\|\Delta\theta_{i,k}\|_{D^{-1}}\}$ monotonously decreases as the iteration number k increases, as long as $\|S_{i,k}\|_D$ is nonzero. The monotonous decrease of $\{\|\Delta\theta_{i,k}\|_{D^{-1}}\}$ implies $\|S_{i,k}\|_D \mapsto 0$ as $k \mapsto \infty$, since $\{\|\Delta\theta_{i,k}\|_{D^{-1}}\}$ is bounded from below. ∎

Remark 4.3 *RILA 1 only uses S_i at the kth iteration to update the parameters, while RILA 2 considers the values of S_i at both the kth and $(k-1)$th iterations. RILA 2 is inspired by the adaptation law in [124]. The difference is that the adaptation coefficients in RILA 2 are iteration-varying instead of constant values. This modification will accelerate the convergence process.*

Remark 4.4 *Both RGDA and EKF algorithm need to calculate the derivative $H_i(k)$, where the computational complexity is determined by the structure of the fault estimators. RILA 2, though avoids the calculation of derivatives, has to call signum functions, and more memories are needed to store variables at previous iterations. The learning rates in RILA 1 and RILA 2 need to be carefully selected using a trial-and-error method, in order to guarantee a fast convergence of the estimation error.*

The proposed fault diagnosis scheme using HOSMDs and iterative Neuron PID estimators is implemented using the following algorithm:

- Step 1: Based on (4.1) - (4.4), obtain the first order derivative of system output y using HOSMDs (4.9) or (4.10).
- Step 2: Design an iterative neuron PID observer based on (4.13) and (4.34).
- Step 3: If all states are estimated by HOSMDs, then activate the INPID estimator (4.34) at $t = T_m$. Otherwise, $\hat{M}_{2,i}(k) = 0$ and goes to Step 1.
- Step 4: Update the parameters of the INPID fault estimator using either of the four algorithms (4.37), (4.42), (4.44), and (4.45).
- Step 5: Compare $\hat{M}_{2,i}(k)$ with a predetermined threshold to detect fault.
- Step 6: Use $\hat{M}_{2,i}(k)$ to isolate and estimate fault.

4.5.2 Application to a Large Angle Satellite Control System

In this section, the proposed fault diagnosis scheme is applied to a satellite with large angle attitude maneuvers [145], [146], [147]. The dynamics of the satellite are described as follows:

$$J_M\dot{\omega} = -S(\omega)J_M\omega + T_d + B_1u \tag{4.53}$$

where $\omega = [\omega_1,\ \omega_2,\ \omega_3]^\top$ is the angular velocity. J_M is the symmetric moment of the inertia matrix:

$$J_M = \begin{bmatrix} J_{11} & -J_{12} & -J_{13} \\ -J_{12} & J_{22} & -J_{23} \\ -J_{13} & -J_{23} & J_{33} \end{bmatrix}$$

with J_{ii} being the moment of inertia along the ith axis. T_d is the disturbance torque input, and $u = [u_1\ u_2\ u_3\ u_4]^\top$ is the control input. B_1 is the control matrix as follows,

$$B_1 = \begin{bmatrix} -\beta_1 & \beta_1 & -\beta_1 & \beta_1 \\ -\beta_2 & -\beta_2 & \beta_2 & \beta_2 \\ -\beta_3 & \beta_3 & \beta_3 & -\beta_3 \end{bmatrix}$$

where $\beta_1 = \dfrac{2d_1d_2}{D_0}\lambda$, $\beta_2 = d_2 - \dfrac{d_2}{D_0}l\lambda$, $\beta_3 = d_1 + \dfrac{d_1}{D_0}l\lambda$, and $D_0 = \sqrt{d_1^2 + d_2^2}$. The satellite parameters used in the simulation are listed in Table 4.1.

Table 4.1: Parameters of a large angle satellite

Parameters	Values (unit)
Moment of inertia J_{11}	5.5384 (kg m^2)
Moment of inertia J_{12}	0.0276 (kg m^2)
Moment of inertia J_{13}	0.0242 (kg m^2)
Moment of inertia J_{22}	5.6001 (kg m^2)
Moment of inertia J_{23}	0.0244 (kg m^2)
Moment of inertia J_{33}	4.2382 (kg m^2)
Angle canted from x-axis λ	5 (deg)
Distance from center of mass l	0.5 (m)
Geometric parameter 1 d_1	0.1 (m)
Geometric parameter 2 d_2	0.2 (m)

The skew symmetric matrix $S(\omega)$ is

$$S(\omega) = \begin{bmatrix} 0 & -\omega_3 & \omega_2 \\ \omega_3 & 0 & -\omega_1 \\ -\omega_2 & \omega_1 & 0 \end{bmatrix}.$$

Quaternions were invented as a result of searching for hypercomplex numbers that could be represented by points in three dimensional space. Quaternions have no inherent geometric singularity as do Euler angles. Moreover, quaternions are well suitable for realtime computation since only products and no trigonometric relations exist in the quaternion kinematic differential equations. Thus, spacecraft orientation is now commonly presented in terms of quaternions. The kinematics of the satellite is written as

$$\begin{cases} \dot{\mathbf{q}} &= \frac{1}{2}\left(q_4 I + S(\mathbf{q})\right)\omega \\ \dot{q}_4 &= -\frac{1}{2}\mathbf{q}^\top \omega \end{cases} \tag{4.54}$$

where $\mathbf{q} = [q_1\ q_2\ q_3]^\top$ and q_4 are the quaternions of the satellite, which satisfy $\mathbf{q}^\top\mathbf{q} + q_4^2 = 1$.

Defining the state vector as $x = [\mathbf{q}^\top \quad q_4 \quad \omega^\top]^\top$, the attitude dynamics is summarized by combining (4.53) and (4.54) as

$$\dot{x} = f(x) + B(x)u + g_1(x)T_d \tag{4.55}$$

$$y = [q_1,\ q_2,\ q_3,\ q_4]^\top \tag{4.56}$$

where

$$f(\mathbf{q},\, q_4,\, \omega) = \begin{bmatrix} \frac{1}{2}(q_4\omega + S(\mathbf{q})\omega) \\ -\frac{1}{2}\mathbf{q}^\top\omega \\ -J_M^{-1}S(\omega)J_M\omega \end{bmatrix}, B = \begin{bmatrix} \mathbf{0} \\ 0 \\ J_M^{-1}B_1 \end{bmatrix}, g_1 = \begin{bmatrix} \mathbf{0} \\ 0 \\ J_M^{-1} \end{bmatrix}.$$

Based on (4.54), we can obtain

$$\begin{bmatrix} \omega_1 \\ \omega_2 \\ \omega_3 \end{bmatrix} = 2 \begin{bmatrix} q_4 & -q_3 & q_2 \\ q_3 & q_4 & -q_1 \\ -q_2 & q_1 & q_4 \end{bmatrix}^{-1} \begin{bmatrix} \dot{q}_1 \\ \dot{q}_2 \\ \dot{q}_3 \end{bmatrix}. \tag{4.57}$$

Therefore, (4.55) - (4.57) belong to the class of nonlinear systems (4.1)-(4.4).

Using (4.57) and third order sliding mode differentiators, we can estimate the system unmeasurable state ω. Then, an iterative neuron PID diagnostic observer is designed according to (4.34).

In the simulation, we assume the system is subject to random uncertainties $0.03 * rand$. The system output is assumed to be subject to random noises with $\varsigma = 0.2\% * rand$; i.e., $y_{measure} = y(1+\varsigma)$, where *rand* is a Gaussian white noise signal. Four cases are considered to verify the performance of the proposed fault diagnosis scheme. In these four cases, the upper bound of the dead-zone operator is set to $\epsilon_i = 0.005$.

Case 1: Single incipient fault $f_a^{(1)}(t)$ with RILA 2–An incipient fault $f_a^{(1)}(t)$ is assumed to occur in the dynamics of state ω_1; i.e.,

$$f_a^{(1)}(t) = 3\beta(t-4)\sin(2\pi t/4). \tag{4.58}$$

Case 2: Single incipient fault $f_a^{(2)}(t)$ with RILA 1–An incipient fault $f_a^{(2)}(t)$ is assumed to occur in the dynamics of state ω_2; i.e.,

$$f_a^{(2)}(t) = -2.5\beta(t-4)\sin(2\pi t/2). \tag{4.59}$$

Case 3: Single incipient constant fault $f_a^{(3)}(t)$ with EKF algorithm–An incipient fault $f_a^{(3)}(t)$ is assumed to occur in the dynamics of state ω_3; i.e.,

$$f_a^{(3)}(t) = 2.8\beta(t-4)\big(1-\exp(-(t-4)/0.2)\big). \tag{4.60}$$

Case 4: Multiple faults $f_a^{(3)}(t)$ with RGDA–An incipient fault $f_a^{(2)}(t)$ and an abrupt constant fault $f_a^{(3)}(t)$ are assumed to occur in the dynamics of state ω_2 and ω_3, respectively; i.e.,

$$f_a^{(2)}(t) = \beta(t-4)\big(-0.75\sin(2\pi t/4) - 0.8\sin(2\pi t/2) - 0.9\sin(2\pi t)\big) \quad (4.61)$$

$$f_a^{(3)}(t) = 2.5\beta(t-5)\big(1-\exp(-(t-5)/0.2)\big). \quad (4.62)$$

The simulation results for these four cases are shown from Figure 4.4 to Figure 4.12. Figures 4.4, 4.7, 4.9 and 4.11 show that the system output will deviate from their normal values when a fault or faults occur. Figure 4.5 demonstrates that the unmeasurable states $\omega_1 \sim \omega_3$ can be accurately estimated by using third order sliding mode differentiators and system dynamics. Figure 4.6, 4.8, 4.10, 4.12 characterize the faults and outputs of the three INPID fault estimators using the four parameter update algorithms, respectively. If we choose the threshold for fault detection to be ± 0.5, after the system states are estimated via the HOSMDs, robust fault detection can be successfully achieved. The spikes in the output of the fault estimators prior to the onset of any fault can be explained by the estimation errors caused by the HOSMDs and the parameter update algorithms. Moreover, after a fault occurs, only the estimator that corresponds to the faulty state specifies the fault, and other estimators remain zero or close to zero. Comparing the proposed four robust parameter update algorithms, though different algorithms are tested using different cases, their estimation performances are similar. In-depth investigation of the computational complexity and real-time issues of these algorithms needs further work. These simulation results demonstrate that the proposed fault diagnosis scheme can successfully isolate and estimate a single fault as well as multiple faults.

4.6 Conclusions

In this chapter, a fault diagnosis scheme using high order sliding mode differentiators and learning approaches was investigated in a class of nonlinear systems, where the system state were represented by a nonlinear function of the system output and its derivatives. Through HOSMDs, the system state was estimated, and then a diagnostic

observer was designed using the obtained state information and learning approaches. A neural adaptive observer and an iterative neuron PID observer were developed to isolate and estimate the faults. After theoretical analysis, the proposed two fault diagnosis observers were applied to a satellite attitude control system and a large angle satellite control system, respectively. The simulation results showed the effectiveness of the proposed fault diagnosis schemes.

A HOSMDs-based fault diagnostic observer offers a new way to diagnose faults, which is different from traditional observer-based approaches. Its strength lies in its capability to deal with difficult cases where traditional observer-based fault diagnosis schemes might fail [148], [149]. The relationship between the traditional observer-based approaches and the method in this chapter needs further exploration.

The necessity of using high order sliding mode differentiators is a limitation when the measurement noise is present. Therefore, designing new input/output relation based fault diagnosis schemes, which do not depend on high order derivatives of the output, is a topic of future research.

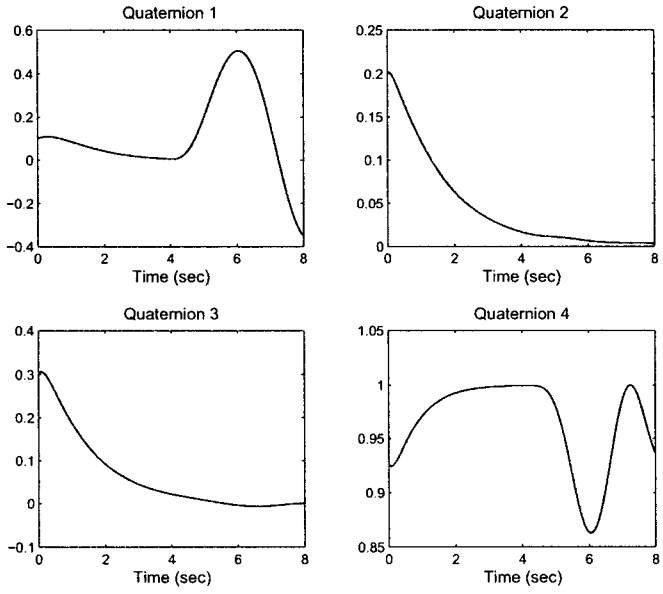

Figure 4.4: Measured quaternions in case 1

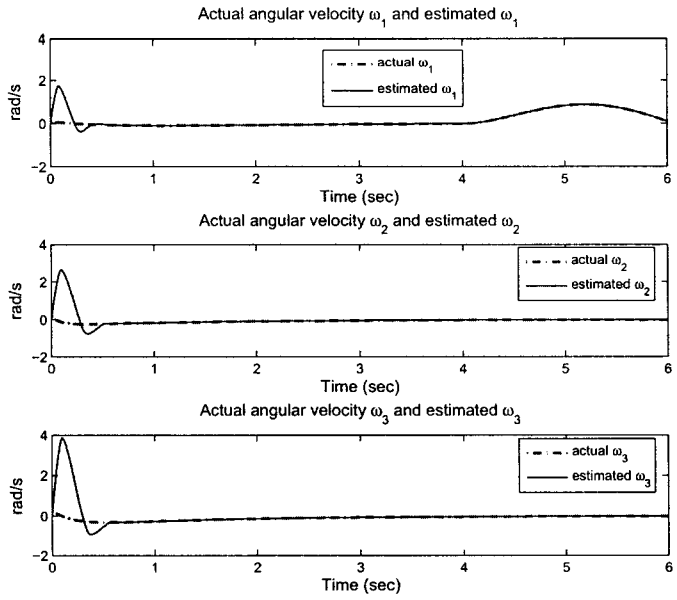

Figure 4.5: Actual states and estimated states using HOSMDs

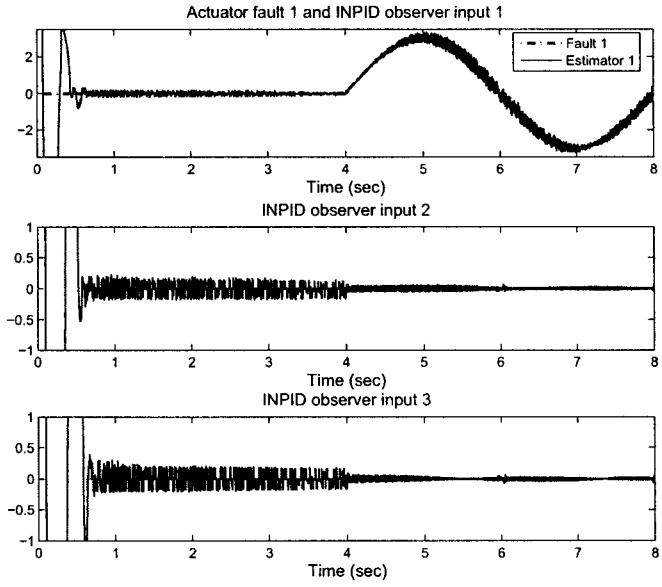

Figure 4.6: Characteristics of fault $f_a^{(1)}(t)$ and estimators in case 1

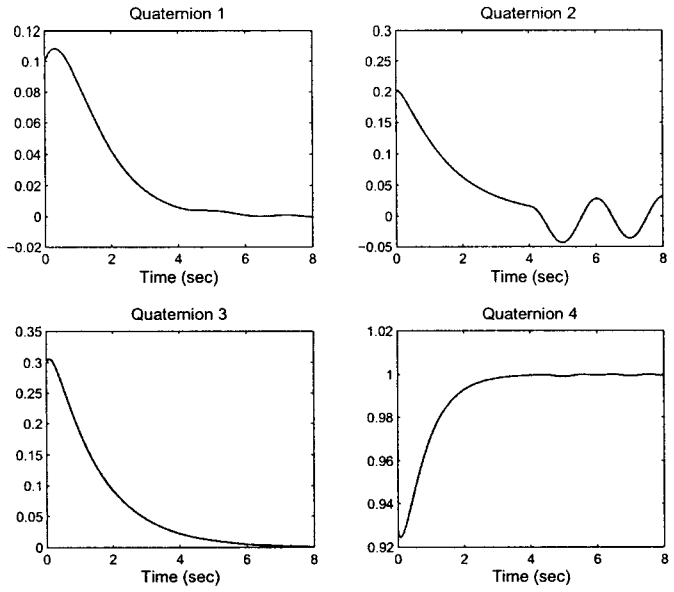

Figure 4.7: Measured quaternions in case 2

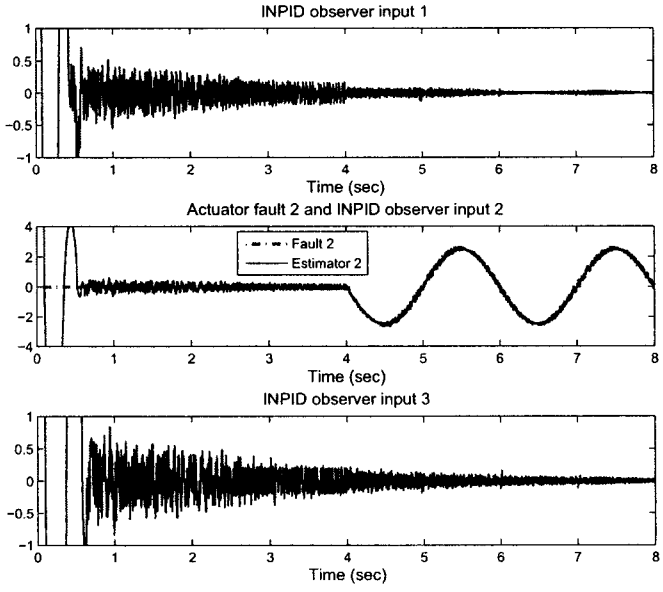

Figure 4.8: Characteristics of fault $f_a^{(2)}(t)$ and estimators in case 2

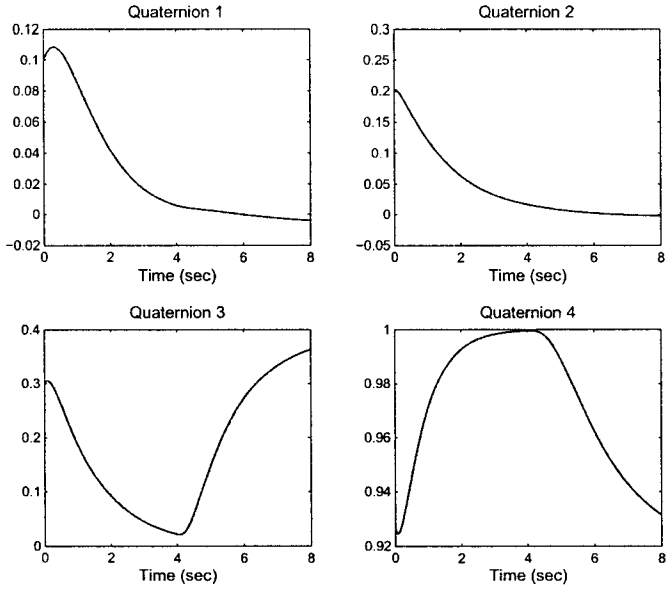

Figure 4.9: Measured quaternions in case 3

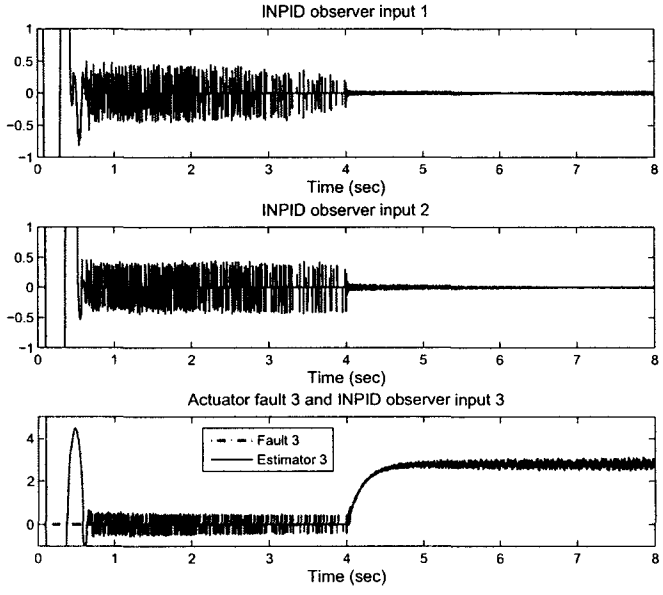

Figure 4.10: Characteristics of fault $f_a^{(3)}(t)$ and estimators in case 3

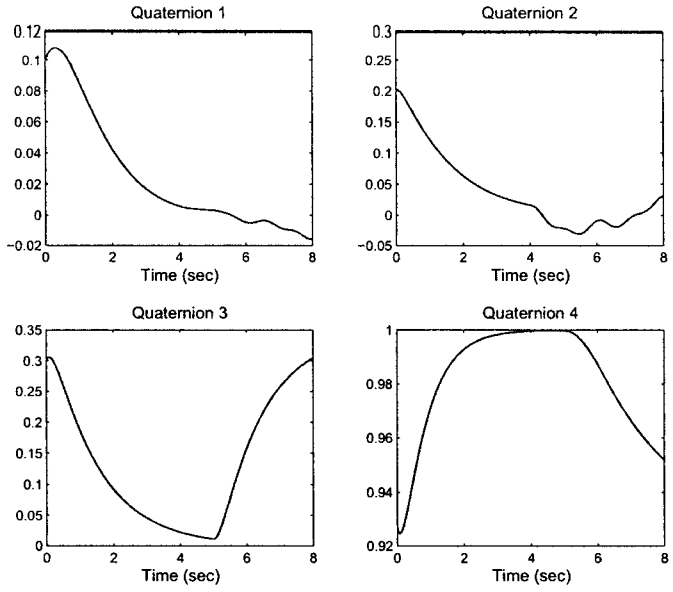

Figure 4.11: Measured quaternions in case 4

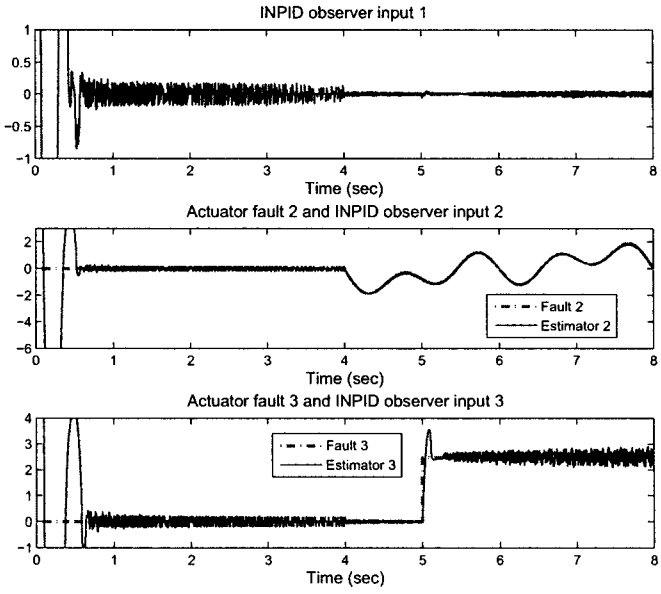

Figure 4.12: Characteristics of faults $f_a^{(2)}(t)$ and $f_a^{(3)}(t)$ and estimators in case 4

Chapter 5

Fault Diagnosis Using Second Order Sliding Mode and Wavelet Networks

In this chapter, a robust fault diagnosis scheme which synthesizes the techniques of second order sliding mode and wavelet networks is proposed for a class of nonlinear systems.

5.1 Introduction

In Chapter 3, a framework for designing robust fault diagnosis schemes using sliding mode and learning approaches was proposed, where the sliding mode eliminates the effect of uncertainties and approximation errors on state estimation and additional online estimators are used to characterize various faults. Although online fault estimators based on neural networks and an iterative learning algorithm were studied in previous chapters, for a specific problem, an *ad hoc* fault estimator is preferred in order to simplify the algorithm and satisfy the real-time computation requirements.

Due to its inherent robustness to system uncertainties, generic sliding mode has been used in the design of fault diagnostic observers, where the sliding mode restrains the state estimation error within a small bound around zero prior to the occurrence

of faults in the presence of system uncertainties and approximation errors.

In addition to first order sliding mode, high order sliding mode techniques have also been studied and used for system observation by many researchers. For example, the super-twisting algorithm provides the best possible asymptotic accuracy of the derivative estimation at each sampling time [73], [74], [113], [114], [116], [66]. In summary, the existing high order sliding mode observers hold the following attractive features: 1) Robustness with respect to unknown inputs, 2) The possibility to use the equivalent output injection to identify the unknown inputs, 3) Observation of unmeasurable states without low-pass filtering, and 4) Finite-time convergence for the systems with an arbitrary relative degree. Last but not least, a high order sliding mode can reduce, or even avoid, chattering if the parameters are carefully selected.

Based on the advantages mentioned above, high order sliding mode has been used in model-based fault diagnosis in recent years; e.g., [50], [26], [149], [87]. One fault diagnosis scheme using high order sliding mode observers is to reconstruct faults by appropriately manipulating the equivalent output injection signal. Through direct reconstruction, short-term faults quickly distinguish themselves, and detection and isolation are easily implemented. This approach is feasible for a class of nonlinear systems with a relative degree more than one, which is not applicable for many traditional observers. Another possible approach is to design an observer in such a way that the sliding motion is destroyed in the presence of faults. In this case, online estimators are needed to characterize the faults.

Moreover, inspired by feed-forward neural networks and wavelet decomposition theory, a new type of network, named wavelet network, was proposed a few years ago [88]. Wavelet networks preserve the universal approximation ability and have an explicit link between the network coefficients and some appropriate transforms. These two distinguishing properties guarantee that wavelet networks can be treated as an alternative to neural networks in nonlinear function approximation. Moreover, wavelet networks have been used to identify and classify signal features to diagnose faults [150].

This chapter establishes a nonlinear observer for the robust fault diagnosis in a class of nonlinear systems, which was studied in Chapter 3. The diagnostic observer

has the following characteristics: 1) The second order sliding mode algorithm is utilized to observe the system state in the presence of system uncertainties. This strategy prevents parameter drifting during the fault estimation caused by uncertainties and approximation errors. 2) The wavelet networks can obtain the same approximation accuracy as traditional neural networks with a simpler structure [88], [151], which simplifies the procedure of choosing online fault estimators. The observer is designed such that the sliding motion is destroyed when a fault occurs. Thereafter, wavelet networks based estimators are adopted to isolate and identify the fault. The theoretical analysis is verified by applying the proposed FD scheme to a multiple satellite formation flying system.

The remaining part of this chapter is organized as follows. Section 5.2 presents a mathematical description of the system to be studied. In Section 5.3 and 5.4, a nonlinear diagnostic observer is designed using second order sliding mode and wavelet networks. After theoretically analyzing the convergence of the diagnostic second order sliding mode observer, the proposed fault diagnosis scheme is applied to a multiple satellite formation flying system. Section 5.5 gives some simulation results that demonstrate the performance of the proposed robust fault diagnosis scheme.

5.2 Problem Formulation

The class of nonlinear dynamic systems in this chapter is described in the state space form as

$$\begin{aligned} \dot{x}_1 &= x_2 \\ \dot{x}_2 &= f(t,x,u) + \xi(t,x,u) + \beta(t-T_f) f_a(t,x,u) \\ y &= x_1 \end{aligned} \tag{5.1}$$

where $x = [x_1, x_2]^\top$ is the state vector. The nominal system dynamics are represented by the function $f(t, x_1, x_2, u)$, the internal uncertainties are denoted by the term $\xi(t, x_1, x_2, u)$, and $f_a(t, x_1, x_2, u)$ describes the dynamics of the process faults, which are defined as additive actuator faults and/or component faults. The time profile

function $\beta(t-T_f)$ is still a step function, which is 1 when $t > T_f$, otherwise, it is zero. T_f is the beginning time of the faults.

The solutions to (5.1) are understood in Filippov's sense. We assume that the system dynamics function $f(t,x,u)$ and the uncertainty function $\xi(t,x,u)$ are Lebesgue-measurable in any compact region of x. Another two assumptions are introduced for designing and analyzing the observer.

Assumption 5.1 Two positive constants k_1 and k_2 exist such that

$$|f(t,x_1,x_2,u) - f(t,\hat{x}_1,\hat{x}_2,u)| \leq k_1|x_1-\hat{x}_1| \tag{5.2}$$

$$\left|\frac{df(t,x_1,x_2,u) - df(t,\hat{x}_1,\hat{x}_2,u)}{dt}\right| \leq k_2|x_2-\hat{x}_2|. \tag{5.3}$$

Assumption 5.2 The uncertainty function $\xi(t,x,u)$ satisfies

$$|\xi(t,x,u)| < \xi^+ \tag{5.4}$$

$$\left|\frac{d\xi(t,x,u)}{dt}\right| < \delta\xi^+ \tag{5.5}$$

where ξ^+ and $\delta\xi^+$ are two positive numbers.

The task of this work is to develop a finite-time convergent observer for fault detection, isolation, and estimation of the system (5.1) where only output $y(t)$ is measurable. The relative degree from u to y is two. For the sake of simplicity, only the scalar case x_1, $x_2 \in \Re$ is considered. The vector case can be analyzed by constructing a bank of observers in parallel for each component of x in the same way.

5.3 Diagnostic Observer Design Using Second Order Sliding Mode

5.3.1 Second Order Sliding Mode Observer

Based on the system dynamics (5.1), a nonlinear observer is proposed as follows:

$$\begin{aligned} \dot{\hat{x}}_1 &= \hat{x}_2 + z_1, & \hat{x}_1(0) = x_1 \\ \dot{\hat{x}}_2 &= f(t, \hat{x}_1, \hat{x}_2, u) + z_2 + \beta(t - T_m)\hat{M}_2(t), & \hat{x}_2(0) = 0 \\ \hat{y} &= \hat{x}_1 \end{aligned} \tag{5.6}$$

where $\hat{x}_1$ and $\hat{x}_2$ are the estimated states, z_1 and z_2 are the correction variables, and $\hat{M}_2(t)$ is a vector of online estimators used to characterize the process faults. Wavelet networks based fault estimators are discussed in detail in Section 5.4. The term T_m is the beginning time that enables the wavelet networks. In order to investigate the properties of the sliding mode and the online estimators more clearly, we assume that $T_x < T_m < T_f$, where T_x is the time when state x_2 is observed by the second order sliding mode. Hence, the online fault estimation does not intervene with the state observation using the second order sliding mode.

The correction variables z_1 and z_2 are expressed as

$$\begin{cases} z_1 = \lambda_1 |\tilde{x}_1|^{1/2} \text{sign}(\tilde{x}_1) + v_1 \\ \dot{v}_1 = \alpha_1 \text{sign}(\tilde{x}_1) \end{cases} \tag{5.7}$$

and

$$\begin{cases} z_2 = 0 & \text{if } \dot{\tilde{x}}_1 \neq 0, \tilde{x}_1 \neq 0 \\ \quad = \lambda_2 |z_1|^{1/2} \text{sign}(z_1) + v_2 & \text{if } \dot{\tilde{x}}_1 = 0, \text{and } \tilde{x}_1 = 0 \\ \dot{v}_2 = \alpha_2 \text{sign}(z_1) \end{cases} \tag{5.8}$$

where $\tilde{x}_1 = x_1 - \hat{x}_1$ and $\tilde{x}_2 = x_2 - \hat{x}_2$ are denoted as the state estimation errors, and "sign" is the signum function.

Remark 5.1 *In the above second-order sliding mode observer, we use an anti-peaking structure [115], [66], where $\tilde{x}_1$ and $\tilde{x}_2$ reach the sliding manifold one by one in a recursive way; that is, $\tilde{x}_1$ reaches the manifold before $\tilde{x}_2$.*

Considering the system dynamics before $\tilde{x}_1$ reaches the sliding manifold, we have

$$\begin{aligned} \dot{\tilde{x}}_1 &= \tilde{x}_2 - \lambda_1 |\tilde{x}_1|^{1/2} \text{sign}(\tilde{x}_1) - v_1 \\ \dot{v}_1 &= \alpha_1 \text{sign}(\tilde{x}_1) \\ \dot{\tilde{x}}_2 &= F(t, x_1, \hat{x}_1, x_2, \hat{x}_2, u) \end{aligned} \tag{5.9}$$

where $F(\cdot) = f(t, x_1, x_2, u) - f(t, \hat{x}_1, \hat{x}_2, u) + \xi(t, x_1, x_2, u)$. Based on Assumption 5.1 and 5.2, we have

$$|F(t, x_1, \hat{x}_1, x_2, \hat{x}_2, u)| < k_1 |x_1 - \hat{x}_1| + \xi^+ \tag{5.10}$$

$$\left| \frac{dF(t, x_1, \hat{x}_1, x_2, \hat{x}_2, u)}{dt} \right| < k_2 |x_2 - \hat{x}_2| + \delta\xi^+ \tag{5.11}$$

for any possible t, x_1, $\hat{x}_1$, x_2, $\hat{x}_2$, and u.

5.3.2 Convergence Analysis

The convergence property of a super-twisting second order sliding mode observer has been provided by Davila *et al.* [74], where the function $F(t, x_1, \hat{x}_1, x_2, \hat{x}_2, u)$ is bounded by a constant f^+. Here, we are ready to use a similar approach to investigate the convergence of the proposed second-order sliding mode observer (5.6)-(5.8), where function $F(\cdot)$ only satisfies conditions (5.10) and (5.11).

Theorem 5.1 *The first variable pairs* $(\hat{x}_1, \dot{\hat{x}}_1)$ *converge to* $(x_1, \dot{x}_1)$ *in finite time, if condition (5.10) holds for system (5.1) and the parameters of the observer (5.7) are selected according to the following criteria:*

$$\alpha_1 > k_1 \tilde{x}_{1_M} + \xi^+ \quad or \quad \alpha_1 > \sqrt{k_1}\, \dot{\tilde{x}}_{1_0} + \xi^+ \tag{5.12}$$

$$\lambda_1 > \frac{4\alpha_1}{\sqrt{\alpha_1 - \xi^+}} \tag{5.13}$$

where $\tilde{x}_{1_M}$ *and* $\dot{\tilde{x}}_{1_0}$ *are defined later.*

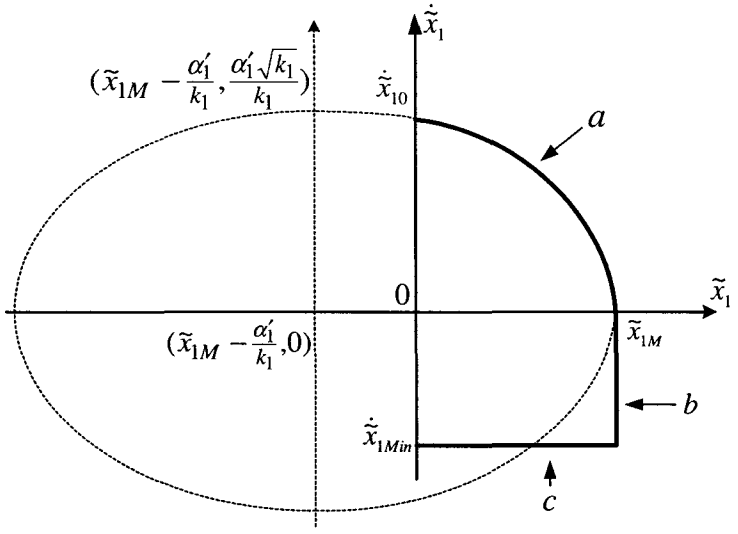

Figure 5.1: The boundedness curve for the finite time convergence of $\tilde{x}_1$

Proof: From (5.9) and (5.10), the state estimation errors, $\tilde{x}_1$ and $\tilde{x}_2$, satisfy the following differential inclusion:

$$\begin{aligned} \dot{\tilde{x}}_1 &= \tilde{x}_2 - \lambda_1 |\tilde{x}_1|^{1/2} \text{sign}(\tilde{x}_1) - v_1 \\ \dot{v}_1 &= \alpha_1 \text{sign}(\tilde{x}_1) \\ \dot{\tilde{x}}_2 &\in [-k_1|\tilde{x}_1| - \xi^+, k_1|\tilde{x}_1| + \xi^+] \end{aligned} \tag{5.14}$$

Here and in the following part of this chapter, all differential inclusions are defined in the Filippov sense. Using the identity $d|x|/dt = \dot{x}\ \text{sign}(x)$, we obtain the derivative of $\dot{\tilde{x}}_1$ with $\tilde{x}_1 \neq 0$ as

$$\ddot{\tilde{x}}_1 \in [-k_1|\tilde{x}_1| - \xi^+, k_1|\tilde{x}_1| + \xi^+] - \frac{1}{2}\lambda_1 \frac{\dot{\tilde{x}}_1}{|\tilde{x}_1|^{1/2}} - \alpha_1 \text{sign}(\tilde{x}_1) \tag{5.15}$$

The inclusion (5.15) is a mathematical description of the boundedness curve drawn in Figure 5.1. Since the initial observer states are set to $(\hat{x}_1, \hat{x}_2) = (x_1, 0)$, the trajectory enters the half-plane $\tilde{x}_1 > 0$ with a positive initial value $\dot{\tilde{x}}_{1_0} = \tilde{x}_2$ and the half-plane $\tilde{x}_1 < 0$ with a negative value of $\tilde{x}_2$.

In quadrant 1 ($\tilde{x}_1 > 0, \dot{\tilde{x}}_1 > 0$), the trajectory is confined between the axis $\tilde{x}_1 = 0$, $\dot{\tilde{x}}_1 = 0$, and the trajectory of the equation $\ddot{\tilde{x}}_1 = k_1\tilde{x}_1 - \alpha_1'$, where $\alpha_1' = \alpha_1 - \xi^+$. We

define $\dot{\tilde{x}}_{1_0}$ as the intersection of this curve with the axis $\tilde{x}_1 = 0$, and we let $\tilde{x}_{1_M}$ be the intersection of this curve with the axis $\dot{\tilde{x}}_1 = 0$. Solving the differential equation $\ddot{\tilde{x}}_1 = k_1\tilde{x}_1 - \alpha_1'$, we obtain a general solution as

$$\tilde{x}_1 = C_1 e^{\sqrt{k_1}t} + C_2 e^{-\sqrt{k_1}t} + \frac{\alpha_1'}{k_1} \tag{5.16}$$

where C_1 and C_2 are two coefficients to be determined.

Setting the time from $(0, \dot{\tilde{x}}_{1_0})$ to $(\tilde{x}_{1_M}, 0)$ be t_M, we have the following four boundary conditions:

$$\begin{aligned}
\dot{\tilde{x}}_{1_0} &= C_1\sqrt{k_1}e^{\sqrt{k_1}t_0} - C_2\sqrt{k_1}e^{-\sqrt{k_1}t_0} \\
&= \sqrt{k_1}(C_1 - C_2) && (5.17)\\
\dot{\tilde{x}}_{1_M} &= C_1\sqrt{k_1}e^{\sqrt{k_1}t_M} - C_2\sqrt{k_1}e^{-\sqrt{k_1}t_M} = 0 && (5.18)\\
\tilde{x}_{1_0} &= C_1 + C_2 + \frac{\alpha_1'}{k_1} = 0 && (5.19)\\
\tilde{x}_{1_M} &= C_1 e^{\sqrt{k_1}t_M} + C_2 e^{-\sqrt{k_1}t_M} + \frac{\alpha_1'}{k_1} && (5.20)
\end{aligned}$$

where $t_0 = 0$ is the initial time.

From (5.17) and (5.19), we obtain

$$\begin{aligned}
C_1 &= \frac{1}{2}\Big(\frac{\dot{\tilde{x}}_{1_0}}{\sqrt{k_1}} - \frac{\alpha_1'}{k_1}\Big) && (5.21)\\
C_2 &= -\frac{1}{2}\Big(\frac{\alpha_1'}{k_1} + \frac{\dot{\tilde{x}}_{1_0}}{\sqrt{k_1}}\Big) && (5.22)
\end{aligned}$$

and from (5.18), we have

$$e^{2\sqrt{k_1}t_M} = \frac{\dfrac{\alpha_1'}{k_1} + \dfrac{\dot{\tilde{x}}_{1_0}}{\sqrt{k_1}}}{\dfrac{\alpha_1'}{k_1} - \dfrac{\dot{\tilde{x}}_{1_0}}{\sqrt{k_1}}}. \tag{5.23}$$

Consequently, based on (5.20), we eliminate t_M, and attain

$$\Big(\tilde{x}_{1_M} - \frac{\alpha_1'}{k_1}\Big)^2 + \Big(\frac{\dot{\tilde{x}}_{1_0}}{\sqrt{k_1}}\Big)^2 = \Big(\frac{\alpha_1'}{k_1}\Big)^2. \tag{5.24}$$

Two equivalent inequalities can be obtained from above deduction:

$$\frac{\alpha_1'}{k_1} - \frac{\dot{\tilde{x}}_{1_0}}{\sqrt{k_1}} > 0 \tag{5.25}$$

$$\frac{\alpha_1'}{k_1} - \tilde{x}_{1_M} > 0 \tag{5.26}$$

Therefore, the trajectory of the boundedness curve in quadrant 1 is described by an elliptical equation [see Figure 5.1, line (a)].

$$\left(\tilde{x}_1 + \frac{\alpha_1'}{k_1} - \tilde{x}_{1_M}\right)^2 + \left(\frac{\dot{\tilde{x}}_1}{\sqrt{k_1}}\right)^2 = \left(\frac{\alpha_1'}{k_1}\right)^2 \tag{5.27}$$

with $\tilde{x}_1 > 0, \dot{\tilde{x}}_1 > 0$.

From the above analysis, we can easily see that $\tilde{x}_{1_M}$ is the maximal $\tilde{x}_1$. Therefore, according to (5.12) and (5.15), we obtain for $\tilde{x}_1 > 0$, $\dot{\tilde{x}}_1 > 0$

$$\ddot{\tilde{x}}_1 \leq k_1\tilde{x}_1 + \xi^+ - \alpha_1 \text{sign}(\tilde{x}_1) - \frac{1}{2}\lambda_1 \frac{\dot{\tilde{x}}_1}{|\tilde{x}_1|^{1/2}} < 0 \tag{5.28}$$

Hence, the trajectory goes down to the axis $\dot{\tilde{x}}_1 = 0$ and enters into the fourth quadrant.

Then, consider the boundedness curve in quadrant 4 ($\tilde{x}_1 > 0$, $\dot{\tilde{x}}_1 < 0$), where based on (5.28), $\dot{\tilde{x}}_1$ continues to decrease until $\ddot{\tilde{x}}_1$ returns back to zero from a negative value. Therefore, the boundedness curve consists of two parts. The first part drops down from $(\tilde{x}_{1_M}, 0)$ to $(\tilde{x}_{1_M}, \dot{\tilde{x}}_{1_{Min}})$, where $\ddot{\tilde{x}}_{1_{Min}} = 0$ implies $\dot{\tilde{x}}_{1_{Min}}$ reaches the smallest value of $\dot{\tilde{x}}_1$ [see Figure 5.1, line (b)].

Let the right-hand side of (5.15) be zero in the worst case; we have $\dot{\tilde{x}}_{1_{Min}} = -\frac{2}{\lambda_1}(k_1\tilde{x}_{1_M} + \alpha_1'')\tilde{x}_{1_M}^{1/2}$, where $\alpha_1'' = \alpha_1 + \xi^+$. Since, in quadrant 4, $\dot{\tilde{x}} < 0$, the trajectory approaches $\tilde{x}_1 = 0$. Thus, the second part of the boundedness curve in the fourth quadrant is the horizontal trajectory from $(\tilde{x}_{1_M}, \dot{\tilde{x}}_{1_{Min}})$ to $(0, \dot{\tilde{x}}_{1_{Min}})$ [see Figure 5.1, line (c)].

Based on (5.12), (5.13), and (5.24), we derive

$$|\dot{\tilde{x}}_{1_{Min}}| < |\dot{\tilde{x}}_{1_0}|. \tag{5.29}$$

If we define $\dot{\tilde{x}}_{1_{Min}} = \dot{\tilde{x}}_{1_1}, \dot{\tilde{x}}_{1_2}, \ldots, \dot{\tilde{x}}_{1_i}, \ldots$ as the intersection points of system (5.9)'s trajectory starting from $(0, \dot{\tilde{x}}_{1_0})$ with the axis $\tilde{x}_1 = 0$, inequality (5.29) ensures the finite-time convergence of the state $(0, \dot{\tilde{x}}_{1_i})$ to $\tilde{x}_1 = \dot{\tilde{x}}_1 = 0$. ∎

Remark 5.2 *The boundedness curve that consists of segments (a), (b), and (c) is the "worst" case of the trajectory. Actually, $(\tilde{x}_1, \dot{\tilde{x}}_1)$ moves along the direction of (a), (b), (c) within the boundedness curve.*

Remark 5.3 *The choice of α_1 and λ_1 depends on the bound of uncertainty and the initial state estimation error in the worst case. The theoretical result is consistent with that when only the bound of $F(\cdot)$ is known. In applications, a sufficiently large α_1 is preferred in order to satisfy (5.12) and (5.13).*

Now, we consider the finite time convergence of $\tilde{x}_2$. Obviously, when $\tilde{x}_1$ reaches the sliding manifold, i.e., $\dot{\tilde{x}}_1 = 0$, $z_1 = \tilde{x}_2$, the dynamics of $\tilde{x}_2$ become

$$\begin{aligned} \dot{\tilde{x}}_2 &= F(t, x_1, \hat{x}_1, x_2, \hat{x}_2) - \lambda_2 |\tilde{x}_2|^{1/2} \text{sign}(\tilde{x}_2) - v_2 \\ \dot{v}_2 &= \alpha_2 \text{sign}(\tilde{x}_2). \end{aligned} \tag{5.30}$$

Similarly computing the derivative of $\dot{\tilde{x}}_2$ with $\tilde{x}_2 \neq 0$, we obtain

$$\ddot{\tilde{x}}_2 \in [-k_2|\tilde{x}_2| - \delta\xi^+, k_2|\tilde{x}_2| + \delta\xi^+] - \frac{1}{2}\lambda_2 \frac{\dot{\tilde{x}}_2}{|\tilde{x}_2|^{1/2}} - \alpha_2 \text{sign}(\tilde{x}_2) \tag{5.31}$$

Because (5.31) has a similar form as (5.15), the finite-time convergence of $\tilde{x}_2$ can be proved in the same way as Theorem 5.1.

Remark 5.4 *Note that the traditional sliding mode techniques are a special case of the high order sliding mode, and they can be considered as first order sliding mode.*

Remark 5.5 *The sliding mode parameters λ_i and α_i can not be chosen too large because, in this work, the sliding mode is deemed only to eliminate the effect of the uncertainties.*

5.4 Fault Diagnosis Using Second Order Sliding Mode and Wavelet Networks

5.4.1 Robust Fault Detection Scheme

In model-based fault diagnosis schemes, a residual or residuals are usually generated for diagnosing faults. The proposed fault diagnosis scheme is required to not only detect the occurrence of a fault, but it also should determine its location and estimate its magnitude. Here, the measurable output estimation error can be selected as the residual for robust fault detection; i.e.,

$$\begin{cases} \text{No fault occurs, and } \hat{M}_2(t) \text{ is set to zero} & \text{if } |\tilde{x}_1(t)| < \epsilon_f \\ \text{Fault has occured, and } \hat{M}_2(t) \text{ works} & \text{if } |\tilde{x}_1(t)| \geq \epsilon_f \end{cases}$$

where ϵ_f is a threshold for robust fault detection. With the help of the sliding mode, ϵ_f can be set very small to increase the sensitivity without losing the robustness. Moreover, when additive faults occur, the online estimator $\hat{M}_2(t)$ is used to determine the location and to estimate the magnitude of the faults.

Remark 5.6 *When the nonlinear system (5.1) is without any fault, i.e., $f_a(t) = 0$, ideally, the states of observer (5.6) should be identical to the states of the practical system (5.1), and $\hat{M}_2(t)$ is supposed to be zero. When a fault $f_a(t)$ occurs, the sliding mode motion is supposed to be destroyed, and the estimator $\hat{M}_2(t)$ is triggered to specify the fault.*

5.4.2 Fault Estimator Design Using Wavelet Networks

Based on wavelet transform theory, wavelet networks were proposed to be an alternative to neural networks with respect to nonlinear function approximation. In this section, we build three-layer wavelet networks as the online fault estimators.

The proposed three-layer wavelet networks are comprised of an input layer (the i layer), a wavelet layer (the ij layer), and an output layer (the o layer). The schematic diagram of this wavelet networks model is shown in Figure 5.2. The relationship

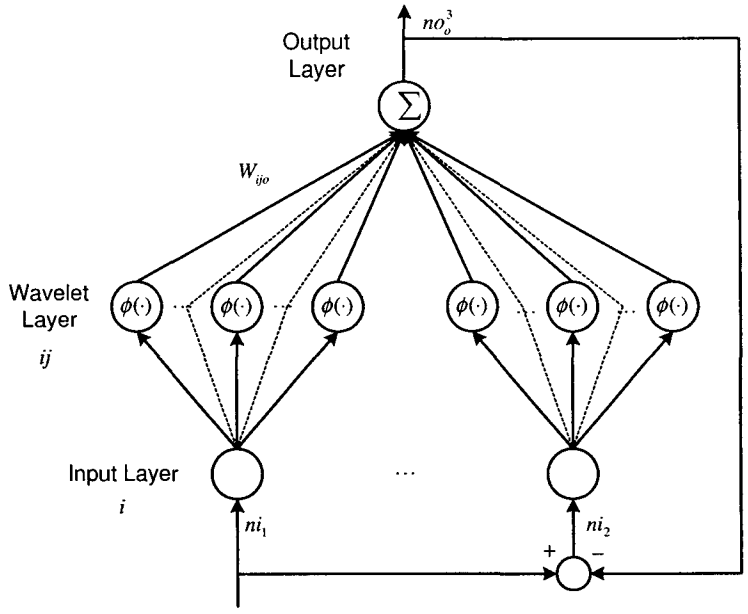

Figure 5.2: Structure of the three-layer wavelet networks

between the input and output of each node i in the input layer is represented as follows:

$$\text{net}_i^1 = ni_i, \quad no_i^1 = f_i^1(\text{net}_i^1) = \text{net}_i^1, \quad i = 1, \cdots, p \tag{5.32}$$

where ni_i is the input of the wavelet networks in which $ni_1 = z_1$, and $ni_2 = z_1 - \hat{M}_2$. Moreover, in the wavelet layer, a family of wavelets is established by performing translations and dilations on a single fixed function called the mother wavelet. In this study, the first derivative of a Gaussian function, $\phi(x) = -x\exp(-x^2/2)$, is selected as the mother wavelet. This mother wavelet function has a universal approximation property, because it can be regarded as a differentiable version of the Haar mother wavelet, just as the sigmoid is the differentiable version of a step function [151]. For the ijth node in the wavelet layer, we have

$$\text{net}_{ij}^2 = \frac{no_i^1 - c_{ij}}{\sigma_{ij}} \tag{5.33}$$

$$\begin{aligned} no_{ij}^2 &= \phi_{ij}(\text{net}_{ij}^2) \\ &= -\text{net}_{ij}^2 \exp\big(-(\text{net}_{ij}^2)^2/2\big), \quad j = 1, \cdots, q \end{aligned} \tag{5.34}$$

where c_{ij} and σ_{ij} are, respectively, the translation and dilation in the jth term of the ith input no_i^1 to the node of the mother wavelet layer, and q is the total number of wavelets with respect to the corresponding input node.

In the output layer, the single node o is labelled as $\sum$, which adds all input signals together; i.e.,

$$\text{net}_o^3 = \sum_{ij} W_{ijo}^3 no_{ij}^2 \tag{5.35}$$

$$no_o^3 = f_o^3(\text{net}_o^3) = \text{net}_o^3, \quad o = 1 \tag{5.36}$$

where $no_o^3 = \hat{M}_2(t)$ is the output of the wavelet networks, the connection weight W_{ijo}^3 is the output action strength of the oth output associated with the ijth wavelet, and no_{ij}^2 is denoted as the ijth input to the node of the output layer.

5.4.3 Parameter Update Algorithm

After determining the structure of the wavelet networks, we need to select an adaptive algorithm to update the parameters during the process of fault diagnosis. Firstly, a vector that includes all the parameters of the wavelet networks is defined as

$$\hat{\theta} = [W_{11o}^3, \cdots, W_{pqo}^3, c_{11}, \cdots, c_{pq}, \sigma_{11}, \cdots, \sigma_{pq}]^\top. \tag{5.37}$$

The parameters of the wavelet networks can be updated by many optimization algorithms, which have been widely used for neural networks. Here, the EKF-like algorithm is adopted again as

$$K(t) = P(t)H(t)\left[H(t)^\top P(t)H(t) + R(t)\right]^{-1} \tag{5.38}$$

$$\dot{P}(t) = -\mathcal{B}_1 K(t)H(t)^\top P(t) \tag{5.39}$$

$$\dot{\hat{\theta}}(t) = \mathcal{B}_2 K(t) z_1(t) \tag{5.40}$$

where $K(t) \in \Re^{(3pq)}$ is the gain matrix, $P(t) \in \Re^{(3pq)\times(3pq)}$ is the covariance matrix of the state estimation error, and $H(t) \in \Re^{(3pq)}$ is the derivative of the state estimation $\hat{x}_2$ with respect to the parameter vector $\hat{\theta}$; i.e., $H(t) = \dfrac{\partial \hat{x}_2}{\partial \hat{\theta}}$. The terms $\mathcal{B}_1$ and $\mathcal{B}_2$

are two positive update rates. $R(t) \in \Re$ is the estimated covariance of measurement noise. Here, $R(t)$ is estimated as

$$\dot{R}(t) = \frac{e^2(t) - R(t)}{t} \tag{5.41}$$

where $e(t) = z_1(t) - \hat{M}_2(t)$.

$H(t)$ is derived using the chain rule and back-propagation algorithm as

$$\begin{aligned}
\frac{\partial \hat{x}_2}{\partial W^3_{ijo}} &= -\frac{\partial \hat{x}_2}{\partial \hat{M}_2}\Big(\frac{ni_i - c_{ij}}{\sigma_{ij}}\Big)\exp\Big(-\frac{(ni_i - c_{ij})^2}{2\sigma^2_{ij}}\Big) \\
\frac{\partial \hat{x}_2}{\partial c_{ij}} &= \frac{\partial \hat{x}_2}{\partial \hat{M}_2} W^3_{ijo}\Big(\frac{1}{\sigma_{ij}} - \frac{(ni_i - c_{ij})^2}{\sigma^3_{ij}}\Big)\exp\Big(-\frac{(ni_i - c_{ij})^2}{2\sigma^2_{ij}}\Big) \\
\frac{\partial \hat{x}_2}{\partial \sigma_{ij}} &= \frac{\partial \hat{x}_2}{\partial \hat{M}_2} W^3_{ijo}\Big(\frac{ni_i - c_{ij}}{\sigma^2_{ij}} - \frac{(ni_i - c_{ij})^3}{\sigma^4_{ij}}\Big)\exp\Big(-\frac{(ni_i - c_{ij})^2}{2\sigma^2_{ij}}\Big).
\end{aligned} \tag{5.42}$$

The convergence of this EKF-like algorithm was analyzed in Chapter 3.

Prior to any fault, only the second order sliding mode works to estimate the state of the system. The convergence of the state estimation error was investigated in Section 5.3.2. After the occurrence of any process fault, the dynamics of the state estimation error are described as

$$\dot{\tilde{x}}_1 = \tilde{x}_2 - z_1 \tag{5.43}$$

$$\dot{\tilde{x}}_2 = f(x,t) - f(\hat{x},t) + \xi(x,t) - z_2 + f_a(t) - \hat{M}_2(t) \tag{5.44}$$

where z_1 and z_2 are defined in (5.7) and (5.8).

Based on the universal nonlinear approximation ability of wavelet networks, optimal parameters W^*_{ijo}, c^*_{ij}, and σ^*_{ij} exist such that

$$|f_a(t) - \hat{M}_2(W^*_{ijo}, c^*_{ij}, \sigma^*_{ij})| = |\delta_f(t)| < \bar{\delta} \tag{5.45}$$

where $\bar{\delta}$ is a finite bound for the network approximation error. Therefore, we can define $F'(x,\hat{x},u,t) = f(x,u,t) - f(\hat{x},u,t) + \xi(x,u,t) + \delta_f(t)$. Based on (5.10), (5.11), and Theorem 5.1, the convergence of $\tilde{x}_1$ and $\tilde{x}_2$ after the occurrence of faults can be analyzed similarly to that in Section 5.3.2.

The proposed fault diagnosis scheme using second order sliding mode and wavelet networks is implemented by the following algorithm:

- Step 1: Set parameters λ_1, λ_2, α_1, and α_2 of the correction variables z_1 and z_2.
- Step 2: Initialize the wavelet networks $\hat{M}_2(t)$.
- Step 3: Build a nonlinear diagnostic observer based on (5.6).
- Step 4: Activate $\hat{M}_2(t)$ at $t = T_m$, and update the parameters of the wavelet networks $\hat{M}_2(t)$ using an EKF-like algorithm.
- Step 5: Derive output estimation error $\tilde{x}_1$ based on system dynamics (5.1) and the observer (5.6).
- Step 6: Compare $|\tilde{x}_(t)|$ with a predetermined diagnostic threshold ϵ_f.
- Step 7: If $|\tilde{x}_(t)| < \epsilon_f$, no fault occurs, the fault estimator $\hat{M}_2(t)$ is set to zero, and goes to Step 4. Otherwise, fault has occurred.
- Step 8: Use $\hat{M}_2(t)$ to isolate and estimate fault.

5.5 Application to a Multiple Satellite Formation Flying System

In this section, we apply the proposed fault diagnosis scheme to a multiple satellite formation flying system.

5.5.1 Dynamics of a Multiple Satellite Formation Flying System

An MSFF system is composed of a cluster of interdependent micro-satellites that communicate with each other and share payload, data, and missions. Relative distances and orientations between the participating micro-satellites are controlled. In this section, the MSFF fleet is only composed of a leader satellite and a follower satellite. The leader satellite provides a reference motion trajectory and the follower satellite

navigates in the neighborhood of the leader satellite based on the desired relative trajectory.

The nonlinear position dynamics of the follower satellite relative to the coordinate frame of the leader satellite is described in [152]

$$m_f\ddot{q} + C\dot{q} + N + F_d = u_f \tag{5.46}$$

where $C(\omega)$ denotes the Coriolis-like matrix

$$C = 2m_f\omega \begin{bmatrix} 0 & -1 & 0 \\ 1 & 0 & 0 \\ 0 & 0 & 0 \end{bmatrix} \tag{5.47}$$

$N(q, \omega, \rho, u_l)$ denotes the following nonlinear vector

$$N = \begin{bmatrix} m_f MG\dfrac{q_x}{\|\rho + q_x\|^3} - m_f\omega^2 q_x + \dfrac{m_f}{m_l}u_{lx} \\ m_f MG\Big(\dfrac{q_y + \|\rho\|}{\|\rho + q\|^3} - \dfrac{1}{\|\rho\|^2}\Big) - m_f\omega^2 q_y + \dfrac{m_f}{m_l}u_{ly} \\ m_f MG\dfrac{q_z}{\|\rho + q\|^3} + \dfrac{m_f}{m_l}u_{lz} \end{bmatrix}$$

and $F_d \in \Re^3$ is the total constant disturbance force vector. The parameters of the system (5.46) are listed in Table 5.1. If we choose state vector as $x = [q_x, q_y, q_z, \dot{q}_x, \dot{q}_y, \dot{q}_z]^\top$, (5.46) can be described by (5.1). Therefore, the proposed fault diagnosis schemes in this chapter can be applied to a multiple satellite formation flying system represented by (5.46).

The designed relative trajectory is given as

$$q_d(t) = \begin{bmatrix} 100\sin(4\omega t)(1 - \exp(-0.05t^3)) \\ 100\cos(4\omega t)(1 - \exp(-0.05t^3)) \\ 0 \end{bmatrix} \text{(m)}. \tag{5.48}$$

The controller is designed using the method in [152], and the parameters of the controller are selected as

$$\alpha = \text{diag}(0.2, 0.2, 0.475) \tag{5.49}$$

$$K = \text{diag}(500, 300, 1500) \tag{5.50}$$

$$\Gamma = \text{diag}(500, 50, 300, 600, 850, 480). \tag{5.51}$$

Table 5.1: Parameters of the MSFF system

Parameter	Value (unit)
Earth's mass M	5.974×10^{24}(kg)
Leader's mass m_l	1550 (kg)
Follower's mass m_f	410 (kg)
Universal gravity constant G	6.673×10^{-11}(kg $\cdot$ m^3 $\cdot$ s^2)
Leader's position ρ	$[0, 4.224 \times 10^7, 0]^\top$(m)
Angular velocity ω	7.272×10^{-5}(rad $\cdot$ s^{-1})
Disturbance force T_d	$[-1.025, 6.248, -2.415] \times 10^{-5}$(N)
Leader's control force u_l	$[0, 0, 0]^\top$(N)

5.5.2 Simulation and Analysis

The simulation is implemented at a frequency of 2kHz since the high order sliding mode algorithm is implemented. The gains of the second order sliding mode terms are set to $\alpha_i = 0.5$ and $\lambda_i = 1$ via a trial-and-error method. In the EKF-like parameter update algorithm, $P(0) = 100I_{42}$, and $R(0) = 2 \times 10^{-4}$. We use the method in [88] to initialize the wavelet networks, and the domains are set to $\mathcal{D}_1 = [-1000, 1000]$, and $\mathcal{D}_2 = [-2000, 2000]$. Since $p = 2$ and $q = 7$, there are totally 14 wavelet functions in the wavelet layer of each wavelet network. In the simulation, we set $\hat{x}(0) = [0.45; -6.2; -201; 0.5; 0.75; -0.65]^\top$. The wavelet network is assumed to be activated at the 10th *sec*; i.e. $T_m = 10$. One incipient fault and one abrupt fault are assumed to occur in the dynamics of $\dot{q}_y$ and $\dot{q}_z$, respectively, and their dynamics are

$$f_a^{(2)}(t) = 150 \times \beta(t - 18)\sin(2\pi t/4) \tag{5.52}$$

$$f_a^{(3)}(t) = 200 \times \beta(t - 22) \tag{5.53}$$

Moreover, it is assumed that u_f is subject to disturbances, which are set to $2 * rand$, where $rand$ is a Gaussian white noise signal. The system output is subject to measurement noise with $\varsigma = 0.5\% * rand$, i.e., $y_{measure} = y(1 + \varsigma)$.

The simulation results are shown from Figure 5.3 to Figure 5.5. Figure 5.3 illustrates the reference trajectory and the actual outputs of the faulty system. The

actual system output deviates from their nominal values after the occurrence of any process fault.

Figure 5.4 demonstrates the dynamics of the system states and observer states (The states x_4-x_6 are shown for the sake of illustration and discussion only) in the initial regulation phase by using the second order sliding mode. The results show that with the help of the proposed second order sliding mode, the system states can be estimated within a finite of time. Moreover, the observer state $\hat{x}_2$ begins to approach the actual state x_2 after the system output $\tilde{x}_1$ reaches the sliding manifold. This phenomenon is consistent with the theoretical analysis in the observer design.

Figure 5.5 characterizes the fault dynamics and the outputs of the wavelet networks based fault estimators. The activation of wavelet networks generates a large amount of chattering in all the output variables of wavelet networks at the 10th *sec* because the wavelet networks need time to update the parameters to track a trajectory. When the incipient fault occurs, due to the compensation of wavelet networks, there is no large chattering. However, chattering still exist in the fault estimation, which is due to random system uncertainties and measurement noises. Moreover, when multiple faults occur, only the wavelet networks that correspond to the faulty states specify the dynamics of the faults, and the wavelet networks associated with other healthy states return zero or close to zero. Therefore, this robust fault diagnosis scheme is effective for fault isolation and estimation of single fault as well as multiple faults.

5.6 Conclusions

In this chapter, a robust fault diagnosis scheme using second order sliding mode and wavelet networks was proposed for the class of nonlinear systems that can be formulated into a triangular input form. The second order sliding mode was used to achieve finite-time robust state estimation in the presence of uncertainties. The wavelet networks, as an alternative to feed-forward neural networks, was used to estimate the off-nominal behavior of the system caused by faults. The convergence of the second order sliding mode observer was proved theoretically, and the performance of the

proposed fault diagnosis scheme was tested by applying it to a multiple satellite formation flying system, where the dynamics between the leader satellite and the follower satellite were considered. The simulation results illustrate that wavelet networks can achieve a similar approximation performance to neural networks.

Although the basic idea of this fault diagnosis scheme is the same as that in Chapter 3, the use of second order sliding mode and wavelet networks provides versatility for the design of fault diagnosis schemes. For example, second order sliding mode avoids the use of filtering, which may cause time delay and bias in the computation of equivalent output injection signal. Wavelet networks have some valuable properties such as signal features identification and classification. Further investigation as well as applications of these properties to the design of fault diagnosis approaches should be the topics of future work. Moreover, in-depth comparison between wavelet networks and neural networks in terms of their computational complexity and real-time implementation issues need to be investigated in the future.

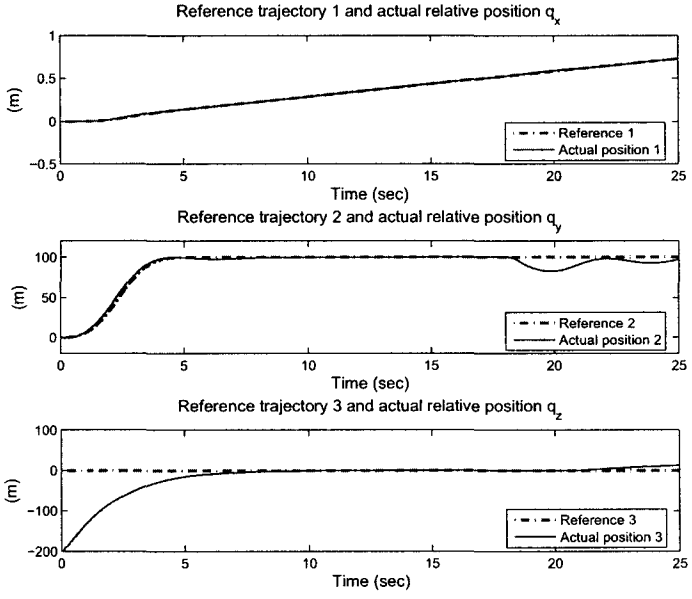

Figure 5.3: System outputs under multiple process faults

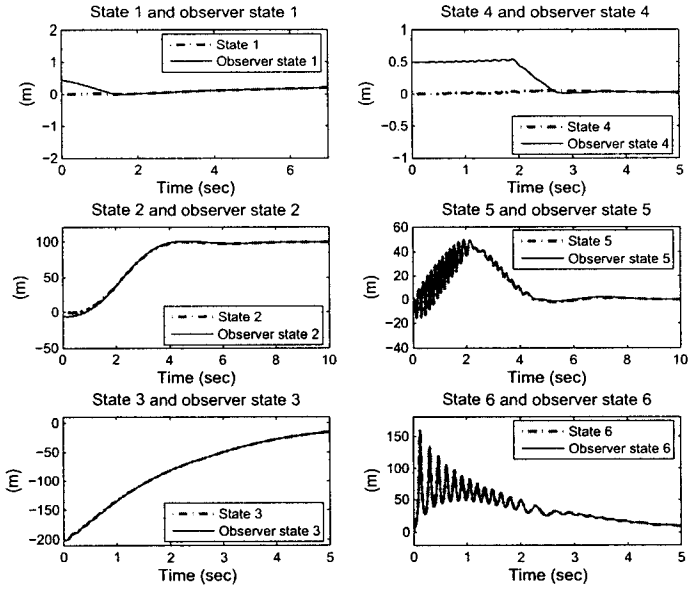

Figure 5.4: States and their estimations using second order sliding mode observer

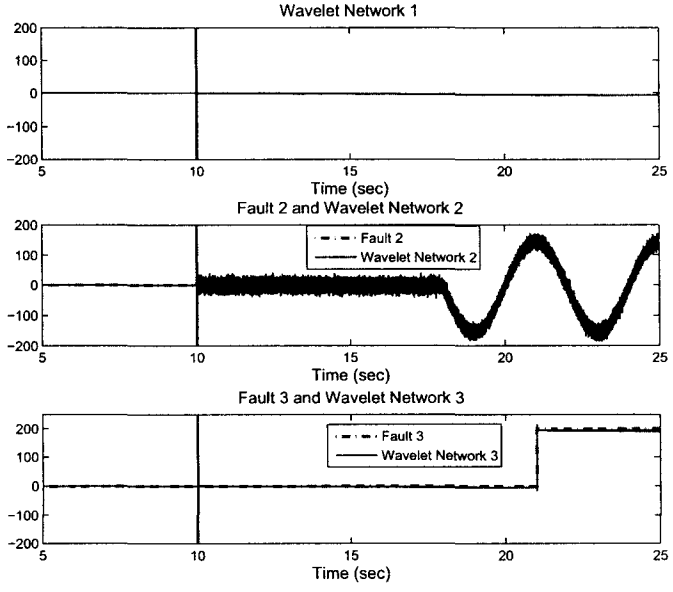

Figure 5.5: Output of wavelet networks under multiple process faults

Chapter 6

Fault Diagnosis in Nonlinear Systems Using Fuzzy-Neural and Sliding Mode Approaches

In this chapter, the fault diagnosis schemes using sliding mode and learning approaches will be extended to a class of nonlinear systems which can be represented by Takagi-Sugeno (TS) fuzzy models.

6.1 Introduction

In previous chapters, we investigated the fault diagnosis problems for two classes of nonlinear systems: one class of systems is of triangular input form, and the other class of systems with a special structure where the unmeasurable states can be represented by nonlinear functions of the system outputs and their derivatives. The satisfactory performance of the proposed fault diagnosis schemes using sliding mode and learning approaches naturally inspires us to extend this class of methods to more general nonlinear systems.

Since the first theoretical results presented by Zadeh [153] and the first application in the area of the process control by Mamdani and Assilian [154], fuzzy logic/models have been widely applied to the modeling and control of nonlinear systems. In the

existing fuzzy methods, the Takagi-Sugeno (TS) fuzzy approach has been extensively studied and used in nonlinear system modeling and control. The basic idea of this approach is to decompose the model of a nonlinear system into a set of linear subsystems which are associated using nonlinear weighting functions. Then, the control task is carried out by using the well-formulated linear control theory. The TS fuzzy models of a nonlinear system can be obtained in two principal ways: 1) black box identification via fuzzy clustering techniques, and 2) linearization of an existing nonlinear plant model around the centers of the fuzzy regions partitioning the state space. The TS fuzzy approaches play an important role in the modeling and control of nonlinear systems due to the wide availability of TS fuzzy models for nonlinear systems.

In real applications, the state of a system is often not directly available. Under such circumstances, one key step in the controller design is to determine the state from the system response to some input over a certain period of time. For linear systems, a Luenberger observer can solve this problem if the system is observable. For nonlinear systems, the systematic design methods of fuzzy observers have attracted a great deal of attention from many researchers, since, by using fuzzy models, some linear observer design methods can be extended to nonlinear systems. In the fuzzy controller/observer design, linear matrix inequality (LMI) is a main tool used to guarantee certain performance criteria. A thorough analysis of stability and simultaneous design of fuzzy controllers and observers can be found in [95]. Further study on fuzzy observer design are provided in the literatures, such as [91], [92], [93], [94], [96], [97], [98], [155].

Moreover, fuzzy logic/model-based fault diagnosis has also been significantly investigated in recent years; e.g., [96], [101], [103], [104]. One class of methods is to build a group of local linear models using TS fuzzy models to describe the original nonlinear systems. As a result, the fault diagnosis schemes for linear systems can be extended to nonlinear systems [101]. The second class of methods is to treat the fuzzy models in the same way as neural networks, since both of them possess the same approximation ability of nonlinear functions in a compact set. The third class of approaches is to make full use of the powerful reasoning capabilities of fuzzy logic, and in this case, fuzzy models are usually used to evaluate the residual signals and

classify the faults [99].

This research is motivated by extending the previous work on TS fuzzy observers, neural networks, and sliding mode observers to the fault diagnosis of a class of nonlinear systems which are not confined to triangular input forms [156]. In this work, a fuzzy-neural observer (FNO) and a fuzzy-neural sliding mode observer (FNSMO) are proposed for the purpose of fault detection, isolation, and estimation in a class of nonlinear systems that can be represented by TS fuzzy models. When no fault has occurred yet, a fuzzy controller and a fuzzy observer are used to stabilize the system and to estimate its state, respectively. Then, a three-layer neural network is established to isolate and estimate the fault after it occurs. In order to achieve robust fault diagnosis, a sliding mode term is utilized to deal with the effect of system uncertainties and approximation errors. A modified back-propagation (BP) algorithm is used to update the parameters of the observer so that the stability of the proposed observer-based system can be analyzed by Lyapunov's direct method. In the simulation, the proposed FD scheme is applied to a reduced-order satellite orbital control system to demonstrate its performance.

The remainder of this chapter is structured as follows. In Section 6.2, the class of dynamic systems under study is formulated and some preliminaries are given. In Section 6.3 and 6.4, two diagnostic observers using TS fuzzy-neural models and TS fuzzy-neural models with sliding mode are designed for fault diagnosis. The stabilities of these two observer-based fault diagnosis schemes are also rigorously proved in these two sections. Then, the proposed fault diagnosis scheme is offered in Section 6.5. After that, a simulation example is given in Section 6.6, and conclusions are presented in Section 6.7.

6.2 Problem Formulation

Consider the nominal dynamics of a class of nonlinear systems:

$$\begin{aligned} \dot{x} &= f(x,u,t) \\ y &= g(x,t) \end{aligned} \tag{6.1}$$

where $x \in \Re^n$ is the state vector, $y \in \Re^p$ is the output vector, and $u \in \Re^m$ is the control input vector of the system. The state function $f : \Re^n \times \Re^m \times \Re^+ \rightarrow \Re^n$ and the measurement function $g : \Re^n \times \Re^+ \rightarrow \Re^p$ are both smooth vector fields.

As proved in [95], (6.1) can be represented or approximated by a TS fuzzy model with linear rule consequence. The TS fuzzy model consists of a set of fuzzy rules, where the ith rule is

$$\begin{array}{l} \text{If } z_1 \text{is } \mu_1^i(z_1), \ldots \text{and } z_r \text{ is } \mu_r^i(z_r) \\ \text{Then} \left\{ \begin{array}{rcl} \dot{x} & = & A_i x + B_i u \\ y & = & C_i x \end{array} \right. \end{array} \tag{6.2}$$

where the vector of premise variables $z \in \Re^r$ is a subset of y and $\mu_j^i : \Re \rightarrow [0,\ 1]$. The function $\mu_j^i(z_j)$ is the jth membership function in the ith rule which is applied to the jth premise variable.

The global TS fuzzy system is then written as

$$\begin{array}{rcl} \dot{x} & = & \sum_{i=1}^{l} h_i(z)(A_i x + B_i u) \\ y & = & \sum_{i=1}^{l} h_i(z) C_i x \end{array} \tag{6.3}$$

where l is the number of fuzzy rules, and

$$h_i(z) = \frac{\omega_i(z)}{\sum_{i=1}^{l} \omega_i(z)} \qquad \omega_i(z) = \prod_{j=1}^{r} \mu_j^i(z_j). \tag{6.4}$$

Thus, the nonlinear system (6.1) with modeling uncertainties and process faults can be described using a TS model as

$$\begin{array}{rcl} \dot{x} & = & \sum_{i=1}^{l} h_i(z)(A_i x + B_i u) + \eta(t) + \mathcal{B}(t - T_f) f_a(t) \\ y & = & \sum_{i=1}^{l} h_i(z) C_i x \end{array} \tag{6.5}$$

where $\eta(t) \in \Re^n$ represents the system uncertainties, which is assumed to be bounded by a constant, i.e., $\|\eta(t)\| < \bar{\eta}$. The function vector $f_a(t) \in \Re^n$ denotes the process

faults in the system, which is composed of actuator faults and/or component faults. The time profile function $\mathcal{B}(t - T_f)$ is 1 when $t \geq T_f$; otherwise it is zero. Time T_f represents the beginning time of the faults.

Remark 6.1 *Usually, the fuzzy models of a nonlinear system can be constructed by identifying fuzzy models using input-output data or directly by derivation from given nonlinear system equations. Therefore, establishing fuzzy models is an effective way to study nonlinear systems using linear system methods.*

Remark 6.2 *The purpose of this study is to timely detect, correctly isolate, and accurately estimate the process faults in the presence of uncertainties for the class of nonlinear systems that can be described by TS fuzzy models.*

6.3 Diagnostic Fuzzy-Neural Observer

In this section, a nonlinear diagnostic observer is proposed for the purpose of robust fault diagnosis. Firstly, a TS fuzzy Luenberger observer is constructed to estimate the states in the fault-free case. Then, after a fault occurs, a recurrent dynamic neural network is established to characterize the location and magnitude of the fault.

6.3.1 Observer Design Using Fuzzy-Neural Models

For the faulty system (6.5), a fuzzy-neural Luenberger observer is designed as

$$\begin{aligned} \dot{\hat{x}}(t) &= \sum_{i=1}^{l} h_i(z)\{A_i\hat{x} + B_i u + L_i(y(t) - \hat{y}(t))\} \\ &\quad + \mathcal{B}(t - T_m)\hat{M}(t) \\ \hat{y}(t) &= \sum_{i=1}^{l} h_i(z) C_i \hat{x}(t) \end{aligned} \tag{6.6}$$

where $\hat{x} \in \Re^n$ and $\hat{y} \in \Re^p$ are the state vector and output vector of the observer, respectively. The term $L_i \in \Re^{n\times p}$ is the gain for the local linear observer in the center of the ith fuzzy region. The observer input $\hat{M}(t) \in \Re^n$ is designed to estimate the

faults, and T_m is the time to start $\hat{M}(t)$. In order to separately demonstrate the properties of the fuzzy models and the neural networks based fault estimators, we assume that $\hat{M}(t)$ is not activated until all the states are estimated by the TS fuzzy Luenberger observer, and no fault occurs prior to the activation of the fault estimator; i.e., $T_m < T_f$.

The classic LMI-based fuzzy controller and observer design method are used to construct the gain L_i in the fuzzy observer [95]. Consequently, the system states are able to be observed by the TS fuzzy observer within a finite time before the occurrence of a fault. The matrices A_i, B_i, and C_i can be obtained through identification using input-output data or directly derived from given nonlinear system dynamics. In this work, we use the second method to attain these matrices.

The dynamic neural network-based fault estimator is of the following structure:

$$\hat{M}(t) = \hat{W}\sigma(\hat{V}\bar{x}(t)) \tag{6.7}$$

where $\bar{x}(t) = [\tilde{y}(t-\tau)^\top \ \hat{M}(t-\tau)^\top]^\top$ is the input of the neural network, $\tilde{y} = y - \hat{y}$ is the output estimation error, $\hat{W}$ and $\hat{V}$ are two parameters of the estimator, and τ is the time delay. The activation function is selected to be a sigmoidal function:

$$\sigma(\hat{V}_i\bar{x}) = \frac{1 - \mathrm{e}^{-2\hat{V}_i\bar{x}}}{1 + \mathrm{e}^{-2\hat{V}_i\bar{x}}}$$

where $\hat{V}_i$ is the ith row of $\hat{V}$, and $\sigma_i(\hat{V}_i\bar{x})$ is the ith element of $\sigma(\hat{V}\bar{x})$.

After the occurrence of a fault, the estimation error dynamics become

$$\begin{aligned}
\dot{\tilde{x}}(t) &= \sum_{i=1}^{l}\sum_{j=1}^{l} h_i(z)h_j(z)(A_i - L_iC_j)\tilde{x} \\
&\quad +\eta(t) + f_a(t) - \hat{W}\sigma(\hat{V}\bar{x}(t)) \\
\tilde{y}(t) &= \sum_{i=1}^{l} h_i(z)C_i\tilde{x}(t)
\end{aligned} \tag{6.8}$$

Since L_i is designed to guarantee the stability of the estimation error dynamics without any fault, the input of the neural networks is zero at T_m. Thus, $\hat{M}(t)$ still keeps zero during the time interval $t \in [T_m, T_f)$. When $t \geq T_f$, the fault $f_a(t)$ breaks the stability of the estimation error dynamics and the neural networks are triggered to approximate the fault.

6.3.2 Parameter Update Algorithm

For a neural network based observer, usually, a learning strategy should be established to update its parameters after the structure of the observer is determined. For example, back-propagation algorithm is a popular way to train neural networks. The parameter update law should be defined in such a way that the stability of the observer can be guaranteed.

Defining a cost function $J = \frac{1}{2}\tilde{y}^2$, we design a similar parameter update law as that in [157],

$$\dot{\hat{W}}_{i,j} = -\rho_1 \frac{\partial J}{\partial \hat{W}_{i,j}} - \rho_2 \|\tilde{y}\| \hat{W}_{i,j} \tag{6.9}$$

$$\dot{\hat{V}}_{i,j} = -\rho_3 \frac{\partial J}{\partial \hat{V}_{i,j}} - \rho_4 \|\tilde{y}\| \hat{V}_{i,j} \tag{6.10}$$

where $\hat{W}_{i,j}$ and $\hat{V}_{i,j}$ are the (i,j)th element of $\hat{W}$ and $\hat{V}$, ρ_1, $\rho_3 > 0$ are the learning rates, and ρ_2 and ρ_4 are small positive numbers. The second terms on the right hand side of above equations are the e-modification terms which are used to guarantee robustness.

Based on the chain rule of derivative, we have

$$\frac{\partial J}{\partial \hat{W}_{i,j}} = \frac{\partial J}{\partial \tilde{y}} \cdot \frac{\partial \tilde{y}}{\partial \tilde{x}} \cdot \frac{\partial \tilde{x}}{\partial \hat{M}} \cdot \frac{\partial \hat{M}}{\partial \hat{W}_{i,j}} \tag{6.11}$$

$$\frac{\partial J}{\partial \hat{V}_{i,j}} = \frac{\partial J}{\partial \tilde{y}} \cdot \frac{\partial \tilde{y}}{\partial \tilde{x}} \cdot \frac{\partial \tilde{x}}{\partial \mathrm{net}_{\hat{V}}} \cdot \frac{\partial \mathrm{net}_{\hat{V}}}{\partial \hat{V}_{i,j}} \tag{6.12}$$

where $\mathrm{net}_{\hat{V}} = \hat{V}\bar{x}$.

Based on the cost function and (6.8), we obtain

$$\frac{\partial J}{\partial \hat{W}_{i,j}} = (\tilde{y}^\top \tilde{C} d_{xM})_{1\times i} \cdot \sigma_j \tag{6.13}$$

$$\frac{\partial J}{\partial \hat{V}_{i,j}} = (\tilde{y}^\top \tilde{C} d_{xV})_{1\times i} \cdot \bar{x}_j \tag{6.14}$$

where $\tilde{C} = \sum_{i=1}^{l} h_i(z) C_i$, and

$$d_{xM} = \frac{\partial \tilde{x}}{\partial \hat{M}} \qquad d_{xV} = \frac{\partial \tilde{x}}{\partial \mathrm{net}_{\hat{V}}}. \tag{6.15}$$

Using (6.11)-(6.15), we can formulate the update laws into a matrix form as

$$\dot{\hat{W}} = -\rho_1(\tilde{y}^\top \tilde{C} d_{xM})^\top (\sigma(\hat{V}\bar{x}))^\top - \rho_2 \|\tilde{y}\| \hat{W} \tag{6.16}$$

$$\dot{\hat{V}} = -\rho_3(\tilde{y}^\top \tilde{C} d_{xV})^\top \bar{x}^\top - \rho_4 \|\tilde{y}\| \hat{V}. \tag{6.17}$$

Instead of using the static approximation of the gradients (6.15) in [157], the dynamics of d_{xM} and d_{xV} can be derived based on (6.8) as

$$\dot{d}_{xM} = \tilde{A} d_{xM} - I \tag{6.18}$$

$$\dot{d}_{xV} = \tilde{A} d_{xV} - \hat{W}(I - \Lambda(\hat{V}\bar{x})) \tag{6.19}$$

where $\tilde{A} = \sum_{i=1}^{l} \sum_{j=1}^{l} h_i(z) h_j(z)(A_i - L_i C_j)$, and $\Lambda(\hat{V}\bar{x}) = \text{diag}\{\sigma_i^2(\hat{V}_i \bar{x})\}$.

During the updating process of the neural networks parameters, we first initialize d_{xM} and d_{xV} to be zero matrices, and then we dynamically update d_{xM} and d_{xV} using equations (6.18) and (6.19). Correspondingly, the updated d_{xM} and d_{xV} are substituted into (6.16) and (6.17) to compute the parameters $\hat{W}$ and $\hat{V}$.

6.3.3 Stability Analysis

Based on the universal approximation ability of neural networks model, on the compact set, we have

$$\epsilon_1(t) = f_a(t) - \hat{M}(W, V, \bar{x}, t) \tag{6.20}$$

where $\epsilon_1(t)$ is the bounded neural network approximation error, and W and V are fixed optimal parameters which are selected such that the L_2-norm distance between $f_a(t)$ and $\hat{M}(W, V, \bar{x}, t)$ is minimized.

We assume that the upper bounds on the fixed ideal parameters W and V satisfy

$$\|W\|_F \leq W_M \tag{6.21}$$

$$\|V\|_F \leq V_M \tag{6.22}$$

where $\|\cdot\|_F$ is the Frobenius norm of a matrix.

Substituting (6.20) into (6.8), we obtain

$$\dot{\tilde{x}}(t) = \tilde{A}\tilde{x} + \tilde{W}\sigma(\hat{V}\bar{x}) + \epsilon_2(t) + \eta(t) \tag{6.23}$$

$$\tilde{y}(t) = \tilde{C}\tilde{x}(t) \tag{6.24}$$

where $\tilde{W} = W - \hat{W}$, and $\epsilon_2(t) = W[\sigma(V\bar{x}) - \sigma(\hat{V}\bar{x})] + \epsilon_1(t)$ is a bounded disturbance term, i.e., $\|\epsilon_2(t)\| \leq \bar{\epsilon}_2$, due to the boundedness of W, the boundedness of sigmoidal function, and the boundedness of the uncertainty and approximation error.

The stability of the fuzzy-neural observer is guaranteed in the following theorem, where we use the proposed modified back-propagation algorithm to update its parameters.

Theorem 6.1 *Consider the TS fuzzy system (6.3) and its fuzzy-neural observer (6.6). If the parameters of the neural networks are updated according to (6.16)-(6.19), then the state estimation error $\tilde{x}$, the parameter estimation errors, $\tilde{W}$, $\tilde{V}$, and the output estimation error $\tilde{y}$ are all bounded.*

Proof: We first prove the boundedness of $\tilde{x}$ and $\tilde{W}$. Consider a positive definite Lyapunov function candidate:

$$V_s = \frac{1}{2}\tilde{x}^\top P_1 \tilde{x} + \frac{1}{2} tr(\tilde{W}^\top \tilde{W}) \tag{6.25}$$

where P_1 is a symmetric positive definite matrix satisfying

$$\tilde{A}^\top P_1 + P_1 \tilde{A} = -Q$$

in which Q is a positive definite matrix, and $\tilde{W}$ can be further written as

$$\dot{\tilde{W}} = \rho_1(\tilde{y}^\top \tilde{C} d_{xM})^\top (\sigma(\hat{V}\bar{x}))^\top + \rho_2 \|\tilde{y}\| \hat{W} \tag{6.26}$$

Since $\tilde{A}$ is designed to be Hurwitz using the LMI method, according to (6.18), d_{xM} is stable and converges to $\tilde{A}^{-1}$.

Based on (6.23) and (6.26), the time derivative of V_s is

$$\begin{aligned} \dot{V}_s &= \frac{1}{2}\dot{\tilde{x}}^\top P_1 \tilde{x} + \frac{1}{2}\tilde{x}^\top P_1 \dot{\tilde{x}} + tr(\tilde{W}^\top \dot{\tilde{W}}) \\ &= -\frac{1}{2}\tilde{x}^\top Q \tilde{x} + \tilde{x}^\top P_1(\tilde{W}\sigma(\hat{V}\bar{x}) + \epsilon_2 + \eta) \\ &\quad + tr[\tilde{W}^\top l_1 \tilde{x}\sigma(\hat{V}\bar{x})^\top + \tilde{W}^\top \rho_2 \|\tilde{C}\tilde{x}\|(W - \tilde{W})] \end{aligned} \tag{6.27}$$

where $l_1 = \rho_1 d_{xM}^{\top} \tilde{C}^{\top} \tilde{C}$.

Using the properties of the matrix trace and sigmoidal function in [157], we have

$$tr[\tilde{W}^{\top} l_1 \tilde{x} \sigma^{\top}] \leq \|\tilde{W}\| \|l_1\| \|\tilde{x}\| \sigma_m \tag{6.28}$$

$$tr[\tilde{W}^{\top} \rho_2 \|\tilde{C}\tilde{x}\| \hat{W}] \leq (W_M \|\tilde{W}\| - \|\tilde{W}\|^2) \rho_2 \|\tilde{C}\| \|\tilde{x}\| \tag{6.29}$$

where σ_m is defined such that $\|\sigma^{\top}\| \leq \sigma_m$.

Therefore, (6.27) can be further written as

$$\begin{aligned}
\dot{V}_s &\leq -\frac{1}{2}\lambda_{\min}(Q)\|\tilde{x}\|^2 + \|\tilde{x}\|\|P_1\|(\|\tilde{W}\|\sigma_m + \bar{\epsilon}_2 + \bar{\eta}) \\
&\quad + \sigma_m \|\tilde{W}\| \|l_1\| \|\tilde{x}\| + (W_M \|\tilde{W}\| - \|\tilde{W}\|^2)\rho_2 \|\tilde{C}\| \|\tilde{x}\| \\
&= -\frac{1}{2}\lambda_{\min}(Q)\|\tilde{x}\|^2 - \beta_1 \|\tilde{x}\| \|\tilde{W}\|^2 + \beta_2 \|\tilde{x}\| \|\tilde{W}\| + \beta_3 \|\tilde{x}\| \\
&\leq -\frac{1}{2}\lambda_{\min}(Q)\|\tilde{x}\|^2 - \beta_1 \|\tilde{x}\| (\|\tilde{W}\| - \frac{\beta_2}{2\beta_1})^2 + (\frac{\beta_2^2}{4\beta_1} + \beta_3)\|\tilde{x}\| \\
&\leq -\frac{1}{2}\lambda_{\min}(Q)\|\tilde{x}\|^2 + (\frac{\beta_2^2}{4\beta_1} + \beta_3)\|\tilde{x}\|
\end{aligned} \tag{6.30}$$

where

$$\beta_1 = \rho_2 \|\tilde{C}\| \tag{6.31}$$

$$\beta_2 = \sigma_m(\|P_1\| + \|l_1\|) + \rho_2 W_M \|\tilde{C}\| \tag{6.32}$$

$$\beta_3 = \|P_1\|(\bar{\epsilon}_2 + \bar{\eta}). \tag{6.33}$$

Thus, from (6.30), when

$$\|\tilde{x}\| > \frac{\beta_2^2 + 4\beta_1\beta_3}{2\lambda_{\min}(Q)\beta_1} = b_1 \tag{6.34}$$

$\dot{V}_s < 0$, which means $\dot{V}_s$ is negative definite outside the ball with radius b_1 described as $\chi_1 = \{\tilde{x} \mid \|\tilde{x}\| \leq b_1\}$. When $\tilde{x}$ is increased outside of the ball χ_1, the negative of $\dot{V}_s$ results in reducing V_s and $\tilde{x}$. This analysis shows the ultimate boundedness of $\tilde{x}$.

Now, consider the boundedness of the parameter error $\tilde{W}$. Based on (6.16), the dynamics of $\tilde{W}$ can be written as

$$\begin{aligned}
\dot{\tilde{W}} &= \rho_1(\tilde{y}^{\top}\tilde{C}d_{xM})^{\top}(\sigma(\hat{V}\tilde{x}))^{\top} + \rho_2\|\tilde{y}\|W - \rho_2\|\tilde{y}\|\tilde{W} \\
&= -\rho_2\|\tilde{y}\|\tilde{W} + \rho_2\|\tilde{y}\|W + \kappa_1(\tilde{x}_1, \hat{V})
\end{aligned} \tag{6.35}$$

where

$$\kappa_1(\tilde{x}_1, \hat{V}) = \rho_1(\tilde{y}^\top \tilde{C} d_{xM})^\top (\sigma(\hat{V}\bar{x}))^\top \tag{6.36}$$

We can see that $\kappa_1(\cdot)$ is bounded since $\tilde{x}$, $\sigma(\cdot)$, and $\tilde{C}$ are all bounded, d_{xM} is bounded because $\tilde{A}$ is a stable matrix. Given the ideal weight W is fixed, (6.35) can be treated as a linear system with bounded input $\rho_2\|\tilde{y}\|W + \kappa_1(\tilde{x}_1, \hat{V})$. Obviously, system (6.35) is stable since ρ_2 is positive and the input is bounded. Therefore, the boundedness of $\tilde{W}$ is guaranteed.

The boundedness of $\tilde{W}$ implies the boundedness of $\hat{W}$. From (6.19), d_{xV} is also bounded since $\sigma_i^2(\cdot)$ is a bounded function, and $\tilde{A}$ is a stable matrix.

The dynamic equation of $\tilde{V}$ is

$$\begin{aligned} \dot{\tilde{V}} &= \rho_3(\tilde{y}^\top \tilde{C} d_{xV})^\top \bar{x}^\top + \rho_4\|\tilde{y}\|\hat{V} \\ &= -\rho_4\|\tilde{y}\|\tilde{V} + \rho_3(\tilde{y}^\top \tilde{C} d_{xV})^\top \bar{x}^\top + \rho_4\|\tilde{y}\|V \end{aligned} \tag{6.37}$$

The second and third terms on the right hand side of (6.37) are both finite because $\tilde{x}$, $\hat{W}$, $\sigma(\cdot)$, $\tilde{C}$, d_{xV} are all bounded, and ρ_3 and ρ_4 are both positive finite values. Consequently, we can conclude that the boundedness of $\tilde{V}$ is also ensured. ∎

6.4 Fuzzy-Neural Sliding Mode Observer

From the above stability analysis of the fuzzy-neural observer, the fault estimation accuracy might be affected by the system uncertainties and neural networks approximation errors. Therefore, we modify the fuzzy-neural observer (6.6) by adding a signum function

$$\begin{aligned} \dot{\hat{x}}(t) &= \sum_{i=1}^{l} h_i(z)\{A_i\hat{x} + B_i u + L_i(y(t) - \hat{y}(t))\} \\ &\quad + \mathcal{B}(t - T_m)\hat{M}(t) + \gamma P_1^{-1}\tilde{C}^\top \mathrm{sign}(\tilde{y}) \\ \hat{y}(t) &= \sum_{i=1}^{l} h_i(z) C_i \hat{x}(t) \end{aligned} \tag{6.38}$$

where $\gamma > 0$, and P_1 is defined in Theorem 6.1.

Then, the estimation error dynamics become

$$\begin{aligned} \dot{\tilde{x}}(t) &= \tilde{A}\tilde{x} + \tilde{W}\sigma(\hat{V}\bar{x}) + \epsilon_2(t) + \eta(t) - \gamma P_1^{-1}\tilde{C}^\top \text{sign}(\tilde{y}) \\ \tilde{y}(t) &= \tilde{C}\tilde{x}(t) \end{aligned} \tag{6.39}$$

Regarding the stability of above dynamics, we have the following theorem.

Theorem 6.2 *Consider the TS fuzzy system (6.3) and the fuzzy-neural sliding mode observer (6.38). If the parameters of the neural networks model are updated according to (6.16)-(6.19), then $\tilde{x}$, $\tilde{W}$, $\tilde{V}$, and $\tilde{y}$ are all bounded, and $\tilde{x}$ can converge to a small bound.*

Proof: The proof procedure is similar to that in theorem 6.1. We still use the Lyapunov function (6.25), and its time derivative is rewritten as

$$\begin{aligned} \dot{V}_s &= \frac{1}{2}\dot{\tilde{x}}^\top P_1\tilde{x} + \frac{1}{2}\tilde{x}^\top P_1\dot{\tilde{x}} + tr(\tilde{W}^\top\dot{\tilde{W}}) \\ &= -\frac{1}{2}\tilde{x}^\top Q\tilde{x} + \tilde{x}^\top P_1(\tilde{W}\sigma(\hat{V}\bar{x}) + \epsilon_2) + \tilde{x}^\top P_1\eta - \tilde{y}^\top\gamma\text{sign}(\tilde{y}) \\ &\quad + tr[\tilde{W}^\top l_1\tilde{x}\sigma(\hat{V}\bar{x})^\top + \tilde{W}^\top\rho_2\|\tilde{C}\tilde{x}\|(W - \tilde{W})] \end{aligned} \tag{6.40}$$

Still using inequalities (6.28) and (6.29), we have

$$\begin{aligned} \dot{V}_s &\leq -\frac{1}{2}\lambda_{\min}(Q)\|\tilde{x}\|^2 + \|\tilde{x}\|\|P_1\|(\|\tilde{W}\|\sigma_m + \bar{\epsilon}_2) + \bar{\eta}\|\tilde{x}^\top P_1\| - \gamma\|\tilde{y}\| \\ &\quad + \sigma_m\|l_1\|\|\tilde{W}\|\|\tilde{x}\| + (W_M\|\tilde{W}\| - \|\tilde{W}\|^2)\rho_2\|\tilde{C}\|\|\tilde{x}\| \\ &\leq -\frac{1}{2}\lambda_{\min}(Q)\|\tilde{x}\|^2 - \beta_1\|\tilde{x}\|\|\tilde{W}\|^2 + \beta_2\|\tilde{x}\|\|\tilde{W}\| + \beta_3\|\tilde{x}\| - \gamma\|\tilde{y}\| \\ &\leq -\frac{1}{2}\lambda_{\min}(Q)\|\tilde{x}\|^2 - \beta_1\|\tilde{x}\|(\|\tilde{W}\| - \frac{\beta_2}{2\beta_1})^2 + (\frac{\beta_2^2}{4\beta_1} + \beta_3)\|\tilde{x}\| - \gamma\|\tilde{y}\| \\ &\leq -\frac{1}{2}\lambda_{\min}(Q)\|\tilde{x}\|^2 + (\frac{\beta_2^2}{4\beta_1} + \beta_3)\|\tilde{x}\| - \gamma\|\tilde{y}\| \end{aligned} \tag{6.41}$$

where β_1, β_2 and β_3 are defined in (6.31), (6.32) and (6.33).

Based on (6.41), we have, when

$$\|\tilde{x}\| > \frac{\beta_2^2 + 4\beta_1\beta_3 + \sqrt{(\beta_2^2 + 4\beta_1\beta_3)^2 - 32\gamma\beta_1^2\lambda_{\min}(Q)\|\tilde{y}\|}}{4\lambda_{\min}(Q)\beta_1} = b_2 \tag{6.42}$$

$\dot{V}_s < 0$, $\tilde{x}$ is ultimately bounded by a ball with a radius b_2; i.e., $\chi_2 = \{\tilde{x} \mid \|\tilde{x}\| \leq b_2\}$. Comparing b_1 and b_2, based on the properties of quadratic functions, we obtain $b_2 \leq b_1$. ∎

Remark 6.3 *When the sliding mode term exactly counteracts the effect of modeling uncertainty, the convergence of $\|\tilde{x}\|$ to a smaller bound implies a more accurate fault estimation. If the sliding mode gain, γ, is too large, the sliding mode may eliminate the effect of fault and uncertainties, which are both treated as unknown inputs. Therefore, the sliding mode gain γ should be carefully selected, in order to distinguish the effect of fault and uncertainties. The methods for updating the sliding mode gain can be found in [158].*

6.5 Robust Fault Diagnosis Schemes

In model-based fault diagnosis strategies, a diagnostic residual is usually generated. Due to the universal existence of system uncertainties and noises, robust fault diagnostic strategies are necessary to avoid false alarms. One robust FD approach uses a dead-zone operator in the parameter update algorithm which makes the online fault estimators only approximate the signal with a magnitude above a predefined threshold [31]. However, this method reduces the accuracy of fault estimation. Another approach to realize robust fault diagnosis is to set a nonzero threshold for the generated residual when making a diagnostic decision.

In this work, after all the states are estimated by using the TS fuzzy models, we use the output error or the output estimation error to detect the fault; i.e.

$$\begin{cases} \text{No fault occurs} & \text{if } \|e_y(t)\| < \epsilon_f \\ \text{Fault occurs, and } \hat{M}(t) \text{ works} & \text{if } \|e_y(t)\| \geq \epsilon_f \end{cases} \tag{6.43}$$

or

$$\begin{cases} \text{No fault occurs} & \text{if } \|\tilde{y}(t)\| < \epsilon'_f \\ \text{Fault occurs, and } \hat{M}(t) \text{ works} & \text{if } \|\tilde{y}(t)\| \geq \epsilon'_f \end{cases} \tag{6.44}$$

where $e_y(t) = y_d - y$ is the system output error, y_d is the reference trajectory, and ϵ_f and ϵ'_f are two thresholds for robust fault detection. The choice of ϵ_f and ϵ'_f relies on the system characteristics and the diagnosis scheme in use.

In addition, a single residual is usually not sufficient for all the tasks of fault diagnosis. Therefore, the neural networks based estimator $\hat{M}(t)$ is used to achieve fault isolation and estimation.

The proposed fault diagnosis scheme using fuzzy-neural and sliding mode approaches is implemented in the following steps.

- Step 1: Construct TS fuzzy model for nominal nonlinear system (6.1) using (6.3).
- Step 2: Determine gain L_i for local linear observer using the LMI method.
- Step 3: Design a neural network based fault estimator $\hat{M}(t)$ based on (6.7), and activate $\hat{M}(t)$ at $t = T_m$.
- Step 4: Construct a fuzzy-neural Luenberger observer (6.6) or a fuzzy-neural sliding mode observer (6.38), and obtain $e_y(t)$ and $\tilde{y}(t)$.
- Step 5: Compare $\|e_y(t)\|$ with ϵ_f, or compare $\|\tilde{y}(t)\|$ with ϵ'_f to detect fault based on (6.43) and (6.44).
- Step 6: Update the parameters, $\hat{W}$ and $\hat{V}$, of the neural network based fault estimator $\hat{M}(t)$.
- Step 7: Use $\hat{M}(t)$ to isolate and estimate faults.

6.6 Application to a Satellite Orbital Control System

In this section, we apply the proposed fuzzy-neural observer and fuzzy-neural sliding mode observer to the fault diagnosis for a point mass satellite dynamic system [135]. Firstly, we design a TS fuzzy controller for the nominal control system. Then, the

fuzzy-neural observer and fuzzy-neural sliding mode observer are established, respectively. The fault diagnosis performance using these two observers are demonstrated and analyzed.

A fourth-order satellite model is considered in [135] as

$$\begin{aligned} \dot{r} &= v & r(0) &= r_0 \\ \dot{v} &= rw^2 - \frac{k}{mr^2} + \frac{u_1}{m} & v(0) &= 0 \\ \dot{\phi} &= w & \phi(0) &= 0 \\ \dot{\omega} &= -\frac{2v\omega}{r} + \frac{u_2}{mr} & \omega(0) &= \omega_0 \end{aligned} \tag{6.45}$$

where $m = 200$kg is the mass of the satellite, (r, ϕ) are the polar coordinates of the satellite, v is the radial speed, and ω is the angular speed. Control inputs u_1 and u_2 are the radial and tangential thrust forces, respectively. When the control purpose is to track the output r and ω to their constant reference trajectory r_r and ω_r, the equation $\dot{\phi} = \omega$ can be omitted.

By choosing $x = [x_1\ x_2\ x_3]^\top = [r\ v\ \omega]^\top$, and $y = [r\ \omega]^\top$, the reduced-order system is formulated as

$$\begin{aligned} \dot{x}_1 &= x_2 & x_1(0) &= r_0 \\ \dot{x}_2 &= x_1 x_3^2 - \frac{k}{mx_1^2} + \frac{u_1}{m} & x_2(0) &= 0 \\ \dot{x}_3 &= -\frac{2x_2x_3}{x_1} + \frac{u_2}{mx_1} & x_3(0) &= \omega_0 \end{aligned} \tag{6.46}$$

The parameter $k = K_E m$, where $K_E = 3.986 \times 10^5 \text{km}^3/\text{s}^2$, is derived from the parameters of the Earth ($M_E = 5.974 \times 10^{24}$kg). The satellite is first observed in perigee 375 km above the surface of the Earth, $r_0 = R_E + 375$km ($R_E = 6.378 \times 10^3$km). The initial angular speed, ω_0, is computed using the orbital mechanics $\omega_0 = \sqrt{(e_{orbit}+1)K_E/r_0^3}$, where $e_{orbit} = 0.162$ is the eccentricity.

In the design of the fuzzy controller and observer, we define the nonlinear terms as $z_1(x_1, x_3) = x_3^2 - \frac{k}{mx_1^3}$, $x_2(x_1, x_3) = \frac{x_3}{x_1}$, and $z_3(x_1, x_3) = \frac{1}{x_1}$. As a result, the state matrix and control matrix become

$$A = \begin{bmatrix} 0 & 1 & 0 \\ z_1 & 0 & 0 \\ 0 & -2z_2 & 0 \end{bmatrix} \quad B = \begin{bmatrix} 0 & 0 \\ \frac{1}{m} & 0 \\ 0 & \frac{z_3}{m} \end{bmatrix}$$

We assume that the output variables satisfy $x_1 \in [r_{\min}, r_{\max}]$ and $x_3 \in [\omega_{\min}, \omega_{\max}]$, where, in the simulation, $r_{\min} = 0.9r_0$, $r_{\max} = 1.1r_0$, $\omega_{\min} = -4$ rad/hr, and $\omega_{\max} = 4$ rad/hr. Thus, we obtain

$$\begin{aligned} z_1^{\max} &= \omega_{\max}^2 - \frac{k}{mr_{\max}^3} & z_1^{\min} &= -\frac{k}{mr_{\min}^3} \\ z_2^{\max} &= \frac{\omega_{\max}}{r_{\min}} & z_2^{\min} &= \frac{\omega_{\min}}{r_{\min}} \\ z_3^{\max} &= \frac{1}{r_{\min}} & z_3^{\min} &= \frac{1}{r_{\max}} \end{aligned} \tag{6.47}$$

The nonlinear term z_1 can be represented by

$$\begin{aligned} \mu_1^1 z_1^{\max} + \mu_1^2 z_1^{\min} &= z_1 \\ \mu_1^1 + \mu_1^2 &= 1 \end{aligned} \tag{6.48}$$

So, the membership functions μ_1^1 and μ_1^2 are

$$\mu_1^1 = \frac{z_1 - z_1^{\min}}{z_1^{\max} - z_1^{\min}} \tag{6.49}$$

$$\mu_1^2 = \frac{-z_1 + z_1^{\max}}{z_1^{\max} - z_1^{\min}} \tag{6.50}$$

and μ_2^1, μ_2^2, μ_3^1, and μ_3^2 are similarly derived.

Since the TS model has three nonlinear terms, eight fuzzy rules are needed. The membership functions for these eight fuzzy rules are computed using (6.4). The output tracking controller is designed by using the approach in [98], where the feedback gain for the controller and observer are calculated by solving a group of LMIs. The controller output is assumed to be subject to uncertainty $u_d = 2\% * rand$, and the measurement noise is set with $\varsigma = 0.2\% * rand$, i.e., $y_{measure} = y(1 + \varsigma)$, where $rand$ still represents Gaussian white noise.

In this simulation, the three-layer neural networks is of a structure $5 \times 5 \times 3$, and training the neural networks before using it for online fault isolation and estimation is recommended. In the parameter update law, (6.18) and (6.19), the learning rates are set to be $\rho_1 = \rho_3 = 20$, and the damping coefficients are $\rho_2 = \rho_4 = 0.1$. The initial values of d_{xM} and d_{xV} are a zero vector and zero matrix, respectively. The sliding mode gain γ is set to be 0.0025 using a trial-and-error method.

The simulation results are shown from Figure 6.1 to Figure 6.5. Figure 6.1 illustrates the performance of output tracking and state observation using TS fuzzy models when the system is fault-free.

In the simulation, we assume that only an incipient fault occurs in the second state at the 16th hour, and the neural networks is enabled at the 15th hour. Figure 6.2 shows the norm of the output error and the norm of the output estimation error, respectively, when a fuzzy-neural sliding mode observer is used. Both of these two signals can be used to detect the occurrence of faults. However, different threshold are needed for each case. For the norm of output error, after the system output tracks the trajectory, the threshold is chosen as $\epsilon_f = 0.05$. For the norm of output estimation error, the threshold is set to $\epsilon_f = 0.001$. After a fault occurs, $e_y(t)$ and $\|\tilde{y}\|$ quickly exceed their respective threshold. However, in order to isolate and estimate the fault, we need to use other signals.

Figure 6.3 portrays the characteristics of the fault functions and the three outputs of the neural networks when using the diagnostic fuzzy-neural observer. When a fault occurs, only the neural network output that corresponds to the faulty state specifies the dynamics of the fault, and the other neural networks outputs associated with the healthy states remain close to zero. This phenomenon illustrates the fault isolation and estimation abilities of the proposed FNO-based fault diagnosis scheme. Due to the approximation errors and system uncertainties, fault estimation errors exist.

Figure 6.4 demonstrates the reference states, actual states, and estimated states when using the fuzzy-neural sliding mode observer. When a fault occurs, the actual states and output significantly deviate from their nominal values. Additionally, the fuzzy-neural sliding mode observer can accurately estimate the states, since the sliding mode and neural networks compensate the effect of the fault and system uncertainties.

Figure 6.5 exhibits the same fault function and the three outputs of the neural networks when using the fuzzy-neural sliding mode observer. Comparing the fault diagnostic results with those using the fuzzy-neural observer in Figure 6.3, we achieve better performance in fault estimation using FNSMO, though the chattering caused by sliding mode might increase as well. The peaks in fault estimation is due to the introduction of measurement noise to sliding mode, and the coupling peaks can be

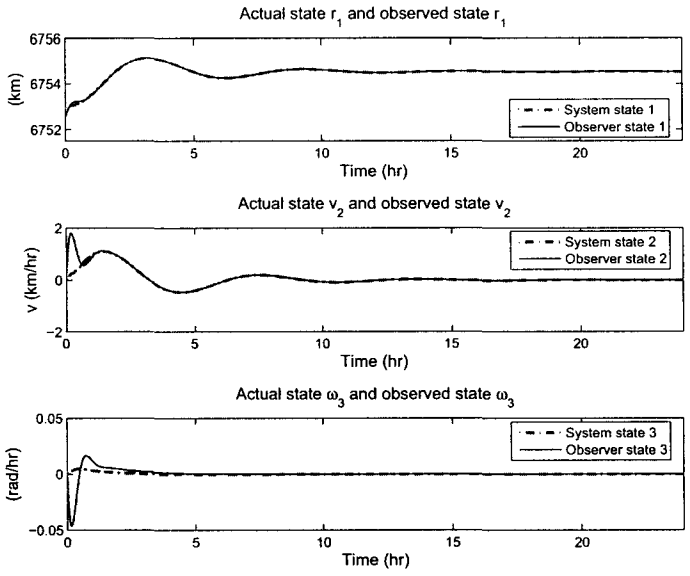

Figure 6.1: System states and observer states using a TS fuzzy control and observer in the fault-free case

reduced using a filter. Extensive work can be found in [87]. Another issue is there is no coupling peaks in the fault estimation in Figure 6.3 because neural network itself has redundancy and is tolerant to measurement noises.

6.7 Conclusions

In this chapter, a robust fault diagnosis scheme using TS fuzzy models, neural networks, and sliding mode was proposed for a class of nonlinear systems which can be represented by the TS fuzzy models. In order to generate diagnostic residuals, a fuzzy-neural observer and a fuzzy-neural sliding mode observer were designed, respectively. In the proposed fuzzy-neural observer, the TS fuzzy model was integrated with a neural networks based estimator which was used to characterize the possible faults. The sliding mode in the second diagnostic observer helps to reduce the effect of the system uncertainties and approximation errors in the fault estimation. The parameters of these two observers were updated using a modified back-propagation

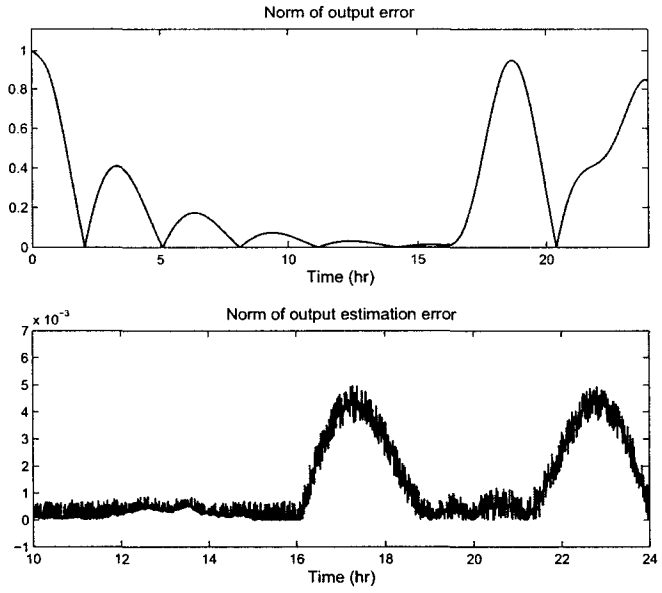

Figure 6.2: Norm of the output error and the output estimation error using FNSMO under an incipient fault

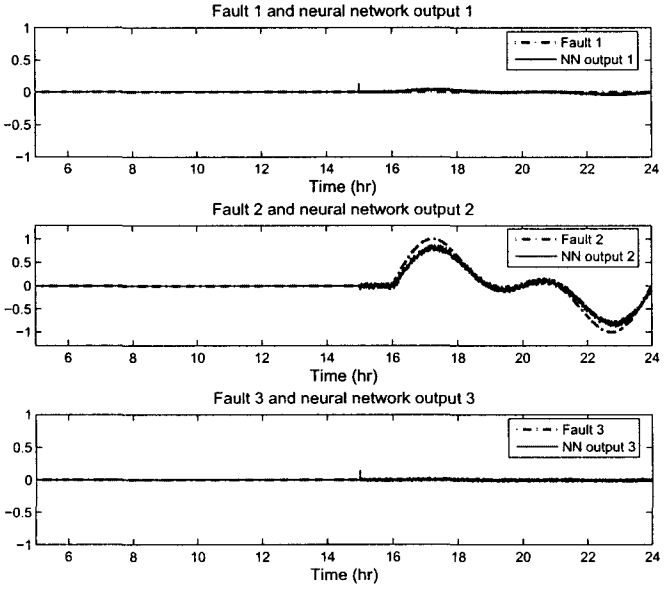

Figure 6.3: Outputs of the fuzzy-neural observer under an incipient fault

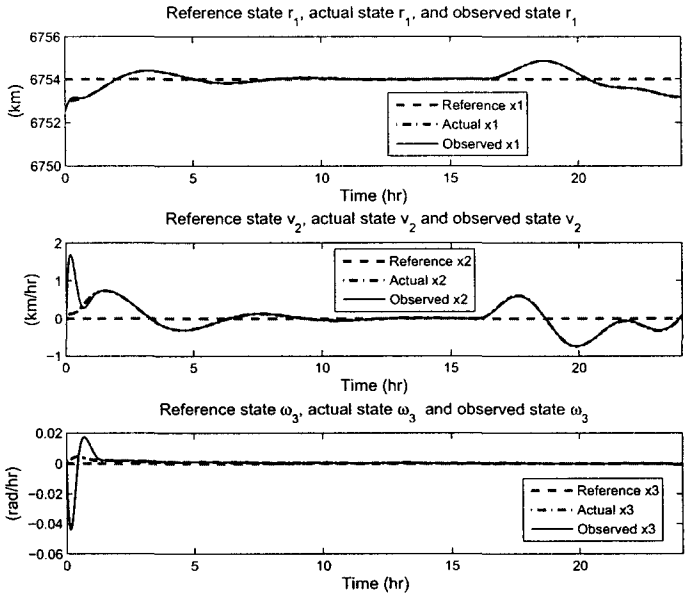

Figure 6.4: Nominal states, actual states and observed states using fuzzy-neural sliding mode observer under an incipient fault

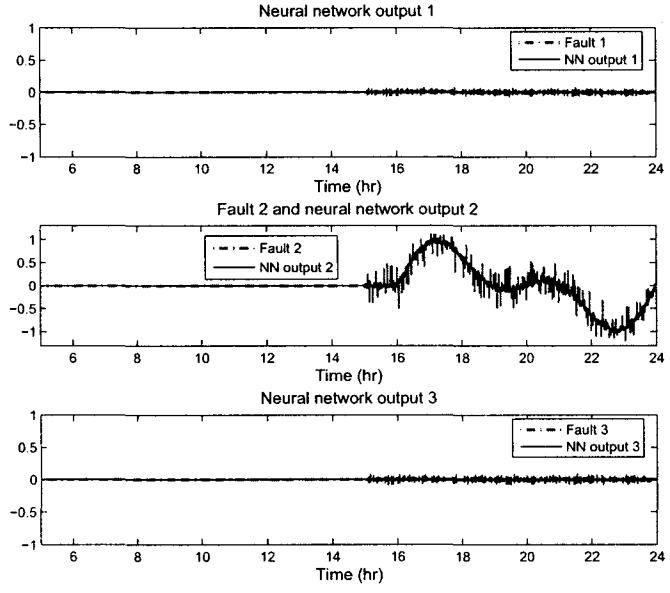

Figure 6.5: Outputs of the fuzzy-neural sliding mode observer under an incipient fault

algorithm, where the stability of the proposed fault diagnosis scheme can be rigorously analyzed. After the theoretical analysis, the proposed robust fault diagnosis scheme was applied to a reduced-order satellite orbital control system. The simulation results demonstrate its satisfactory performance.

Although via TS fuzzy models, the fault diagnosis schemes using sliding mode and learning approaches can be applied to a more general class of nonlinear systems, the complexity of fuzzy models makes solving the LMIs difficult in real applications. Therefore, building suitable fuzzy models becomes the primary task of using TS fuzzy observers in fault diagnosis, and this area still needs in-depth research.

In addition, in this chapter, only the system modeling capability of fuzzy models was used. Since fuzzy models have many other attractive features, further applications of fuzzy models or integration of fuzzy models with other techniques in fault diagnosis should be a topic of future research.

Chapter 7

Fault Diagnosis in Nonlinear Systems Using High Order Sliding Mode Differentiators and an Uncertainty Observer

In this chapter, an actuator fault detection, isolation, and estimation scheme using high order sliding mode differentiators and a neural networks based uncertainty observer is proposed for the class of nonlinear systems which have been studied in Chapter 4.

7.1 Introduction

One of the most popular model-based fault diagnosis approaches is observer-based techniques, which include the use of the estimation error as the diagnostic residual, and reconstruction of the outputs of the system of interest with the aid of observers. Although the available observer design methods provide freedom for achieving the required performance, efficient fault diagnosis relies on the robustness of the diagnostic residual to modeling uncertainties and noises. A straightforward method to create

robustness with respect to uncertainties and noises is to generate unknown input decoupled residuals. There are three classes of time domain solutions: 1) unknown input observer (UIO) based approaches, e.g., [159]; 2) eigenstructure assignment approaches, e.g., [160]; and 3) sliding mode observer based approaches, e.g., [56], [57], [70], [66]. The advantage of the decoupling methods lies in the fact that they can detect a small-magnitude fault, even if large modeling errors are present.

The above approaches are originally based on linear multivariable models, which can not cover many practical systems with strong nonlinearity. The inherent nonlinear nature of real systems makes exact or approximate decoupling difficult. Therefore, robust fault diagnosis problems for nonlinear systems have attracted a great deal of attentions in the past few years. One class of approaches uses learning strategies, in which the fault is estimated using online approximators [28], [29], [31]. The robustness is achieved through modifying the parameter update law of the approximators. Only the bound information of the uncertainties is used to design a threshold for robust fault detection. However, uncertainties with large magnitude probably affect the sensitivity of the diagnosis scheme to faults. Hence, some researchers considered designing fault diagnosis algorithms using the explicit information of the uncertainty. For example, the information of the uncertainty is first estimated using a recursive approach or an adaptive approach, and then it is used to generate a diagnostic residual. If an accurate estimation of the uncertainty is achieved, the fault signature on the residual becomes more evident [161], [162]. This class of methods increases the sensitivity of the diagnosis schemes to the fault. However, previous work only investigated discrete-time systems with known nonlinearity, and all the states were available through first order difference operators.

Moreover, fault diagnosis techniques based on sliding mode observers and/or differentiators have been significantly investigated in the past few years. In some previous works, the aim of building sliding mode observers was to reconstruct faults, which is different from residual generation methods. By using a system transformation and equivalent output injection, the faults can be directly reconstructed, so the detection, isolation, and estimation of the faults become straightforward. For those systems where the relative degree from the input to the output is more than one, high order

sliding mode observers/differentiators demonstrate advantages over some traditional observers [87], [149].

In this chapter, we take advantage of the high order sliding mode differentiators (HOSMDs), and extend current fault diagnosis schemes using uncertainty estimation approaches to a class of nonlinear systems. Correspondingly, a robust actuator fault detection, isolation, and estimation scheme is designed. Unlike previous fault diagnosis schemes using HOSMDs and learning approaches, the explicit information of the uncertainty is estimated and used to achieve higher sensitivity to the faults, while keeping robustness in the presence of uncertainties. Theoretically, the robustness, sensitivity, and stability of the fault diagnosis scheme will be rigorously studied. Practically, the proposed fault diagnosis scheme will be applied to a satellite attitude control system, and simulation results illustrate its effectiveness.

The remaining sections of this chapter are organized as follows. In Section 7.2, the system under study is formulated and some assumptions are given. In Section 7.3, a new fault detection scheme using high order sliding mode differentiators and neural networks based uncertainty observers is proposed, and some theoretical properties of this fault diagnosis scheme are analyzed. Section 7.4 provides two approaches to isolate and estimate faults. Thereafter, the proposed fault diagnosis scheme is applied to a satellite attitude control system which has been studied in Section 7.5. Finally, conclusions are presented in Section 7.6.

7.2 Problem Formulation

The class of nonlinear dynamic systems in this study is the same as that in Chapter 4, which is again presented here as

$$\dot{x}_1 = h(x_1, x_2) \tag{7.1}$$

$$\dot{x}_2 = f(x_1, x_2) + Bu(t) + \eta(t) \tag{7.2}$$

$$x_2 = h^{\dagger}(x_1, \dot{x}_1) \tag{7.3}$$

$$y = x_1 \tag{7.4}$$

where $x_1 \in \Re^n$, $x = [x_1^\top, x_2^\top]^\top$ is the vector of system states, and $u(t) = [u_1, \cdots, u_m]^\top$ and $y(t)$ are the system input and output vectors, respectively. The function vector $f(x_1, x_2) = [f_1(x_1, x_2), \cdots, f_n(x_1, x_2)]^\top$ and $h(x_1, x_2) = [h_1(x_1, x_2), \cdots, h_n(x_1, x_2)]^\top$ describe the dynamics in system state and output, and $\eta(t) = [\eta_1(t), \cdots, \eta_n(t)]^\top$ represents the uncertainty vector. Moreover, $B \in \Re^{n \times m}$ is the control matrix, and in (7.3), $h^\dagger$ is a nonlinear function, which implies the state x_2 can be described as a nonlinear function of the system output and its derivative.

For the sake of designing and analyzing the actuator fault diagnosis scheme conveniently, the following assumptions are introduced.

Assumption 7.1 All the functions in $f(x_1, x_2)$ and $h(x_1, x_2)$ are known.

Assumption 7.2 The state function $f(x_1, x_2)$ is differentiable at $\hat{x}_2$, which is

$$A = \left.\frac{\partial f}{\partial x}\right|_{x=\hat{x}_2}$$

where A is an $n \times n$ matrix. So, the following equation can be derived through series expansion of $f(x)$ at $\hat{x}_2$.

$$f(x_1, x_2) - f(x_1, \hat{x}_2) = A\tilde{x}_2 + \xi(x_1, x_2) - \xi(x_1, \hat{x}_2) \tag{7.5}$$

where $\xi(x_1, x_2)$ is the nonlinear part of the system dynamics.

Assumption 7.3 The nonlinear component $\xi(x_1, x_2)$ is Lipschitz at $\tilde{x}_2$ with a known constant k_ξ; that is,

$$\|\xi(y, x_2) - \xi(y, \hat{x}_2)\| < k_\xi \|x_2 - \hat{x}_2\|. \tag{7.6}$$

Assumption 7.4 Matrix A is stable, which implies a symmetric positive definite matrix Γ_1 exists such that

$$A^\top \Gamma_1 + \Gamma_1 A = -Q \tag{7.7}$$

where Q is also a positive definite matrix. Even the matrix A is unstable, we can stabilize the linear part of the system by using a Luenberger gain.

Assumption 7.5 Matrix B is of full column rank.

Assumption 7.6 The ith system uncertainty function $\eta_i(t)$ is bounded by a constant $\bar{\eta}_i$, i.e., $|\eta_i(t)| \leq \bar{\eta}_i$.

The purpose of this study is to design an actuator fault detection, isolation, and estimation scheme for system (7.1)-(7.4) under Assumption 7.1-7.6.

7.3 Fault Detection Using High Order Sliding Mode Differentiators and an Uncertainty Observer

7.3.1 State Estimation Using HOSMDs

For the dynamic systems (7.1)-(7.4), we can still use the high order sliding mode differentiators and (7.3) to estimate the state x_2. In order to obtain the first order and second order derivatives of the system output, we use a third order sliding mode differentiator, which is written again as:

$$\begin{aligned}
\dot{z}_0 &= v_0 \\
v_0 &= -\lambda_0 |z_0 - y|^{3/4} sign(z_0 - y) + z_1 \\
\dot{z}_1 &= v_1 \\
v_1 &= -\lambda_1 |z_1 - v_0|^{2/3} sign(z_1 - v_0) + z_2 \\
\dot{z}_2 &= v_2 \\
v_2 &= -\lambda_2 |z_2 - v_1|^{1/2} sign(z_2 - v_1) + z_3 \\
\dot{z}_3 &= -\lambda_3 sign(z_3 - v_2)
\end{aligned} \tag{7.8}$$

where $\lambda_0 \sim \lambda_3$ are positive diagonal coefficient matrices.

When there is no measurement noise and all the coefficients are properly selected, the third order sliding mode differentiator (7.8) can achieve

$$z_0 = y;\ z_1 = \dot{y};\ z_2 = \ddot{y} \tag{7.9}$$

Even though measurement noise exists, if the magnitude of the measurement noise is known, the boundedness of the derivative estimation error can be theoretically guaranteed [84].

Correspondingly, the system unmeasurable state x_2 can be estimated using the following function:

$$x_{2D} = h^{\dagger}(x_1, \dot{x}_{1D}) \tag{7.10}$$

where $\dot{x}_{1D}$ is the calculated derivative of x_1 using the third order sliding mode differentiator.

7.3.2 Design of Uncertainty Observer

Some researchers have used uncertainty observers to design nonlinear controllers [163], [164], where the estimation of the uncertainty is used to assist controller design to eliminate the effect of uncertainty on the systems.

In model-based fault detection, isolation, and estimation schemes, a diagnostic residual is usually generated. For dynamic systems with modeling uncertainties, we need to design robust fault detection strategies to determine whether a fault occurs or not. One way to achieve robust fault detection is to use a nonzero threshold which is established based on the magnitude of the uncertainty. However, this strategy passively makes use of partial information of the uncertainty. The robustness is achieved, but the sensitivity of the fault diagnosis scheme is sacrificed.

In this study, we design an observer that is able to successfully characterize the uncertainty. The estimated dynamics of the uncertainty is then used to generate a residual. If the system function is known and the uncertainty dynamics is accurately obtained, then the residual signal for fault detection could be very small before the occurrence of any fault.

The proposed uncertainty observer is as follows,

$$\dot{\hat{x}}_2 = f(y, \hat{x}_2) + Bu + \hat{M}_1(t), \quad \hat{x}_2(0) = x_{2D}(0) \tag{7.11}$$

$$x_{2D} = h^{\dagger}(y, \dot{y}_D) \tag{7.12}$$

where $\dot{y}_D$ is the first-order derivative of y computed via the third order sliding mode differentiator, and x_{2D} is the estimated state using y and $\dot{y}_D$. If the third order sliding mode differentiator can exactly calculate the derivative of y, then x_{2D} is completely equal to x_2. Moreover, in (7.11), $\hat{M}_1(t)$ is the observer input, which is used to estimate the magnitude of the uncertainty. Since $\hat{M}_1(t)$ is supposed to specify the uncertainty only, it is distinguished from the fault with respect to its amplitude, i.e.,

$$\hat{M}_{1,i}(t) = \begin{cases} -\bar{\eta}_i & \text{if} \quad M_{1,i}(t) < -\bar{\eta}_i \\ M_{1,i}(t) & \text{if} \quad |M_{1,i}(t)| \leq \bar{\eta}_i \\ \bar{\eta}_i & \text{if} \quad M_{1,i}(t) > \bar{\eta}_i \end{cases} \tag{7.13}$$

where $M_{1,i}(t)$ is the ith $(i = 1, \cdots, n)$ element of $M_1(t)$, which is described as

$$M_1(t) = W\sigma(V\bar{x}) \tag{7.14}$$

in which $\bar{x} = [M_1^\top(t-\tau), \tilde{x}_{2D}^\top(t-\tau)]^\top$, $\tilde{x}_{2D} = x_{2D} - \hat{x}_2$, τ is the time delay. The activation function $\sigma(\cdot)$ is the tangent hyperbolic function.

In this study, we use a popular back-propagation algorithm to update $\hat{W}$ and $\hat{V}$. Define a cost function $J = \frac{1}{2}\tilde{x}_2^2$, the update law is formulated into a matrix form as

$$\dot{\hat{W}} = -\rho_1 \frac{\partial J}{\partial \hat{W}} - \rho_2 \|\tilde{x}_{2D}\| \hat{W} \tag{7.15}$$

$$\dot{\hat{V}} = -\rho_3 \frac{\partial J}{\partial \hat{V}} - \rho_4 \|\tilde{x}_{2D}\| \hat{V} \tag{7.16}$$

where $\rho_1, \rho_3 > 0$ are the learning rates, and ρ_2, ρ_4 are small positive numbers. The second terms on the right side of above equations are e-modification terms to guarantee robustness in estimation.

Based on the chain rule of derivative, we have

$$\frac{\partial J}{\partial \hat{W}} = \frac{\partial J}{\partial \tilde{x}_2} \cdot \frac{\partial \tilde{x}_2}{\partial \hat{M}_1} \cdot \frac{\partial \hat{M}_1}{\partial \hat{W}} \tag{7.17}$$

$$\frac{\partial J}{\partial \hat{V}} = \frac{\partial J}{\partial \tilde{x}_2} \cdot \frac{\partial \tilde{x}_2}{\partial \text{net}_V} \cdot \frac{\partial \text{net}_V}{\partial \hat{W}} \tag{7.18}$$

where $\text{net}_V = \hat{V}\bar{x}$.

When $x_2 = x_{2D}$ is valid through using the high order sliding mode differentiators, we have $\tilde{x}_2 = \tilde{x}_{2D}$. Subtracting (7.11) from (7.2), we get the dynamics of the unmeasurable state estimation error, i.e.,

$$\begin{aligned} \dot{\tilde{x}}_2 &= \dot{\tilde{x}}_{2D} = f(y, x_{2D}) - f(y, \hat{x}_2) + \eta(t) - \hat{M}_1(t) \\ &= A\tilde{x}_2 + \xi(y, x_{2D}) - \xi(y, \hat{x}_2) + \eta(t) - \hat{M}_1(t). \end{aligned} \tag{7.19}$$

Based on (7.17), (7.18), and (7.19), the update law is

$$\dot{\hat{W}} = -\rho_1(\tilde{x}_{2D}^\top d_{xM})^\top(\sigma(\hat{V}\bar{x}))^\top - \rho_2\|\tilde{x}_{2D}\|\hat{W} \tag{7.20}$$

$$\dot{\hat{V}} = -\rho_3(\tilde{x}_{2D}^\top d_{xV})^\top \bar{x}^\top - \rho_4\|\tilde{x}_{2D}\|\hat{V}. \tag{7.21}$$

where

$$d_{xM} = \frac{\partial \tilde{x}}{\partial \hat{M}_1} \qquad d_{xV} = \frac{\partial \tilde{x}}{\partial \mathrm{net}_V} \tag{7.22}$$

Using a static approximation of the gradients, we have

$$d_{xM} = A^{-1} \tag{7.23}$$

$$d_{xV} = A^{-1}\hat{W}(I - \Lambda(\hat{V}\bar{x})) \tag{7.24}$$

where $\Lambda(\hat{V}\bar{x}) = diag\{\sigma_i^2(\hat{V}_i\bar{x})\}$.

7.3.3 Stability Analysis

Based on the nonlinear approximation ability of neural networks, there exists a pair of optimal parameters W^* and V^* such that on a compact set we have

$$\epsilon_1(t) = \eta(t) - M_1(W^*, V^*, \tilde{x}_{2D}, t) \tag{7.25}$$

where $\epsilon_1(t)$ is the bounded approximation error using neural networks. The optimal parameters W^* and V^* are selected such that the L_2-norm distance between $\eta(t)$ and its estimation is minimized. Usually, this approximation error is very small if the structure and learning algorithm of the neural networks are carefully chosen.

We assume that the upper bounds on the optimal parameters W^* and V^* satisfy that

$$\|W^*\|_F \leq W_M \tag{7.26}$$

$$\|V^*\|_F \leq V_M \tag{7.27}$$

where $\|\cdot\|_F$ is the Frobenius norm of a matrix.

Substituting (7.25) into (7.19), when no fault occurs, we obtain

$$\begin{aligned}\dot{\tilde{x}}_2 &= f(y, x_{2D}) - f(y, \hat{x}_2) + \eta(t) - \hat{M}_1(t) \\ &= A\tilde{x}_2 + \xi(y, x_{2D}) - \xi(y, \hat{x}_2) + \tilde{W}\sigma(\hat{V}\bar{x}) + \epsilon_2\end{aligned} \tag{7.28}$$

where $\tilde{W} = W^* - \hat{W}$, and $\epsilon_2 = W^*[\sigma(V^*\bar{x}) - \sigma(\hat{V}\bar{x})] + \epsilon_1$ is a bounded disturbance term, i.e., $\|\epsilon_2\| = \bar{\epsilon}_2$, due to the boundedness of W^*, the boundedness of sigmoidal function, and the boundedness of approximation error.

Stability of the fault diagnosis algorithm is analyzed in the following theorem.

Theorem 7.1 *For system (7.1)-(7.4) under Assumption 7.1-7.6, if the high order sliding mode differentiators and the proposed uncertainty observer are used, the state estimation error $\tilde{x}_2$, the parameter estimation error $\tilde{W}$ and $\tilde{V}$ are all bounded.*

Proof: First, we prove the boundedness of $\tilde{x}$ and $\tilde{W}$. Consider a Lyapunov candidate:

$$V_s = \frac{1}{2}\tilde{x}_2^\top \Gamma_1 \tilde{x}_2 + \frac{1}{2}tr(\tilde{W}^\top \tilde{W}) \tag{7.29}$$

where Γ_1 satisfies Assumption 7.4.

Based on (7.20), we obtain

$$\dot{\tilde{W}} = \rho_1(\tilde{x}_2^\top d_{xM})^\top(\sigma(\hat{V}\bar{x}))^\top + \rho_2\|\tilde{x}_2\|\hat{W}. \tag{7.30}$$

Using (7.28) and (7.30), the time derivative of V_s is

$$\begin{aligned}\dot{V}_s &= \frac{1}{2}\dot{\tilde{x}}_2^\top \Gamma_1 \tilde{x}_2 + \frac{1}{2}\tilde{x}_2^\top \Gamma_1 \dot{\tilde{x}}_2 + tr(\tilde{W}^\top \dot{\tilde{W}}) \\ &= -\frac{1}{2}\tilde{x}_2^\top Q\tilde{x}_2 + \tilde{x}_2^\top \Gamma_1(\xi(x_1, x_2) - \xi(x_1, \hat{x}_2)) \\ &\quad + \tilde{x}_2^\top \Gamma_1 \tilde{W}\sigma(\hat{V}\bar{x}) + \tilde{x}_2^\top \Gamma_1 \epsilon_2 \\ &\quad + tr[\tilde{W}^\top \rho_1 d_{xM}^\top \tilde{x}_2 \sigma^\top + \tilde{W}^\top \rho_2 \|\tilde{x}_2\|\hat{W}].\end{aligned} \tag{7.31}$$

Based on the properties of matrix trace and sigmoidal function, we have

$$tr(\tilde{W}^\top \rho_1 d_{xM}^\top \tilde{x}_2 \sigma^\top) \leq \rho_1 \sigma_m \|\tilde{W}\| \|d_{xM}\| \|\tilde{x}_2\| \tag{7.32}$$

$$tr(\tilde{W}^\top \rho_2 \|\tilde{x}_2\| \hat{W}) \leq (W_M \|\tilde{W}\| - \|\tilde{W}\|^2) \rho_2 \|\tilde{x}_2\| \tag{7.33}$$

where σ_m is a bound of σ, i.e., $\|\sigma^\top\| \leq \sigma_m$.

According to (7.32) and (7.33), (7.31) can be further written as

$$\begin{aligned}
\dot{V}_s &\leq -\frac{1}{2}\lambda_{\min}(Q)\|\tilde{x}_2\|^2 + k_\xi \|\Gamma_1\| \|\tilde{x}_2\|^2 \\
&\quad + \|\tilde{x}_2\| \|\Gamma_1\| \|\tilde{W}\| \sigma_m + \|\tilde{x}_2\| \|\Gamma_1\| \bar{\epsilon}_2 - \rho_2 \|\tilde{x}_2\| \|\tilde{W}\|^2 \\
&\quad + \rho_1 \sigma_m \|\tilde{W}\| \|d_{xM}\| \|\tilde{x}_2\| + W_M \|\tilde{W}\| \|\tilde{x}_2\| \rho_2 \\
&= -\gamma \|\tilde{x}_2\|^2 - \beta_1 \|\tilde{x}_2\| \|\tilde{W}\|^2 + \beta_2 \|\tilde{x}_2\| \|\tilde{W}\| + \beta_3 \|\tilde{x}_2\| \\
&\leq -\gamma \|\tilde{x}_2\|^2 - \beta_1 \|\tilde{x}_2\| (\|\tilde{W}\| - \frac{\beta_2}{2\beta_1})^2 + (\frac{\beta_2^2}{4\beta_1} + \beta_3) \|\tilde{x}_2\| \\
&\leq -\gamma \|\tilde{x}_2\|^2 + (\frac{\beta_2^2}{4\beta_1} + \beta_3) \|\tilde{x}_2\|
\end{aligned} \tag{7.34}$$

where

$$\gamma = \frac{1}{2}\lambda_{\min}(Q) - k_\xi \|\Gamma_1\| \tag{7.35}$$

$$\beta_1 = \rho_2 \tag{7.36}$$

$$\beta_2 = \sigma_m(\|\Gamma_1\| + \rho_1 \|d_{xM}\|) + \rho_2 W_M \tag{7.37}$$

$$\beta_3 = \|\Gamma_1\| \bar{\epsilon}_2 \tag{7.38}$$

where d_{xM} is bounded due to the stability of matrix A.

Thus, from (7.34), we can see that when

$$\|\tilde{x}_2\| > \frac{\beta_2^2 + 4\beta_1\beta_3}{4\beta_1\gamma} = b_1 \tag{7.39}$$

$\dot{V}_s < 0$, which means $\dot{V}_s$ is negative outside the ball with radius b_1 described as $\chi = \{\tilde{x}_2 | \|\tilde{x}_2\| \leq b_1\}$. When $\tilde{x}_2$ increases outside of the ball χ, the negative of $\dot{V}_s$ results in reducing V_s and $\tilde{x}_2$, which shows the boundedness of $\tilde{x}_2$.

Then, we consider the boundedness of $\tilde{W}$, which can be written as

$$\dot{\tilde{W}} = -\rho_2 \|\tilde{x}_2\| \tilde{W} + \rho_2 \|\tilde{x}_2\| W^* + \rho_1 d_{xM}^\top \tilde{x}_2 \sigma^\top. \tag{7.40}$$

The second and third terms on the right side of (7.40) are bounded, since $\tilde{x}_2$, σ, and W^* are all bounded, and d_{xM} is bounded, because A is a stable matrix. (7.40) can be considered as a linear system with bounded input. Therefore, (7.40) is stable, since ρ_2 is positive and input is bounded. Consequently, the boundedness of $\tilde{W}$ is guaranteed. The boundedness of $\tilde{W}$ implies the boundedness of $\hat{W}$.

From (7.24), d_{xV} is also bounded since $\sigma_i^2(\cdot)$ is a bounded function, and A is a stable matrix. The dynamic equation of $\tilde{V}$ can be written as

$$\dot{\tilde{V}} = -\rho_4\|\tilde{x}_2\|\tilde{V} + \rho_3 d_{xV}^{\top}\tilde{x}_2\bar{x}^{\top} + \rho_4\|\tilde{x}_2\|V^* \tag{7.41}$$

where the second and third terms on the right side of 7.41 are both finite, because $\tilde{x}_2$, $\hat{W}$, σ, d_{xV} are all bounded, and ρ_3 and ρ_4 are both finite positive numbers. Therefore, the boundedness of $\tilde{V}$ is ensured. ∎

Before a fault occurs, no matter what the magnitude of uncertainty is, if $\eta(t)$ can be precisely estimated by the neural network model $M_1(t)$, $\|\epsilon_2\|$ would approach zero, which means the residual $\tilde{x}_2$ will converge to a very small bound, prior to the occurrence of a fault.

7.3.4 Robustness Analysis

As we design model-based fault detection strategies, we expect the generated residual would be as small as possible prior to any fault, so it could be more sensitive to the occurrence of faults. In addition, we also expect the robustness property of the fault detection schemes is not affected.

The dynamics of $\tilde{x}_2$ prior to the occurrence of any fault is described as

$$\dot{\tilde{x}}_2 = A\tilde{x}_2 + \xi(y, x_{2D}) - \xi(y, \hat{x}_2) + \eta - \hat{M}_1, \qquad \tilde{x}_2(0) = 0. \tag{7.42}$$

The initial condition $\tilde{x}_2(0) = 0$ is guaranteed when the derivatives of y can be exactly obtained by HOSMDs.

During the time interval $[0, t_e)$, where $0 < t_e < T$, (T is the beginning time of any

fault), we get $\tilde{x}_2$ by solving the differential equation (7.42)

$$\begin{aligned}\tilde{x}_2 &= \int_0^{t_e} e^{A(t_e-\tau)}(\xi(y,x_{2D}) - \xi(y,\hat{x}_2))d\tau \\ &\quad + \int_0^{t_e} e^{A(t_e-\tau)}(\eta(\tau) - \hat{M}_1(\tau))d\tau \end{aligned} \tag{7.43}$$

Taking the norm on both sides of (7.43), we have the following inequality

$$\begin{aligned}\|\tilde{x}_2\| &\leq \int_0^{t_e} \|e^{A(t_e-\tau)}\| \left\|\xi(y,x_{2D}) - \xi(y,\hat{x}_2)\right\| d\tau \\ &\quad + \int_0^{t_e} \|e^{A(t_e-\tau)}\| \left\|\eta(\tau) - \hat{M}_1(\tau)\right\| d\tau \\ &\leq \int_0^{t_e} k_\xi \|e^{A(t_e-\tau)}\| \|\tilde{x}_2\| d\tau + \int_0^{t_e} \|e^{A(t_e-\tau)}\| \|\epsilon_2\| d\tau. \end{aligned} \tag{7.44}$$

Using Gronwall's Lemma, we have

$$\begin{aligned}\|\tilde{x}_2\| &\leq \left(\int_0^{t_e} \|e^{A(t_e-\tau)}\| \|\epsilon_2\| d\tau\right) \exp\left(\int_0^{t_e} k_\xi \|e^{A(t_e-\tau)}\| d\tau\right) \\ &< \left(\bar{\epsilon}_2 \int_0^{\infty} \|e^{A\tau}\| d\tau\right) \exp\left(k_\xi \int_0^{\infty} \|e^{A\tau}\| d\tau\right) \\ &= \bar{\epsilon}_2 \lambda_x \exp(k_\xi \lambda_x) = \epsilon_3 \end{aligned} \tag{7.45}$$

where $\bar{\epsilon}_2$ is defined as $\max_{t\in[0,T]}\{\|\epsilon_2(t)\|\}$, and λ_x is

$$\lambda_x = \int_0^{\infty} \|e^{At}\| dt \tag{7.46}$$

which is bounded according to Assumption 7.4.

From (7.45), as long as the uncertainty observer does not reach its bound η_0 due to the occurrence of a fault, $\tilde{x}_2$ would stay within a bound ϵ_3. The magnitude of this bound depends on the estimation accuracy of the uncertainty. If $\hat{M}_1(t)$ can exactly characterize the uncertainty $\eta(t)$, $\|\tilde{x}_2\|$ will approach zero ultimately. This conclusion is consistent with that in Section 7.3.3.

7.3.5 Fault Sensitivity Analysis

In addition to robustness, another important property of a fault diagnosis scheme is its sensitivity to faults.

The following theorem characterizes the set of additive actuator faults that can be detected by the proposed fault diagnosis scheme.

Theorem 7.2 *Consider the proposed fault diagnosis scheme using high order sliding mode differentiators and uncertainty observers. If a time $t_x > 0$ exists such that the actuator fault u_f^i satisfies the condition*

$$\int_{T_x}^{T_x+t_x} \left\| e^{A(T_x+t_x-\tau)} \sum_{i=1}^{m} B_i u_f^i(\tau) \right\| d\tau \;>\; 2\bar{\epsilon}_2 \lambda_x \tag{7.47}$$

then the fault will be detected, i.e., $\|\tilde{x}_2\| > \epsilon_3$.

Proof: During the time interval between the occurrence of a fault and the saturation of $\hat{M}_1(t)$, the dynamics of $\tilde{x}_2$ become

$$\dot{\tilde{x}}_2 \;=\; A\tilde{x}_2 + \xi(y, x_{2D}) - \xi(y, \hat{x}_2) + \sum_{i=1}^{m} B_i u_f^i + \eta - \hat{M}_1, \qquad \tilde{x}_2(0) = 0 \tag{7.48}$$

where B_i is the ith column of B, u_f^i is the additive fault in the ith actuator, and T_x is the beginning time of a fault.

For any $t_x > 0$, the solution of (7.48) is given by

$$\begin{aligned} \tilde{x}_2 \;=\; & \int_0^{T_x+t_x} e^{A(T_x+t_x-\tau)} (\xi(y, x_{2D}) - \xi(y, \hat{x}_2)) d\tau \\ & + \int_0^{T_x+t_x} e^{A(T_x+t_x-\tau)} (\eta - \hat{M}_1) d\tau \\ & + \int_{T_x}^{T_x+t_x} e^{A(T_x+t_x-\tau)} \sum_{i=1}^{m} B_i u_f^i(\tau) d\tau. \end{aligned} \tag{7.49}$$

Taking norm of (7.49) and using Gronwall's lemma, we have

$$\begin{aligned} \|\tilde{x}_2\| \;&<\; \left(\bar{\epsilon}_2 \lambda_x + \int_{T_x}^{T_x+t_x} \left\| e^{A(T_x+t_x-\tau)} \sum_{i=1}^{m} B_i u_f^i(\tau) \right\| d\tau \right) \exp(k_\xi \lambda_x) \\ &=\; \epsilon_3 + e^{k_\xi \lambda_x} \int_{T_x}^{T_x+t_x} \left\| e^{A(T_x+t_x-\tau)} \sum_{i=1}^{m} B_i u_f^i(\tau) \right\| d\tau. \end{aligned} \tag{7.50}$$

According to the triangular inequality, we obtain

$$\|\tilde{x}_2\| > e^{k_\xi \lambda_x} \int_{T_x}^{T_x+t_x} \left\| e^{A(T_x+t_x-\tau)} \sum_{i=1}^{m} B_i u_f^i(\tau) \right\| d\tau - \epsilon_3. \tag{7.51}$$

Therefore, when

$$\int_{T_x}^{T_x+t_x} \left\| e^{A(T_x+t_x-\tau)} \sum_{i=1}^{m} B_i u_f^i(\tau) \right\| d\tau > 2\bar{\epsilon}_2 \lambda_x \tag{7.52}$$

the following inequality is guaranteed:

$$\|\tilde{x}_2\| > \epsilon_3 \tag{7.53}$$

which indicates the fault is detected. ∎

From (7.52), the threshold for robust fault detection also depends on the bound of the approximation error ϵ_2. When $\hat{M}_1(t)$ can accurately estimate the uncertainty, the threshold becomes very small, and the detection of faults becomes easier.

7.4 Fault Reconstruction Using HOSMDs

Although fault detection is the primary task in fault diagnosis, in real applications, in order to counteract the effect of faults, we need to distinguish the faults according to their locations and even their magnitudes. In this section, we introduce two methods that can be used for fault isolation and estimation.

For the system (7.1)-(7.4), since the uncertainty and fault are coupled after the fault occurs, we can only estimate the combinational effect of the fault and uncertainty. For the nominal system of (7.1)-(7.4), the control value u can be calculated through the following way, if x_2 and $\dot{x}_2$ are available.

$$u = (B^\top B)^{-1} B^\top (\dot{x}_2 - f(x_1, x_2)) \tag{7.54}$$

where x_2 and $\dot{x}_2$ can be obtained by using y, $\dot{y}$, and $\ddot{y}$, which are computed via the high order sliding mode differentiators. Consequently, the reconstructed control signal is

$$\hat{u} = (B^\top B)^{-1} B^\top (\dot{x}_{2D} - f(x_1, x_{2D})) \tag{7.55}$$

where $\dot{x}_{2D}$ is the derivative of x_{2D} using HOSMDs.

Denote the control signal in a healthy (normal) system as u^*, which is usually obtained through controller design. When the system is fault-free, $\hat{u} = u^*$. However, when an actuator fault is present, $\hat{u}$ deviates from u^*. Therefore, based on (7.55) and the normal control signals, we define the following signal to isolate and reconstruct fault:

$$r = \hat{u} - u^* \tag{7.56}$$

where $r = [r_1, \cdots, r_m]^\top$ is the residual vector.

In a noise free situation, $r_i \neq 0$, $(i = 1, \cdots, m)$ means the ith actuator is faulty. If the magnitude of the uncertainty and noise is small, the magnitude of r_i would still keep below a small threshold, δ_f, before the onset of any fault. If any one of the magnitudes of r_i, $(i = 1, \cdots, m)$ is above the threshold, we can specify the location and type of the fault.

The proposed fault diagnosis scheme using HOSMDs and uncertainty observers is implemented in the following algorithm:

- Step 1: Obtain bounds of system uncertainties, i.e., $\bar{\eta}_i$.
- Step 2: Obtain $\dot{y}_D$ from system output using HOSMDs (7.8).
- Step 3: Design an uncertainty observer based on (7.11) to (7.14).
- Step 4: Update $\hat{W}$ and $\hat{V}$ based on (7.15) and (7.16).
- Step 5: Generate residual $\|\tilde{x}_2\|$.
- Step 6: Compare $\|\tilde{x}_2\|$ with a threshold ϵ_3 to detect fault.
- Step 7: Calculate control signal u^* for the healthy system.
- Step 8: Reconstruct control signal $\hat{u}$ based on (7.55).
- Step 9: Reconstruct fault signal r based on (7.56).
- Step 10: Compare r_i with δ_f to isolate fault.
- Step 11: Use r_i to estimate fault.

7.5 Application to a Satellite Attitude Control System

In this section, we apply the proposed fault detection, isolation, and estimation method to a satellite attitude control system. Consider a satellite flying in a circular orbit in an inverse square gravitational field. We assume that the attitude of the satellite has no effect on the orbit. The motion dynamics of the satellite about its center of the mass is given in [110] as

$$I\dot{\omega} + \tilde{\omega}I\omega = 3\omega_0^2\tilde{\xi}_c I\xi_c + u + T_d \tag{7.57}$$

where $\omega = [\omega_1, \omega_2, \omega_3]^\top$ is the angular velocity vector of the satellite, $I = diag\{I_1, I_2, I_3\}$ is the principal axis moments of inertia of the satellite, $u = [u_1, u_2, u_3]^\top$ is the control torque vector, $T_d = [T_{d1}, T_{d2}, T_{d3}]^\top$ is the disturbance torque vector, and the vector ξ_c is defined as

$$\xi_c = \begin{bmatrix} -\sin\theta_1 \cos\theta_2 \\ \cos\theta_1 \sin\theta_3 + \sin\theta_1 \sin\theta_2 \cos\theta_3 \\ \cos\theta_1 \cos\theta_3 - \sin\theta_1 \sin\theta_2 \sin\theta_3 \end{bmatrix} \tag{7.58}$$

where θ_1, θ_2, θ_3 are the pitch, yaw, and roll angles, respectively.

The notation $\tilde{\omega}$ stands for the skew symmetric form of the vector ω, i.e.,

$$\tilde{\omega} = \begin{bmatrix} 0 & -\omega_3 & \omega_2 \\ \omega_3 & 0 & -\omega_1 \\ -\omega_2 & \omega_1 & 0 \end{bmatrix}. \tag{7.59}$$

The relationship between the angular velocity and the measurable Euler angles is formulated as

$$\begin{aligned} \omega_1 &= (\omega_0 + \dot{\theta}_1)\sin\theta_2 + \dot{\theta}_3 \\ \omega_2 &= (\omega_0 + \dot{\theta}_1)\cos\theta_2 \cos\theta_3 + \dot{\theta}_2 \sin\theta_3 \\ \omega_3 &= -(\omega_0 + \dot{\theta}_1)\cos\theta_2 \sin\theta_3 + \dot{\theta}_2 \cos\theta_3 \end{aligned} \tag{7.60}$$

where ω_0 is a constant used to denote the orbital angular velocity of the satellite.

The system state variables are chosen as $x = [\theta^\top, \omega^\top]^\top$. The dynamics of the satellite is described as

$$\dot{x} = \begin{bmatrix} R^{-1}(\theta)(\omega - \omega_c(\theta)) \\ I^{-1}(-\tilde{\omega} I\omega + 3\omega_0^2 \tilde{\xi}_c I \xi_c) \end{bmatrix} + \begin{bmatrix} 0 \\ I^{-1} \end{bmatrix} u + \begin{bmatrix} 0 \\ I^{-1} \end{bmatrix} T_d \tag{7.61}$$

where

$$\begin{aligned} R(\theta) &= \begin{bmatrix} \sin\theta_2 & 0 & 1 \\ \cos\theta_2 \cos\theta_3 & \sin\theta_3 & 0 \\ -\cos\theta_2 \sin\theta_3 & \cos\theta_3 & 0 \end{bmatrix} \\ \omega_c(\theta) &= \begin{bmatrix} \omega_0 \sin\theta_2 \\ \omega_0 \cos\theta_2 \cos\theta_3 \\ -\omega_0 \cos\theta_2 \sin\theta_3 \end{bmatrix}. \end{aligned} \tag{7.62}$$

The parameters of this satellite are given in Chapter 2. Since our research focuses on the fault diagnosis in actuators, we directly use the controller design method in [110]. In order to make the system output smooth enough that its derivatives can be accurately obtained through HOSMDs, we replace the discontinuous term *sign* in the controller by its continuous approximation as

$$sign(x) \approx \frac{x}{|x| + \delta} \tag{7.63}$$

where δ is a small positive number.

In the simulation, we assume that a fault occurs in the third actuator at the $10th$ second; i.e.,

$$f_a^{(3)}(t) = -5\beta(t - 10)(1 - e^{\frac{-(t-10)}{0.15}}) \tag{7.64}$$

where $\beta(t)$ is still a time profile function defined in Chapter 3.2. The control torque is disturbed by $\varsigma_u = 1\% * rand$; i.e., $T_d = \varsigma_u u$, while the Euler angles have measurement noise with $\varsigma_y = 0.5\% * rand$; i.e., $\theta_{measure} = (1 + \varsigma_y)\theta$, where $rand$ is a Gaussian white noise.

The uncertainty observer is assumed not to be activated until the $7.5th$ second. The reason for this assumption is that we expect that the derivatives of the system

output can be exactly attained via HOSMDs before we start to estimate the uncertainties. Otherwise, when $x_{2D} \neq x_2$, the calculated estimation error $\tilde{x}_{2D}$ is probably not equal to the real $\tilde{x}_2$. The assumption that any fault is present after the activation of the uncertainty observers guarantees no false alarm occurs prior to the start of the uncertainty observer.

The sampling time of the simulation is set to 5×10^{-4}. The four coefficients $\lambda_0 \sim \lambda_3$ in the third order sliding mode differentiator are all set to be 40. In the parameter update algorithm, $\rho_1 = \rho_3 = 15$, and $\rho_2 = \rho_4 = 0.08$. The neural network is pre-trained before being used, in order to achieve a good performance in the estimation of the uncertainty.

The simulation results are illustrated from Figure 7.1 to Figure 7.5. Figure 7.1 shows the unmeasurable states ω_1, ω_2, ω_3 and their estimations using third order sliding mode differentiators and (7.60). The estimated states ω_1 to ω_3 can approximate the real states in a very short time, if the third order sliding mode differentiators work well.

Figure 7.2 demonstrates the difference between the real unmeasurable states and the calculated states in the presence of an actuator fault. It can be seen that prior to the occurrence of any fault, the state estimation error decreases as the exact derivative of the system output is obtained. When an actuator fault occurs, $\|\tilde{x}_2\|$ will be quickly above a threshold, e.g., 0.5, which indicates the onset of the fault. Moreover, under the performance of the uncertainty observer, the state estimation error is almost reduced to zero between the activating time of the uncertainty observer and the beginning time of the fault. This result shows the sensitivity of the fault diagnosis scheme increases by using the uncertainty observer.

Figure 7.3 portrays the characteristics of the uncertainties in the system dynamics and their estimation using the neural networks model we discussed in Section 7.3. The bound of $\hat{M}_1(t)$ is set to $\eta_0 = 2 \times 10^{-3}$. From Figure 7.3, $\hat{M}_1(t)$ can basically estimate the uncertainties during the period [7.5, 10] seconds. The uncertainty estimation error is due to the introduction of measurement noises into the high order sliding mode differentiators. After the onset of the fault, at least one uncertainty estimator becomes saturated. This phenomenon also signals the presence of the fault.

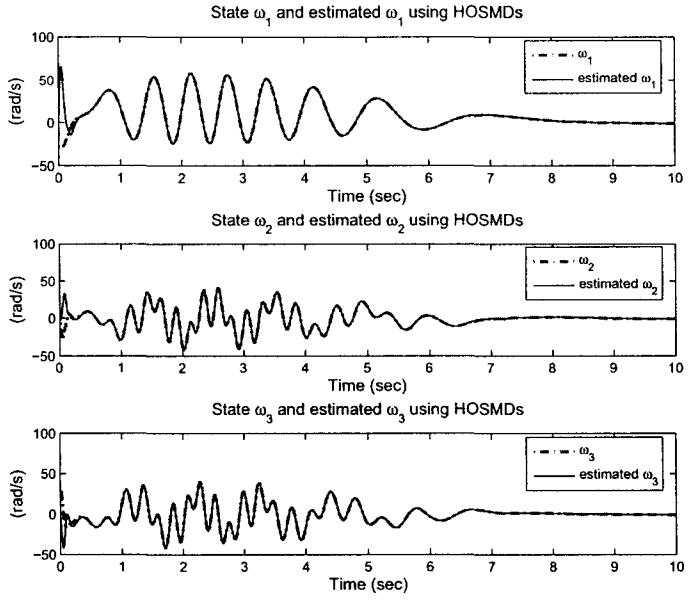

Figure 7.1: Unmeasurable states and their estimations using high order sliding mode differentiators

Figure 7.4 and 7.5 exhibit the fault isolation and reconstruction results using the third order sliding mode differentiators. When neither uncertainty nor noise is present, the fault reconstruction signal can precisely characterize the fault. A small threshold of 0.05 is successful enough to be used in the fault isolation. In addition, for the system with small-magnitude of uncertainties and measurement noises, the fault reconstruction signal can still specify the fault with certain accuracy. However, in this case, the threshold for a correct fault isolation needs to be updated to 0.5 or above. The mismatch between the reconstructed fault and the actual fault is also due to the introduction of measurement noise into HOSMDs. This issue has been discussed in Chapter 4 and some suggestive remarks are given in [87].

7.6 Conclusions

In this chapter, a fault diagnosis scheme using high order sliding mode differentiators and uncertainty observers was studied for a class of nonlinear systems. In the proposed

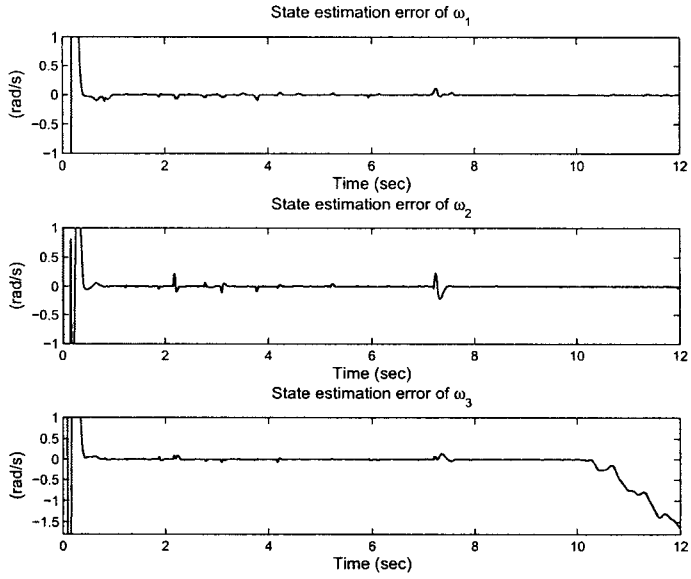

Figure 7.2: Calculated state estimation error in the presence of a fault in the third actuator

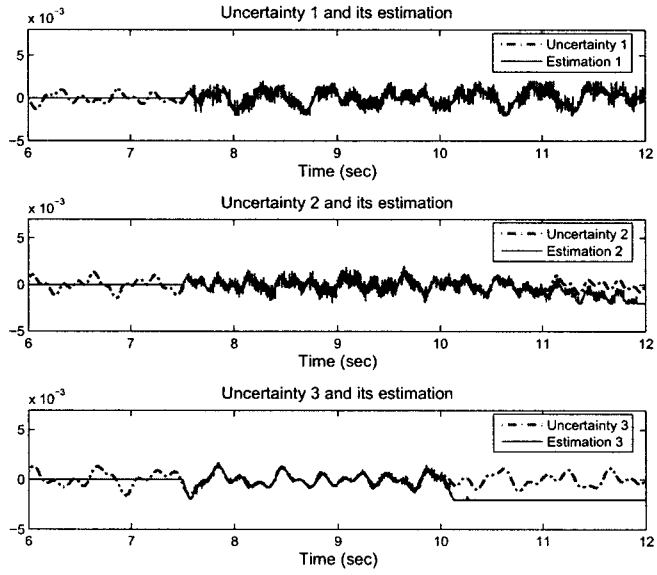

Figure 7.3: Uncertainties and their estimation using neural networks in the presence of a fault and measurement noise

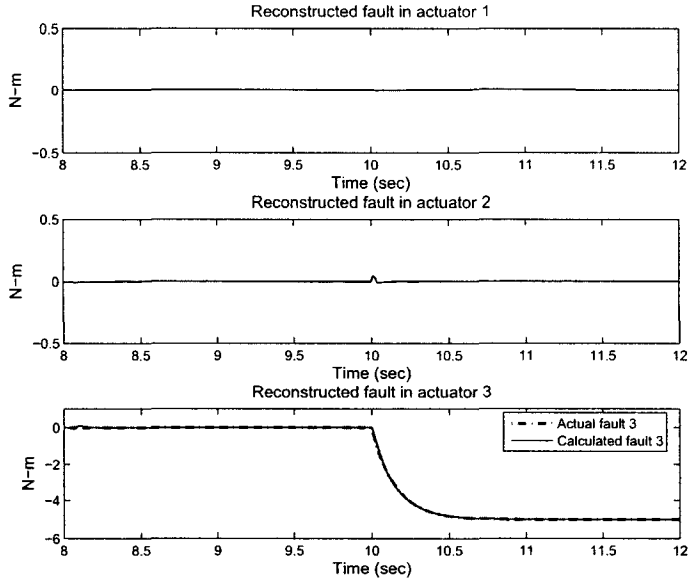

Figure 7.4: Reconstructed fault and actual fault in uncertainty-free case

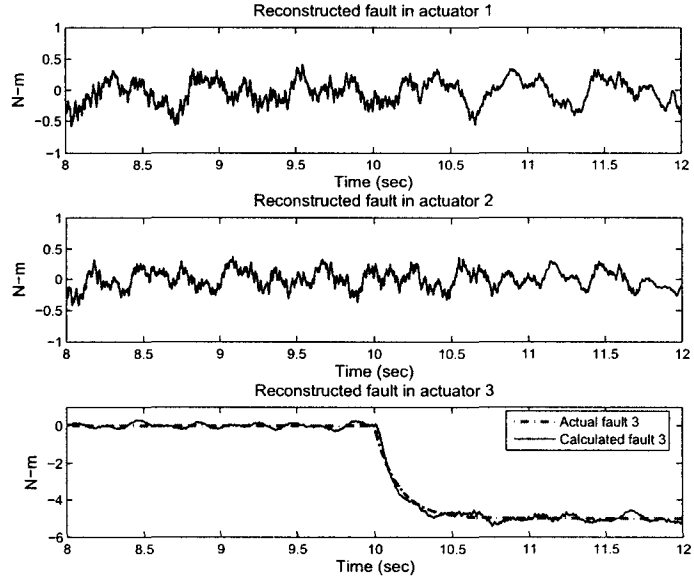

Figure 7.5: Calculated fault and actual fault in the presence of uncertainty and measurement noise

fault diagnosis algorithm, the system uncertainty was first estimated using a neural networks model. Then, the estimation of the uncertainty was used in the generation of a diagnostic residual. As a result, the magnitude of the diagnostic residual prior to the occurrence of any fault was reduced, and, correspondingly, the sensitivity of the fault diagnosis scheme increases. Moreover, fault reconstruction was achieved by using the high order sliding mode differentiators. The reconstructed signal makes the fault isolation and estimation straightforward. The analytical properties of the proposed fault diagnosis scheme were then rigorously proved. After that, an example that applies the proposed fault diagnosis scheme to a satellite attitude control system was given, and the simulation results demonstrated the effectiveness of this fault diagnosis strategy.

Since high order sliding mode differentiators are used to provide exact derivatives of the output, the performance of this fault diagnosis scheme is still affected by the measurement noise and the sampling interval in discrete time implementation. Therefore, methods to guarantee the real-time computational requirement need to be carefully considered in practical applications.

Another important issue to be further investigated is how to select a suitable upper bound for the uncertainty observer. Although a larger upper bound may be more tolerant to the approximation error, it also reduces the sensitivity to faults. In comparison, a small bound, though more sensitive to faults, will probably cause false alarms in fault detection.

Chapter 8

Conclusions and Future Work

In this Chapter, the whole thesis is summarized and then some topics are pointed out for further investigation.

8.1 Conclusions

In this thesis, fault detection, isolation, and estimation problems were studied in a systematic way for several classes of nonlinear systems. In order to deal with the uncertainties encountered in these systems, sliding mode observers, high order sliding mode observers/differentiators, and various learning approaches were used to design different robust fault diagnosis schemes. In addition, the applications of the proposed fault diagnosis schemes to a series of satellite control systems were carried out in this thesis. The contributions of this thesis are the subjects of several publications [139], [162], [156], [158], [165], [166], [167], [149]. The key features are summarized as follows.

- Since satellites belong to a class of safety-critical systems, the health monitoring and fault diagnosis for satellite control systems become very important and have been investigated in this thesis. According to the generations and operations of different satellites, several typical satellite control systems were considered in

this thesis: satellite attitude control systems, large angle satellite attitude control systems, flexible satellite control systems, satellite orbital control systems, and multiple satellite formation flying systems. Although different satellite systems have distinct characteristics and work on different missions, their dynamics can be classified based on their mathematical descriptions. The satellite control systems belong to mechatronic systems, which are usually formulated by second order ordinary differential equations. Using state space forms, the mathematical models of the satellite control systems mentioned above can be divided into two classes. The first class of dynamic systems have triangular input forms, where the unmeasurable state is directly the derivative of the system output. In the second class of systems, the unmeasurable state can be written as nonlinear functions of the system output and its derivatives. Therefore, in this thesis, the proposed fault diagnosis schemes are mainly designed for these two classes of systems and applied to the satellite control systems mentioned above.

- Inspired by previous iterative learning observer-based fault diagnosis approaches, a bank of PI-type repetitive learning observers were designed for a class of nonlinear Lipschitz systems. The generalized observer structure was chosen for each observer so that only the coefficients which determine the learning rate have to be selected. The simple architecture of this class of fault diagnosis scheme makes it feasible in real applications.

- One important contribution of this thesis is, for a class of uncertain nonlinear systems, which have triangular input forms, a framework of robust fault diagnosis schemes using sliding mode and learning approaches was proposed to achieve fault detection, isolation, and estimation. Unlike some fault diagnosis strategies using sliding mode observers, where the system uncertainties and faults are both treated as unknown inputs and the fault signal is reconstructed through processing the equivalent output injection signal, the proposed fault diagnosis schemes distinguish the system uncertainties from the faults by using time-varying sliding mode switching gains. An iterative learning algorithm and an iterative fuzzy model were used to design the sliding mode switching gains, respectively. As

a result, the sliding mode switching gain is large at the beginning regulation phase to accelerate the state estimation process, and then it decreases in the fault estimation phase to guarantee that other online estimators only specify the faults.

- Moreover, besides the classic sliding mode observers, second order sliding mode observers were also used to eliminate the effect of system uncertainties. The second order sliding mode not only preserves features such as robustness to system uncertainties, and finite-time convergence in state estimation, but it also reduces or even removes the chattering. In addition, the high order sliding mode approaches offer an efficient way to deal systems with a relative degree greater than one.

- In the above framework of fault diagnosis schemes, three classes of online estimators were used to characterize the faults. The first class is the neural networks based estimators, which can successfully estimate the faults due to the powerful approximation ability of the neural networks. The second class of diagnostic estimators are wavelet networks, which may achieve the same approximation capability as neural networks with a reduced-size network architecture. The third class of fault estimators were based on iterative learning algorithms, where the parameters of the estimators are iteratively updated in order to reduce the overshoot and transient process in the estimation of fault functions.

- For a class of satellite attitude control systems, although their mathematical descriptions do not satisfy triangular input forms, the unmeasurable state can be represented by nonlinear functions of the output and its derivatives. Towards this class of nonlinear systems, high order sliding mode differentiators were used to calculate the derivatives of the system output and then the unmeasurable state was obtained according to the system dynamic equations and calculated derivatives. The zero initialization of the estimation error dynamics helps to achieve satisfactory estimation of the faults. In this circumstance, neural adaptive estimators and iterative neuron PID estimators are used to estimate

the faults, respectively. The neural adaptive estimators have a simple structure and only the numbers of previous inputs and outputs need to be determined. Additionally, the proposed iterative neuron PID estimators integrate the advantages of the neural networks and the iterative learning algorithms, where the convergence rate is accelerated and the overshoot and transient process are reduced or even eliminated in the fault estimation.

- In order to extend the robust fault diagnosis schemes to more general nonlinear systems, a fault diagnosis strategy using learning and sliding mode approaches was designed for the nonlinear systems which can be represented by TS fuzzy models. A TS fuzzy observer was designed to estimate all the states by solving a group of linear matrix inequalities. Neural networks based estimators were then integrated with the TS fuzzy models to build a fuzzy-neural observer, which is used to detect, isolate, and estimate possible faults. Although a stable parameter update law is used to guarantee the stability of the proposed fault diagnosis scheme, uncertainties and approximation errors still affect the accuracy of the fault estimation. Therefore, the sliding mode term is then synthesized with the fuzzy-neural observer to establish a fuzzy-neural sliding mode observer, which is robust to the uncertainties and approximation errors, and is able to estimate the fault with better performance.

- Unlike most existing robust fault diagnosis schemes which only use the bound information of the uncertainties, a novel fault diagnostic observer was designed to generate residual. In the proposed fault diagnosis scheme, high order sliding mode differentiators were used to estimate the unmeasurable state, and then the system uncertainty was characterized in an explicit way by using neural networks based learning approaches, so that the information of the system uncertainty can be directly used in the residual generation. If the uncertainty estimation is successfully achieved, the diagnostic residual is not affected by the system uncertainties, and the fault detection becomes easier.

In summary, the research in this thesis demonstrates that the proposed fault diagnosis schemes using sliding mode and learning techniques are effective in dealing

with fault detection, isolation, and estimation for several classes of satellite control systems. The versatile sliding mode and learning approaches provide multiple choices for real applications.

8.2 Future Work

The proposed fault diagnosis schemes in this thesis are all model-based, more specifically, observer-based approaches. Therefore, their performance, to some extent, depends on the accuracy of the mathematical models of the systems under study, although certain robust techniques are used. Moreover, since many other types of challenging system complexities need to be dealt with, the area of fault diagnosis for nonlinear systems still attracts many researchers. Some possible future studies are listed as follows.

- In most cases of this thesis, only the actuator faults and additive component faults were considered. However, in more realistic cases, the faults are possibly represented by multiplicative faults, which are coupled with the system dynamics. To deal with the multiplicative faults, more robust approaches are necessary, and the structure of the systems need to be deeply investigated. Moreover, an implicit assumption of this thesis is that the output measurement is accurate and no fault occurs in the sensors. However, sensor faults, such as scalings errors, dead zone, and parameter drift possibly exist in real systems. Therefore, sensor fault diagnosis for various nonlinear systems should be carefully studied in the future work.

- In this thesis, only the fault detection, isolation, and estimation problems were studied. However, successful fault diagnosis is not the ultimate goal in many real applications. The systems should have some fault accommodation strategies to deal with the effect of faults. An analytical solution is to design fault tolerant controllers through system or controller reconfiguration. The passive fault tolerant control can be classified into robust control, and the active fault tolerant controller design needs specific information about the faults. Therefore,

correct fault isolation and accurate fault estimation can be very helpful in the design of fault accommodation strategies.

- Additionally, neural networks, fuzzy logic/models, and wavelet networks were used in this thesis, where only their partial characteristics have been used in the fault diagnosis schemes. This situation is partly because the designed fault diagnosis schemes are quantitative model-based. If the model-based FD methods are integrated with other types of techniques, for example, the memory, association, and prediction features of neural networks, the reasoning and decision capabilities of fuzzy models, and the signal processing abilities of wavelet networks and so on, then the quantitative model-based, the qualitative model based, and even the process history based fault diagnosis methods can be synthesized in a systematic way. We can predict that the reliability and effectiveness of the innovative fault diagnosis methods will significantly increase and they can deal with more complicated systems.

Bibliography

[1] R. Clark, "Instrument fault detection," *IEEE Transactions on Aerospace and Electronic Systems*, vol. 14, pp. 456–465, 1978.

[2] R. Patton, P. Frank, and R. Clark, *Fault Diagnosis in Dynamic Systems: Theory and Applications.* Prentice-Hall: Englewood Cliffs, New Jersey, 1989.

[3] J. Gertler, *Fault Detection and Diagnosis in Engineering Systems.* Marcel Dekker: New York, 1998.

[4] J. Chen and R. Patton, *Robust Model-Based Fault Diagnosis for Dynamic Systems.* Kluwer Academic Publishers: Boston, 1999.

[5] P. Frank, R. Patton, and R. Clark, *Issues of Fault Diagnosis for Dynamic Systems.* Springer-Verlag: London, 2000.

[6] S. Simani, C. Fantuzzi, and R. Patton, *Model-based Fault Diagnosis in Dynamic Systems Using Identification Techniques.* Springer-Verlag: Berlin, 2003.

[7] P. Frank, "Fault diagnosis in dynamic systems using analytical and knowledge-based redundancy - a survey and some new result," *Automatica*, vol. 26, pp. 459–474, 1990.

[8] V. Venkatasubramanian, R. Rengaswamy, K. Yin, and S. Kavuri, "A review of process fault detection and diagnosis: part I: quantitative model-based methods," *Computers and Chemical Engineering*, vol. 27, pp. 293–311, 2003.

[9] V. Venkatasubramanian, R. Rengaswamy, K. Yin, and S. Kavuri, "A review of process fault detection and diagnosis: part II: qualitative models and search strategies," *Computers and Chemical Engineering*, vol. 27, pp. 313–326, 2003.

[10] V. Venkatasubramanian, R. Rengaswamy, K. Yin, and S. Kavuri, "A review of process fault detection and diagnosis: part III: process history based methods," *Computers and Chemical Engineering*, vol. 27, pp. 327–346, 2003.

[11] V. Kapila, A. Sparks, J. Buffington, and Q. Yan, "Spacecraft formation flying: Dynamics and control," in *Proceedings of the American Control Conference*, pp. 4137–4141, 1999.

[12] P. Wang and D. Yang, "PD-fuzzy formation control for spacecraft formation flying in elliptical orbits," *Aerospace Science and Technology*, vol. 7, pp. 561–566, 2003.

[13] E. Tehrani, K. Khorasani, and S. Tafazoli, "Dynamic neural network-based estimator for fault diagnosis in reaction wheel actuator of satellite attitude control system," in *Proceedings of International Joint Conference on Neural Networks*, pp. 2347–2352, 2005.

[14] N. Tudoroiu and K. Khorasani, "Satellite fault diagnosis using a bank of interacting kalman filters," *IEEE Transactions on Aerospace and Electronic Systems*, vol. 43, pp. 1334–1350, 2007.

[15] Z. Li, L. Ma, and K. Khorasani, "Fault diagnosis of an actuator in the attitude control subsystem of a satellite using neural networks," in *Proceedings of International Joint Conference on Neural Networks*, pp. 2658–2663, 2007.

[16] H. Azarnoush and K. Khorasani, "Fault detection in spacecraft attitude control system," in *Proceedings of International Conference on Systems, Man, and Cybernetics*, pp. 726–733, 2007.

[17] H. Talebi, R. Patel, and K. Khorasani, "Fault detection and isolation for uncertain nonlinear systems with application to a satellite reaction wheel actuator," in *Proceedings of International Conference on Systems, Man, and Cybernetics*, pp. 3140–3145, 2007.

[18] A. Barua and K. Khorasani, "Intelligent model-based hierarchical fault diagnosis for satellite formations," in *Proceedings of International Conference on Systems, Man, and Cybernetics*, pp. 3191–3196, 2007.

[19] N. Meskin and K. Khorasani, "Fault detection and isolation in a redundant reaction wheels configuration of a satellite," in *Proceedings of International Conference on Systems, Man, and Cybernetics*, pp. 3153–3158, 2007.

[20] T. Jiang and K. Khorasani, "A fault detection, isolation and reconstruction strategy for a satellites attitude control subsystem with redundant reaction wheels," in *Proceedings of International Conference on Systems, Man, and Cybernetics*, pp. 3146–3152, 2007.

[21] H. Talebi and K. Khorasani, "A robust fault detection and isolation scheme with application to magnetorquer type actuators for satellites," in *Proceedings of International Conference on Systems, Man, and Cybernetics*, pp. 3165–3170, 2007.

[22] H. Wang and S. Daley, "Actuator fault diagnosis: an adaptive observer-based technique," *IEEE Transactions on Automatic Control*, vol. 41, pp. 1073–1078, 1996.

[23] H. Wang, Z. Huang, and S. Daley, "On the use of adaptive rules for actuator and sensor fault diagnosis," *Automatica*, vol. 33, pp. 217–225, 1997.

[24] B. Jiang and M. Staroswiecki, "Adaptive observer design for robust fault estimation," *International Journal of Systems Science*, vol. 33, pp. 767–775, 2002.

[25] A. Xu and Q. Zhang, "Nonlinear system fault diagnosis based on adaptive estimation," *Automatica*, vol. 40, pp. 1181–1193, 2004.

[26] W. Chen and M. Saif, "Adaptive actuator fault detection, isolation and accommodation in uncertain systems," *International Journal of Control*, vol. 80, pp. 45–63, 2007.

[27] M. Polycarpou, "Stable learning scheme for failure detection and accommodation," in *Proceedings of IEEE International Symposium on Intelligent Control*, pp. 315–320, 1994.

[28] M. Polycarpou and A. Helmicki, "Automated fault detection and accommodation: a learning systems approach," *IEEE Transactions on System, Man, and Cybernetics*, vol. 25, pp. 1447–1458, 1995.

[29] A. Vemuri and M. Polycarpou, "Robust nonlinear fault diagnosis in input-output systems," *International Journal of Control*, vol. 68, pp. 343–360, 1997.

[30] M. Demetriou and M. Polycarpou, "Incipient fault diagnosis of dynamical systems using online approximators," *IEEE Transactions on Automatic Control*, vol. 43, pp. 1612–1617, 1998.

[31] A. Trunov and M. Polycarpou, "Automated fault diagnosis in nonlinear multivariable systems using a learning methodology," *IEEE Transactions on Neural Networks*, vol. 11, pp. 91–101, 2000.

[32] M. Polycarpou and A. Trunov, "Learning approach to nonlinear fault diagnosis: detectability analysis," *IEEE Transactions on Automatic Control*, vol. 45, pp. 806–812, 2000.

[33] X. Zhang, M. Polycarpou, and T. Parisini, "A robust detection and isolation scheme for abrupt and incipient faults in nonlinear systems," *IEEE Transactions on Automatic Control*, vol. 47, pp. 576–593, 2002.

[34] S. Naidu, E. Zafirou, and T. Mcavoy, "Use of neural networks for failure detection in a control system," *IEEE Control Systems Magazine*, vol. 10, pp. 49–55, 1990.

[35] A. Bernieri, M. D'Apuzzo, L. Sansone, and M. Savastano, "A neural network approach for identification and fault diagnosis on dynamic systems," *IEEE Transactions on Instrumentation and Measurements*, vol. 43, pp. 867–873, 1994.

[36] T. Marcu and L. Mirea, "Robust detection and isolation of process faults using neural networks," *IEEE Control Systems Magazine*, vol. 17, pp. 72–79, 1997.

[37] J. Theocharis and V. Petridis, "Neural network observer for induction motor control," *IEEE Control Systems Magazine*, vol. 14, pp. 26–37, 1994.

[38] Y. Kim, F. Lewis, and C. Abdallah, "A dynamic recurrent neural-network-based adaptive observer for a class of nonlinear systems," *Automatica*, vol. 33, pp. 1539–1543, 1997.

[39] D. Strobl, U. Lenz, and D. Schroder, "Systematic design of stable neural observers for a class of nonlinear systems," in *Proceedings of IEEE International Conference on Control Applications*, pp. 377–382, 1997.

[40] A. Alessandri, M. Baglietto, T. Parisini, and R. Zoppoli, "A neural state estimator with bounded errors for nonlinear systems," *IEEE Transactions on Automatic Control*, vol. 44, pp. 2028–2042, 1999.

[41] J. Choi and J. Farrell, "Adaptive observer for a class of nonlinear systems using neural networks," in *Proceedings of IEEE International Symposium on Intelligent Control*, pp. 114–119, 1999.

[42] T. Fretheim, R. Shoureshi, and T. Vincent, "A general approach to nonlinear output observer design using neural network models," in *Proceedings of the American Control Conference*, pp. 924–928, 2000.

[43] M. Ahmed and S. Riyaz, "Design of dynamic neural observers," *IEE Proceedings of Control Theory and Applications*, vol. 147, pp. 257–266, 2000.

[44] A. Delgado, M. Hou, and C. Kambhampati, "Neural observer by coordinate transformation," *IEE Proceedings of Control Theory and Applications*, vol. 152, pp. 698–706, 2005.

[45] P. Kabisatpathy, A. Barua, and S. Sinha, "Artificial neural network model based observers," *IEEE Circuits and Devices Magazine*, vol. 21, pp. 18–26, 2005.

[46] H. Zhang, C. Chan, K. Cheung, and H. Jin, "Sensor fault diagnosis for systems with unknown nonlinearity using neural network based nonlinear observers," in *UKACC International Conference on Control*, pp. 981–986, 1998.

[47] P. Kabore and H. Wang, "A B-spline neural network based actuator fault diagnosis in nonlinear systems," in *Proceedings of the American Control Conference*, pp. 1139–1144, 2001.

[48] A. Alessandri, "Fault diagnosis for nonlinear systems using a bank of neural estimators," *Computers in Industry*, vol. 52, pp. 271–289, 2003.

[49] W. Chen and M. Saif, "An iterative learning observer-based approach to fault detection and accommodation in nonlinear systems," in *Proceedings of the 40th IEEE Conference on Decision and Control*, pp. 4469–4474, 2001.

[50] W. Chen and M. Saif, "A robust iterative learning observer-based fault diagnosis of time delay nonlinear systems," in *Proceedings of the 15th Triennial World Congress of IFAC*, 2002.

[51] W. Chen and M. Saif, "Fault diagnosis and accommodation in nonlinear time-delay systems," in *Proceedings of the American Control Conference*, pp. 4255–4260, 2003.

[52] W. Chen, M. Saif, and B. Shafai, "Fault detection in a class of differential-algebraic systems," in *Proceedings of the American Control Conference*, pp. 4398–4402, 2004.

[53] W. Chen and M. Saif, "An iterative learning observer for fault detection and accommodation in nonlinear time-delay systems," *International Journal of Robust and Nonlinear Control*, vol. 16, pp. 1–19, 2006.

[54] Z. Bien and J. Xu, *Iterative Learning Control, Analysis, Design, Integration and Applications*. Kluwer Academic Publishers: Boston, 1998.

[55] Y. Chen and C. Wen, *Iterative Learning Control, Convergence, Robustness and Applications*. Springer-Verlag: London, 1999.

[56] C. Edwards, S. Spurgeon, and R. Patton, "Sliding mode observers for fault detection and isolation," *Automatica*, vol. 36, pp. 541–553, 2000.

[57] C. Tan and C. Edwards, "Sliding mode observers for detection and reconstruction of sensor faults," *Automatica*, vol. 38, pp. 1815–1821, 2002.

[58] C. P. Tan and C. Edwards, "Sliding mode observers for reconstruction of simultaneous actuator and sensor faults," in *Proceedings of the 42nd IEEE Conference on Decision and Control*, pp. 1455–1460, 2003.

[59] C. P. Tan and C. Edwards, "Multiplicative fault reconstruction using sliding mode observers," in *Proceedings of the 5th Asian Control Conference*, pp. 957–962, 2004.

[60] C. Edwards, "A comparison of sliding mode and unknown input observers for fault reconstruction," in *Proceedings of the 43rd IEEE Conference on Decision and Control*, pp. 5279–5284, 2004.

[61] X. Yan and C. Edwards, "Robust sliding mode observer-based actuator fault detection and isolation for a class of nonlinear systems," in *Proceedings of the 44th IEEE Conference on Decision and Control, and the European Control Conference*, pp. 987–992, 2005.

[62] H. Alwi and C. Edwards, "Robust sensor fault estimation for tolerant control of a civil aircraft using sliding modes," in *Proceedings of the American Control Conference*, pp. 5704–5709, 2006.

[63] X. Yan and C. Edwards, "Fault reconstruction/estimation using a sliding mode observer," in *Proceedings of the 45th IEEE Conference on Decision and Control*, pp. 5573–5578, 2006.

[64] R. Sreedhar, B. Fernandez, and G. Masada, "Robust fault detection in nonlinear systems using sliding mode observers," in *Proceedings of IEEE Conference on Control Application*, pp. 715–721, 1993.

[65] W. Chen, M. Saif, and Y. Soh, "A variable structure adaptive observer approach for actuator fault detection and diagnosis in uncertain nonlinear systems," in *Proceedings of the American Control Conference*, pp. 2674–2678, 2000.

[66] Y. Xiong and M. Saif, "Sliding mode observer for nonlinear uncertain systems," *IEEE Transactions on Automatic Control*, vol. 46, pp. 2012–2017, 2001.

[67] L. Li and D. Zhou, "Fast and robust fault diagnosis for a class of nonlinear systems: detectability analysis," *Computers and Chemical Engineering*, vol. 28, pp. 2635–2646, 2004.

[68] T. Yeu and S. Kawaji, "Sliding mode observer based fault detection and isolation in descriptor systems," in *Proceedings of the American Control Conference*, pp. 4543–4548, 2002.

[69] B. Jiang and F. Chowdhury, "Observer-based fault diagnosis for a class of nonlinear systems," in *Proceedings of the American Control Conference*, pp. 5671–5675, 2004.

[70] T. Floquet, J. Barbot, W. Perruquetti, and M. Djemai, "On the robust fault detection via a sliding mode disturbance observer," *International Journal of Control*, vol. 77, pp. 622–629, 2004.

[71] W. Chen and M. Saif, "Actuator fault isolation and estimation for uncertain nonlinear systems," in *Proceedings of the IEEE International Conference on Systems, man and Cybernetics*, pp. 2560–2565, 2005.

[72] W. Chen and M. Saif, "Application of sliding mode observers for actuator fault detection and isolation in linear systems," in *Proceedings of IEEE Conference on Control Applications*, pp. 1479–1484, 2005.

[73] T. Boukhobza and J. Barbot, "High order sliding modes observer," in *Proceedings of the 37th IEEE Conference on Decision and Control*, pp. 1912–1917, 1998.

[74] J. Davila, L. Fridman, and A. Levant, "Second-order sliding mode observer for mechanical systems," *IEEE Transactions on Automatic Control*, vol. 50, pp. 1785–1789, 2005.

[75] Y. Shtessel and A. Poznyak, "Parameter identification of affine time varying systems using traditional and high order sliding modes," in *Proceedings of the American Control Conference*, pp. 2433–2438, 2005.

[76] L. Fridman, A. Levant, and J. Davila, "High-order sliding mode observer for linear systems with unknown inputs," in *Proceedings of the International Workshop on Variable Structure Systems*, pp. 202–207, 2006.

[77] A. Benallegue, A. Mokhtari, and L. Fridman, "Feedback linearization and high order sliding mode observer for a quadrotor UAV," in *Proceedings of the International Workshop on Variable Structure Systems*, pp. 365–372, 2006.

[78] N. Msirdi, A. Rabhi, M. Ouiadsine, and L. Fridman, "First and high order sliding mode observers to estimate the contact forces," in *Proceedings of the International Workshop on Variable Structure Systems*, pp. 274–279, 2006.

[79] V. Lebastard, Y. Aoustin, F. Plestan, and L. Fridman, "Absolute orientation estimation based on high order sliding mode observer for a five link walking biped robot," in *Proceedings of the International Workshop on Variable Structure Systems*, pp. 373–378, 2006.

[80] N. Msirdi, A. Rabhi, L. Fridman, J. Davila, and Y. Delanne, "Second order sliding mode observer for estimation of velocities, wheel sleep, radius and stiffness," in *Proceedings of the American Control Conference*, pp. 3316–3321, 2006.

[81] J. Davila, L. Fridman, and A. Poznyak, "Observation and identification of mechanical systems via second order sliding modes," *International Journal of Control*, vol. 79, pp. 1251–1262, 2006.

[82] S. Baev, I. Shkolnikov, Y. Shtessel, and A. Poznyak, "Parameter identification of nonlinear system using traditional and high order sliding modes," in *Proceedings of the American Control Conference*, pp. 2634–2639, 2006.

[83] A. Levant, "Robust exact differentiation via sliding mode technique," *Automatica*, vol. 34, pp. 379–384, 1998.

[84] A. Levant, "High-order sliding modes, differentiation and output-feedback control," *International Journal of Control*, vol. 76, pp. 924–941, 2003.

[85] A. Levant, "Homogeneity approach to high order sliding mode design," *Automatica*, vol. 41, pp. 823–830, 2005.

[86] H. Saadaoui, I. Leon, M. Djemai, N. Manamanni, and J. Barbot, "High order sliding mode and adaptive observers for a class of switched systems with unknown parameters: a comparative study," in *Proceedings of the 45th IEEE Conference on Decision and Control*, pp. 5555–5560, 2006.

[87] C. Edwards, L. Fridman, and M.-W. Thein, "Fault reconstruction in a leader/follower spacecraft system using higher order sliding mode observers," in *Proceedings of the American Control Conference*, pp. 408–413, 2007.

[88] Q. Zhang and A. Benveniste, "Wavelet networks," *IEEE Transactions on Neural Networks*, vol. 3, pp. 889–898, 1992.

[89] J. Zhang, G. Walter, Y. Miao, and W. Lee, "Wavelet neural networks for function learning," *IEEE Transactions on Signal Processing*, vol. 43, pp. 1485–1497, 1995.

[90] X. Ma, Z. Sun, and Y. He, "Analysis and design of fuzzy controller and fuzzy observer," *IEEE Transactions on Fuzzy Systems*, vol. 6, pp. 41–51, 1998.

[91] A. Fayaz, "On the Sugeno-type fuzzy observers," in *Proceedings of the 38th IEEE Conference on Decision and Control*, pp. 4828–4833, 1999.

[92] R. Palm and D. Driankov, "Towards a systematic analysis of fuzzy observers," in *Proceedings of the 18th International Conference of the North American Fuzzy Information processing Society*, pp. 179–183, 1999.

[93] P. Bergsten and R. Palm, "Thau-Luengerger observers for TS fuzzy systems," in *Proceedings of the ninth IEEE International Conference on Fuzzy Systems*, pp. 671–676, 2000.

[94] P. Bergsten, R. Palm, and D. Driankov, "Fuzzy observers," in *Proceedings of the IEEE International Fuzzy Systems Conference*, pp. 700–703, 2001.

[95] K. Tanaka and H. Wang, *Fuzzy Control Systems Design and Analysis: A Linear Matrix Inequality Approach.* John Wiley and Sons Inc.: New York, 2001.

[96] P. Bergsten, R. Palm, and D. Drankov, "Observers for Takagi-Sugeno fuzzy systems," *IEEE Transactions on Systems, Man, and Cybernetics - Part B: Cybernetics*, vol. 32, pp. 114–121, 2002.

[97] C. Ting, "An adaptive fuzzy observer-based approach for chaotic synchronization," *International Journal of Approximate Reasoning*, vol. 35, pp. 97–114, 2005.

[98] K. Lian and J. Liou, "Output tracking control for fuzzy systems via output feedback design," *IEEE Transactions on Fuzzy Systems*, vol. 14, pp. 628–639, 2006.

[99] R. Isermann, "On fuzzy logic applications for automatic control, supervision, and fault diagnosis," *IEEE Transactions on Systems, Man, and Cybernetics - Part A: Systems and Humans*, vol. 28, pp. 221–235, 1998.

[100] H. Schneider and P. Frank, "Observer-based supervision and fault detection in robots using nonlinear and fuzzy logic residual evaluation," *IEEE Transactions on Control Systems Technology*, vol. 4, pp. 274–282, 1996.

[101] R. Patton, J. Chen, and C. Lopez-Toribio, "Fuzzy observers for nonlinear dynamic systems fault diagnosis," in *Proceedings of the 37th Conference on Decision and Control*, pp. 84–89, 1998.

[102] B. Castillo-Toledo and J. Anzurez-Marin, "Model-based fault diagnosis using sliding mode observers to Takagi-Sugeno fuzzy model," in *Proceedings of the IEEE International Symposium on Intelligent Control*, pp. 652–657, 2005.

[103] J. Anzurez-Martin and B. Castillo-Toledo, "The fault diagnosis problem: sliding mode fuzzy dedicated observers approach," in *Proceedings of IEEE International Conference on Fuzzy Systems*, pp. 1322–1328, 2006.

[104] F. J. Uppal, R. Patton, and M. Witczak, "A neuro-fuzzy multiple-model observer approach to robust fault diagnosis: based on the DAMADICS benchmark problem," *Control Engineering Practice*, vol. 14, pp. 699–717, 2006.

[105] J. Suykens, J. Vandewalle, and B. Moor, *Artificial Neural Networks for Modelling and Control of Nonlinear Systems.* Kluwer Academic Publishers: Netherlands.

[106] J. Suykens, J. Vandewalle, and B. D. Moor, "NL_q theory: checking and imposing stability of recurrent neural networks for nonlinear modeling," *IEEE Transactions on Signal Processing.*

[107] J. Zamarreno and P. Vega, "State space neural network properties and application," *Neural Networks*, vol. 11, pp. 1099–1112, 1998.

[108] J. Suykens, B. Moor, and J. Vandewalle, "Robust local stability of multilayer recurrent neural networks," *IEEE Transactions on Neural Networks*, vol. 11, pp. 222–229, 2000.

[109] V. Chobotov, *Spacecraft Attitude Dynamics and Control.* Krieger Publishing Company: Malabar, FL, 1991.

[110] S. Singh and A. Iyer, "Nonlinear decoupling sliding mode control and attitude control of spacecraft," *IEEE Transactions on Aerospace and Electronic Systems*, vol. 25, pp. 621–633, 1989.

[111] S. Drakunov, "Sliding mode observers based on equivalent control method," in *Proceedings of the 31st Conference on Decision and Control*, pp. 2368–2369, 1992.

[112] V. Utkin, *Sliding Modes in Control and Optimization.* Springer-Verlag: Heidelberg, Berlin, 1992.

[113] C. Edwards and S. Spurgeon, "On the development of discontinuous observers," *International Journal of Control*, vol. 59, pp. 1211–1229, 1994.

[114] S. Drakunov and V. Utkin, "Sliding mode observers. tutorial," in *Proceedings of the 34th Conference on Decision and Control*, pp. 3376–3378, 1995.

[115] J. Barbot, T. Boukhobza, and M. Djemai, "Sliding mode observer for triangular input form," in *Proceedings of the 35th Conference on Decision and Control*, pp. 1489–1490, 1996.

[116] I. Haskara, U. Ozguner, and V. Utkin, "On sliding mode observers via equivalent control approach," *International Journal of Control*, vol. 71, pp. 1051–1067, 1998.

[117] F. Floret-Ponetet and F. Lamnabhi-Lagarrigue, "Parametric identification methodology using sliding modes observer," *International Journal of Control*, vol. 74, pp. 1743–1753, 2001.

[118] A. Koshkouei and A. Zinober, "Sliding mode state observation for nonlinear systems," *International Journal of Control*, vol. 77, pp. 118–127, 2004.

[119] K. Veluvolu, Y. Soh, W. Cao, and Z. Liu, "Observer with multiple sliding modes for a class of nonlinear uncertain systems," in *Proceedings of American Control Conference*, pp. 2445–2450, 2005.

[120] R. Lopez and R.M.Yescas, "State estimation for nonlinear systems under model uncertainties: a class of sliding mode observers," *Journal of Process Control*, vol. 15, pp. 362–370, 2005.

[121] W. Chen and M. Saif, "Novel sliding mode observers for a class of uncertain systems," in *Proceedings of the American Control Conference*, pp. 2622–2627, 2006.

[122] G. Wheeler, C. Su, and Y. Stepanenko, "A sliding mode controller with improved adaptation laws for the upper bounds on the norm of uncertainties," in *Proceedings of the American Control Conference*, pp. 2133–2137, 1997.

[123] G. Wheeler, C. Su, and Y. Stepanenko, "A sliding mode controller with improved adaptation laws for the upper bounds on the norm of uncertainties," *Automatica*, vol. 34, pp. 1657–1661, 1998.

[124] G. Monsees and J. Scherpen, "Adaptive switching gain for a discrete-time sliding mode controller," in *Proceedings of American Control Conference*, pp. 1639–1643, 2000.

[125] V. Mkrtchian and A. Lazayan, "Application of neural network in sliding mode control," in *Proceedings of the IEEE Conference on Control Applications*, pp. 653–657, 2000.

[126] G. Monsees and J. Scherpen, "Adaptive switching gain for a discrete-time sliding mode controller," *International Journal of Control*, vol. 75, pp. 242–251, 2002.

[127] W. Perruquetti and J. Barbot, *Sliding Mode Control in Engineering.* Marcel Dekker Inc.: New York, 2002.

[128] R. Schneider and P. Frank, "Fuzzy logic based threshold adaption for fault detection in robots," in *Proceedings of Conference on Control Applications*, pp. 1127–1132, 1994.

[129] M. Rank and H. Niemann, "Norm based threshold selection for fault detectors," in *Proceedings of American Control Conference*, pp. 2027–2031, 1998.

[130] S. Ding, P. Zhang, P. Frank, and E. Ding, "Threshold calculation using LMI-technique and its integration in the design of fault detection systems," in *Proceedings of Conference on Decision and Control*, pp. 469–474, 2003.

[131] J. Stoustrup, H. Niemann, and A. la Cour-Harbo, "Optimal threshold functions for fault detection and isolation," in *Proceedings of American Control Conference*, pp. 1782–1787, 2003.

[132] Z. Shi, F. Gu, B. Lennox, and A. Ball, "The development of an adaptive threshold for model-based fault detection of a nonlinear electro-hydraulic system," *Control Engineering Practice*, vol. 13, pp. 1357–1367, 2005.

[133] T. Hsiao and M. Tomizuka, "Threshold selection for timely fault detection in feedback control systems," in *Proceedings of American Control Conference*, pp. 3303–3308, 2005.

[134] L. Ljung and T. Söderström, *Theory and Practice of Recursive Identification.* MIT Press: Massachusetts, 1983.

[135] R. Marino and P. Tomei, *Nonlinear Control Design, Geometric, Adaptive and Robust.* Prentice Hall: UK, 1995.

[136] Z. Li, R. Zhao, Y. Li, and D. Sun, "Real-time predictable control based on single-neuron PSD controller," in *Proceedings of the Second International Conference on Machine Learning and Cybernetics*, pp. 720–725, 2003.

[137] S. Singh and R. Zhang, "Adaptive output feedback control of spacecraft with flexible appendages by modeling error compensation," *Acta Astronautica*, vol. 54, pp. 229–243, 2004.

[138] K. Karray, A. Grewal, M. Glaum, and V. Modi, "Stiffening control of a class of nonlinear affine systems," *IEEE Transactions on Aerospace and Electronic Systems*, vol. 33, pp. 473–484, 1997.

[139] Q. Wu and M. Saif, "Neural adaptive observer based fault detection and identification for satellite attitude control systems," in *Proceedings of the American Control Conference*, pp. 1054–1059, 2005.

[140] S. Ibrir, "Online exact differentiation and notion of asymptotic algebraic observers," *IEEE Transactions on Automatic Control*, vol. 48, pp. 2055–2060, 2003.

[141] A. L.-J. R.M. Guerra and J. Rincon-Pasaye, "Fault estimation using algebraic observers," in *Proceedings of the American Control Conference*, pp. 438–442, 2007.

[142] N. Wang and P. Ji, "Neuron PID variable structure control," in *Proceedings of IEEE Asia-Pacific Conference on Circuit and Systems*, pp. 319–322, 2000.

[143] W. Chang, R. Hwang, and J. Hsieh, "A multivariable online adaptive PID controller using auto-tuning neurons," *Engineering Applications of Artificial Intelligence*, vol. 16, pp. 57–63, 2003.

[144] S. Barnett, *Matrices in Control Theory.* Van Nostrand Reinhold: New York, 1971.

[145] L. Show, J. Juang, and C. Yang, "Nonlinear H_∞ robust control for satellite large angle attitude maneuvers," in *Proceedings of American Control Conference*, pp. 1357–1362, 2001.

[146] L. Show, J. Juang, and Y. Jan, "An LMI-based nonlinear attitude control approach," *IEEE Transactions on Control Systems Technology*, vol. 11, pp. 73–83, 2003.

[147] H. Bang, M. Tahk, and H. Choi, "Large angle attitude control of spacecraft with actuator saturation," *Control Engineering Practice*, vol. 11, pp. 989–997, 2003.

[148] W. Chen and M. Saif, "Actuator fault diagnosis for uncertain linear systems using a high-order sliding-mode robust differentiator (HOSMRD)," *International Journal of Robust and Nonlinear Control*, vol. 18, pp. 413–426, 2008.

[149] Q. Wu and M. Saif, "Robust fault detection and diagnosis for a multiple satellite formation flying system using second order sliding mode and wavelet networks," in *Proceedings of the American Control Conference*, pp. 426–431, 2007.

[150] W. Chen, Q. Qian, and X. Wang, "Wavelet neural network based transient fault signal detection and identification," in *Proceedings of International Conference on Information, Communications and Signal Processing*, pp. 377–1381, 1997.

[151] Y. Oussar, I. Rivals, L. Personnaz, and G. Dreyfus, "Training wavelet networks for nonlinear dynamic input-output modeling," *Neurocomputing*, vol. 20, pp. 173–188, 1998.

[152] W. Dixon, S. Nagarkatti, D. Dawson, and A. Behal, *Nonlinear Control of Engineering Systems–A Lyapunov-Based Approach.* Birkhauser: Boston, 2003.

[153] L. Zadeh, "Fuzzy sets," *Information Control*, vol. 8, pp. 338–353, 1965.

[154] E. Mamdani and S. Assilian, "An experiment in liguistic synthesis with a fuzzy logic controller," *International Journal of Man Machine Studies*, vol. 7, pp. 1–13, 1975.

[155] W. Chen and M. Saif, "Design of a TS based fuzzy nonlinear unknown input observer with fault diagnosis applications," in *Proceedings of American Control Conference*, pp. 2545–2550, 2007.

[156] Q. Wu and M. Saif, "Robust fault diagnosis for a satellite system using a neural sliding mode observer," in *Proceedings of the 44th IEEE Conference on Decision and Control, and European Control Conference ECC 2005 (CDC-ECC'05)*, pp. 7668–7673, 2005.

[157] F. Abdollahi, H. Talebi, and R. Patel, "A stable neural network-based observer with applications to flexible-joint manipulators," *IEEE Transactions on Neural Networks*, vol. 17, pp. 118–129, 2006.

[158] Q. Wu and M. Saif, "Robust fault detection and diagnosis in a class of nonlinear systems using a neural sliding mode observer," *International Journal of Systems Science-Special Issue on Advances in Sliding Mode Observation and Estimation*, vol. 38, pp. 881–899, 2007.

[159] M. Saif and Y. Guan, "A new approach to robust fault detection and identification," *IEEE Transactions on Aerospace and Electronic Systems*, vol. 29, pp. 685–695, 1993.

[160] R. Patton and J. Chen, "Robust fault detection of jet engine sensor systems using eigenstructure assignment," *Journal of Guidance, Control and Dynamics*, vol. 15, pp. 1491–1497, 1992.

[161] F. Caccavale and L. Villani, "Fault diagnosis for industrial robots," in *Fault Diagnosis and Fault Tolerance for Mechatronic Systems, Recent Advances* (L. Villani, ed.), pp. 85–108, Springer-Verlag: Berlin, 2003.

[162] Q. Wu and M. Saif, "Robust fault diagnosis for satellite attitude systems using neural state space models," in *Proceedings of the International Conference on Systems, Man, and Cybernetics*, pp. 1955–1960, 2005.

[163] F. Lin, R. Wai, C. Lin, and D.-C. Liu, "Decoupled stator-flux-oriented induction motor drive with fuzzy neural network uncertainty observer," *IEEE Transactions on Industrial Electronics*, vol. 47, pp. 356–367, 2000.

[164] J. Gonzalez, R. Aguilar, J. Alvarez-Ramirez, and M. Barron, "Nonlinear regulation for a continuous bioreactor via a numerical uncertainty observer," *Chemical Engineering Journal*, vol. 69, pp. 105–110, 1998.

[165] Q. Wu and M. Saif, "Robust fault diagnosis for a satellite large angle attitude system using an iterative neuron PID (INPID) observer," in *Proceedings of the American Control Conference*, pp. 5710–5715, 2006.

[166] Q. Wu and M. Saif, "Observer-based robust process fault detection and diagnosis for a satellite system with flexible appendages," in *Proceedings of the 45th Conference on Decision and Control*, pp. 2183–2188, 2006.

[167] Q. Wu and M. Saif, "Repetitive learning observer based actuator fault detection, isolation, and estimation with application to a satellite attitude control system," in *Proceedings of the American Control Conference*, pp. 414–419, 2007.

[168] Y. Xiong and M. Saif, "Robust and nonlinear fault diagnosis using sliding mode observers," in *Proceedings of the 40th IEEE Conference on Decision and Control*, pp. 567–572, 2001.

[169] A. Alessandri, "Sliding mode estimators for a class of nonlinear systems affected by bounded disturbances," *International Journal of Control*, vol. 76, pp. 226–236, 2003.

[170] F. Caccavale and L. Villani, "An adaptive observer for fault diagnosis in nonlinear discrete-time systems," in *Proceedings of American Control Conference*, pp. 2463–2468, 2004.

[171] W. Chen, Q. Qian, and X. Wang, "Wavelet neural network based transient fault signal detection and identification," in *International Conference on Information, Communications and Signal Processing*, pp. 1377–1381, 1997.

[172] C. Yang and Y. Sun, "Mixed H_2/H_∞ sate-feedback design for micorsatellite attitude control," *Control Engineering Practice*, vol. 10, pp. 951–970, 2002.

[173] B. Wie, *Space Vehicle Dynamics and Control.* American Institute of Aeronautics and Astronautics Inc.: Reston, 1998.